Free Solution Capillary Electrophoresis for Purity and Identification of Synthetic Oligonucleotides on Polymer Modified Capillary Surfaces

A thesis submitted for fulfilment of the degree of Doctor of Philosophy

Kerrilee Evelyn Allan

BTech (Forensic & Analytical Chemistry), BSc (Hons)

Flinders UNIVERSITY

Adelaide, South Australia

Faculty of Science & Engineering

School of Chemical & Physical Sciences

Supervised by

Associate Professor Amanda V. Ellis (School of Chemical and Physical Sciences)

Co-supervised by

Associate Professor Claire E. Lenehan (School of Chemical and Physical Sciences)

February 2012

Declaration

I certify that this thesis does not incorporate without acknowledgment any material previously submitted for a degree or diploma in any university; and that to the best of my knowledge and belief it does not contain any material previously published or written by another person except where due reference is made in the text.

_____

Kerrilee E. Allan on _____/_____/_____

Acknowledgments

My first thanks must go to my supervisor Associate Professor Amanda Ellis. You tackled my candidature with both brutal honesty and unexpected kindness.
And for that and all else, I thank you.

I would also like to thank my co-supervisor Associate Professor Claire Lenehan for the little bits of support and guidance, and helping me get back on track when I derailed.

To my office mate Noni, I'd like to formally thank you for labouring over both the AFM and the editing of this thesis for me.
I have found a true friend in you and I can't thank you enough for everything.

Special thanks to Auntie Diane for taking the time to do the final proof-reading for me.
I hope it was at least insightful!

Many, many thanks go to Dad, Mum & Graeme, Andrew, Anthony, Nana & Grandad, Dain & Andrew Blok. It has been almost as much of a journey for you as it has for me.
You are my best friends and I love you.

And to all those I have whinged and gossiped to, and played, partied, and shared precious memories with (especially Jez, Ra, Sophie, & Jacqueline), you are simply amazing!

Abstract

This thesis describes a capillary electrophoretic method to determine the identity and purity of oligonucleotides (ODNs) and phosphorothioate antisense oligonucleotides (PS-ODNs) using cationic copolymers as a dynamic coating, based on monomers of ethylpyrrolidine methacrylate (EPyM) and methyl methacrylate (MMA). ODNs are short fragments of single-stranded (ss) or double-stranded (ds) deoxyribonucleic acid (DNA) and their uses range from biological systems to drug delivery and pharmaceutical analysis. In particular, antisense oligonucleotides (AS-ODNs) have a role as therapeutic molecules which inhibit expression of target genes by binding to a specific RNA sequence, blocking the translation process. AS-ODNs exist in various modified forms of which PS-ODNs are the most common. It is therefore necessary to have methods in place to determine the identity and purity of these modified AS-ODNs.

Capillary electrophoresis (CE) has been extensively used for separation of DNA fragments focusing on large strands. Consequently, there is a significant gap in the literature regarding the analysis of short strands of DNA (such as ODNs). DNA strands below the DNA persistence length (p_{DNA}) are rod-like and non-free draining, and exhibit different migration patterns in free solution compared to larger strands which cannot be separated in this way. Operating in free solution has the advantage of only requiring surface confined capillary modification for electroosmotic flow (EOF) suppression allowing for charge-based separation in which larger, more negatively strands exhibit a greater mobility.

In this thesis, homopolymers and copolymers based on EPyM and MMA were prepared by conventional free radical (CFR) and reversible addition-fragmentation chain transfer (RAFT) polymerisation. This work reports for the first time the use of a RAFT block copolymer for the separation of ODNs. Polymer solutions were prepared for surface-confined capillary modification via physical adsorption and the adsorptive properties (onto silicon (Si) wafers) were investigated via atomic force microscopy (AFM). It was observed that the effectiveness of these polymers for capillary surface modification via adsorption was highly dependent on the polymer concentration, tacticity and hence, stereochemistry. A dilute polymer solution of CFR poly(ethylpyrrolidine methacrylate-*co*-methyl methacrylate)

(PEPyM-*co*-PMMA) random copolymer (1 mg mL^{-1}) provided a homogenous surface coating owing to the polymer chains being hydrodynamically separated allowing for adsorption as individual globules. Whereas the RAFT poly(ethylpyrrolidine methacrylate-*block*-methyl methacrylate) (PEPyM-*b*-PMMA) block copolymer provided an uneven and incomplete surface coverage owing to the rigidity of the polymer chains.

Enhanced CE separation of ODNs (ds and ss) ranging from 16 - 20 base pairs (bp) (containing the same 16 base (b) sequence) was achieved in free solution on a capillary dynamically coated with CFR PEPyM-*co*-PMMA random copolymer (21/79). Fast and efficient surface modification was achieved on bare fused-silica capillaries activated with hydrochloric acid (HCl), H_2O, sodium hydroxide (NaOH) and Tris(hydroxymethyl)aminomethane (Tris)-borate (100 mM)/urea (7M) buffer, by flushing with polymer solution and H_2O followed by a final treatment with running buffer. 1 bp resolution (R_s) and was seen for long (30 cm) and short (8 cm) capillaries with partial R_s of the 16 bp and 17 bp mixture. Co-migration of some strands was attributed to ODN-ODN interactions during migration. These interactions were confirmed by the 16 bp peak migration time (t_m) not being additive within each mixture. The 1 bp R_s achieved for the complementary sequence strands was improved by up to 37 % for separation of dsODNs containing non-complementary sequences. Interestingly, separation of a dsODN mixture containing two 16 bp strands of different sequences resulted in partial R_s (0.52) suggesting that the free solution mobility of dsODNs was sequence dependent. Differential mobilities for ssODN fragments of the same length were also observed.

The method described herein was capable of resolving mixtures of PS-ODNs and ODNs, (including R_s of ss impurities from ds fragments) indicating that this method is suitable for determining ODN and PS-ODN purity. Both ODN and PS-ODN mobility was found to be proportional to an increase in bp length, suggesting the separation mechanism is based on the free solution mobility and ion-pairing between the surface and the analyte. The developed method has the advantage of fast and simple preparation, easy regeneration, extended capillary life-time, unrestricted polymer solubility, and enhanced stability under harsh conditions (high voltage and temperature, and extreme pH).

Publications

The publications originating from the work within this thesis are as follows:

Papers

Kerrilee E. Allan; Claire E. Lenehan; Dmitriy A. Khodakov; Hilton J. Kobus; Amanda V. Ellis, High-performance capillary electrophoretic separation of double-stranded oligonucleotides using a poly(ethylpyrrolidine methacrylate-*co*-methyl methacrylate) coated capillary, *Electrophoresis* **2012**, *33*, 1-10

Conference Proceedings

Kerrilee E. Allan, Polymeric Surface Modification of Capillaries for the Separation of DNA by Capillary Electrophoresis. Oral presentation at the *European Polymer Congress (EPF2011) and XII Congress of the Specialized Group of Polymers (GEP)*, Granada, Spain, **2011**

Kerrilee E. Allan, Random versus block copolymers for dynamic coatings for capillary electrophoretic separation of DNA. Oral presentation at the *32nd Australasian Polymer Symposium (APS)*, Coffs Harbour, NSW, **2011**

Kerrilee E. Allan, Capillary electrophoretic separation of double-stranded DNA oligonucleotides using a PEPyM-*co*-PMMA dynamically coated capillary. Poster presentation at the *ANZFSS 20th International Symposium on the Forensic Sciences*, Sydney, NSW, **2010**

Kerrilee E. Allan, Investigation of PEPyM-*co*-PMMA copolymer as a dynamic coating for capillary electrophoretic separation of DNA fragments. Oral presentation at the *ARNAM/ARCNN 2010*, Adelaide, SA, **2010**

Kerrilee E. Allan, Capillary electrophoretic determination of double-stranded DNA through an intercalating dye using the zone-passing technique, Poster presentation at the *ANZFSS 19th International Symposium on the Forensic Sciences*, Melbourne, Vic., **2008**

Table of Contents

List of Figures

List of Tables

List of Schemes

List of Abbreviations and Symbols

[*M*]	Concentration of monomer (via integration)
[M_0]	Initial concentration of monomer (via integration)
[η]	Intrinsic viscosity
$\sum_k$	Particle (*k*) surface area
μ_{app}	Apparent electrophoretic mobility
μ_{BRF}	BRF mobility
μ_{BRM}	BRM mobility
μ_{CR}	CR mobility
$\mu_{CR(tot)}$	Total CR mobility
μ_{EOF}	Electroosmotic mobility
μ_{ep}	Electrophoretic mobility
μ_o	Free solution mobility
μ_{obs}	Observed electrophoretic mobility
μ_{rep}	Reptation mobility
A	Adenine
a_0	Contour length of one DNA bp
ACN	Acetonitrile
ACPA	4,4'azobis(4-cyanovaleric acid)
AFM	Atomic force microscopy
AIBN	Azo-*bis*-isobutyrylnitrile
APS	Ammonium persulphate
AS-ODN	Antisense oligonucleotide
b	(DNA) base
b	Kuhn length
BGE	Background electrolyte
bp	(DNA) base pair
BRF	Biased reptation with fluctuations
BRM	Biased reptation model
Bu_3SnH	Tributylstannane
C	Cytosine
c	Concentration
c*	Overlap concentration
C16-HEC	C16-derivatised 2-hydroxyethyl cellulose
cat-HEC	Cationised hydroxyethylcellulose

$CDCl_3$	Chloroform, deuterated
CE	Capillary electrophoresis
CEP	Capillary electrophoresis phase
CFR	Conventional free radical
CGE	Capillary gel electrophoresis
c_k	Bulk concentration of '*k*' ions
CMS	Current monitoring system
c_{opt}	Optimum polymer concentration
CR	Constraint release
CTA	Chain transfer agent
D	Tangential distance of chain
$\bar{d}$	Mean difference
d6-DMSO	Dimethylsulphoxide, deuterated
DEAEMA	2-(diethylamino)ethyl methacrylate
DMF	Dimethylformamide
DMF	Diethylmalonate
DNA	Deoxyribonucleic acid
ds	Double-stranded
dsAS-ODN	Double-stranded antisense oligonucleotide
dsDNA	Double-stranded DNA
dsODN	Double-stranded oligonucleotide
dsPS-ODN	Double-stranded phosphorothioate antisense oligonucleotide
D_t	Translational diffusion coefficient
E	Total field strength
EDL	Electric double layer
EDTA	Ethylenediaminetetraacetic acid
EOF	Electroosmotic flow
epoxy-PDMA	Poly(dimethylacrylamide-*co*-allylglycidyl ether)
epoxy-poly(AG-AA)	Poly(acrylamide-*co*-allyl-β-D-glucopyranoside-*co*-allylglycidy ether)
EPy	*N*-(2-hydroxyethyl)-2-pyrrolidine
EPyM	Ethylpyrrolidine methacrylate
ez_k	Charge of ion '*k*'
F	Faradays constant
F_{drag}	Average drag force acting on the DNA due to one polymer
FTIR	Fourier transform infrared

G	Guanine
g	Grams
g	Polymer globule
GPC	Gel permeation chromatography
h	Hours
H_3PO_4	Hydrogen phosphate
HCl	Hydrochloric acid
HEC	Hydroxyethylcellulose
HMC	Hydroxypropylmethylcellulose
HPLC	High performance liquid chromatography
I_B	Bjerrum length
id	Capillary inner diameter
k	Boltzmann constant
K	Constant of proportionality
K*	Mark-Houwink-Sakurada constant
kDA	Kilodaltons
L	Litres
L	Molecular chain length
L_c	DNA contour length
L_d	Length to the detector (effective capillary length)
LIF	Laser induced fluorescence
L_p	Polymer contour length
L.O.D	Limit of detection
LPA	Linear polyacrylamide
L_t	Total capillary length
m	Metres
M	Moles per litre (mol L^{-1})
MALDI	Matrix-assisted laser desorption/ionisation
MALLS	Multi-angle laser light scattering
MC	Methylcellulose
M_{DNA}	Base pair length of DNA
min	Minutes
MMA	Methyl methacrylate
M_n	Average number molecular mass
mol	Moles
MPTS	γ-methacryloxypropyltrimethoxysilane
M_w	(Average weight) molecular mass

N	Molecular length
n	Mean number of polymer chains in contact with the DNA
N	Theoretical plates
N_A	Avogadro's number
NaCl	Sodium chloride
NaDM	Sodium diethylmalonate
NaH_2PO_4	Dihydrogen sodium phosphate
NaOH	Sodium hydroxide
N_{bl}	Number of globules per chain
N_k	Total number of Kuhn segments
NMR	Nuclear magnetic resonance
N_p	Number of polymer molecules
$N_{polymer}$	Degree of polymerisation of the polymer
od	Capillary outer diameter
ODN	Oligonucleotide
OHP	Outer Helmholtz plane
p	Persistence length
Pa	Pascals
PAM	Polyacrylamide
Pd(A)	Polydeoxyadenylic acid
Pd(T)	Polydeoxythymidylic acid
PDEA	Polydiethylacrylamide
PDEAEMA	Poly(diethylaminoethyl methacrylate)
PDEAEMA-*co*-PMMA	Poly(diethylaminoethyl methacrylate-*co*-methyl methacrylate)
PDI	Polydispersity index
PDMA	Polydimethylacrylamide
PDMA-*co*-PEPyM	Poly(*N*,*N*-dimethylacrylamide-*co*-ethylpyrrolidine methacrylate)
PDMA-*co*-PMAEM	Poly(*N*,*N*-dimethylacrylamide-*co*-4-(ethyl)-morpholine methacrylamide)
p_{DNA}	Persistence length of DNA
PEG	Polyethylene glycol
PEO	Polyethylene oxide
PEPyM	Poly(ethylpyrrolidine methacrylate)
PEPyM-*b*-PMMA	Poly(ethylpyrrolidine methacrylate-*block*-methyl methacrylate)
PEPyM-*co*-PMMA	Poly(ethylpyrrolidine methacrylate-*co*-methyl methacrylate)
PHEA	Poly-*N*-hydroxyethylacrylamide

PMMA	Poly(methyl methacrylate)
poly(AA-EE)	Poly(acryloylaminoethoxyethanol)
poly(AG-AA)	Polyacrylamide-*co*-allyl-*β*-D-glucopyranoside
poly(Agal-AA)	Poly(acrylamide-co-allyl-D-galactopyranoside)
polyE-323	Bis(3-aminopropylamino)ethane
PPS	Potassium persulphate
PS-ODN	Phosphorothioate oligonucleotide
PSS	Polystyrenesulfonate
PVP	Polyvinylpyrrolidone
Q	Total particle charge
R	Gas constant
r	Capillary radius
RAFT	Reversible addition-fragmentation chain transfer
R_g	Radius of gyration/migrating particle radius
RMS	(Roughness) root mean squared
RNA	Ribonucleic acid
R_p	Radius of the polymer chains
R_s	Resolution (of peaks)
RSD	Relative standard deviation
s	Seconds
SCLRP	Surface-confined living radical polymerisation
s_d	Standard deviation
SEC	Size exclusion chromatography
SECE	Size exclusion capillary electrophoresis
SEI	Short-end injection
Si	Silicon
SNP	Single nucleotide polymorphism
ss	Single-stranded
ssAS-ODN	Single-stranded antisense oligonucleotide
ssDNA	Single-stranded DNA
ssODN	Single-stranded oligonucleotide
ssPS-ODN	Single-stranded phosphorothioate antisense oligonucleotide
star-PEO	Star-polyethylene oxide
STRs	Short tandem repeats
T	Thymine
t	Time
T	Temperature

TA	Tris-acetate
TAE	Tris-acetate-EDTA
TAPS	*N*-tris(hydroxymethyl)methyl-3-aminopropanesulfonic acid
TBE	Tris-borate-EDTA
t_{calc}	Calculated *t* value for *t*-test
TEA	Triethylamine
TEC	Transient entanglement coupling
TEMED	*N*,*N*,*N'*,*N'*-tetramethylethane-1,2-diamine
THF	Tetrahydrofuran
t_{int}	Injection time
T_m	Melting temperature
t_m	Migration time
TMS	Tetramethyl silane
Tris	Tris(hydroxymethyl)aminomethane
TrisCl	Tris chloride
t_{table}	*t* value from the table of *t*-distribution values for *t*-test
UV	Ultraviolet
UV-Vis	Ultraviolet-visible
V	Applied voltage
v	Volume
V_{DNA}	Velocity of the DNA
V_{inj}	Injection voltage
v_{int}	Volume of sample introduced/injected
V_n	Electrophoretic velocity of a DNA molecule with n polymers attached
V_{par}	Particle volume
V_p	Curvilinear velocity of the reptating polymer chains
V_s	Surface potential
W_h	Peak width at half height
α_{MHS}	Mark-Houwink-Sakurada constant
β	Ratio of τ_p to τ_{DNA}
γ	$(\rho_{solvent}/\rho_{polymer})$ x $(N_{polymer})^{1+v}$
δ	Chemical shift
δ	Thickness of the EDL
ΔP	Change in pressure
ε	Reduced electric field
ε_o	Permittivity of vacuum

ε_b	Dielectric constant of the fluid
ζ	Zeta potential
η	Viscosity of solution
η_s	Viscosity of solvent
κ	Inverse Debye length
κ^{-1}	Debye screening length
μ	Micro
v	Velocity
v_c	Average number of chain centres/cm^3
v_{EOF}	EOF velocity
v_F	Flory's exponent
ξ	Polymer screening length
$\bar{\xi}$	Mesh size normalised to the DNA Kuhn length
ξ_b	Pore (mesh) size
ξ_f	DNA friction coefficient per bp
π	Pi
ρ	Density
σ	Surface charge density
τ_{DNA}	Release time of the polymer from the DNA
τ_p	Release time of the DNA from the polymer
ψ	Electric potential

1 Introduction and literature review

1.1 Synopsis

Background information relative to this thesis is given with focus upon capillary electrophoresis (CE) in free solution. Specific attention is directed toward the modification of capillaries with polymers for application to free solution CE of short rod-like oligonucleotides (ODNs) that are non-free draining in nature. In order to understand the migration of deoxyribonucleic acid (DNA), it is necessary to be familiar with the separation mechanisms currently described in literature and these are highly dependent on the type of surface modification employed. As such each of the separation mechanisms are discussed in turn. In addition, the types of polymer surface modifications are classified and described, concentrating on physically adsorbed dynamic polymer surfaces for the regulation of surface charge.

The respective background information relating to polymer synthesis and characterisation can be found in Chapter 3 (Sections 3.3 and 3.4). Refer to Section 7.2 in Chapter 7 for the introduction and literature regarding therapeutic antisense oligonucleotides (AS-ODNs), focusing on phosphorothioate antisense oligonucleotides (PS-ODNs).

1.2 Principles of CE separation of DNA

1.2.1 Background on DNA

DNA is a helical molecule composed of nucleotide units bound together forming either single-strands (ss) or double-strands (ds) [1, 2]. Each nucleotide unit (shown in Figure 1.1) consists of a sugar (2'-deoxyribose), a phosphate and a nitrogenous base [3].

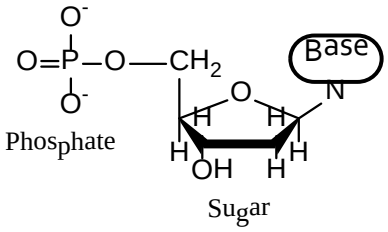

Figure 1.1. Structure of a nucleotide.

There are four different types of nitrogenous bases in DNA, shown in Figure 1.2, which include adenine (A), thymine (T), guanine (G) and cytosine (C).

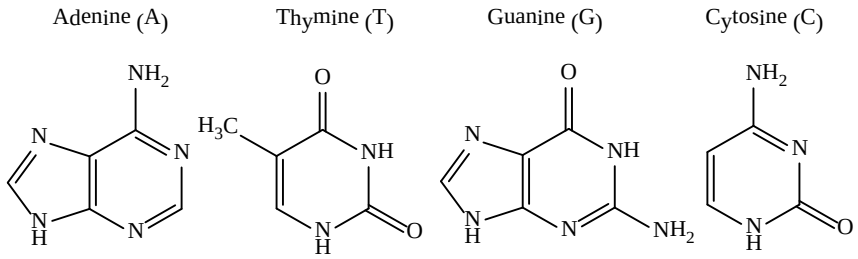

Figure 1.2. Structure of amine bases in DNA.

In order to create a single-strand of DNA (ssDNA), nucleotides are linked together via phosphodiester bonds between the phosphate and the sugar of adjacent nucleotides (shown in Figure 1.3, left) [3]. The phosphate-sugar backbone is non-informational, and provides structural support to the molecule. Importantly for the work described later, it provides DNA with a negative charge density which is critical for electrophoresis [4].

Finally, to form double-stranded DNA (dsDNA) two polynucleotide strands are held together via hydrogen bonding and hydrophobic forces between complementary base pairing of C and G, and T and A bases (see Figure 1.3, right). The strands then intertwine, forming the well-recognised double helix.

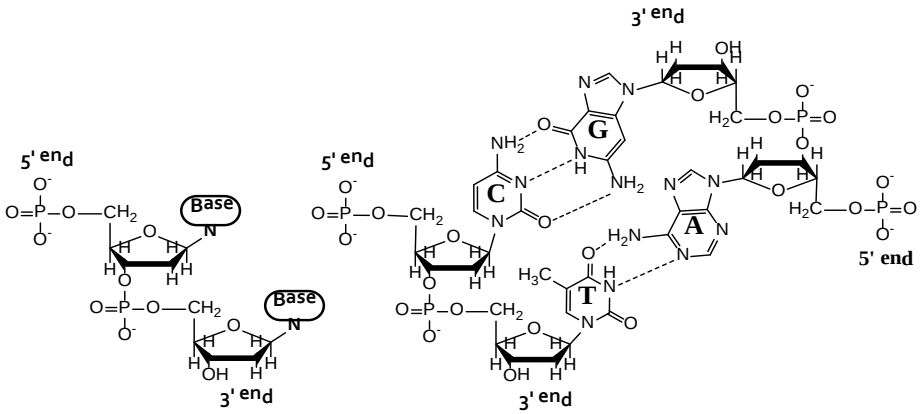

Figure 1.3. Structure of ssDNA formed by linked nucleotides (left). Complementary base pairing between C and G, and T and A (right) to form dsDNA.

The proposed structure of the DNA double helix has a diameter of 10 Å in which each adjacent base on the one strand is separated by a distance of 3.4 Å [5]. By making the assumption that the angle between adjacent bases is 36^{o}, Watson & Crick [5] determined that the structure repeated itself after 10 b, leading to a repeat length of ~34 Å (see Figure 1.4).

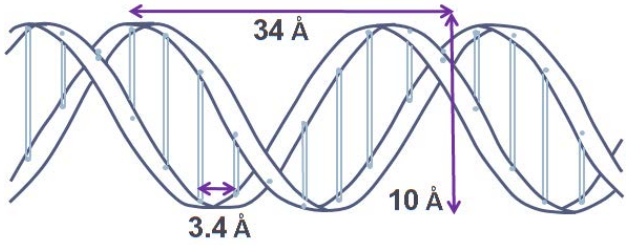

Figure 1.4. Structure of the DNA double helix showing the dimensions.

These dimensions are dependent on the conformation of the double helix. In some solutions, or more specifically during electrophoresis, the helical structure can undergo conformational changes [6, 7]. The persistence length of DNA (p_{DNA}), which describes the stiffness of the DNA chain, has been reported for dsDNA to be somewhere between 500 Å and 900 Å (~147 - 260 b) [8, 9]. Below the p_{DNA}, the dsDNA chains behave as a rod, and above this length the behaviour of the chains can be best described mathematically as a random walk [8, 9]. Of great importance to this thesis is that the p_{DNA} can greatly affect the way that the DNA will migrate during electrophoresis (see Section 1.4). The following describes the fundamentals of electrophoresis, in particular capillary electrophoresis and electroosmotic flow (EOF) within microchannels for DNA separation.

1.2.2 Fundamentals of CE

CE separates components in a solution under the application of a high voltage in a capillary (typically 50 µm - 100 µm in diameter and 20 cm - 50 cm in length) based on ion mass and charge [10]. Traditional CE uses a positive polarity (injection at the anode, with detection at the cathode) generating a cathodic EOF which moves in the same direction as the detected analytes. Positive polarity is most commonly used for separation of analytes that are positively or negatively charged. However, in the case of negatively charged species in which the electrophoretic mobility (μ_{ep}) is greater than the EOF, a negative polarity (cathode to anode) is used [11]. A schematic of the migration of ions through a capillary under a negative applied voltage is shown in Figure 1.5.

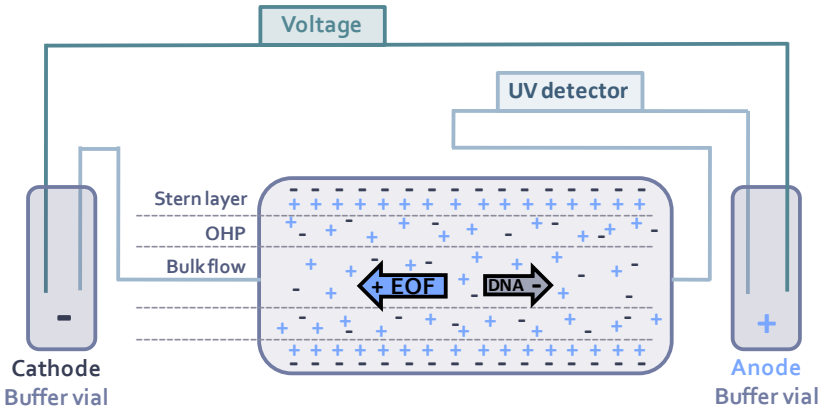

Figure 1.5. Diagram of ion movement through a fused-silica capillary using a negative applied voltage.

The surface of the capillary is typically made of hydroxylated fused-silica, and hence has silanol surface functional groups [12, 13]. The silanol groups on the silica capillary are deprotonated by washing with a basic solution prior to addition of the buffer. Deprotonation results in a negative charge along the interior of the capillary [12, 13] which attracts the positive counterions (cations) from the buffer forming an electric double layer (EDL). This layer has two parts; a static layer (the Stern layer) and a more diffuse layer, known as the outer Helmholtz plane (OHP) [4, 14]. When an electric field is applied, the cations in the diffuse layer migrate towards the cathode carrying their water of hydration, and so the solution 'flows'. This is the EOF, which propels the buffer and solvent towards the cathode (Figure 1.5) [8, 12, 13, 15].

1.2.3 Surface and analyte charge theories

Surface and analyte charge theories are related to how the surface potential affects the migration of molecules, focussing on successful separation of short DNA strands in free solution. For simplicity, this thesis defines free solution to be electrophoresis of an analyte without the addition of polymers to the BGE (i.e., non-sieving), in which migration is a factor of the charge of the analyte and the diffuse ion atmosphere. The following introduces the relevant equations to experimentally derive the electroosmotic and electrophoretic velocities and mobilities required for complete analysis of DNA separation.

1.2.3.1 Electro-migration of background electrolytes

In order to explain the mobility of a large charged ion immersed in a solution of smaller charged particles, one must first consider the mobility of the smaller ions and the forces they instil upon the migrating ion (e.g., DNA). This is directly related to the thickness (concentration) of the electrolyte counterions on the surface and their static or diffuse nature for the formation of the EDL and thus subsequent EOF under an applied voltage. As previously mentioned, the EDL consists of a static Stern layer of immobile ions, and a diffuse OHP layer of mobile ions. The thickness of the Stern layer is given by the Bjerrum length (I_B), shown by Equation 1.1 [4],

$$I_B = \frac{e^2}{(4\pi\varepsilon_b\varepsilon_o kT)}$$

Equation 1.1

where ε_b is the dielectric constant of the fluid, k is the Boltzmann constant, ε_o is the permittivity of vacuum, and T is temperature (in Kelvin). The equilibrium distribution of mobile ions, according to mean-field theory, can be determined by the Poisson-Boltzmann equation, shown by Equation 1.2 [4],

$$\varepsilon_b\varepsilon_o\nabla^2 V_{par} = -e\sum_k z_k c_k \exp\left(\frac{-ez_k V_{par}}{kT}\right)$$

Equation 1.2

where ez_k is the charge, c_k is the bulk concentration of 'k' ions, V_{par} is the particle volume, and $\sum_k$ is the particle (k) surface area. Linearisation of Equation 1.2

conveys the Debye-Hückel theory which describes the screening of the electric fields in the electrolyte and is applicable to the OHP, shown by Equation 1.3 [4],

$$V_{\mathrm{p}}(\mathrm{x}) = V_{\mathrm{s}}\mathrm{e}^{-\kappa X}$$

Equation 1.3

where V_s is the surface potential and κ^{-1} is the Debye screening length given by Equation 1.4 [4].

$$\kappa^{-1} = \left(\frac{\varepsilon_{\mathrm{b}}\varepsilon_{\mathrm{o}}kT}{e^2\sum_{\mathrm{k}} z_{\mathrm{i}}^2 c_{\mathrm{i}}}\right)^{1/2}$$

Equation 1.4

In relation to DNA in electrolytes, κ^{-1} describes the thickness of the diffuse ion atmosphere surrounding the DNA, which modulates the interactions with other charged species in the solution [16]. As κ^{-1} varies inversely with the square root of ionic strength, the electrostatic shielding of the DNA is decreased with increasing ionic strength, and the migration in free solution will therefore be reduced by increased interactions with other charged species [16].

As κ^{-1} is directly related to the diffuse layer, the thickness of the EDL (δ) can therefore be defined by Equation 1.5 as,

$$\delta = \left(\frac{\varepsilon_{\mathrm{b}}\varepsilon_{\mathrm{o}}RT}{2cF^2}\right)^{1/2}$$

Equation 1.5

where R is the gas constant and F is Faradays constant, and these two equations (Equation 1.4 and 1.5) are interchangeable. The properties and the thickness of the EDL define the mobility of a charged molecule during free solution electrophoresis. These surface properties are exploited in this thesis to enable charge-based separations of ODNs and PS-ODNs on modified capillaries in free solution (see Chapters 5 - 7).

Now that the surface properties have been defined, the electro-migration of larger charged species (such as DNA) in a charged electrolyte solution can be determined.

1.2.3.2 Electro-migration of DNA in charged solutions

Application of an electric field causes the ion cloud (of given thickness, κ^{-1}), consisting of excess counterions surrounding the polyelectrolyte, to be dragged in the opposite direction (related to the EOF) to the migrating polyelectrolyte, resulting in hydrodynamic interactions with the DNA. Therefore, by decreasing the thickness (by increasing ion concentration) of κ^{-1}, the drag/friction will decrease as the mean free path of the buffer ions will be reduced and this effectively decreases the EOF, as κ^{-1} describes the EDL. In free solution, this decreases the migration of the DNA (by increasing the solution viscosity according to Equation 1.6 and 1.7). This can be explained by considering two scenarios; a thick Debye layer where migrating particle radius (R_g) < κ^{-1}, and a thin Debye layer where R_g >> κ^{-1}. The electrophoretic mobility of a spherical particle for a thick Debye layer can be determined by Equation 1.6 [17],

$$\mu_{ep} = \frac{v}{E} = \frac{Q}{6\pi\eta_s R_g}$$

Equation 1.6

where Q is the total particle charge, and η_s is the solvent viscosity. Equation 1.6 demonstrates that the mobility is dependent on a ratio of the particle size and charge. Given that the charge scales proportionally with an increase in size for DNA, the mobility will be the same regardless of the size. For a thin Debye layer, the velocity becomes independent of the DNA particle size and shape and the μ_{ep} can be described by the Smoluchowski equation, according to Equation 1.7 [4],

$$\mu_{ep} = \frac{\varepsilon_b \varepsilon_o \zeta}{\eta_s}$$

Equation 1.7

where $\zeta = \delta\sigma/\varepsilon_o\varepsilon_b$ is the zeta potential which characterises the diffuse layer [18]. For a thin Debye layer, the size and shape independence described by Equation 1.7 represents the μ_{ep} of DNA restricted only by the surrounding ion cloud. By ignoring the Stern layer, the μ_{ep} of a charged polyelectrolyte is expressed by the Debye-Hückel limit as a function of surface charge density (σ) and described by Equation 1.8 [4],

$$\mu_{ep} = \frac{\sigma}{4\pi\eta_s\kappa}$$

Equation 1.8

where κ is the inverse Debye length. Equation 1.7 and 1.8 (for a thin Debye layer) both show that the μ_{ep} of an unhindered molecule will be independent of size and shape, and this is due to the screening of hydrodynamic interactions. Therefore, to facilitate charge-based separation of short DNA strands in free solution, it is necessary to operate in the thin Debye layer regime. According to a review by Viovy [4], the Smoluchowski equation (shown by Equation 1.7) can also be used to theorise the EOF. This is because it describes the motion of a charged surface in relation to the surrounding liquid and hence corresponds to the mobility of an electrolyte (ion in the OHP) in the vicinity of the Stern layer. The Helmholtz-Smoluchowski equation (combining Equations 1.6 and 1.7) describes the EOF velocity (v_{EOF}) and is expressed by Equation 1.9 [18].

$$v_{EOF} = \frac{\varepsilon_b \varepsilon_o \zeta E}{\eta_s}$$

Equation 1.9

Equation 1.9 states that an increase in viscosity will result in a decrease in the v_{EOF}. This fact is crucial for the work described in this thesis, as separation of ODNs in free solution is reliant upon the ability of the adsorbed polymer on the fused silica capillary to screen the surface charge by increasing the local viscosity [19].

1.2.3.3 Practical considerations for EOF and electrophoretic mobility of DNA

DNA is classified as a free draining macromolecule with a constant linear charge density, meaning that migration in free solution is independent of molecular mass (M_w) [20]. This is evidenced by Equation 1.6 which shows that the mobility of DNA is dependent on both DNA size and charge (expressed as a ratio), implying that size-based separation is not possible in free solution. This is true for DNA molecules above the p_{DNA}, but molecules below the p_{DNA} have been observed to exhibit charge-based migration [20, 21]. The size independent migration of larger DNA molecules is due to both hydrodynamic friction forces felt during migration and total molecular charge being proportional to the length of the molecule. Therefore, for successful electrophoretic separations of DNA above the p_{DNA}, obstacles such as polymer sieving media are required to alter the mobility based on size. This will be discussed further in Section 1.4.

As mentioned previously, in an electric field, the positive counterions on the surface migrate towards the cathode, dragging other hydrated ions along with them. An applied voltage also causes migration of the analyte ions in the bulk solution. The velocity (v) of these ions depends on the properties of the background electrolyte (BGE) and the magnitude of the voltage applied. The μ_{ep} of an analyte can therefore be determined by relating the velocity to the total field strength (E) according to Equation 1.10.

$$\mu_{\mathrm{ep}} = \frac{v}{E}$$

Equation 1.10

The μ_{ep} of a given analyte is independent of the applied voltage and capillary used, and characteristic of buffer properties (such as composition, ionic strength and pH). The apparent mobility (μ_{app}) can be determined from the CE electropherogram using the migration time of the analyte [22] and is expressed by Equation 1.11,

$$\mu_{\mathrm{app}} = \frac{L_{\mathrm{d}} L_{\mathrm{t}}}{\mathrm{t_m V}}$$

Equation 1.11

where L_d is the length to the detector (effective capillary length), L_t is the total capillary length, t_m is the migration time of the analyte, and V is the applied voltage. The μ_{ep} is also dependent on the EOF mobility of the system, and by taking this into account, the observed (and overall) mobility (μ_{obs}) of an analyte can be determined by Equation 1.12 [8],

$$\mu_{\mathrm{obs}} = \mu_{\mathrm{app}} - \mu_{\mathrm{EOF}}$$

Equation 1.12

where, μ_{EOF} is the electroosmotic mobility. According to Equation 1.12, a neutral analyte migrating solely due to the EOF will have a μ_{obs} equal to the μ_{EOF}, and can therefore be used as a neutral marker to determine the μ_{EOF} from Equation 1.11 using the t_m.

Equations 1.10 - 1.12 are crucial to the work in this thesis as they are used to determine the velocity and mobility of the EOF in polymer coated capillaries; and hence characterise the migration of ODNs and PS-ODNs in free solution on these capillaries based on their calculated mobilities (see Chapters 5 - 7).

1.2.3.4 EOF suppression by surface modification

A major contributing factor to CE separation is the existence of the EOF. Although this can be utilised in some CE applications, conventional DNA analysis requires the reduction of EOF for successful and efficient separation. As was observed by Figure 1.5, the EOF moves in the opposite direction to the negatively charged migrating species. Coating the capillary surface with polymers slows down the EOF by shielding the surface from the EDL. This is achieved by altering the charge distribution along the surface of the capillary depending on the coating material used. Coating provides flexibility in the separation of analytes by allowing control of the analyte and the buffer mobility [12, 13, 23-28]. The theory behind EOF elimination was first described by Hjertén in 1985 [23] using Equation 1.13 expressed as,

$$\mu_{\mathrm{EOF}} = \frac{\varepsilon_{\mathrm{b}}}{4\pi}\int_{\mathrm{o}}^{\zeta}\frac{1}{\eta_{\mathrm{s}}}d\psi$$

Equation 1.13

where ψ is the electric potential. Equation 1.13 predicts that the integral value approaches zero when the viscosity in the EDL close to the wall approaches infinity [23], suggesting that the EOF can be suppressed by increasing the viscosity in the EDL [18, 20]. This can be simply achieved by coating the surface with polymers. The thickness and the density of the polymer layer can control the viscosity of the EDL, meaning that a thicker coating will prevent the EOF in the region of high potential [13]. This thesis focuses on the use of polymers adsorbed onto the surface from solution, to shield the surface charge by increasing the viscosity of the EDL (see Chapter 3 for polymer synthesis and Chapter 4 for the polymer modified surface characterisation).

1.3 Capillary surface modification for DNA analysis

This section highlights the necessity to modify capillary surfaces for the separation of ssDNA and dsDNA of varying lengths, and introduces a classification system for the different types of coatings available. This thesis focuses on various types of surface modification with polymers for charge-based separation in free solution.

1.3.1 Polymer wall coatings

Research has shown that CE analysis of various analytes is improved by capillary surface modification to reduce and manipulate the EOF and surface-analyte interactions [11, 12, 22]. In some of these cases, surface modification is absolutely essential for separation of the analyte. This is particularly true for DNA separations [18, 26, 29–34]. Electrophoretic separation of DNA and RNA requires special attention due to the fact that these molecules have a constant mass-to-charge ratio irrespective of length [11]. Hence, on bare capillaries, all strands migrate together and are unresolved [28, 35, 36]. Therefore, to enable size separation of DNA, the capillary surface needs to be modified. Successful surface modification of a silica capillary slows down or reverses the EOF, manipulates surface/analyte interactions and ultimately alters the mobility of the DNA [17]; thereby improving the resolution (R_s) and repeatability. It is necessary to manipulate the interface between the DNA and the coated surface in order to maximize DNA separation [17, 37]. The most successful separations on modified capillaries are achieved using polymers as sieving media [28, 38-43]. However, this is not always necessary, especially for the separation of short DNA fragments (< ~170 base pairs (bp)). In particular, R_s of short fragments of DNA in free solution has been observed using surface confined polymer coatings [20, 21, 44] without sieving polymers. This is discussed in detail in Section 1.4.1. Surface confined polymer coatings are confined to the surface and do not provide any sieving properties. They are used mainly to suppress the EOF allowing for charge-based separation dependent on the free solution mobility of small polyions. The work described in this thesis utilises these types of coatings by tailoring the surface for specific analyte (ODN) interactions which are able to improve the R_s (see Chapters 5 and 6).

The most common CE application for DNA separation is of forensically relevant DNA (such as short tandem repeats (STRs), restriction fragments and single nucleotide polymorphisms (SNPs), including DNA sequencing), which are typically strands greater than ~100 b (or bp) [1, 33, 43, 45-51]. Consequently, DNA analysis has predominantly focussed on the separation of long fragments of DNA (typically ssDNA). While extensive research has been conducted on the use of coatings for the separation of ssDNA [26, 52-55] and large fragments of dsDNA [26, 52, 53, 56] there is a significant gap in the literature regarding the analysis of

short fragments of dsDNA and ODNs. The aim of this thesis is to develop a simplified method for separation of synthetic ODNs, less than 20 bp, for application to future forensic microfluidic applications and therapeutics.

The advantage of using polymers for surface modification is the ability to tailor the coating for a specific purpose or analyte [52]. CE of DNA has been in development for a few decades leading to an extensive amount of literature available encompassing a number of applications, in particular for forensic analysis (sequencing, genotyping and mutation detection, etc.) [57-64] and, more recently, pharmaceuticals (therapeutic ODNs, drug purity, AS-ODNs, etc.) [65-76]. Due to the fact that CE methods are developed for specific purposes, there are limitations within each method according to the size and structure of DNA each method is capable of separating [52, 77]. For example, Chu *et al.* [52] proposed that due to the difference in the p_{DNA} between dsDNA and ssDNA that the separation media should be tailored. This means that a method developed for the separation of dsDNA may not be able to resolve ssDNA and vice versa. This also applies to the size of the DNA, as migration in polymer matrices is heavily dependent on both the radius of the DNA and the polymer chains. In addition, polymer topology and architecture plays a crucial role in determining CE performance in which the type of separation media used determines the way the DNA migrates and hence the R_s [78]. Again, this is dependent on the size of the DNA fragments being analysed. This is discussed further in Section 1.4.

1.3.2 Surface modification classification

Classification of capillary coatings has become quite complicated with the vast number of polymers available. The simplest way to classify polymer surface coatings is either as covalently attached (static) or physically adsorbed (dynamic) [12]. Static coatings involve permanent covalent bonding between the capillary surface and the coating compound and are non-regenerative. These are subject to degradation from run to run and hence suffer from poor repeatability [17]. Dynamic coatings rely on adsorptive interactions and as such are non-permanent and can easily be regenerated, enhancing the repeatability [12]. The term dynamic can refer to any coating that is physically adsorbed to the capillary wall, but is

more commonly associated with coatings in which a small amount of coating agent is dissolved in the separation buffer [18, 25, 26, 38, 56]. However, this is not essential as some dynamic coatings use post-run regeneration as an alternative to buffer additives [25, 77, 79-81].

For the purpose of this review, polymer coatings have been classified according to Table 1.1. These classifications can overlap or be used simultaneously. The coating classifications are listed in the relative chronological order of scientific development.

Table 1.1. Classification of polymer surface modifications.

Classification	Sub-classification	Description
Static		*A permanent/covalent attachment of polymer to the capillary surface*
	Capillary gel electrophoresis (CGE) [40, 42, 48, 60, 61, 65, 75, 82]	Adapted from slab-gel electrophoresis, CGE preparation involves the covalent attachment and growth of polymer *in-situ* creating a permanent gel within the capillary.
	Covalent surface confined coatings [13, 23, 27, 83-86]	The polymer is covalently attached to the capillary inner surface creating a permanent polymer layer (not necessarily sieving).
Dynamic		*A non- or semi-permanent physical adsorption of polymer onto the capillary surface from a polymer or buffer solution*
	Polymer-buffer sieving solutions [15, 38, 87]	A small amount of polymer is added to the running buffer. This coating often does not suppress the EOF and a polymer pre-coat is used.

Classification	Sub-classification	Description
	Polymer solutions as sieving media [26, 35, 43, 54, 88, 89]	Sieving media involves filling the capillary with polymer solution prior to electrophoresis. The polymer solution is removed and replaced after each run. The polymer acts as a sieving media for the analyte and can also physically adsorb onto the surface. In cases in which the polymer used is incapable of suppressing the EOF, a polymer pre-coat is used. The concentration of the polymer solution used defines the separation mechanism and the analytes in which it is capable of separating.
	Physically adsorbed surface confined coatings [77, 79-81, 88, 90-92]	These types or coating involve flushing the capillary with a polymer solution allowing to polymer to physically adsorb to suppress the EOF and surface/analyte interactions. Polymers used for these coatings generally have a high affinity for the surface and the coating is deemed semi-permanent and is regenerated by flushing with polymer solution between runs. No polymer is added to the run buffer.
Polymer pre-coat		*This can be either static or dynamic (semi-permanent physically adsorbed coating). The aim of the pre-coat is to suppress the EOF to be used in conjunction with dynamic polymer surfaces (either as sieving or polymer-buffer)*

The work described in this thesis is based on a dynamic physically adsorbed surface coating from a dilute copolymer solution. It does not require any surface pre-coat or polymer in the run buffer. Nor does it involve any exhaustive coating preparation or polymerisation *in situ.*

1.4 Separation mechanisms

Separation of DNA is governed by well-established mechanisms. These mechanisms generally depend on the type of coating involved, the M_w and concentration of the polymer used, and the size and shape of the analyte.

Free solution mobility was shown to be governed by the mobility of the analyte based on its charge density and was only applicable to rod-like, non-free draining DNA molecules below the p_{DNA} [16, 93, 94]. In fact, free solution mobility cannot be used to separate larger DNA molecules above the p_{DNA} owing to their free draining behaviour which is related to their conformation [9, 95]. Free solution electrophoresis of DNA requires surface modification to eliminate the EOF and to improve the R_s. A full evaluation of the separation mechanisms described in this thesis demonstrated that the mobility of the short DNA fragments (ODNs) was dependent on the free solution mobility on polymer modified surfaces (strongly related to the theories described in Section 1.2.3), tailored to improve R_s based on ion-pairing. Therefore, this mechanism termed 'free solution mobility' will be discussed first.

1.4.1 Free solution mobility

This thesis concentrates on migration of short strands of dsODNs in free solution. Free solution refers to electrophoresis in the absence of polymer gels or sieving media and describes the mobility of an analyte under applied electric fields [9, 20, 21, 44, 93, 94, 96]. The capillary surface is coated to eliminate/reduce the EOF, so that the mobility will primarily depend on the analyte properties in the chosen buffer. Free solution mobility can be used to determine the physical properties of DNA, such as the dependence of DNA mobility on M_w, sequence, and BGE ionic strength, as well as determining the diffusion coefficients of both ss and ds short fragments of DNA [93].

DNA is classified as a free draining macromolecule with a constant linear charge density and therefore migration in free solution should be independent of M_w [20]. This trend in mobility has been predicted by Ferguson plots (plots of the log of electrophoretic mobility of the analyte versus the polymer concentration) for gel

electrophoresis separations [97]. However, extrapolation of these plots of varying M_w DNA does not lead to free solution, but instead leads to a decrease in μ_{ep} with an increase in DNA size, which is typical for DNA-matrix interactions [20]. However, in the absence of sieving media, free solution mobility is dependent on the effective charge of the analyte (Q) and solvent friction (f), but given that both Q and f are proportional to the number of bases in the molecule this will predict mobilities that are independent of M_w [98]. The expression for free solution mobility (μ_o) is represented by Equation 1.14 [16, 20, 93, 95],

$$\mu_o = Q/f$$

Equation 1.14

where $f = (6\pi\eta_s R_g)$ is the friction coefficient [96]. By substituting f into Equation 1.14 this leads to an expression that is synonymous to Equation 1.6 which describes that free solution electrophoresis of a free draining molecule will be independent of size, which has been observed experimentally [8, 20, 96].

However, Equation 1.14 cannot be used to describe the free solution electrophoresis of short strands of DNA. In free solution, these short molecules have been shown to exhibit M_w dependence during electrophoresis, in which the mobility increases with increasing size [20, 21, 93, 94]. The M_w dependence on the mobility of short DNA fragments is said to be polyelectrolyte in nature [20, 21].

Unfortunately, there are no clear analytical and mathematical expressions to describe the true mobility of short rod-like molecules in free solution. Although there have been several attempts which make various assumptions and contradictions [99], none of these theories can accurately compare to experimental values determined by other free solution methods. This highlights the complexity of this mechanism and how the mobility of short strands of DNA in free solution is highly dependent on the DNA physical properties in the chosen BGE. Nevertheless, the μ_o can easily be determined from experimental values of the DNA t_m, despite the lack of defined complementary theories of the mechanism of the mobility. This can be expressed by Equations 1.11 and 1.12.

1.4.1.1 Molecular mass dependence of mobility in free solution

The key to the M_w independence for free draining molecules is related to their conformation during electrophoresis in free solution. As DNA molecules above their p_{DNA} adopt a random coil conformation, these molecules are treated as spheres and their mobility is described by Equations 1.6 and 1.14. However, due to the rigid rod-like structure of short strands of DNA, they cannot be treated as free draining molecules [8]. From studies of short strands of both ssDNA and dsDNA in free solution, it was observed that mobility increased with increasing M_w. Stellwagen *et al.* [20] studied the free solution mobility in Tris(hydroxymethyl)aminomethane (Tris)-acetate-ethylenediaminetetraacetic acid (TAE) and Tris-borate-EDTA (TBE) buffer showing that μ_o is independent of DNA size between ~400 bp and 48.5 kbp. Interestingly, below ~400 bp the mobility increases with increasing DNA size. The authors also observed higher mobilities in the TBE buffer due to the formation of DNA-borate complexes [20].

As previously stated, due to discrepancies surrounding the theory behind this trend, there are no clear expressions to define this. In spite of this, the one conclusion that can be drawn and agreed upon by the literature is that the mobility is related to a polyelectrolyte effect; how this relates to the M_w trend is still under discussion. In short, the M_w dependence on the mobility of smaller DNA fragments has been attributed to the rod-like conformation of the strands, hydrodynamic coupling between monomer subunits of small polyions [9, 95, 96, 100, 101], and solvent friction caused by interactions with the diffuse counterion atmosphere [21, 96]. Cottet *et al.* [101] developed Scheme 1.1 which introduces a relevant model of the mobility dependence on molecular size and conformation of migrating molecules, in free solution according to the polyelectrolyte migration theory. This model was developed from the migration behaviour of polystyrenesulfonate (PSS) molecules.

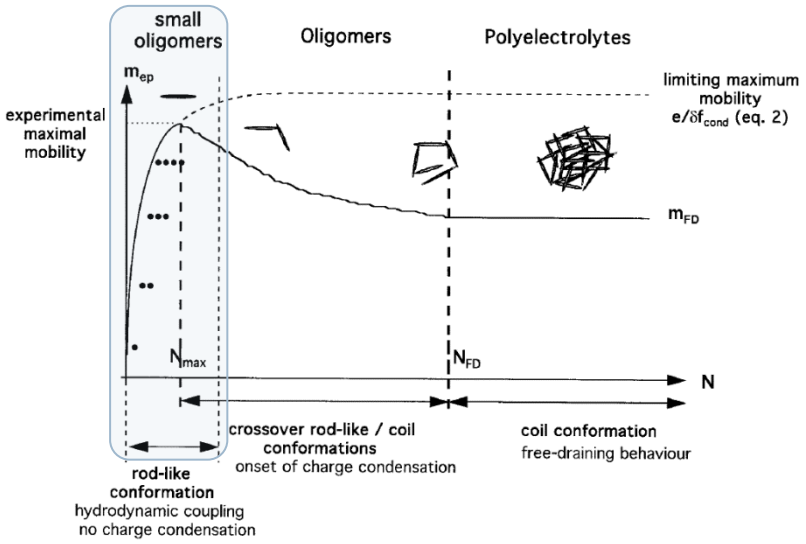

Scheme 1.1. Schematic representation of the mobility of PSS molecules based on size and conformation and how this relates to hydrodynamic coupling and counterion condensation. The highlighted area indicates the region in which the method described in this thesis operates. Adapted from [101].

Scheme 1.1 demonstrates how the mobility of a polyelectrolyte is related to the conformation and size. For small charged rod-like molecules, mobility increases with increasing size until the molecule begins to undergo a conformational change to a coil with the onset of charge condensation. After this, the mobility is size independent as the molecule becomes free draining. The area highlighted by the box in Scheme 1.1 is of significance to this thesis, indicating the region in which the method described herein operates.

1.4.1.1.1 Hydrodynamic coupling and Coulomb interactions

Hydrodynamic coupling can be rationalised by the fact that movement of a molecule during electrophoresis causes disturbances in the solvent which transmits through the fluid and is felt' by the migrating molecule along the chain [9]. The more fluctuations 'felt' by the molecule, the slower the migration; hence hydrodynamic coupling is more prevalent in smaller molecules [101]. There is much discrepancy in the literature to explain how the observed M_w cut-off dependence of the mobility is related to hydrodynamic coupling. It has been proposed that as the M_w of the migrating molecule increases, the hydrodynamic coupling is screened by the friction from the counterion cloud starting to form along the molecule [101]. This suggests that hydrodynamic coupling does not occur at large M_w. However, it has been reported that as the hydrodynamic friction

is related to the diffusion, the lack of hydrodynamic interactions (for larger molecules) would lead to the prediction of mobilities that decrease with increasing M_w, which is not the case experimentally. Therefore, it was proposed that the observed M_w independence on mobility above the p_{DNA} is related to the electrostatic screening of the Coulomb interactions [99, 102]. What this means is that the M_w dependence of DNA below the p_{DNA} is governed by hydrodynamic interactions, and once the p_{DNA} has been exceeded, screening of Coulomb interactions occurs and M_w independence is observed [99, 101, 102].

1.4.1.1.2 Molecular length

In an attempt by Stellwagen *et al.* [20] to explain the M_w dependence by relating the mobility to the molecular length of the DNA, the Einstein equation for the frictional coefficient ($f = kT/D_t$) was substituted into Equation 1.14 to give the Nernst-Einstein equation represented by Equation 1.15 [8, 20],

$$\mu_o = \frac{QD_t}{kT}$$

Equation 1.15

where D_t is the translational diffusion coefficient. Due to the fact that the diffusion coefficient of DNA decreases as $L^{-0.6}$ (where L is the molecular chain length), Equation 1.15 predicts a decrease in mobility with an increase in L [20]. In fact, the opposite is observed experimentally for short DNA fragments, meaning that the mobility dependence on M_w is not directly related to L [20].

1.4.1.1.3 Counterion condensation and rod-like conformation

In a further study by Stellwagen & Stellwagen [8], it was determined that the initial report of μ_o independence in TBE and TAE buffers with ~400 bp dsDNA was inaccurate (see Section 1.4.1.1), and using μ_{ep} markers to increase the accuracy of the study, the authors determined the M_w cut-off to be ~170 bp. The approximate contour length of DNA containing 170 bp is 58 nm (assuming the repeat length is 0.34 nm (refer to Figure 1.4)) which corresponds approximately to the p_{DNA} of dsDNA in the reported buffer conditions. This better corresponds to the transition from rod-like to random coil [8]; therefore the size independent μ_o observed for free draining DNA fragments greater than the p_{DNA} has been attributed to the equal

scaling of the drag (friction) and driving forces with molecular size [9] due to the conformational change from rod-like to random coil [8, 30, 96]. In addition, counterion condensation occurs once the molecule has transformed from rod-like to random coil, effectively reducing the charge of the molecule, resulting in size-independent migration [101].

1.4.1.1.4 Solvent (electrolyte) friction

Electrolyte friction is an additional frictional force induced by the migration of the analyte [20] and is related to interactions of the DNA with the diffuse counterion atmosphere. This is an electrophoretic effect which accounts for the viscous drag created by the migration of the counterions and the DNA in opposite directions [16]. Shorter strands are said to experience solvent friction more than larger strands and this is related to the drag force, owing, again, to the rod-like structure and the fact that the shorter fragments are not free draining [93]. Solvent friction is said to be less effective during transformation from a rod to a free draining coil [44]. This is because the hydrated counterions in the coil interior migrate in the opposite direction to the DNA, making it permeable to the solvent (hence experiencing less friction) [103].

1.4.1.1.5 Charge density

Given that electrophoresis is a factor of the mass and the charge of a molecule, smaller molecules typically have greater mobilities as they are lighter, but in the case of DNA in which charge scales with size, to enable separation in free solution it would seem logical that migration must be a factor of the charge. Acknowledging that free solution electrophoresis results in faster mobilities for larger strands (still below their p_{DNA}), it is evident that this inversed migration is a factor of the electric charge density of the molecule. The significance of charge density upon μ_o of ssDNA was investigated by Dong *et al*. [93]. The authors used constant length (16 b) ODNs modified with phosphoramidate linkages (in place of phosphodiester linkages) to regulate the charge of the oligomer, and compared the μ_o trends to those observed for regular variable length (2 bp - 20 bp) ODNs (shown by Figure 1.6). In agreement with μ_o trends observed for dsDNA, the μ_o increased with increasing charge. However, the rate of increase was greater for the variable length

phosphodiester ODNs, owing primarily to the frictional forces experienced during migration (not to be confused with solvent friction) being greater for the larger variably charged phosphoramidate oligomers. What this shows is that while the mobility is most definitely a factor of the charge, it is also somewhat dependent on the size and the frictional forces it experiences. This study showed that the charge of the oligomers dominated the mobility, and this can be explained by the frictional forces, which are less for smaller molecules meaning that if these forces dominated, the migration order would be from smallest to largest (in terms of size).

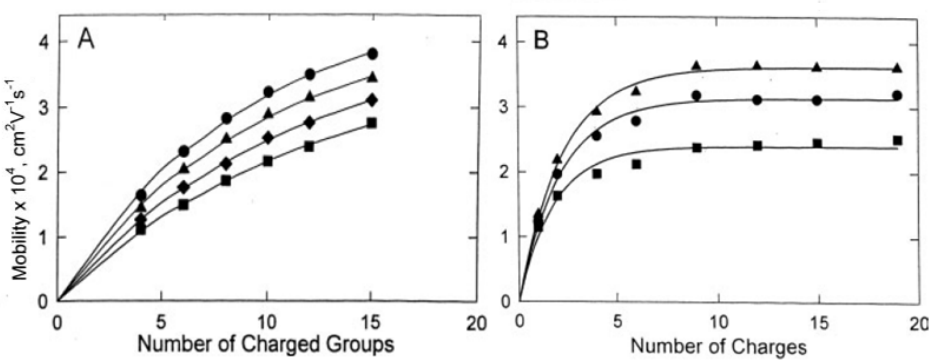

Figure 1.6. Dependence of the μ_{ep} on the number of negatively charged phosphate residues in the oligomer. Variably charged oligomers (A) in 10 mM (●); 20mM (▲); 40mM (♦); and 80 mM (■) cacodylate buffer, pH 6.7. Variable sized oligomers (B) in 25 mM (▲); 50 mM (●); and 200 mM (■) TA buffer, pH 7.4. Adapted from [93].

In summary, and significant to the work described herein, the rod-like conformation of the shorter strands means that counterion condensation does not occur and that μ_o increases with increasing M_w due to screening of the hydrodynamic coupling between subunits [101]. In addition, shorter strands are said to experience solvent friction more than larger strands owing, again, to the rod-like structure and the fact that the shorter fragments are non-free draining [93].

1.4.1.2 Sequence dependent mobilities

The μ_o has been observed to be sequence dependent for both ssDNA and dsDNA molecules with preferential counterion ion binding to the A-tract [8, 103]. An A-tract is represented by consecutive adenine residues in a DNA helix, and bending of the helix can be observed if it contains four or more of these A-tracts. This bending can contribute to slower μ_o of these fragments, but for this to occur, more than five A-tracts need to be present [103]. Counterion binding to the DNA also results in slower observed mobilities, and these counterions have been shown to

preferentially bind to DNA molecules containing A-tracts [103]. Stellwagen *et al.* [103] measured the mobility of 20 bp DNA oligomers with and without A-tracts and found that the BGE (TAE and Tris-acetate (TA)) counterions preferentially bind to molecules containing A-tracts, and in addition, binding was most prevalent for the sequences that contained two runs of AAATTT. Whether or not there is a sequence dependence observed for random DNA sequences has not yet been investigated. Therefore this thesis investigates the random sequence dependence of ssODNs (Section 5.3.1) and dsODNs (Sections 6.2.1.3 and 6.3.1) in free solution.

1.4.1.3 Effect of conductivity and ionic strength on mobility

The μ_o was predicted by Manning [104] to decrease linearly with the logarithm of ionic strength of the BGE (achieved by increasing the concentration of the BGE) [93] and this has been shown experimentally [16, 105]. However, by maintaining a constant BGE concentration and altering the conductivity by adding various amounts of salt, the change in mobility is quite different [105].

Stellwagen & Stellwagen [105] investigated the conductivity and ionic strength effects on the differential mobilities of a high M_w dsDNA fragment (linear pUC19, 2686 bp) and a 20 bp oligomer (dsA5) in TAE buffer with and without the addition of NaCl. Increasing the concentration of the TAE buffer resulted in longer t_m of both fragments. Interestingly, the peak shapes were relatively Gaussian and the t_m did not change if the fragments were injected separately or in a mixture. This indicated that there were no DNA-DNA or DNA-buffer interactions occurring and the $Tris^+$ ions behaved as simple phosphate counterions. However, decreasing the TAE concentration to below 5 mM promoted DNA-buffer interactions only for the pUC19 (indicated by distorted peak shapes) suggesting these interactions were size-dependent. Conversely, the t_m for individual injections of each fragment did not correspond to the t_m when injected as a mixture, indicating that there were in fact DNA-DNA interactions occurring at low ionic strengths. The dsA5 fragment began to experience DNA-buffer interactions only when the BGE concentration was below 1 mM [105].

Upon addition of NaCl from 2 mM to 10 mM into the BGE (18 mM TAE), the μ_o initially decreased then became independent of salt concentration and finally decreased after the addition of ~50 mM NaCl. The peak shapes remained Gaussian for both fragments and the mobility trends for both fragments were very similar indicating the mobility patterns were size-independent. The independence of salt concentration observed between 10 mM and 50 mM was attributed to the exchange of Na^+ ions for $Tris^+$ ions in the counterion cloud around the DNA molecule. The dependence of DNA μ_o on the conductivity of the solution is shown in Figure 1.7.

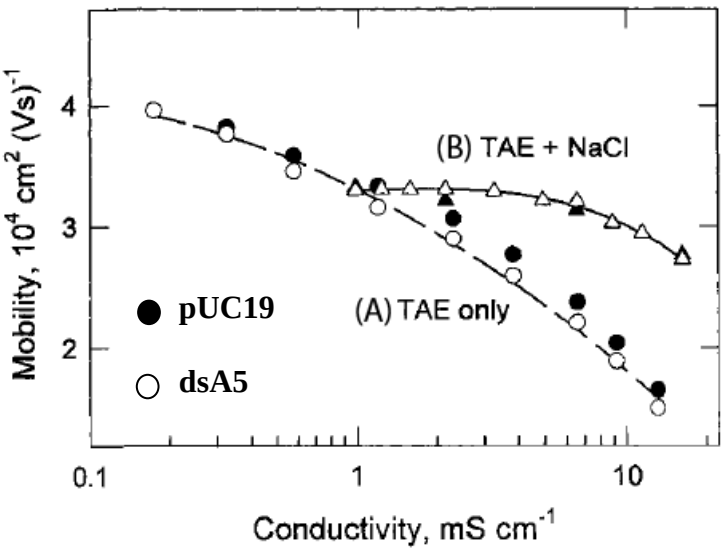

Figure 1.7. Comparison of free solution mobility of pUC19 and dsA5 in TAE buffer at varying concentrations, and 18 mM TAE buffer containing varying amounts of NaCl [105].

The μ_o of the ds fragments were compared to their corresponding ss fragments. The mobility of the sspUC19 was reduced in comparison to the dspUC19; however, the mobilities of the ssA5 fragments were no different to those determined for the dsA5 fragment. This indicates a size-dependence on the differential mobility of ss and ds fragments only above a certain M_w [105].

In general, for electrophoresis, the BGE concentration is much greater than the DNA concentration, resulting in an engulfment of the negatively charged DNA by a diffuse counterion atmosphere which effectively modulates (or shields) interactions with other charged molecules in the solution. In order to further investigate these electrostatic shielding effects of the DNA, Stellwagen & Stellwagen [16] conducted a similar study using diethylmalonate (DM) buffer and Tris-acetate buffers with or without the addition of NaCl or TrisCl to determine the

free solution mobility of 20 bp dsDNA. The authors again observed a decrease in mobility with an increase in buffer concentration for the DM buffer. Addition of either NaCl or TrisCl also resulted in a decrease in mobility with increasing ionic strength. The observed trend was linear if the counterion in the salt was the same as the counterion in the buffer (i.e., NaCl added to NaDM or TrisCl added to TrisDM), but a non-linear trend was observed when the counterion of the salt was different to the buffer counterion. In the former case, the mobility dependence on ionic strength is attributed to the electrostatic shielding of the DNA by the ion cloud. In the latter case the mobility decreases either more rapidly than expected or slower than expected, depending on whether the limiting equivalent conductivity of the salt counterion is less or greater than the limiting equivalent conductivity of the BGE counterion [16].

The work described in this thesis investigates the ionic strength effects on the R_s of synthetic ODN and PS-ODN mixtures by increasing the buffer counterion concentration and by the addition of ionic salts (see Sections 6.3.2 and 7.3.2).

1.4.2 Other models

The most commonly referred to mechanisms for the use of sieving media are the Ogston [34, 95-98] and reptation models (including the biased reptation model (BRM) and biased reptation with fluctuations (BRF)) [34, 97, 99-101], which govern the separation of ssDNA and dsDNA fragments in polymer gels. More recently, due to the emergence of polymer solutions and dynamic coatings, some relatively new models have been proposed, such as constraint-release (CR) [34, 98, 112-115], transient entanglement coupling (TEC) [7, 29, 35, 115, 116], and a size-exclusion capillary electrophoresis (SECE) based mechanism [37]. These will be discussed in turn in the following and are grouped as either gel electrophoresis mechanisms (Section 1.4.3) or mechanisms in polymer solutions (Section 1.4.5).

To fully understand the migration of DNA in a given system, it is necessary to first evaluate the possible separation mechanisms and what governs each one. The Ogston model (see Section 1.4.3.2) was proven to be suitable for describing the migration of spherical particles smaller than the pore size of the gel and cannot

account for larger elongated molecules [29]. The reptation models (Section 1.4.3.3) were therefore developed to describe the migration of these larger molecules [34, 110, 111]. Ferguson plots (Section 1.4.3.1) can be used to differentiate between the two mechanisms based on the linearity of a plot of the log of electrophoretic mobility of the analyte versus the polymer concentration [97, 117].

It was found that separations in entangled (semi-dilute) polymer solutions can be described by the CR model (see Section 1.4.5.3.1), which is an adaptation of the reptation models. CR was found to only be applicable to the migration of larger DNA fragments through a network of smaller entangled polymer chains [114]. Separations in dilute/ultra-dilute and low M_w polymer solutions were revealed to be governed by TEC (Section 1.4.5.4.1) and SECE (Section 1.4.5.4.2), in which TEC involves entanglement of the DNA with the polymer chains, dependent on the ratio of the DNA and the polymer chain length [35]. All these mechanisms describe size-based separation of DNA with a migration order of shortest to longest, except the SECE based mechanism which exhibits migration in the reverse order using low M_w polymer solutions as sieving media for the separation of short fragments of dsDNA [37].

1.4.3 Gel electrophoresis mechanisms

The more common theories/mechanisms describing the separation of DNA using electrophoresis are based around the use of gel electrophoresis [29]. This is due to the extensive use of gels (either slab-gel or CGE) for many decades. Consequently, although these mechanisms are the most understood, they have limitations when applied to different polymer systems, such as polymer solutions (in particular dilute polymer solutions). Gel separations are based on the theory that the gel forms a network of pores for the DNA to be driven through by electrophoresis and the mechanism of migration is described by either the Ogston or reptation models [4, 29, 30, 34, 98, 107, 109-112, 118-120]. The following will discuss each of the models in detail.

1.4.3.1 Ferguson plots

Ferguson plots were developed to explain the migration of an analyte in a polymer network. These plots can be used to differentiate between the migration mechanism taking place (Ogston sieving or reptation), as the application of these models is related to the analyte size, and the size is related to the orientation. By plotting the log of electrophoretic mobility of the analyte versus the polymer gel concentration (Ferguson plot), the orientation of the analyte can be determined during electrophoresis [97, 120]. A linear plot is representative of migration as spherical particles (denoting Ogston sieving of small particles) while a non-linear plot is representative of migration as non-spherical particles (denoting reptation of larger particles). Thus, deviation from linearity in a single plot can give the M_w at which the migration changes from Ogston sieving to reptation. Analyte orientation (and radius of gyration, R_g) is therefore important in migration of particles through gel pores of a given size, as it will ultimately determine the mechanism of separation.

1.4.3.2 Ogston model

The Ogston sieving model was the first mechanism proposed for the migration of flexible 'polymers' using gel electrophoresis [98]. This model was based on a mathematical theory developed by Ogston [107] which defines the distribution of spaces within a random network of chains and the penetration of these spaces by an object with a smaller radius. The Ogston model therefore describes the movement of an analyte as a globular object within a randomly distributed porous network with an R_g smaller than the pore size (ξ_b) (also referred to as mesh size) [98]. This model predicts that smaller analytes will migrate faster as they can access a larger number of pores, whereas analytes with a larger R_g would be unable to permeate the network [29, 98, 120]. According to Chrambach & Rodbard [109, 121], the DNA molecule diffuses across the surface searching for pores large enough to pass through, implying that electrophoretic mobility is proportional to the volume of pores which allow passage (shown by Scheme 1.2).

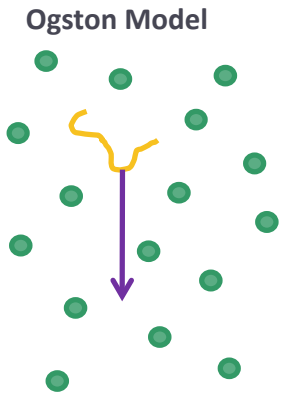

Scheme 1.2. DNA migration in polymer matrices obeying the Ogston model where $R_g < \xi_b$. Adapted from [34, 98, 120].

Ogston [107] derived a simple expression to describe the migration of a particle based on its ability to penetrate a gel network and the free rotation of the particle within this network, defined by Equation 1.16,

$$P_{D>R_g} = exp - \left(2\pi v_c L r^2 + \frac{4\pi}{3} v_c {R_g}^3\right)$$

Equation 1.16

where D is the tangential distance of chain or the chain end from the origin, R_g is the migrating particle radius, and v_c is the average number of chain centres/cm^3. The Ogston model has been successfully applied to smaller DNA molecules under low applied voltages [122] using starch [97] and polyacrylamide (PAM) [109, 123] networks. Although it cannot explain the non-linear curves observed in the plots for some larger and/or non-spherical particles, as it only dealt with the distribution of spaces in a suspension available to a spherical molecule [109] rather than the migration of the molecule through these spaces. Therefore in 1970, Rodbard & Chrambach [109] developed the extended Ogston model (Equation 1.17) to explain deviations from linearity in Ferguson plots. This model takes into account the molecular geometry and the retardation coefficients ($K_R = K(R_p + R_g)^2$) which are characteristic to the migrating species through a specific polymer network, and can be derived from the slope of a Ferguson plot [109, 121, 123],

$$\mu_{ep} = \mu_o exp\left[-Kc\left(R_p + R_g\right)^2\right]$$

Equation 1.17

where μ_o is the free solution mobility, K is the constant of proportionality, and R_p is the radius of the polymer chains [34, 120].

Serwer [124] investigated agarose properties, and in particular the concave shape of the Ferguson plot resulting from deformation of the larger random coils of dsDNA during electrophoresis. The aim was to perform a quantitative study on the sieving of non-spherical particles by adapting the extended Ogston model. Tietz & Chrambach [106, 117] also applied this model to estimate the chain dynamics of agarose gels for the separation of proteins and viruses, explaining that migration of random shaped particles through a random chain network can be treated probabilistically in terms of a 'random space-walk'. Tietz [108] then went on to explain the behaviour of larger fragments of DNA during gel electrophoresis using the extended Ogston model. The authors applied a mathematical computational model including local retardation coefficients to account for the effect of the gel concentration on the radius of the DNA and gel chains.

The limitation of the Ogston model lies within the assumption that the DNA migrates as a spherical particle and does not change shape to fit through the smaller pores. It therefore cannot account for the observed migration of larger fragments with radii larger than the pore size [29]. The reptation model was developed for such cases in which the radius of the particle exceeds the pore size (discussed in Section 1.4.3.3).

1.4.3.3 Reptation

Research by de Gennes [110] first introduced the idea of reptation of polymer chains in fixed gels back in 1971 during the time that the Ogston model was in development. It was not until 1982 that this model was applied to electrophoresis of biopolymers by Lerman & Frisch [125]. The reptation model accounts for the saturation of mobility of long DNA at a finite value independent of M_w, contrary to the inaccurate prediction by the Ogston model that the mobility will decrease exponentially [98]. The term reptation (adapted from the reptile-like motion) was developed to explain the migration of a thin flexible molecule by threading through polymer gel pores head on [34, 98, 111, 120] in which the pores vary depending on the gel structure. In the case of a rigid mesh, these pores resemble a tube for the DNA to travel through; whereas the pores are better represented by globules (also termed blobs, but for consistency, these will be referred to as globules) in a flexible

network [34]. Experimental data shows that in cases where $R_g > \xi_b$, the μ_{rep} decays inversely with M_w before tapering off at a fixed value defined by the electric field according to Equation 1.18 [98],

$$\mu_{rep} \sim \frac{N}{N^2} = \frac{1}{N}$$

Equation 1.18

where N is the molecular length [120].

1.4.3.3.1 Biased reptation model

The model described by Equation 1.18 is very simple and does not take into account the applied field. However, it is evident that large electric fields influence the migration of DNA by changing the DNA configuration and this assumption is no longer valid. Therefore, the BRM was developed to describe this behaviour and is most easily represented by Equation 1.19 [120, 126],

$$\frac{\mu_{BRM}}{\mu_o} \approx \frac{1}{3}\left(\frac{1}{N} + \frac{\varepsilon^2}{3}\right)$$

Equation 1.19

where ε is the reduced electric field [4, 120]. It is evident from Equation 1.19 that an increase in N or E will cause the dependence of electrophoretic mobility on the M_w to decrease, meaning that separation will not occur after a determined M_w. This has been proven experimentally using both agarose [39, 116-118] and PAM [39, 130] gels. Fangman [129] has shown that DNA fragments smaller than ~40 kbp undergo size separation during gel electrophoresis using agarose; although separation of larger fragments required pulsed-electric fields. Lumpkin *et al.* [126] used the reptation model to explain this behaviour.

Application of an electric field causes the strands to become elongated (aligned along the electric field [111]), and the higher the field strength, the more elongated the strand becomes, until it resembles a rod [29, 120]. It is at this point in which all strands essentially behave the same and hence migrate together. Scheme 1.3 shows the migration of DNA via reptation without orientation (small molecules and/or low applied field strength) and biased reptation with orientation (larger molecules and/or high applied field strength).

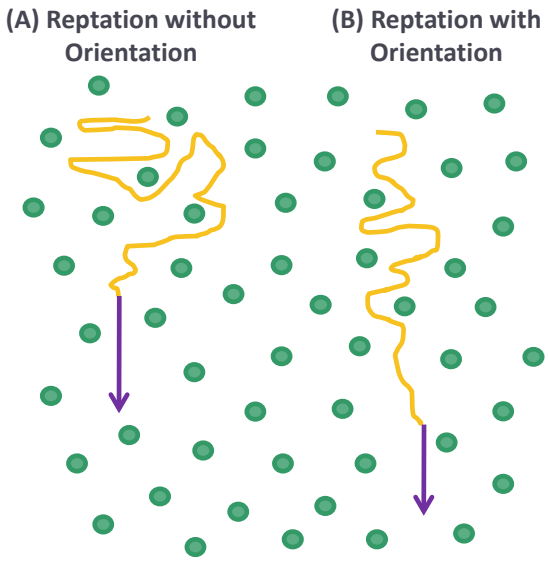

Scheme 1.3. DNA migration in polymer matrices where $R_g > \xi_b$ and obeying reptation without orientation (A) and reptation with orientation (B). Adapted from [34, 98].

In summary, the basic reptation model describes the migration of DNA strands without orientation at low fields, whereas the BRM describes the migration under electric fields that are high enough to cause orientation (elongation) of the strands typically greater than 100 V cm^{-1} - 300 V cm^{-1} [34] and can also account for separation of large fragments of DNA (larger than 40 kbp) [29].

1.4.3.3.2 Biased reptation with fluctuations

Size separation is best achieved using reptation without orientation in which the pore size is independent of polymer M_w. Both these models make the assumption that the DNA chain does not change its length as it migrates [34], however, studies using fluorescence microscopy observed changes in the end-to-end distance of individual DNA strands during electrophoretic migration in agarose gels [131, 132]. Gurrieri *et al.* [132] first captured the migration of a large dsDNA fragment (164 kbp) during conventional gel electrophoresis with a consistent applied field of 10 V cm^{-1} (depicted in Figure 1.8).

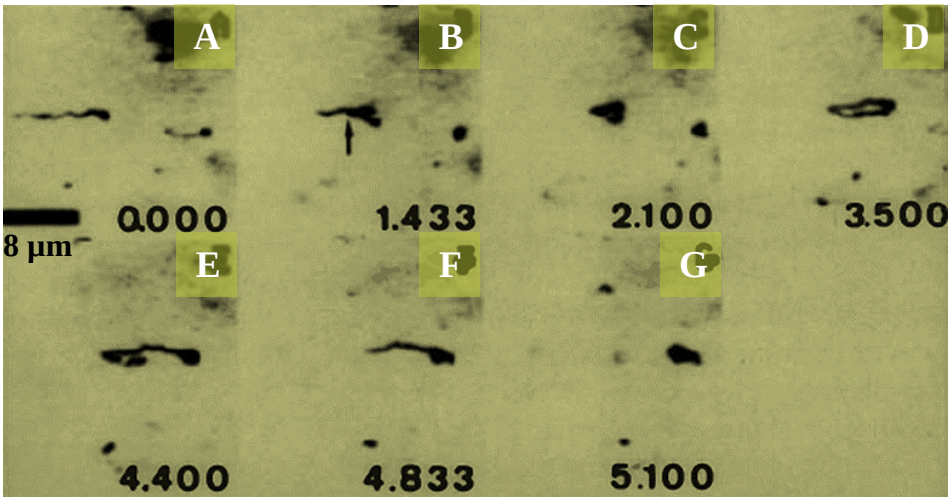

Figure 1.8. Migration of a dsDNA fragment (from left to right) through a thin agarose gel showing reptation and end-to-end conformational changes, captured by fluorescence microscopy at random time periods (numbers are in seconds). The partial extension of the DNA fragment is shown to bunch at the leading end (A). When the fragment encounters an obstacle, it folds onto itself (B) and the trailing end overshoots the leading end (becomes U-shaped) (C) until it bunches up and becomes the leading end (D). This end assists in the fragment moving around the obstacle (E and F) after which it collapses into a globule (G). Adapted from [132].

Duke *et al.* [111] introduced the concept of BRF which takes into account the changes in DNA chain length during migration. As previously stated, the DNA snakes through 'tubes' created by pores in the gel, thus 'feeling' its way through the matrix. As the DNA strands continually probe in and out of the tube looking for new pathways, tube length fluctuations occur (shown by Scheme 1.4) [111].

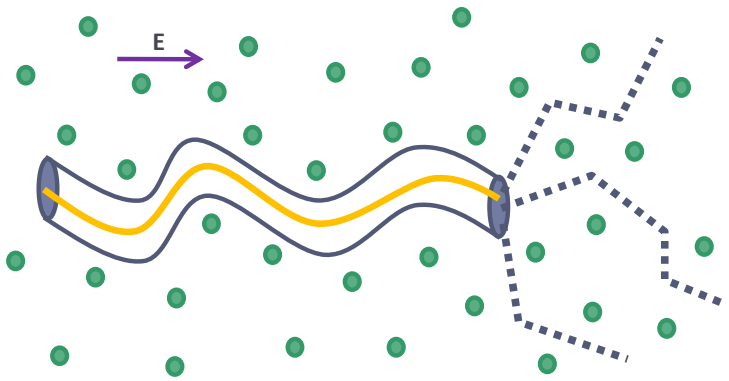

Scheme 1.4. DNA migration through a gel obeying the BRF model. The dashed lines represent the alternative confirmations of the fluctuating chain end sections. *E* refers to the electric field. Adapted from [111].

The BRF model can be used to describe the migration of strands with Kuhn length (gyration radius) smaller or greater than the pore size. When $R_g < \xi_b$ Equation 1.20 can be used to describe the mobility [34],

$$\frac{\mu_{\mathrm{BRF}}}{\mu_{\mathrm{o}}} \cong \bar{\xi}^2 \left[\left(\frac{1}{N_{\mathrm{k}}}\right) + \varepsilon_{\mathrm{o}}\bar{\xi}\right]$$

Equation 1.20

where $\bar{\xi} = \xi_{\mathrm{b}}/b$ (mesh size normalised to the DNA Kuhn length) and $\varepsilon_{\mathrm{o}} = E\, q_{\mathrm{k}}\, b/k\, T$ (electric potential energy per Kuhn length scaled to thermal energy). Equation 1.21 describes the mobility when $R_{\mathrm{g}} > \xi_{\mathrm{b}}$ [34],

$$\frac{\mu_{\mathrm{BRF}}}{\mu_{\mathrm{o}}} = \frac{b}{\xi_{\mathrm{b}}}\frac{1}{3N_{\mathrm{bl}}} = \frac{1}{3N_{\mathrm{k}}}$$

Equation 1.21

where $N_{\mathrm{bl}} = N_{\mathrm{k}}\,(b/\xi_{\mathrm{b}})$ (number of globules per chain), and b is the Kuhn length [98]. This relationship is experimentally relevant for dsDNA migration in PAM gels and has also been applied to low mesh size entangled polymer solutions [98]. It is important to note that this model breaks down in the case of tight gels and/or high field strengths as fluctuations cannot occur, and migration is again represented by the BRM (see Equation 1.19) [34].

1.4.4 Application of gel electrophoresis models to CE in polymer solutions

There has been much debate on the separation mechanisms surrounding polymer solutions, and whether the traditional Ogston and reptation models are applicable to these systems. This heavily depends on the type of polymer solution employed. Indeed, it was initially believed that sieving gels were an absolute necessity for the separation of DNA fragments. That was until 1989 when Zhu *et al.* [133] adapted a non-gel electrophoretic method, initially developed by Bode [134], which used non-crosslinked polymer solutions for the separation of proteins, peptides and DNA. The capillary was first pre-coated by the covalent attachment of linear polyacrylamide (LPA) to reduce EOF and analyte adsorption. Separation of dsDNA fragments was achieved in a dynamic solution by dissolving either methylcellulose (MC) (0.5 % w/v) or hydroxypropylmethylcellulose (HMC) (0.5 % w/v) polymer in the run buffer. The separation mechanism is based upon molecular sieving [133].

Early on, a few theories emerged to explain the migration in polymer solutions to be similar to traditional models in which the polymer forms a porous network in

solution [120, 135]. This is indeed the case if the polymer concentrations are high enough to promote highly entangled solutions which behave the same as physical gels (involving immobile polymer chains) [98]. Other researchers [33, 51] have offered some interesting theories to describe migration involving DNA-polymer interactions in solution but with limited evidence. A study by Grossman & Soane [120] proposed that in order to achieve separation, the polymer chains need to be entangled in order to act as a sieving media for separation of DNA fragments (118 - 1353 bp). The authors used Ferguson plots to apply the Ogston model to the separation of DNA fragments in entangled polymer solutions containing hydroxyethylcellulose (HEC). These plots exhibited a linear range from 0.1 - 0.4 % HEC for 118 - 310 bp indicating Ogston sieving for the smaller strands, but deviated from linearity between 603 bp and 1353 bp indicating a transition to reptation [120].

The most promising adaptation of the BRM for the separation of DNA fragments in non-crosslinked moderately entangled polymer solutions was proposed by Daoud & de Gennes [136], then revisited and remodelled by Viovy *et al.* [34, 113], and is termed CR. This will be discussed in more detail in Section 1.4.5.3.1. In brief, this model describes the dynamic nature of the non-crosslinked polymer network by taking into account the tube dimension fluctuations due to mobile (non-static) polymer chains [34].

The Ogston and reptation models can only successfully describe/predict the mobility of an analyte in highly entangled solutions in which migration of the polymer chains is not possible, and therefore cannot be applied to dilute polymer solutions which are governed by entirely different mechanisms and these will be discussed further in Section 1.4.5.4.

1.4.5 Mechanisms in polymer solutions

In order to understand separation mechanisms in dynamic polymer solutions, it is necessary to first characterise them based on some key parameters. Separation theories need to take into account the overlap (or entanglement) threshold determined by the polymer concentration and/or mass, and the solution viscosity

[98, 120]. These will govern the mechanism involved in the separation. This section describes how the overlap concentration defines the polymer dimensions in solution and how this affects the migration of dsDNA and ssDNA of varying lengths. In addition, it introduces some relatively new separation mechanisms which take into account mobile polymer chains (in comparison to static chains for CGE).

1.4.5.1 Overlap threshold concentration (Φ or c*)*

The overlap threshold concentration (sometimes referred to as the entanglement threshold concentration) defines the concentration at which the polymer chains begin to interact with each other. In some literature it is denoted by ϕ* where ϕ refers to the polymer mass fraction [50, 120]. In other literature it is represented by *c** where *c* is the polymer concentration [34, 98]. Both symbols are referring to the same thing, therefore to be consistent, this review will refer to the overlap (threshold) concentration as being *c**. The *c** can be easily determined from a log-log plot of solution viscosity (η) versus *c* in which the *c** is represented by a deviation from linearity [50, 120]. Braun *et al.* [50] applied this experimental method to determine the *c** to be 0.027 % (w/w), 0.85 % (w/w) and 1.2 % (w/w) for HEC (2 100 000 g mol^{-1}), polyvinylpyrrolidone (PVP) (M_w not specified) and star-polyethyleneoxide (star-PEO) (710 000 g mol^{-1}), respectively. Grossman *et al.* [120] also used this relationship to determine the *c** for HEC (191 000 g mol^{-1}) to be between 0.29 % (w/w) and 0.40 % (w/w) (shown by Figure 1.9).

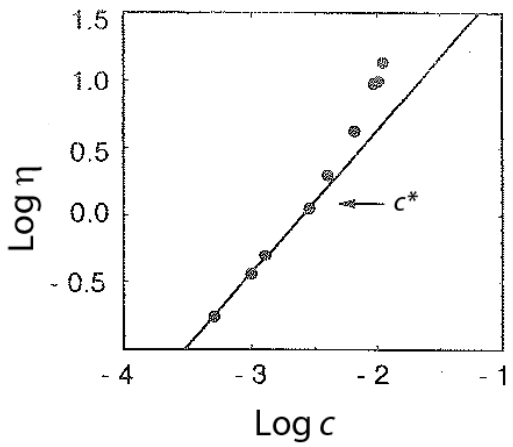

Figure 1.9. Log-log plot of solution viscosity versus PVP concentration to determine *c** (point of deviation away from linearity). Adapted from [120].

After the c^* was reached, there was a significant increase in the slope represented by the promotion of polymer entanglement [29]. The experimental value was compared to a theoretical value determined by Equation 1.22, initially developed by de Gennes [110],

$$c^* \approx N_{\mathrm{p}}{}^{-0.8}$$

Equation 1.22

where N_{p} refers to the number of polymer molecules and can be determined by first determining the M_{w} by a rearrangement of the Mark-Houwink-Sakurada equation represented by Equation 1.23 [120],

$$[\eta] = K^*(M_{\mathrm{w}})^{\alpha_{\mathrm{MHS}}}$$

Equation 1.23

where $[\eta]$ is the intrinsic viscosity, M_{w} refers to that of the polymer, and K^* and α_{MHS} are constants characteristic of a given polymer/solvent system. Equation 1.23 predicts a c^* of 0.39 % (w/w) for HEC, which is in accordance with the experimentally derived value [120]. c^* can also be represented by Equation 1.24 derived by Broseta *et al.* [137],

$$c^* \cong \frac{M_{\mathrm{w}}/N_{\mathrm{A}}}{\frac{4}{3}\pi R_{\mathrm{p}}^3}$$

Equation 1.24

where N_{A} is Avogadro's number. Equation 1.24 takes into account well-defined measurable quantities by universal prefactors; in other words, it becomes independent of the polymer being considered [34] unlike Equation 1.23 which is dependent on the polymer/solvent system. Viovy *et al.* [34] applied Equation 1.23 to theoretically determine c^* for HEC (191 000 g mol^{-1}) under the same concentration conditions as applied by Grossman *et al.* [120].

The discovery of c^* has given rise to three distinctive regimes to describe the polymer conformation in solution [98]. The first regime is referred to as 'dilute', in which the polymer concentration is less than the overlap concentration ($c < c^*$), and describes the polymer chains self-coiling to form globular structures that are hydrodynamically separated from each other. As the polymer concentration increases, the frequency of collisions between polymer coils also increases until the overlap concentration is reached ($c = c^*$) and the polymer coils begin to aggregate.

The 'semi-dilute' regime describes situations in which the polymer concentration exceeds the overlap concentration ($c > c^*$), where the polymer chains are said to be entangled and form a dynamic network [34, 50, 98, 120]. The dilute and semi-dilute regimes are represented schematically in Scheme 1.5A and C, respectively; and Scheme 1.5B represents the overlap between these two regimes ($c = c^*$). The third regime is 'concentrated', which has limited or no application to CE using polymer solutions [98] and therefore is not discussed.

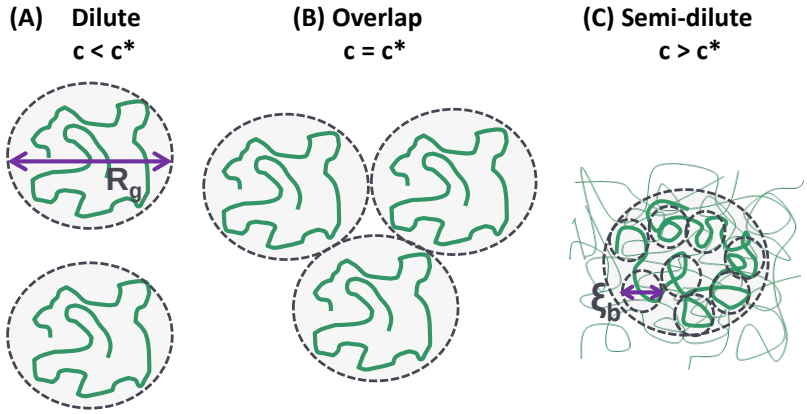

Scheme 1.5. Schematic representation of polymer conformations in dilute solutions (A), at the overlap concentration (B), and in semi-dilute solutions (C). Adapted from [34, 98].

1.4.5.2 Evaluation of polymer dimensions

It is necessary when dealing with polymer solutions to evaluate the polymer dimensions which will vary upon changes in concentration. Dilute polymer solutions are treated as a single chain and hence the polymer dimensions depend on the R_p of the polymer; whereas semi-dilute polymer solutions are entangled, and hence the dimensions rely on the polymer screening length (ξ).

1.4.5.2.1 Dilute (and ultra-dilute) regime

Due to the fact that in the dilute regime the polymer chains are hydrodynamically separated, the polymer dimensions are theoretically defined by the square-average R_p of a single chain according to the Kratky-Porod formula described by Equation 1.25 [98],

$$R_p = \langle R_p^2 \rangle^{1/2} = \left[\frac{1}{12} b^2 (2N_k - 1 + exp2N_k) \right]^{1/2}$$

Equation 1.25

where N_k is the total number of Kuhn segments and b is the Kuhn length of the polymer equal to $2p_{DNA}$. The R_p can also be derived experimentally for single chain (dilute) polymer solutions by determining the intrinsic viscosity ($[\eta]$), and applying Equation 1.26 [98],

$$[\eta] = \frac{\eta - \eta_s}{\eta_s c} \approx \frac{6.2R_p^3}{M_w/N_A}$$

Equation 1.26

where η is the polymer solution viscosity and η_s is the solvent viscosity (without the solute). The intrinsic viscosity is a measure of the contribution of the polymer to the solution viscosity. Therefore, by rearranging Equation 1.26 for R_p^3 and substituting into Equation 1.24, the polymer overlap concentration, c^* can be simply defined by Equation 1.27 [98].

$$c^* = 1.5[\eta]^{-1}$$

Equation 1.27

Equations 1.26 and 1.27 are of particular interest as they are used in this thesis to determine $[\eta]$ and c^* of the polymer solutions synthesised for surface modification of fused-silica capillaries (see Section 4.2).

1.4.5.2.2 Semi-dilute regime

In the case of semi-dilute solutions, where the chains are entangled, the polymer dimensions are defined by ξ which represents the average distance between polymer chains [34, 98], and is expressed by Equation 1.28.

$$\xi = 0.50\, R_p \left(\frac{c}{c^*}\right)^{-3/4}$$

Equation 1.28

In entangled solutions, ξ is related to ξ_b by involving successive independent polymer chains, known as globules [98] and is represented by Equation 1.29.

$$\xi_b = 2.86\xi = 1.43\, R_p \left(\frac{c}{c^*}\right)^{-3/4}$$

Equation 1.29

However, in scales larger than ξ_b, entangled polymer chains are better represented by the number of monomers per globule (g) shown by Equation 1.30 [98].

$$g = c\xi_b^3 \sim \frac{M_w}{N_A}\left(\frac{c}{c^*}\right)^{-5/4}$$

Equation 1.30

Once *c** has been exceeded, the extent of polymer entanglement increases with increasing concentration, forming a tighter mesh with smaller sieving pores [138]. When applied to DNA fragment analysis, this means better separation performance, particularly for short strands; with the detriment of slower t_m due to an increase in DNA-polymer interactions [138]. For highly entangled high M_w polymer solutions, the polymer network is relatively static, hence the mechanism can be explained by the reptation (BRF) model (refer to Section 1.4.3.3.2). However, this is not the case for moderately entangled polymer solutions, which are assumed to be somewhat mobile during electrophoresis [98].

1.4.5.3 Mechanisms in entangled solutions

Entangled polymer solutions (semi-dilute) deal with polymer concentrations above the *c**. For concentrations well above the *c** (termed concentrated polymer solutions), the polymer in solution becomes immobile, and the migration of the DNA can simply be defined by the BRF (refer to Section 1.4.3.3.2). However, for semi-dilute polymer solutions above the *c**, the migration is defined by CR mechanism (refer to Section 1.4.5.3.1) which describes how the reptation of the polymer chains affects the reptation of the migrating DNA.

1.4.5.3.1 Constraint release

The BRF model (refer to Section 1.4.3.3.2) describes the migration of the DNA along 'tubes' formed by pores in the polymer in which the DNA can change its length by probing in and out of the tube looking for new paths. CR is an extension of this reptation model which takes into account fluctuations of the polymer tube, meaning that the polymer molecules themselves also reptate which is said to release the constraints that cause DNA to reptate [30]. A study on the reptation of polymer chains in fixed obstacles by de Gennes [110] introduced the concept of the tube having a finite lifetime due to Brownian reptative motion of all chains, meaning that the reptation model alone is not suitable for describing migration in entangled polymer solutions. This led to the theory of tube renewal by Daoud & de Gennes [136] which was later on termed CR [139]. The CR process is represented by Scheme 1.6.

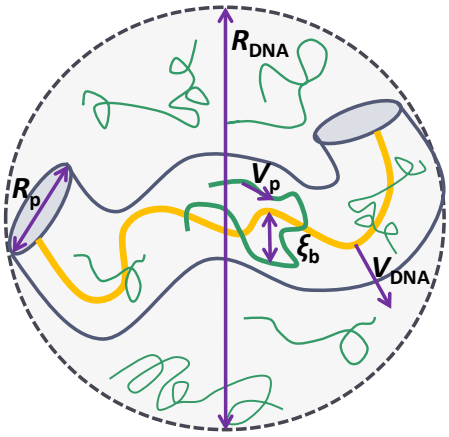

Scheme 1.6. Schematic representation of CR. The DNA chain is surrounded by the 'tube' formed by the polymer globules. V_p is the curvilinear velocity of the reptating polymer chains, V_{DNA} is the velocity of the reptating DNA, R_{DNA} is the radius of the DNA. Adapted from [34, 98].

Preliminary CR theory dealt with the relaxation of chains via reptation within the tube, or motion of the tube itself, otherwise known as Rouse motion. Relaxation was said to be dependent on the reptation of the DNA chain in comparison to the Rouse motion of the tube. Therefore, if the speed of tube renewal is slower than the reptative motion of the DNA, then CR is said to be negligible. This means that CR is dominant in moderately entangled polymers in which the analyte is large and surrounded by smaller polymer chains [34, 98]. Knowing this, the revised model made the assumption that CR is relevant only to large strands of DNA (N_k > 1) migrating in entangled (semi-dilute) polymer solutions. Another important assumption made by this model, is that the DNA is stiff in comparison to the surrounding polymer chains and therefore the DNA dynamics are treated, according to de Gennes [110], as a 'stiff molecule in an entangled melt' [34]. The most significant assumption for this model is that reptation and CR are independent processes and the total CR mobility ($\mu_{CR(tot)}$) is described by Equation 1.31 [34, 98, 112],

$$\mu_{CR(tot)} \cong \mu_{BRF} + \mu_{CR}$$

Equation 1.31

where μ_{BRF} is determined from the BRF model. The mobility contribution from CR (μ_{CR}) can be defined by Equation 1.32 [34, 98, 112].

$$\frac{\mu_{CR}}{\mu_o} = \left(\frac{\xi_b}{R_p}\right)^5 \left(\frac{\xi_b}{b}\right)$$

Equation 1.32

CR describes a migration mechanism that is size independent [34], which means that according to Equation 1.31 size dependent mobility will therefore also depend on the reptation. The assumption that reptation and CR are independent oversimplifies the model which consequently cannot explain the nonlinear migration of large DNA fragments at field strengths above ~50 V cm^{-1} [98].

1.4.5.4 Mechanisms in dilute and low molecular mass solutions

Dilute/ultra-dilute polymer solutions are those that are below the c^*, and from Equation 1.24 it can be observed that the c^* is highly dependent on the polymer M_w and R_p and is therefore specific to each polymer. For polymer solutions below the c^*, a new TEC model was developed [140] to explain the migration of DNA among non-entangled polymer chains. TEC describes the change in velocity of DNA once it becomes entangled with the polymer chains. Migration order is from shortest to longest as the larger the strand, the greater the probability of entanglement. Conversely, there has been one report of a reversed migration order (largest to shortest) using a dilute polymer solution [37]. In order to explain this, a SECE mechanism was proposed. Each mechanism will be detailed in the following.

1.4.5.4.1 Transient entanglement coupling

A TEC mechanism was developed by Barron, *et al.* [140] to describe the separation mechanism in dilute ($c < c^*$) to ultra-dilute polymer solutions ($c << c^*$). This mechanism can account for the M_w dependence of electrophoretic separations, by proposing that the DNA molecules become entangled with the polymer in the solution which consequently migrates as a transient complex [119]. The degree of entanglement (number of collisions and drag) is greater for larger molecules as they have a greater surface area. Therefore their motion will be more retarded and their mobility decreased in comparison to shorter strands [35, 98].

TEC has since been confirmed by epifluorescence videomicroscopy which captured fluorescence images of the dye-labelled DNA molecules as they migrated [116, 141, 142]. A study by Schwinefus & Morris [141] used high speed video fluorescence microscopy to image the migration of a large λ dsDNA fragment (48.5 kbp) in dilute solutions of high M_w HEC (0.008 %, 438 800 g mol^{-1}) (shown by Figure 1.10).

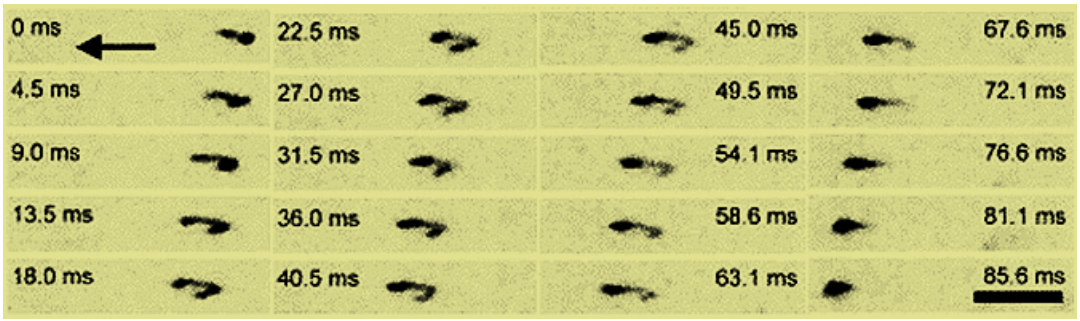

Figure 1.10. Time sequence fluorescence images of λ dsDNA as it migrates through the HEC solution under an applied voltage of 100 V cm^{-1}. Scale bar is 10 µm. The arrow indicates the direction of migration. Adapted from [141].

Figure 1.10 shows that as the fragment encounters a polymer chain in solution (t = 0 ms), they will entangle and the DNA will open from the globular shape and form a characteristic 'U' or 'J' shape (t = 13.5 ms) [29]. The DNA then drags the polymer chain along until they disentangle (t = 54.1 ms), after which the DNA will reform the globular shape until more collisions occur (t = 81.1 ms) [142]. The rate of collisions/entanglements and disentanglements is said to be dependent on the size of the DNA molecule [119].

As entanglements occur, the frictional characteristics of the DNA are altered in a size-dependent fashion. A study on dilute solutions of HEC by Barron *et al.* [35] raised the issue that size separation is highly dependent on the size of the polymer chains and DNA molecules relative to each other. This dependence is confirmed in a model study by Starkweather *et al.* [143] in which below the c^*, the polymer decreases the DNA mobility proportional to an increase in polymer concentration, with the strongest dependence occurring when the polymer and DNA chains are nearly equal in length. Barron *et al.* [35] observed that low M_w HEC (24 000 - 27 000 g mol^{-1}) solutions have little success in the separation of DNA fragments greater than 603 bp in comparison to high M_w HEC (105 000 g mol^{-1}) solutions. The shorter HEC chains have a lower average number of persistence lengths (p),

and therefore are less flexible and less likely to become entangled. Furthermore, the smaller chains provide less frictional drag when entangled, and are also more likely to be displaced rather than entangled [35]. In ultra-dilute polymer solutions, the arms of 'U' or 'J' shape are observed to be quite short indicating less polymer entanglement [7, 141]. Indeed, the use of low M_w polymers in ultra-dilute solutions results in no observable conformational changes from a globular coil to the characteristic 'U' or 'J' shape during migration [116, 119].

The TEC model suggests that there should be no upper limit of DNA fragment size separation using dilute high M_w polymer solutions under constant field strengths [35]. Further investigation into this mechanism by Barron *et al.* [29] discovered that low M_w (24 000 - 27 000 g mol^{-1}) dilute/ultra-dilute HEC polymer solutions are only capable of separating fragments of DNA smaller than ~2 kbp. Whereas, high M_w (90 000 - 105 000 g mol^{-1}) HEC solutions can separate strands greater than 600 bp, but R_s is lost for smaller fragments. In general for electrophoresis of large fragments of DNA, the separation power increases with increasing polymer M_w and concentration along with smaller polydispersities. Polydispersity refers to the distribution of polymer chain lengths in the sample; a smaller polydispersity signifies a more even distribution of change lengths [144]. Therefore in dilute and ultra-dilute solutions, the R_s can be quite poor due to the lower concentration of polymer chains. To improve the performance of the separation it is necessary to maximise the number and/or duration of collisions [98]. One way to improve the R_s in dilute and ultra-dilute solutions is to use uncoated capillaries and negative polarity. The EOF will increase the residence time of the strands in the capillary and hence likelihood of collisions [29, 119].

Hubert *et al.* [145] developed a theory to predict DNA velocity using experimental conditions based on the TEC mechanism. This theory takes into account the deformation and hydrodynamic resistance of the polymer, disengagement time of the DNA and polymer complex, and the average number of polymer molecules dragged by the DNA. The instantaneous electrophoretic velocity of a DNA molecule with *n* polymers attached (V_n) can be expressed by Equation 1.32 [145],

$$V_{\mathrm{n}} = \frac{QE - nF_{\mathrm{drag}}}{M_{\mathrm{DNA}}\xi_{\mathrm{f}}}$$

Equation 1.33

where n represents the mean number of polymer chains in contact with the DNA, $F_{\mathrm{drag}} = \eta_{\mathrm{s}} L_{\mathrm{p}} V_{\mathrm{n}}$ is the average drag force acting on the DNA due to one polymer, M_{DNA} is the bp length of DNA and ξ_{f} is the DNA friction coefficient per bp. The mean velocity of the DNA (for $n >> 1$, $V_{\mathrm{n}} \sim V_{\mathrm{DNA}}$, $p_{\mathrm{DNA}} > R_{\mathrm{p}}$) can be calculated by Equation 1.34 [98, 145],

$$\frac{V_{\mathrm{DNA}}}{V_{\mathrm{o}}} = \left[1 + \gamma c \left(1 + \frac{L_{\mathrm{p}}}{L_{\mathrm{c}}}\right)^{-1}\right]^{-1}$$

Equation 1.34

where γ is represented by $(\rho_{\mathrm{solvent}}/\rho_{\mathrm{polymer}})$ x $(N_{\mathrm{polymer}})^{1+\nu_{\mathrm{F}}}$, where ρ refers to the densities, N_{polymer} is the degree of polymerisation of the polymer and $\nu_{\mathrm{F}} \approx 3/5$ is Flory's exponent, c is the polymer concentration, L_{p} is the polymer contour length and $L_{\mathrm{c}} = N_{\mathrm{DNA}} a_{\mathrm{o}}$ is the DNA contour length in which a_{o} is the contour length (distance between adjacent bases) of one DNA bp (~0.34 nm). Equation 1.35 can be used to determine the optimum polymer concentration (c_{opt}) for separating DNA molecules of size L_{c} according to [98, 145],

$$c_{\mathrm{opt}} = \frac{1}{\gamma} + \frac{\beta L_{\mathrm{p}}}{L_{\mathrm{c}}}$$

Equation 1.35

where β represents the ratio of $\tau_{\mathrm{p}}/\tau_{\mathrm{DNA}}$ where $\tau_{\mathrm{p}} \approx L/2V_{\mathrm{n}}$ is the release time of the DNA from the polymer and $\tau_{\mathrm{DNA}} \approx M_{\mathrm{DNA}} b/2V_{\mathrm{n}}$ is the release time of the polymer from the DNA.

TEC is best applied to separations in which the DNA fragment size and the polymer chain size are relative to each other [35], and the number/duration of collisions are maximised [98]. This is best achieved by increasing the polymer M_{w} of the dilute solutions, and/or the use of non-coated capillaries to increase the residence time of the DNA and hence increase chance of collisions occurring [29, 119]. Interestingly, low M_{w} polymers have been shown to resolve short fragments of DNA, which is again due to the relative size of the DNA to the polymer chains; the smaller DNA fragments can entangle in the smaller polymer chains and hence size separation occurs [29].

1.4.5.4.2 Size exclusion capillary electrophoresis

The first and only reported SECE based dsDNA separation was described by Zhu *et al.* [37] to explain the unusual migration order of short fragments of dsDNA using low M_w LPA polymer solutions. The authors used a low M_w (1500 g mol^{-1}) LPA polymer buffer solution (dissolved in Tris (90 mM), boric acid (330 mM), EDTA (2 mM) buffer) to separate short strands of dsDNA (11, 20 and 22 bp) on a capillary electrophoresis phase (CEP) covalently coated capillary and found an increase in dsDNA mobility with an increase in size indicating that the classic Ogston and reptation sieving mechanisms no longer applied to low M_w solutions. At such low M_w (below the overlap concentration c^* [34, 35, 50, 98, 120]), polymer entanglement does not occur owing to the short chains self-coiling into a globular structure. The short dsDNA strands diffuse through the polymer pores in a similar mechanism to size exclusion chromatography [37]. From a thorough investigation into separation mechanisms, and in particular free solution mobility, it is more likely that the use of such low M_w polymer solutions as sieving media have little to no effect on the migration of short DNA fragments, and the migration is actually based on the free solution mobility.

1.5 Types of polymer coatings in CE

Table 1.1 in Section 1.3.2 provides a classification of the various polymers coatings available for the surface modification of capillaries. Coating the capillary surface slows down the EOF and decreases DNA adsorption onto the capillary surface. Typically when a solute adsorbs onto an untreated capillary surface, the distribution and hence the surface charge becomes non-uniform. This can lead to asymmetric peaks and peak broadening. By coating the capillary, not only does it result in less adsorption due to repulsive forces, it also creates a constant charge distribution along the capillary surface and enhances peak R_s by reducing the interaction between the analyte and the surface [12].

This section describes and introduces the relevant literature for the separation of charged analytes (focussing on DNA) on each of the surfaces described in Table 1.1, with particular attention to dynamic physically adsorbed coatings. Table 1.1 classifies coatings as either static (covalently attached, permanent) or dynamic

(physically adsorbed, non-permanent). The most common static coating for DNA separation revolves around the use of immobile gels to act as sieving media [40, 61, 65, 75, 82]; however, these suffer from a lack of repeatability owing to deterioration of the gel with each run [17]. Surface confined static coatings have been developed to suppress the EOF and reduce surface-analyte interactions. These types of coatings are most useful for the separation of non-free draining molecules (such as proteins and peptides [136-139]), and are therefore not suitable for separations of DNA fragments above the p_{DNA}. However, they can be used as EOF suppressants for the separation of short DNA fragments in free solution [20, 93, 105, 146].

Static coatings cannot be easily regenerated and therefore lack repeatability; this led to the creation of dynamic coatings which show enhanced repeatability due to the ability to regenerate the coating [38, 56, 147, 148]. The method can be fine-tuned for enhanced repeatability by altering the regeneration steps. Dynamic coatings refer to the physical adsorption of the polymer from a solution onto the surface. These coatings can be used as sieving media (much the same effect as using gels) [35, 38, 43, 54, 87], or can be confined to the surface [77, 79, 80, 90, 92]. The former involves either the polymer dissolved in the running buffer, or the capillary filled with the polymer solution prior to electrophoresis for the separation of DNA; the latter, similarly to the covalently attached surface confine polymers, does not involve any molecular sieving and is therefore used as a suppressant of EOF and surface-analyte interactions [26, 56, 91].

This is significant for the work described in this thesis, as these coatings are suitable for the separation of short (non-free draining) DNA strands in free solution [20] (see Chapters 5 - 7).

1.5.1 Static coatings

Static coatings involve the direct covalent attachment of polymer to the capillary surface. This attachment is permanent and therefore cannot be regenerated. These types of coatings can become degraded during electrophoresis due to a number of things, such as the application of high voltages and/or temperatures, harsh pH

conditions, and interactions with analytes removing the polymer from the surface. All these things may easily lead to poor repeatability and a non-uniform surface coverage [11].

Static coatings typically involve either the use of a polymer gel pumped into the capillary (CGE), much like slab-gel electrophoresis, or the covalent attachment and/or growth of the polymer *in situ*. Not all polymers can covalently attach to a capillary surface, therefore it is common to use an intermediate bifunctional molecule as a covalent linker to attach the polymer to the surface. Horvath & Dolnik [12] have defined three main steps in achieving a permanent surface coating:

(1) ***Pre-treatment of the capillary:*** The capillary is cleaned and activated to allow the intermediate layer to bind. This involves etching with sodium hydroxide (NaOH) and leaching with hydrochloric acid (HCl). This combination of etching and leaching enhances the repeatability, when compared to using etching or leaching alone [149].

(2) ***Formation of the intermediate layer:*** A bifunctional molecule (typically a silane) is used to assist in the binding of a polymer to the capillary surface. A bifunctional silane (such as γ-methacryloxypropyltrimethoxysilane (MPTS)) has functional groups available to bind to the silanol surface and other functional groups available to bind to and polymerise the monomers [23].

(3) ***Polymer top layer:*** This layer is generally formed via a free radical polymerisation reaction with the terminal functional group from the bifunctional molecule on the intermediate layer (most commonly a terminal alkene), however polymerisation can be achieved using a molecule with a good leaving group, such as a chloride [13].

1.5.1.1 Gel coatings

CGE provides a sieving medium to allow for the separation of DNA based on size and orientation [22]. The idea of gel-filled capillaries originated from slab-gel electrophoresis on which the first DNA size separation was carried out [22]. These

types of coatings are generally prepared by mixing the polymer gel and forcing it through the capillary with pressure, allowing it to cure inside the capillary (usually overnight) [42, 48, 60, 82]. Separations using these coatings follow the Ogston or reptation models depending on the size of the polymer pores and the size of DNA fragments being separated (see Section 1.4.3). The most commonly used gels comprise of PAM cross-linked with various acrylamide monomer derivatives. PAM gels generally have small pore sizes making them unsuitable for separation of large fragments of DNA. With the development of mixed-bed sols (addition of another polymer), the pore size is able to be tuned by using lower temperatures during curing and monitoring the gelation time (addition of a cross-linker stops the gelation process) [22].

There are a number of mechanisms/models to describe the migration of DNA, and these depend on the polymer matrix, the DNA size and conformation, and whether the DNA is ss or ds (for more detail on separation mechanisms refer to Section 1.4). Taking this into account, a particular gel is capable of separating only a narrow range of DNA. Other serious drawbacks of using gels include the inability to regenerate, formation of bubbles, and deterioration from run to run [17]. These limit the capillary lifetime and seriously hinder the repeatability of separation. Consequently, gel-filled capillaries have become a thing of the past and no longer play a major part in DNA separations.

Owing to the early popularity and success of CGE as a separation technique for DNA (in particular with sequencing), there is a vast amount of literature available, the most relevant of which are summarised in Table 1.2.

Table 1.2. Summary of some CGE methods in the literature.

Ref.	Analyte	Surface	Separation conditions	Results
[42]	Polydeoxyadenylic acid ($Pd(A)_{40-60}$) (40 b - 60 b, 1 b increments), ssODNs (17 b, 70 b and 99 b)	Bis-acrylamide cross-linked PAM gel (7.5 % T and 3.3 % C) containing urea (8.3 M) sieving matrix covalently attached to the capillary surface via MPTS. T refers to the % of monomer and C is the % of cross-linker	400 V cm^{-1}, Tris (0.1 M)-borate (0.25 M)/urea (7 M) buffer, pH 8.3; UV detection; 27 cm - 30 cm L_d	Separation of ss $pd(A)_{40-60}$ was achieved in under 6 min with t_m increasing with increasing bp length
[48]	1000 bp ladder (75 - 12 216 bp), Hae III digest ϕx174 dsDNA fragments (72 bp - 1353 bp) spiked with pBR322 dsDNA (4363 bp) and M13mp18 (7250 bp), $Pd(A)_{20,}$ $Pd(A)_{40-60}$	Bis-acrylamide cross-linked PAM gel (3 % T and 0.5 % C) or LPA (3 - 14 % T) sieving matrices covalently attached to the capillary surface via MPTS	125 V cm^{-1} - 308 V cm^{-1}, Tris-borate (100 mM)-EDTA (2 mM) buffer, pH 8.3 (for separation of ssDNA urea was added to the buffer (7 M)); UV detection; 10 cm - 45 cm L_d	Migration order was from shortest to longest fragments for all PAM gels. Use of lower % C resulted in larger pores sizes and allowed for sieving of much larger fragments. Higher % T in the LPA gels proved to be suitable for ssODN separations

Ref.	Analyte	Surface	Separation conditions	Results
[82]	Polydeoxythymidylic acids ($Pd(T)_{20-160}$ (20 b - 160 b, 20 b increments) and $Pd(A)_{40-60}$	Bis-acrylamide cross-linked PAM gel (3 % - 6 % T and 5 % C) sieving matrix covalently attached to the capillary surface via MPTS	300 V cm^{-1}; Tris (0.1 M)-borate (0.25 M)/urea (7 M) buffer; UV detection; 15 cm and 55 cm L_d	Separation of $pd(A)_{40-60}$ was achieved in 13 min using 6 % T and 5 % C crosslinked gel (15 cm capillary); and 21 min using 3 % T and 5 % C (55 cm capillary)
[40]	$Pd(A)_{40-60}$ and $pd(T)_{1-431}$ (1 b - 431 b), both 1 b increments	Bis-acrylamide cross-linked PAM gel (6 % T and 5 % C) sieving matrix covalently attached to the capillary surface via a non-crosslinked PAM monolayer bonded to MPTS	300 V cm^{-1}; Tris (0.1 M)-borate (0.25 M)/urea (7 M) buffer; UV detection; 40 cm L_d	Separation of $pd(A)_{40-60}$ was achieved in under 35 min with migration order from shortest to longest
[65]	ssODNs (20 b - 50 b), $pd(T)_{12-30}$, $pd(T)_{10-50}$	Cross-linked PAM gel (7.5 %) sieving matrix covalently attached to the capillary surface via MPTS	250 V cm^{-1} - 375 V cm^{-1}; Tris-borate (50 mM)-polyethylene glycol (PEG) (3 %)/urea (7 M) buffer; UV detection; 20 cm L_d	Separation of $pd(T)_{10-50}$ was achieved in under 30 min with migration order of shortest to longest for all mixtures injected

Ref.	Analyte	Surface	Separation conditions	Results
[61]	Fluorescently labelled ssDNA sequencing fragments (46 b - 624 b)	Bis-acrylamide cross-linked PAM gel (4 % T and 5 % C) containing urea (8.3 M) sieving matrix covalently attached to the capillary surface via MPTS	100 V cm^{-1} - 400 V cm^{-1}; laser induced fluorescence (LIF) detection; Tris (0.75 M)-disodium EDTA (10 mM) buffer, adjusted to pH 7.5 with phosphoric acid; 50 cm L_d	Separation/sequencing of fluorescently labelled ssDNA fragments was achieved using the conditions described
[60]	Fluorescently labelled ssDNA sequencing fragments (46 b - 624 b)	Bis-acrylamide cross-linked PAM gel (4 % T and 5 % C) containing urea (8.3 M) sieving matrix covalently attached to the capillary surface via MPTS	150 V cm^{-1}; LIF detection; Tris (0.75 M)-disodium EDTA (10 mM) buffer, adjusted to pH 7.5 with phosphoric acid; 25 cm - 75 cm L_d	Higher field strengths in these gels can be used to increase the efficiency of separation which was proven to be independent of capillary length. Resolution can however be improved by increasing the capillary length
[75]	ssPS-ODNs (18 b - 21 b) (mono-, di-, and tri-phosphodiester analogs)	Polyacrylamide gel (pre-purchased, specifications not listed)	300 V cm^{-1}; UV detection; tris-borate/urea buffer (concentrations not reported); 40 cm L_d	Resolution of a 1/1 mixture of PS-ODNs and monophosphodiester ODNs was not possible with this method. However, it was capable of resolving a mixture of phosphorothioate ODNs 1 - 3 b difference

1.5.1.2 Surface confined static coatings

Surface confined static coatings involve the permanent covalent attachment of the polymer to the capillary inner surface and unlike CGE do not provide molecular sieving. As the name suggests, this type of coating entails polymer confinement to the surface, and results in the suppression of EOF, the formation of a uniform surface charge and the reduction in surface-analyte interactions [12]. This concept is necessary for the separation of proteins which are notorious for sticking to the capillary walls. However, surface-analyte interactions can be utilised when separating similarly sized DNA fragments, in particular when using charged polymers as surface modifiers. Providing surface-analyte interactions are limited, the separation mechanism involved in these types of surface confined coatings should depend on the free solution mobility of the analyte (see Section 1.4.1).

1.5.1.2.1 Linear polyacrylamide

In 1985, Hjertén [23] set the bench mark for surface confined static coatings by introducing the use of LPA as a permanent surface coating in an attempt to move away from CGE to improve repeatability and R_s. This led to acrylamides (and derivatives) being the most widely used materials for a permanent capillary coating [12]. However, PAM is very hydrophilic and is unable to directly bind to the capillary surface. Therefore, a bifunctional silane is used as the surface binder [12]. MPTS is a common bifunctional molecule with the methoxy moiety capable of reacting with the silanol groups on the capillary surface and the acryl groups reacting with monomer acryl groups to produce poly attachment.

Hjertén [23] developed a method to coat narrow glass capillary tubes (3 mm internal diameter) with a monolayer of non-cross-linked PAM (reaction scheme is represented by Scheme 1.7). The glass capillary was initially coated with an aqueous solution of MPTS and acetic acid to create the silane intermediate layer. The solution was left standing for 1 h, and then withdrawn. The capillary was then flushed with water and treated with an aqueous solution containing acrylamide, *N*,*N*,*N'*,*N'*-tetramethylethane-1,2-diamine (TEMED) and potassium persulphate (PPS) for a further 30 min to form the PAM top layer. After the excess polymer solution was removed, the capillary was washed with water and dried [23].

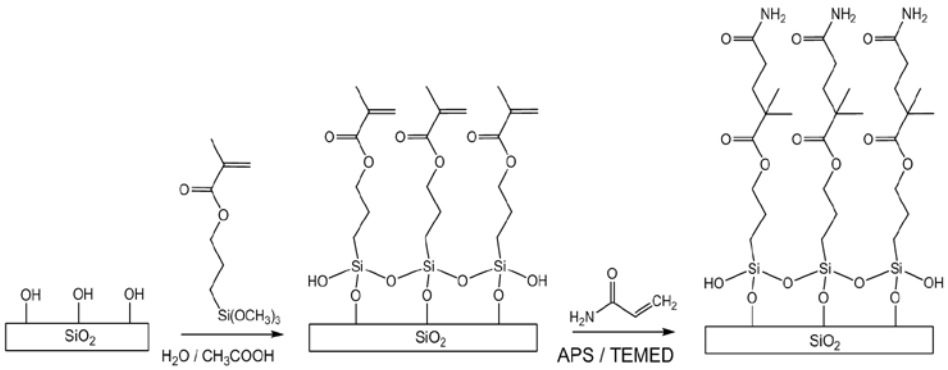

Scheme 1.7. Reaction schematic for preparation of an LPA coated capillary.

The coating method developed by Hjertén [23] was tested on zone electrophoretic analysis of aromatic carboxylic acids (Figure 1.11A) and compared to analysis with a non-coated capillary (Figure 1.11B). The separation and R_s of the peaks were significantly improved using the coated capillary.

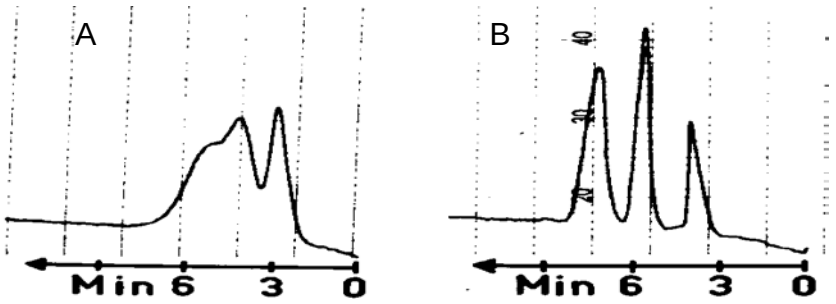

Figure 1.11. Zone electrophoresis of aromatic carboxylic acids in non-coated glass tube (A) and LPA coated capillary (B) [23].

Following the method derived by Hjertén [23], Cifuentes *et al*. [27] investigated LPA coatings in fused-silica capillaries. The process first involved the modification of the silanol groups on the surface using 7-oct-1-enyltrimethoxysilane (bifunctional silane), followed by the attachment of the acrylamide to produce PAM on the surface. Each step involved in the coating procedure needed to be strictly monitored. This is because the coating depended on the quantities and ratios of chemicals used. The size and reactivity of the polymer was controlled by the concentrations of the monomer (acrylamide), activator (TEMED) and initiator (ammonium persulphate (APS)) involved. Kinetic studies performed by the group determined that the rate of aqueous polymerisation of acrylamide was proportional to the square root of the concentration of the initiator (APS), and was dependant on the concentration of monomer (acrylamide) to the power of approximately 1 - 1.5.

Therefore, the M_w of PAM was equal to the concentration of the acrylamide divided by the square root of the concentration of the APS. Keeping this in mind, it was possible to predict the amount of polymer for complete surface coverage. The repeatability was enhanced by using the optimum reaction conditions determined by measuring the EOF and t_m of an internal standard [27]. The coating method developed was tested by CE on basic proteins (lysozyme, ribonuclease A and α-chymotrypsinogen).

Owing to the high success of LPA as a surface coating to reduce/remove the EOF, it is frequently used as a capillary pre-coat for dynamic separations using sieving media [29, 53].

1.5.1.2.2 Surface-confined living radical polymerisation

Surface-confined living radical polymerisation (SCLRP) involves covalently binding polymers to the surface via a self-assembled monolayer which contains reactive groups for the growth of polymer in the presence of the initiator. This technique is an adaptation of the Hjertén [23] LPA method, replacing the bifunctional silane with a different intermediate species containing leaving groups which allow for the growth of a more diverse array of polymers, such as PVP [83] and polystyrene nanoparticles [86]. Huang *et al*. [13] developed a SCLRP method of coating capillaries with PAM using benzyl chloride as the intermediate layer (shown by Scheme 1.8). The benefit of using surface-confined polymerisation is that it restricts the formation of polymer in solution which is responsible for blockages in the capillary. This method also has the advantage of controlling layer thickness by monitoring monomer concentration, as well as enhanced repeatability [13].

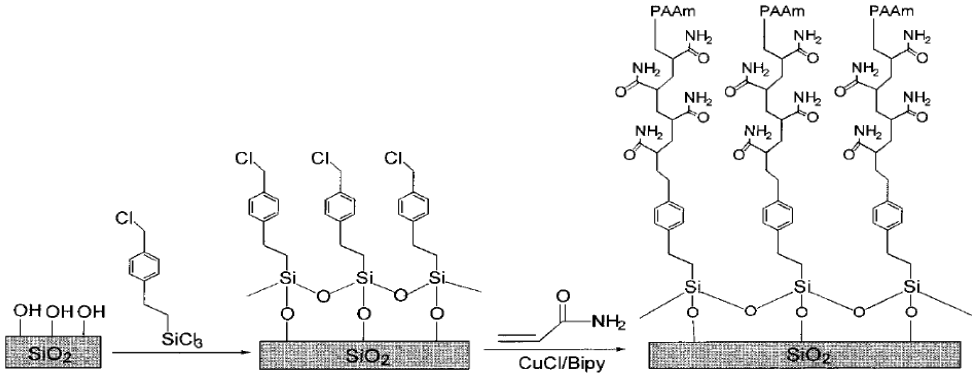

Scheme 1.8. Capillary modification using SCLRP of PAM [13].

This method was proven to work well for the electrophoretic separation of proteins, despite the low stability of PAM when confined to the surface. However, this method was only applied at low pH [13], and may therefore not be suitable for DNA separation at neutral to basic pH without some modification.

1.5.1.3 Other covalently bound polymer coatings

A variety of polymers have been immobilised on capillary surfaces via covalent attachments using intermediate molecules. They provide no sieving ability for DNA separation but are often used as a pre-coat for sieving polymer solutions. Covalent coatings for EOF suppression are detailed in Table 1.3.

Table 1.3. Examples of surface confined covalent polymer coatings for EOF suppression.

Ref.	Analyte	Surface	Separation conditions	Results
[83]	Proteins and peptides	PVP covalently attached to the capillary surface via MPTS	Gradient voltage, linear step from 2.5 kV - 30 kV; phosphate buffers (H_3PO_4 (150 mM), pH 1.45; NaH_2PO_4 (150 mM), pH 4.5; H_3PO_4 (38.5 mM) and (20 mM) NaH_2PO_4, pH 2.0); UV detection; 100 cm - 110 cm L_d	Low pH buffers in conjunction with the modified surface resulted in near elimination of EOF
[84]	Proteins	LPA covalently attached via vinyl surface groups formed by a Grignard reaction with the chlorinated silanol surface	-12 kV, -20 kV or -22 kV; Glutamine (0.05 M), TEA (pH 9.5) buffer and citric acid (0.03 M) buffer, adjusted to pH 2.7 with NaOH (1M); UV detection; 45 cm L_d	The coating caused a reduction in EOF and protein adsorption, resulting in shorter t_m and improved R_s
[85]	Proteins	Covalent attachment of poly(acryloylaminoethoxy ethanol) (poly(AA-EE)) via MPTS	500 V cm^{-1}; bicine-Tris (25 mM) buffer, pH 8.5; UV detection at 214 nm; 32 cm L_d	EOF was negligible with this coating which was stable over 100 h (stability was improved by adding small amounts of poly(AA-EE) to the running buffer)
[86]	Peptides	Derivatised polystyrene nanoparticles (latex diol) or derivatised fullerenes (fullerenol)	20 kV; triethylamine (TEA) (40 mM) buffer adjusted to pH 2.3, and 8.0 (containing acetonitrile (ACN)) (20 % v/v) with phosphoric acid; UV detection coupled to matrix-assisted laser desorption/ionisation (MALDI); 57.5 cm L_d	Coatings were proven to be stable at high and low pH and the EOF was suppressed for both coatings, with a greater reduction observed using latex-diol coating

The production of covalently linked LPA, like the production of many other covalently linked polymeric coatings, is time-consuming and generates an uneven layer of material of unknown thickness [56]. Therefore research is moving towards to use of dynamic solutions as physically adsorbed coatings and sieving media.

1.5.2 Dynamic coatings

Dynamic coatings are promising replacements for CGE and other covalently bound polymers, and are capable of separating ssDNA and dsDNA of varying lengths. A wide range of polymers can be physically adsorbed (such as PVP, polydimethylacrylamide (PDMA) and various acrylamide derivatives [56]) onto the capillary inner wall in order to modulate the surface charge and hydrophobicity. This, along with the relative ease of capillary regeneration, has led to this approach becoming the method of preference for capillary surface modification for separation of various analytes [56, 77, 79-81, 88, 89].

It is a common misconception in literature that dynamic coatings require polymer in the run buffer; in fact, dynamic coatings can simply refer to the physical adsorption of a solute to a surface from a polymer solution. The polymer solution plays an important role in the analyte separation and, in particular, the polymer concentration is important when using the solution as a sieving media (see Section 1.5.2.1). According to Table 1.1 (in Section 1.3.2), dynamic polymer coatings can be organised into 2 main categories; sieving polymer solutions (including polymer-buffer solutions), and surface confined polymer coatings. Each of these rely on the physical adsorption of the polymer from solution onto the capillary surface.

Dynamic coatings are extremely desirable due to the high repeatability [12]. The forces involved in physically adsorbed coatings can involve hydrogen bonding, electrostatic interactions, van der Waals forces [90] and hydrophobic interactions [56]. Coating is achieved by rinsing the capillary with a solution containing the coating material, and in some cases, adding a small amount of the coating material to the run buffer (referred to as polymer-buffer solutions, see Section 1.5.2.1.1). Regeneration of these dynamic coatings can be achieved by removing the surface polymer and repeating the coating procedure. Regeneration is more essential for hydrophilic polymers which are easily removed from the capillary surface by the

aqueous buffer [25]. Therefore, the polymer from the run buffer replaces the bound polymer which is stripped off the surface by the aqueous buffer. When using this method it is necessary to consider the fact that the polymer must possess the ability to displace the water molecules which are strongly attracted to the surface [25]. This is not always possible, and most often requires water soluble polymers.

Some polymers can be used as dynamic coatings which do not require the addition of polymer to the running buffer. These types of coating can be either physically adsorbed surface confined coatings (see Section 1.5.2.2), or sieving polymer solutions containing a polymer that is capable of physically adsorbing to the capillary surface to suppress the EOF (see Section 1.5.2.1.2). More often than not, these polymers are hydrophobic and therefore are not removed from the surface by an aqueous buffer. Chiari *et al.* [25] proposed that hydrophobic polymers have a greater affinity for the surface and often do not require polymer in the run buffer or as much regeneration. When this is the case, the coating is simply regenerated between runs by flushing through fresh polymer solution.

1.5.2.1 Dynamic polymer solutions as sieving media

Dynamic polymer solutions can be used as sieving media either by dissolving the polymer in the running buffer (polymer-buffer solutions) or completely filling the capillary with the polymer solution (sieving polymer solutions). Dynamic coatings using polymer-buffer solutions are prepared by pre-treating the capillary with the polymer-buffer solution prior to electrophoresis to reduce the EOF. The polymer in the running buffer assists in the sieving process and replaces any polymer molecules removed from the surface [12]. Sieving polymer solutions (without polymer added to the buffer) are prepared by completely filling the capillary with the polymer solution which only partially adsorbs to the surface and creates a three-dimensional sieve [12]. The sieving medium is often replaced between runs by refilling the capillary with fresh polymer solution. For both the polymer-buffer solutions and the sieving polymer solutions, in some cases, the capillary requires pre-treatment (activation) or a polymer pre-coat to suppress the EOF. In particular, for polymers that are chosen for their sieving abilities, rather than their ability to suppress the EOF (such as polyacrylamide-*co*-allyl-*β*-D-glucopyranoside (poly(AG-

AA)) [38] and HEC [43, 88]). Dynamic sieving polymers involve the use of polymer solutions which can be of varying concentrations to control the separation mechanism (refer to Section 1.4.5). Dynamic polymer mixtures have also been developed to create interpenetrating networks for polymer sieving [28, 78, 150].

The separation mechanism involved in dynamic polymer solutions will depend on the concentration and the M_w of the polymer, along with the size of the migrating molecule. In dilute/ultra-dilute solutions, the polymer chains are mobile and can entangle with the migrating molecule, altering the mobility. This mechanism is described by TEC (discussed in Section 1.4.5.4.1). In general to achieve high efficiency, the polymer chain length should be relatively similar to the DNA chain length. Therefore, in order to separate larger fragments of DNA using sieving media, high M_w polymers are required, whereas for short fragments of DNA, low M_w polymers achieve the best results. For separation where $c > c^*$, the separation mechanism is said to follow the CR model (refer to Section 1.4.5.3.1) which is dominant for cases in which the analyte is large, surrounded by shorter polymer chains. For cases in which $c >> c^*$, the mechanism is said to revert to the BRF, meaning that shorter fragments can be more efficiently separated.

1.5.2.1.1 Dynamic polymer-buffer solutions for analysis of DNA

A variety of polymers have been dissolved in running buffer for the sieving separation of DNA fragments on bare or modified capillary surfaces. In the case where the chosen sieving polymer is not capable of adsorbing onto the capillary surface to suppress the EOF, pre-coated capillaries are used. Table 1.4 details the types of coatings used as polymer-buffer solutions on both bare and pre-coated capillaries.

Table 1.4. Examples of polymer-buffer solutions as sieving media for the separation of DNA fragments.

Ref.	Analyte	Surface	Separation conditions	Results
[38]	dsDNA (51-587 bp) and ssODNs (40-60 b)	Bare capillary treated with poly(AG-AA)/PDMA polymer-buffer solution	poly(AG-AA) (10 %) and PDMA (0.05 %) were dissolved in TAPS-Tris (100 mM)-EDTA (2 mM) running buffer; 200 V cm^{-1} for dsDNA and 300 V cm^{-1} for ssODN separation; UV detection at 260 nm; 36 cm L_d	The glucose units decreased the viscosity of the polymer solution to allow for easier application. Addition of small amounts (0.05 %) of PDMA to the polymer-running buffer allowed for the dynamic suppression of the EOF. Separation was achieved in 30 min and 20 min for the dsDNA and ssODNs, respectively
[87]	dsDNA fragments (100 bp ladder)	Capillary was pre-treated with PVA (1 %) to suppress the EOF before being treated with HEC polymer-buffer solution	HEC (4.5 %) was dissolved in Tris (20 mM), orthophosphoric acid (10 mM), EDTA (2 mM) running buffer; -298 V cm^{-1}; UV detection at 260 nm; 40 cm L_d	Separation was achieved in 24 min. The authors reported repeatability of the coating for t_m of the 100 bp peak to be 0.54 % for n = 10 (intraday). Interestingly, the repeatability of the larger fragments declined (0.92 % for the 500 bp fragment)
[15]	dsDNA fragments (Hae III digest ϕx174)	Bare capillary treated with PDMA polymer-buffer solution	PDMA (3 %) dissolved in *N*-tris (hydroxymethyl)methyl-3-aminopropanesulf-onic acid (TAPS) (80 mM, pH 7.6) running buffer; -400 V cm^{-1}; 25 ^{o}C; LIF detection at 488 nm; 40 cm L_d	Separation was achieved in 15 min. The authors reported good repeatability of the coating for t_m (0.24 % - 0.27 % for n = 7 intraday and 1.35 - 1.63 % for n = 21 interday)

With the advent of sieving polymer solutions, polymer-buffer coatings are no longer the main focus, although they continue to be the inspiration for development of dynamic polymer solutions which are often modifications of these methods.

1.5.2.1.2 Sieving polymer solutions for EOF suppression and analyte separation

As already stated, not all polymer solutions are capable of acting as both a sieving medium and an EOF suppressant, and in these cases, a polymer pre-coat is used to suppress the EOF. Some examples of these include the use of PDMA pre-coated capillaries filled with HEC polymer sieving solution by Kleemiβ *et al.* [43]; and epoxy-PDMA pre-coated capillaries for the separation of dsDNA fragments using a poly(acrylamide-*co*-allyl-D-galactopyranoside) (poly(Agal-AA)) polymer sieving solution [88]. There are only a few polymer solutions that are capable of acting as both a physically adsorbed surface coating to suppress the EOF and as sieving media for analyte separation. Such polymers include PDMA, poly-*N*-hydroxyethylacrylamide (PHEA), PVP and polyethylene oxide (PEO) [26]. The adsorption mechanism and properties of the coatings are not well known, however, according to Doherty *et al.* [56] the EOF of the coating is related to the polymer hydrophobicity. The underlying principle behind the enhanced adsorptive properties of hydrophobic polymers from dynamic solutions is related to their ability to displace water molecules from the silanol surface. This theory originates from the competition from the solvent for the surface [25]. This property also ensures that the polymer is not removed from the surface by the buffer during electrophoresis.

PDMA is a very versatile polymer for surface modifications (whether for static or dynamic coatings). The hydrophobic properties allow for strong adsorption to the surface, but it is not so strongly hydrophobic that it can still dissolve in water at low concentrations. Water is generally a poor solvent for PDMA which enhances the adsorption from the water solution onto the surface when compared to good solvents. In terms of dynamic coatings, it is preferred that the polymer be dissolved in poor solvents so that adsorption from solution onto the surface is maximised [54]. Hydrophobic polymers also have the advantage of not being easily removed from the surface during electrophoresis in aqueous buffers, creating a more stable

and reproducible surface coating. PDMA also exhibits good sieving properties for biomolecules due to the structure and polymer entanglement threshold. The acrylamide groups are also available for covalent surface attachment to create a permanent static coating/gel [54].

Madabhushi [54] used a high M_w (98 kilodaltons (kDA)), low concentration/viscosity (6.5 % w/v) PDMA polymer solution to separate DNA sequencing extension products. The authors showed that the PDMA effectively coated the capillary surface, suppressing the EOF, and also acted as a sieving media to resolve individual sequencing fragments. The coating was prepared by simply flushing the capillary with the polymer solution for 1 min, with no capillary pre-treatment. The sieving medium was replaced between runs in a similar fashion. The EOF mobility was reduced using the PDMA as a sieving media, when compared to a bare fused-silica capillary, and each coated capillary could be used up to 100 times before it needed to be replaced.

Zhang *et al*. [26] have studied dynamic polymer coatings using PDMA and polydiethylacrylamide (PDEA) as sieving media for the separation of long dsDNA fragments. Coatings were prepared by flushing the capillary with HCl (1 M), water and buffer and finally filling the capillary with polymer dissolved in buffer and leaving it stand for 30 min. The polymer solution was replaced prior to each run. Polymer surface modifications were initially investigated on silicon wafers, using atomic force microscopy (AFM) to image/analyse the surface, and contact angle measurements to determine the hydrophobic surface properties. Multi-angle laser light scattering (MALLS) was used on ultra-dilute polymer solutions to measure the molecular radii of the polymer. AFM showed that both polymers were strongly adsorbed to the silica surface. The authors calculated the size of the 'adsorbing globules' from the AFM images to be above 50 nm. The authors then compared these values to the R_p (~20 nm) determined from MALLS. However, the AFM samples were prepared using 5 % w/v polymer solutions, whereas MALLS was performed using an ultra-dilute 0.01 % w/v polymer solution (0.1 mg mL^{-1}). The concentration of polymers in solution plays a major role in the polymer conformation. At ultra-dilute concentrations ($c < c^*$), the polymer chains self-coil forming a globular structure, whereas at dilute to semi-dilute ($c = c^*$ or $c > c^*$) the

polymer chains begin to entangle [29, 34, 50, 98, 120]. Therefore, the R_p will not be the same for the polymer at different concentrations, and these two techniques cannot be compared for this work.

Electrophoresis performed in PDEA and PDMA polymer solutions 1 % w/v - 4 % w/v (Figure 1.12) showed an increase in DNA R_s with increasing polymer concentration (and hence an increase in t_m) [26]. The R_s in DNA strands increased dramatically between the 1 % solution and the 2 % solution, suggesting a change in polymer morphology between these two concentrations. EOF measurements showed that these coatings were capable of suppressing, but not reversing the cathodic EOF with % RSD values between 1.5 % and 2.3 %.

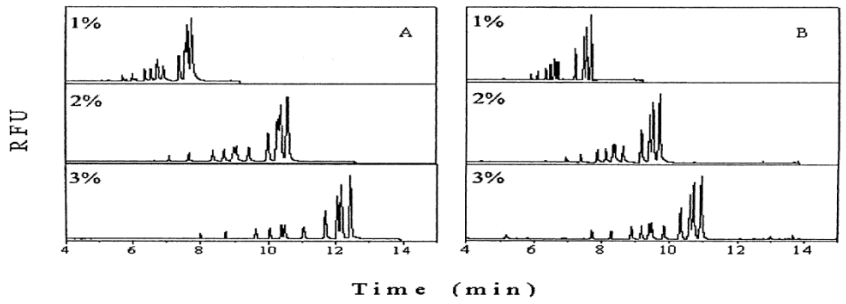

Figure 1.12. CE electropherograms of separation of Hae III digest ϕx174 dsDNA fragments on an uncoated capillary (40 cm L_d) at -400 V cm^{-1} using PDMA (1 - 3 %) sieving matrix (A) and PDEA (1 - 3 %) sieving matrix (B) [26].

Water contact angle measurements were used to investigate the hydrophobicity of the polymers. The contact angle measurement at 25 ^oC increased from 5.48° for the bare fused-silica capillary, to 21.11° and 34.64° for the PDMA and PDEA coated capillaries, respectively [26]. The increase in hydrophobicity of the surface was attributed to the substituted nitrogen groups. The authors proposed that the polymer adsorbs to the surface via hydrogen bonding, and the hydrophobic groups attached to the nitrogen stabilise the surface by repelling the water molecules which aim to displace the polymer. This method showed the suitability of both PDMA and PDEA polymer solutions as a dynamic coating to suppress the EOF and also behave as sieving media [26].

An interesting study on the separation of 19 different dsDNA restriction fragments (72 - 23 130 bp) by Barron *et al.* [35] used HEC as a sieving polymer solution. This polymer did not suppress the EOF and a pre-coat was not used. Therefore

electrophoresis was operated in positive polarity (injection at the anode and detection at the cathode), relying on the EOF to assist in migration of the strands. Resolution of most strands was achieved using HEC (90 000 - 105 000 g mol^{-1}) polymer solutions (0.0025 - 0.45 % in buffer) which caused the larger strands to migrate first (smaller electrophoretic mobility), followed by the smaller strands (larger electrophoretic mobility). The smallest strands (118 and 72 bp) were unresolved. The authors investigated the separation mechanism of DNA separations in dilute polymer solutions and proposed the new mechanism, transient entanglement coupling (refer to Section 1.4.5.4.1 for more details). This method exhibited % RSD values of less than 0.5 % for t_m [35].

A study by Yang *et al.* [89] involved the development of a HEC-*graft*-PAM (HEC-*g*-PAM) polymer to be used as a polymer solution for the effective sieving of dsDNA fragments (72 - 1353 bp). The significance of using a graft polymer is the ability to change the graft length. An increase in graft length showed an improvement for R_s of the dsDNA fragments. In addition, graft polymers form a more stable and immobile entangled mesh with an effective pore size for DNA migration. This novel HEC-*g*-PAM polymer utilised the good sieving properties of hydrophilic PAM and good dynamic coating (and hence EOF suppression) abilities of HEC. Increasing the PAM concentration to achieve effective sieving ($c > c^*$) also resulted in a less effective EOF suppression. Therefore, to maintain a good coating, the ratio of each monomer must be kept relative. To improve the sieving ability of the polymer, whilst maintaining sufficient EOF suppression both the PAM and HEC concentrations needed to be increased. An increase in polymer concentration resulted in greater EOF suppression and enhanced the R_s of the smaller fragments. By increasing the applied voltage, the R_s was decreased.

Polymer solutions used as sieving media and for EOF suppression are most commonly used for the separation of longer fragments of DNA, in particular dsDNA. However, there have been some methods developed for short strand analysis and these are described in Section 1.6.

1.5.2.2 Physically adsorbed surface confined coatings

Due to the chemical nature of dynamic polymers (generally hydrophilic), most of these coating methods require the addition of the polymer to the run buffer to aid in the regeneration of the coating (and act as a sieving medium for separation of biomolecules), however, this is not always necessary. Coatings with high repeatability can be achieved by simply flushing the capillary for a predetermined time to allow polymer adsorption to the surface. Between runs, the coating is regenerated by a short rinse with the polymer solution. These types of coatings are excellent at reducing the EOF and can be tailored to enhance the separation of analytes based on surface interactions [52]. Most of the work on this type of simple system has revolved around proteins. This is because separation of proteins requires surface modification to stop the adsorption of proteins to the capillary wall along with the suppression of EOF. Consequently, because most of these coatings have been developed for protein separation, they create a pH tuneable surface charge in which the surface is generally strongly positive at low pH and weakly positive at high pH [79-81]. For biomolecules such as DNA which are negatively charged, a positively charged surface would promote surface-analyte interactions. However, owing to the constant mass-to-charge ratio of DNA, these surface-analyte interactions have the potential to assist in R_s of individual strands. Physically adsorbed coatings described here behave similarly to the surface confined covalent attachments (see Section 1.5.1.2) and both can be used as polymer pre-coats for dynamic separations (Section 1.5.2.1) or separations in free solution (Section 1.4.1). In addition, depending on the surface-analyte interactions, the separation mechanism involved in these types of physically adsorbed polymer coatings should depend on the free solution mobility of the analyte (see Section 1.4.1).

Iki & Yeung [90] used PEO, a non-ionic hydrophilic polymer, for the separation of basic proteins under acidic conditions. Although PEO is hydrophilic, it is also non-ionic and contains ether groups which are capable of hydrogen bonding to the surface. The coating is reported to be kinetically and thermodynamically stable, meaning it possesses a slow rate of desorption. These properties make it more suitable as a physically adsorbed coating than typical hydrophilic polymers. The R_s of peaks was enhanced by the addition of HCl (0.1 M) to the polymer coating

solutions This is because the HCl reprotonates the capillary silanol surface resulting in more hydrogen bonding sites for the PEO polymer [90]. The authors reported % RSD (n = 5) of protein t_m between 1.4 and 3.9 %. Interestingly, the proteins with a longer t_m have a decreased repeatability.

Building on earlier work using dynamic polymer-buffer solutions [38], Chiari *et al*. [25] also developed a hydrophilic poly(acrylamide-*co*-allyl-β-D-glucopyranoside-*co*-allylglycidy ether) (epoxy-poly(AG-AA)) dynamic polymer solution to physically adsorb to the capillary wall for CE analysis of proteins. Separation efficiency was compared to a hydrophobic poly(dimethylacrylamide-*co*-allylglycidyl ether) (epoxy-PDMA) polymer solution. The structures of these polymers are shown by Figure 1.13.

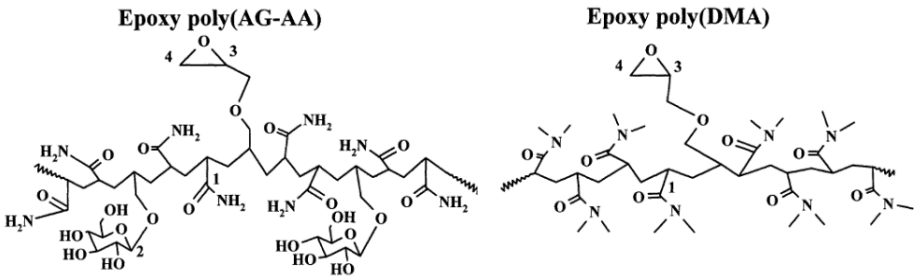

Figure 1.13. Structures of the epoxy polymers [25].

The authors used EOF measurements of a neutral marker (benzyl alcohol) to determine the effectiveness of the coatings. While the EOF mobility was lower (~1.5 x 10^{-9} m^2 V^{-1} s^{-1}) for the epoxy-poly(AG-AA), the coating showed stability for only 20 h, whereas the epoxy-PDMA coating (~4.0 x 10^{-9} m^2 V^{-1} s^{-1}) was proven to be stable for over 40 h before it needed to be regenerated. This enhanced stability is due to the more hydrophobic nature of the epoxy-PDMA meaning that it is more strongly adsorbed to the capillary surface and is therefore not easily removed by the aqueous buffer. Hydrophilic polymers, on the other hand, require polymer in the run buffer. This can be avoided by the inclusion of epoxy groups on the polymer which increases the affinity for the surface. Without the use of polymer in the buffer, the coating requires more frequent regeneration, but the repeatability can be improved [25].

A cationic polymer of bis(3-aminopropylamino)ethane (polyE-323) was synthesised by Hardenborg *et al.* [91] for the surface modification of fused-silica capillaries to separate four basic proteins (α-chymodrypsinogen A, ribonuclease A, cytochrome c, lysozyme). Capillaries were pre-treated by flushing with NaOH (1 M) for 30 min and Milli-Q water for 3 min. The capillary was coated by flushing with polymer solution (non-purified polyamine reaction mixture in acetic acid (0.2 M)) for 1 min and allowing the solution to stand inside the capillary for 1 hr before flushing with buffer (ammonium acetate) for 5 min. The coating procedure was repeated every 5 days to regenerate the coating. PolyE-323 can strongly interact with the surface due to the high density of positive charges available, which are also responsible for reversing the EOF (the EOF becomes anodic). The EOF was investigated between pH 4 - 8 and compared to a bare fused-silica capillary. The EOF increased with increasing pH for the bare capillary, whereas the polyE-323 coated capillary had a consistent EOF across this range (shown by Figure 1.14). Extreme pH conditions were not tested for this polymer, nor was there any mention of the EOF of the coating at pH 9. The EOF with the coated capillary was proven to be repeatable for ~60 injections (0.8 % RSD).

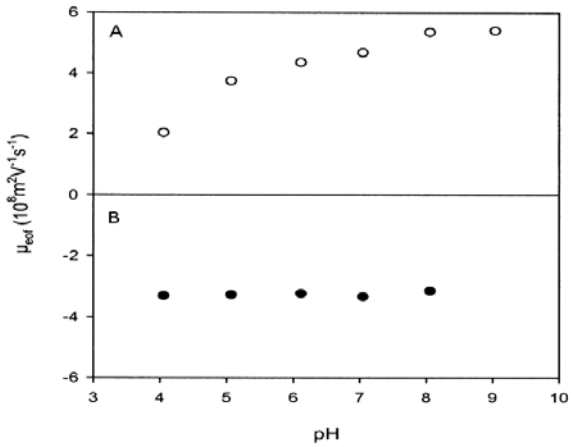

Figure 1.14. Plot of EOF mobility versus pH for a bare fused-silica capillary (A) compared to a polyE-323 coated capillary (B). Adapted from [91].

While creating a positively charged surface is ideal for suppressing and/or reversing the EOF, a high positive charge density, in this case, will not show pH dependency and hence these coatings would not be able to easily resolve negatively charged (or acidic) analytes. Yang *et al.* [92] showed that a cationised hydroxyethylcellulose (cat-HEC) polymer (250 000 g mol^{-1}) is capable of suppressing the EOF when physically adsorbed onto a fused-silica capillary

surface. The cationic property of the cat-HEC polymer allows for the formation of ionic bonds with the deprotonated capillary surface, and any remaining protonated silanol surface groups can hydrogen bond to the HEC. This provides a stable and highly positive surface capable of reversing the EOF. Due to high positive density of the surface, this coating is suitable for the R_s of basic proteins which are repelled by the surface, however, it is not suitable for the separation of acidic proteins which would be attracted to the surface charge and result in peak tailing and insufficient R_s. The coating was developed for the separation of basic proteins and showed a reduction in protein adsorption to the surface. Prior to coating, the capillary was pre-treated with NaOH (0.1 M) for 20 min and deionised water for 10 min. The polymer was dissolved in buffer (0.2 % w/v) and flushed through the capillary for 10 min and left to stand for a further 10 min. Finally the capillary was filled with buffer for 10 min. cat-HEC was synthesised from HEC with varying cationic strengths (shown by Scheme 1.9).

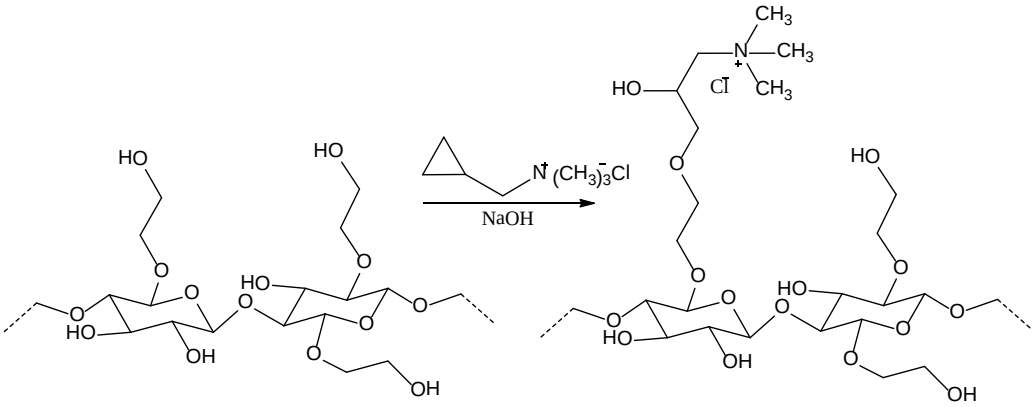

Scheme 1.9. Synthesis of cat-HEC from HEC. Adapted from [92].

The EOF mobility at varying pH (2 - 10) was investigated for three cat-HEC polymers. When compared to the bare fused-silica capillary, the EOF for the HEC coated capillary is reduced and independent of pH, but is still cathodic. Using cat-HEC polymers results in a reversal of EOF (anodic EOF) due to the high density of positive charges on the surface. This anodic EOF was observed at all pH values and was relatively independent of pH. This indicated that the surface was strongly positive and the higher pH values were unable to deprotonate the surface. The cat-HEC showed an improved repeatability for protein t_m (< 1 % RSD) when compared to HEC coated capillaries (2.45 - 3.56 % RSD), supporting the statement that the surface was stabilised by the ionic bonds [92].

The use of copolymer solutions has shown promise for analyte separations due to the potential for tailoring the copolymer composition for specific analyte interactions [52]. The other advantage of using copolymers is the possibility of creating a polymer with hydrophilic character from one monomer (increasing the solubility and potentially decreasing viscosity) and high adsorption properties from the other monomer [138].

Gonzalez *et al*. [77] have developed a dynamic physically adsorbed coating method based on the copolymer poly(*N*,*N*-dimethylacrylamide-*co*-ethylpyrrolidine methacrylate) (PDMA-*co*-PEPyM) (0.1 mg mL^{-1}, M_w not specified) for the separation of basic and acidic proteins. The ethylpyrrolidine methacrylate (EPyM) adds cationic character to the polymer and was ionised at low pH's to create a positive surface charge. Whilst the pKa of EPyM is not known, it is estimated to be approximately 10 owing to the pyrrolidine ring, which explains the surface behaviour at varying pH. PDMA is reasonably hydrophobic and has a good affinity for the surface, making this copolymer an effective coating agent [77]. Investigation into the EOF showed a reduction in the EOF mobilities using the coated capillary when compared to the bare capillary. The authors also found that they could moderate the surface charge by changing the buffer pH, with a near linear trend of EOF mobility versus pH. This moderation can be further tailored by controlling the ratio of EPyM to PDMA. Figure 1.15 shows the EOF mobilities for coated and bare capillaries, presenting the observed trends.

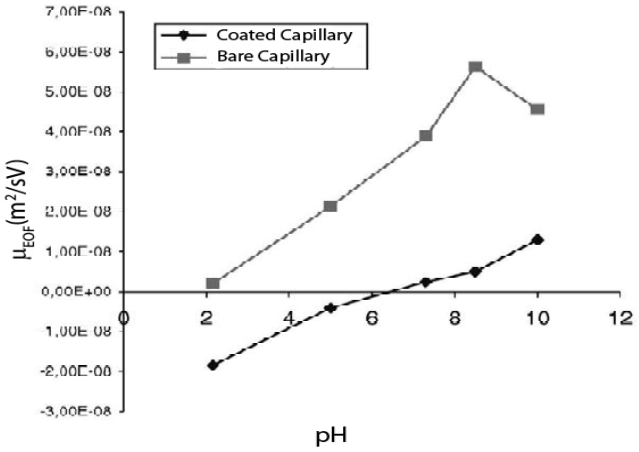

Figure 1.15. EOF mobility versus pH for bare and PDMA-*co*-PEPyM coated fused-silica capillaries [77].

The EOF was anodic under acidic pH, cathodic under basic pH and almost zero at pH 6 - 7. These results indicate that the negative silanol groups are diminished by the application of the positively charged polymer. The authors reported RSD values of 0.75 % (intraday, n = 5) and 3.90 % (interday, n = 15) for the t_m of basic proteins using this coating [77].

A further study using this copolymer by Erny *et al.* [80] separated basic proteins under a negative polarity. The positive surface charge produced as a result of the copolymer coating reduced the adsorption of the proteins onto the capillary walls and, like Gonzalez *et al.* [77], Erny *et al.* [80] observed a reduction in the EOF which the authors attributed to the shielding effect of the copolymer (shown by Figure 1.16). Additionally, the authors showed that the excess positive charge from the non-bound (free) pyridyl groups of EPyM on the capillary surface could be regulated by altering the amount of EPyM in the copolymer. The authors reported % RSD values (n = 3) for the EOF mobilities to be less than 2 % for all coatings. The repeatability was improved at low pH when compared to the bare capillary, however, the opposite was observed at pH values above 6.9 [80].

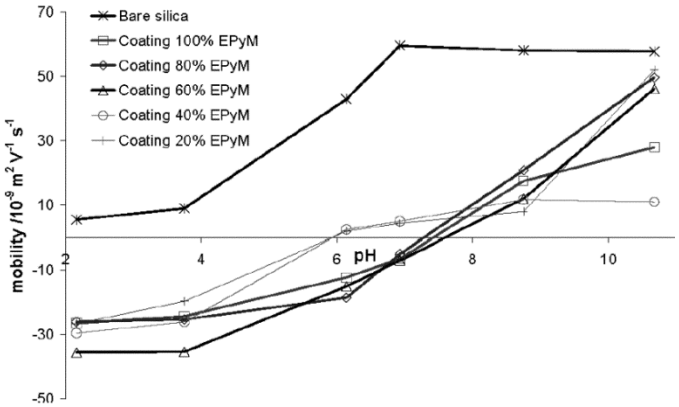

Figure 1.16. EOF mobility versus pH for bare and PEPyM-*co*-PDMA coated fused-silica capillaries [80].

A method developed by Bernal *et al.* [79] also has the advantage of keeping the polymer out of the run buffer. The authors synthesised poly(ethylpyrrolidine methacrylate-*co*-methyl methacrylate) (PEPyM-*co*-PMMA) copolymers (25/75, 50/50, 75/25) to physically adsorb to the capillary surface for enhanced separation of basic proteins (bovine cytochrome *c*, horse cytochrome *c*, and ribonuclease A) and nucleosides (dA, dT, dC, dG, and mdC). The structure of PEPyM-*co*-PMMA can be seen in Figure 1.17.

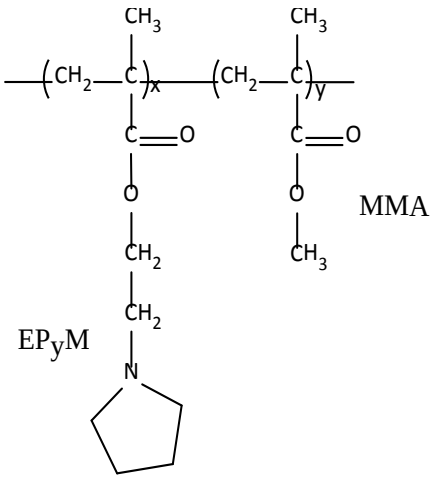

Figure 1.17. Structure of PEPyM-*co*-PMMA copolymer. Adapted from [79].

The hydrophobic nature of the polymer increases its affinity for the surface and hence the lifetime of the coating as it is not easily removed from the surface by the aqueous buffer. Capillary coating was achieved by first dissolving the copolymers in formic acid (100 mM) and ammonium hydroxide (100 mM), and diluting in ethanol or acetone to a final polymer concentration of 1 mg mL^{-1} [79]. Investigation into the monomer ratios showed that, like Erny *et al*. [80], they were able to regulate the surface charge. Analysis of the EOF showed that at acidic pH the amine is ionised, creating a global positive charge and hence an anodic flow. As the pH is increased to basic, there are less positive charges on the surface, leaving the remaining negative silanol groups to predominate, creating a cathodic flow. When compared to the bare capillary, the EOFs were reduced at acidic and basic pH. Interestingly, at neutral pH there was no notable difference between the bare and coated capillary due to the neutral charge of the polymer being unable to change the overall surface charge. Polymer dissolved in ethanol was more successful at suppressing the EOF than using the polymer dissolved in acetone which would most likely be due to a better surface coverage using ethanol. PEPyM-*co*-PMMA is more soluble in acetone and during the coating process may not adsorb from the solution onto the capillary as easily. According to Madabhushi [54], polymers are more effectively physically adsorbed from solution when the solution used is a poor solvent, compared to a good solvent. A 50/50 PEPyM-*co*-PMMA (39 900 g mol^{-1}) in acetone (1 mg mL^{-1}) was chosen as the coating for analysis of proteins and nucleosides. The authors reported high repeatability for

same-day (< 1.9 %) and inter-day (< 0.5%) injections for the μ_{EOF} of the coatings performed at 540.5 V cm^{-1} [79].

Bernal *et al.* [81] then went on to develop a pH tuneable polymer surface for the separation of proteins, nucleotides and organic acids. The authors synthesised a cationic poly(*N*,*N*-dimethylacrylamide-*co*-4-(ethyl)-morpholinemethacrylamide) (PDMA-*co*-PMAEM) copolymer to suppress the EOF and reduce the adsorption of analytes onto the capillary walls. The EOF mobility was investigated at pH 2 - 11, showing a reduction in EOF at all pH values when compared to the bare fused-silica capillary. The EOF was cathodic from pH 7 - 11 and anodic between pH 2 and 5, with a near-zero EOF at pH 6. The EOF can be tailored by changing the amount of PMAEM in the copolymer (i.e., changing the cationic strength). A higher percentage of PMAEM reverses the EOF to a greater extent at low pH, but under basic conditions there is no observable trend. The cationic properties of the polymer create a strongly positively charged surface under acidic pH and weakly positively charged under basic pH. These pH tuneable surfaces can be used for the separation of neutral and charged species (both positive and negative) simply by choosing an appropriate buffer and changing the polarity. The intraday % RSD (n = 5) for all coatings was less than 2.3 % indicating a reasonably stable coating [81].

In summary, the use of dynamic physically adsorbed coatings allows for more simplified and repeatable coatings without the need for polymer added to the running buffer, thereby expanding the range of useful polymers to encompass hydrophilic and hydrophobic polymers. The application is no longer limited by solubility meaning that the high affinity of hydrophobic polymers for a deprotonated capillary surface can be exploited to create a stable, longer lasting surface.

1.6 CE separation of short fragments of DNA

This thesis involves the separation of short fragments of dsODNs and AS-ODNs in free solution on capillaries coated with hybrid cationic copolymers (see Chapters 5 - 7). Therefore this section introduces the relevant literature involving CE separations of ODNs (both ss and ds) on modified capillaries.

Most of the focus on separation of short strands of DNA (along with larger DNA fragments) has been on the ss form and consequently there is limited literature on short dsDNA fragments. The most common way of separating shorter fragments of DNA is by using sieving media; either gels or entangled polymer solutions ($c > c^*$). Although, there have been some investigations on the free solution mobility of low M_w DNA on various surface confined coatings (see Section 1.4.1). Early on, CGE was the most common method for separation of short and large DNA fragments and some of the literature related to low M_w DNA separations can be found in Table 1.2.

Paulus *et al.* [65] developed a CGE method for analysis of the purity of ODNs 20 - 50 b in length using a bis-acrylamide crosslinked PAM covalently attached to the surface via MPTS. Separation of homopolymeric ODNs was achieved on the gel-filled capillaries using Tris (50 mM), boric acid (50 mM), and urea (7 M) run buffer containing PEG (3 %), at 250 V cm^{-1}. The authors also investigated separation of two complementary ss hetero-ODNs differing by 1 b (29 and 30 b). The strands were analysed directly after mixing, and also at 10, 40 and 70 min after mixing (see Figure 1.18 for the separation of the mixture after 10 min hybridisation cycle).

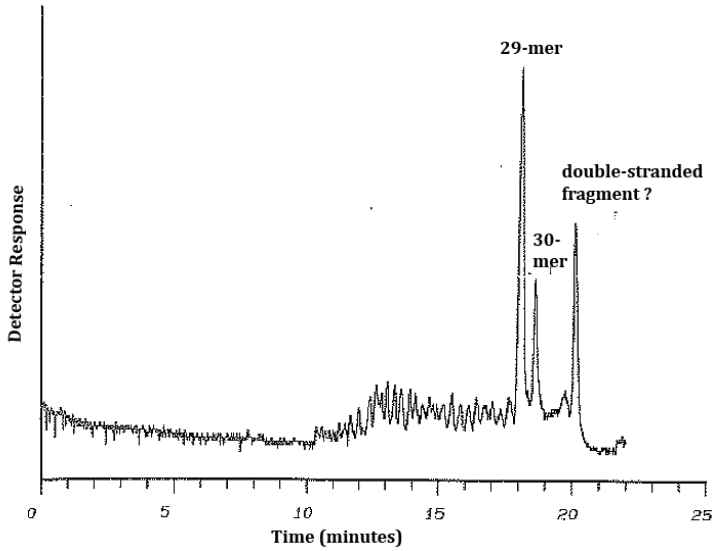

Figure 1.18. CE electropherogram of the separation of two crude, synthetic ssODNs, 29 and 30 b, 10 min after mixing. Separation was performed on a PAM gel capillary (7.5 % T, 3.3 % C) at 250 V cm^{-1} on a 20 cm (L_d), 75 µm id capillary. Adapted from [65].

The presence of two peaks showed that the urea was capable of preventing hybridisation of the two complementary strands on the column directly after mixing; however, analysis of the strands 10 min after mixing showed the presence of a third peak of dsODNs indicating the urea was not capable of denaturing the strands once they hybridised. This peak increased in intensity with increasing time before analysis. The fact that the single-strands could be resolved from the double-strands within 10 - 30 min (along with the single b R_s) indicates that the method could be suitable for analysis of the purity of ODNs. However, CGE capillaries are notorious for low repeatability due to gel degradation and bubble formation, therefore, the same separation efficiency needs to be replicated using regenerative or replaceable polymer solutions.

Khan *et al.* [151] used a semi-dilute HEC (4 %) polymer-buffer (TAPS (25 mM) containing urea (7 M), pH 7) solution as sieving media to separate ODNs ($p(dA)_{12-18}$, $p(dA)_{19-24}$ and $p(dT)_{12-18}$) on a DB-17 (methyl silicon (50 %), phenyl silicone (50 %)) coated capillary. Migration order was from shortest to longest and the use of semi-dilute polymer solution promoted polymer entanglement creating a mesh for the ODNs to traverse. Although the M_w of the polymer was not known, according to Viovy *et al.* [34] the c^* of high M_w HEC (192 000 g mol^{-1}) was ~0.16 % (calculated using Equation 1.24) which was well below the 4 % used by Khan *et al*. [151].

Chiari *et al*. [38] synthesised copolymers of poly(AG-AA) to be used as dynamic sieving polymer solutions for the separation of ssODNs ($pd(A)_{40-60}$) and dsDNA (pBR322 Hae III) on coated and uncoated capillaries. The dynamic coating and sieving ability was tested using the polymer solution in uncoated capillaries and capillaries with a permanent pre-coat to suppress the EOF. The permanent coatings were prepared by use of an intermediate bifunctional silane (MPTS) used to covalently attach poly(AA-EE) copolymer to the surface [85]. ssODN (40 - 60 b) separation required a higher concentration of poly(AG-AA) (10 %) compared to the larger dsDNA (51 - 587 bp) fragment mixture (6 %). The EOF suppression was greater for the coated capillaries resulting in reduced t_m; however, the repeatability of the coating was poor in comparison to the uncoated capillary which used PDMA in the polymer solution to suppress the EOF. The repeatability (n = 20) for the

ODN t_m was between 0.5 % and 0.51 % for the dynamic coating, and 1.07 % and 1.26 % for the permanent coating. The dynamic sieving ability of this copolymer was sufficient for separation of short and long fragments at varying polymer solution concentrations [38] (all presumed to be greater than *c** and entangled).

Polymer solutions have proven to be very useful for separations of DNA of any length. However, some polymers are not as soluble in aqueous buffers, and hence their use as sieving media is restricted. Sjödahl *et al.* [152] used an organic solvent as the liquid base for CE separation of ODN mixtures ($pd(A)_{12-18}$ and $pd(A)_{40-60}$). Two polymer sieving solutions were prepared; one consisted of C16-derivatised 2-hydroxyethyl cellulose (C16-HEC, 5 % w/v) in *N*-methylformamide (NMF) containing ammonium acetate (50 mM). The second solution was a polymer matrix consisting of C16-HEC (4 % w/v) and PVP (5 % w/v). The coatings were prepared by filling the capillary with the polymer mixture and then cutting them to size. C16-HEC had enhanced solubility due to the c16 moieties. These moieties also assisted in strengthening the polymer entanglement giving rise to a greater resistance to shear force from migrating analytes. This method was operated in the semi-dilute to concentrated range in which the $c > c^*$, promoting polymer entanglement [152]. Depending on the degree of entanglement, separation would be based on either BRF (highly entangled, $c >> c^*$) or CR (moderately entangled, $c > c^*$).

Very recently, Li *et al.* [66] analysed ssODNs using a semi-dilute/concentrated low M_w PEG polymer solution in an LPA (covalently attached) pre-coated capillary. Prior to each run, the LPA-coated capillary was preconditioned with buffer (25 mM TBE, pH 8) followed by treatment with PEG (35 000 g mol^{-1}, 20 % w/v in buffer) polymer solution as a sieving matrix. Single b R_s of ssODNs 10 b - 20 b was achieved in under 32 min using 398.4 V cm^{-1} and UV detection at 254 nm [66]. The migration order was from shortest to longest strands. At such high concentrations (above *c**), polymer entanglement occurs, allowing for size-based separation. Depending on the degree of entanglement, separation is based on the BRF model ($c >> c^*$, high entanglement) or the CR model ($c > c^*$, moderate entanglement).

1.7 Summary

The successful CE separation of DNA is based on a highly diverse range of parameters, including DNA length and base pairing (i.e., ss form or ds form); and polymer concentration and M_w. Therefore, the migration of DNA is heavily dependent on its size, along with the M_w and concentration of the polymer involved, whether it be confined to the surface or acting as a sieving medium. As short strands of DNA are rod-like and non-free draining, they exhibit different migration patterns in free solution, when compared to sieving solutions. Sieving polymer solutions provide obstacles to alter the mobility of the DNA based on size which results in the shorter strands having the greater mobility as they can more easily navigate the pores created by the entangled polymer chains; conversely, operating in free solution causes a migration that is based predominantly on the charge, and for DNA strands smaller than the p_{DNA}, the result is a larger (higher charged) species possessing a greater mobility. Unfortunately, free solution electrophoresis (as well as electrophoresis in sieving solutions) is highly influenced by the EOF, which in the case of DNA analysis (negatively charged species), is detrimental to separation. It is therefore necessary to suppress the EOF to enhance DNA migration.

The work described in this thesis uses a dynamic coating from a dilute polymer solution confined to the surface to suppress the EOF. The aim is not to eliminate the EOF entirely, but to utilise the weak cathodic flow to improve the R_s of fragments. In order to achieve this, it is necessary to use a dilute solution so that the physically adsorbed polymer chains can form individual globules on the surface to create a more uniform coating. The concentration of the polymer solution also controls the viscosity of the EDL which influences the EOF. As the polymer is adsorbed to the surface, the viscosity of the EDL increases, and the ions become less mobile. The use of a dilute solution increases the viscosity while still allowing for some ion mobility in the EDL and hence a weak cathodic EOF. Analysis of short strands of dsODNs on the coated capillary (in free solution) indicates that the chosen polymer and concentration is sufficient for the effective control of the EOF and R_s of the strands.

2 Experimental

2.1 Synopsis

This chapter outlines the materials and methods used throughout this thesis. All relevant experimental details for the polymer synthesis, sample preparations (ODNs, PS-ODNs and polymer solutions) and instrumentation used are described herein.

2.2 Materials

This section details all reagents and chemicals used in this study for polymer synthesis and ODN and PS-ODN sample preparation.

2.2.1 Reagents for polymer synthesis

All reagents used for polymer synthesis can be found in Table 2.1 which also details any specific storage or preparation required before use.

Table 2.1. Reagents and solvents used for polymer synthesis.

NAME & PURITY	MANUFACTURER	ADDITIONAL INFO.
4,4'azobis(4-cyanovaleric acid) (ACPA), ≥ 98 %	Sigma-Aldrich, Australia	Used as purchased
Aluminium oxide (basic alumina)	Sigma-Aldrich, Australia	Used as purchased
Benzoyl peroxide, ≥ 98 %	Sigma-Aldrich, Australia	Used as purchased
Chloroform, ≥ 99 %	Sigma-Aldrich, Australia	Used as purchased
2-cyanopropyl-2-dithiobenzoate (CPDB), ≥ 97 %	Strem Chemicals, MA, USA	Used as purchased
2-(diethylamino)ethyl methacrylate (DEAEMA), ≥ 99 %	Sigma-Aldrich, Australia	Removed inhibitor
Dimethylformamide (DMF), ≥ 99 %	Sigma-Aldrich, Australia	Used as purchased
Hexane, AR grade	Ajax Finechem Pty Ltd, Australia	Distilled before use
N-(2-hydroxyethyl)-2-pyrrolidine (EPy), ≥ 99 %	Sigma-Aldrich, Australia	Used as purchased
Magnesium sulphate ($MgSO_4$), anhydrous	BDH Lab Supplies, England	Used as purchased

NAME & PURITY	MANUFACTURER	ADDITIONAL INFO.
Methacryloyl chloride, ≥ 97 %	Sigma-Aldrich, Australia	Used as purchased
Methanol, AR grade	Ajax Finechem Pty Ltd, Australia	Used as purchased
Methyl methacrylate (MMA), ≥ 99 %	Sigma-Aldrich, Australia	Inhibitor removed prior to reaction by running through a column of basic alumina under nitrogen at 0 ^{o}C.
Silica gel, powder	Grace Davison Discovery Sciences, Australia	Used as purchased
Sodium hydroxide (NaOH), pellets	Ajax Finechem Pty Ltd, Australia	Dissolved in Milli-Q water to desired concentration
Tetrahydrofuran (THF), AR grade	Ajax Finechem Pty Ltd, Australia	Used as purchased
Toluene, ≥ 99.8 %	Sigma-Aldrich, Australia	Used as purchased
Triethylamine (TEA), ≥ 99 %	Sigma-Aldrich, Australia	Used as purchased

2.2.2 Chemicals

All other chemicals used in this study can be found in Table 2.2 which also details any specific storage or preparation required before use.

Table 2.2. Chemicals used in this study.

NAME & PURITY	MANUFACTURER	ADDITIONAL INFO.
Acetone, AR grade	Ajax Finechem Pty Ltd, Australia	Used as purchased
Acetone, high performance liquid chromatography (HPLC) grade	Scharlau Chemie, Spain	Filtered through 0.45 µm syringe filters prior to use for gel permeation chromatography (GPC)
Ammonium hydroxide (aqueous ammonia), ACS grade, 28.0 % - 30.0 % NH_3 in H_2O	Sigma-Aldrich, Australia	Diluted in Milli-Q water to desired concentration
Boric acid, for electrophoresis, ≥ 99.5 %	Sigma-Aldrich, Australia	Dissolved in Milli-Q water to make buffer solutions
Chloroform, deuterated ($CDCl_3$), 100 % (99.96 atom %), with tetramethyl silane (TMS), 0.03 % (v/v)	Sigma-Aldrich, Australia	Used as purchased
Dimethylsulphoxide, deuterated (d6-DMSO), ≥ 99.9 %	Cambridge Isotope Laboratories Inc., USA	Used as purchased
Ethanol, AR grade	Ajax Finechem Pty Ltd, Australia	Filtered through 0.45 µm syringe filters prior to use for CE
Formic acid, ACS reagent, ≥ 96.0 %	Sigma-Aldrich, Australia	Diluted in Milli-Q water to desired concentration

NAME & PURITY	MANUFACTURER	ADDITIONAL INFO.
Hydrochloric acid (HCl), AR grade, 36 % in H_2O	Ajax Finechem Pty Ltd, Australia	Diluted in Milli-Q water to desired concentration and filtered through 0.45 µm syringe filters prior to use for CE
Milli-Q water	Not Applicable	Prepared by filtering through resin membrane filters to a resistivity of 18 MΩ cm using a Labconco Waterpro PS. This water was used for all dilutions and aqueous solutions
Sodium chloride (NaCl), BioXtra, ≥ 99.5 %	Sigma-Aldrich, Australia	Used as purchased
Tris-borate (100 mM)/urea (7 M) buffer	Biolab, Australia	pH adjusted using NaOH (1 M) or HCl (1 M) and filtered through 0.45 µm membrane filters
Tris(hydroxymethyl)amino methane (Tris), for electrophoresis, ≥ 99.9 %	Sigma-Aldrich, Australia	Dissolved in Milli-Q water to make buffer solution

2.2.3 DNA samples

2.2.3.1 ssODNs

All ssODNs were purchased from Geneworks, Adelaide, Australia, which were synthesised with 200 nmol starting synthesis scale and purified and de-salted by size exclusion chromatography (SEC) to transfection grade. Table 2.3 details the sequences of the ssODNs and their relative melting temperatures (T_m) and M_w. Initial sequence of the 16 base strands was chosen at random and built upon for the larger strands. How the same base sequence affected separation of different sized strands was investigated, along with the sequence dependence using a 16 bp strand comprising of an entirely different and non-complementary sequence.

Table 2.3. ssODNs used in this study.

BASE #	CODE	SEQUENCE	T_m (^oC)	M_w (g mol^{-1})
16	5'-TTC(16)	5'-TTC TGC TTC TGT CCG G-3'	45.9	4830.2
16	5'-CCG(16)	5'-CCG GAC AGA AGC AGA A-3'	45.9	4933.3
16	5'-CAT(16)	5'-CAT GCA ACG TAC TAG C-3'	43.4	4850.2
16	5'-GCT(16)	5'-GCT AGT ACG TTG CAT G-3'	43.4	4912.3
17	5'-TTC(17)	5'-TTC TGC TTC TGT CCG GC-3'	49.5	5119.4
17	5'-GCC(17)	5'-GCC GGA CAG AAG CAG AA-3'	49.5	5262.5
18	5'-TTC(18)	5'-TTC TGC TTC TGT CCG GCG-3'	52.6	5448.6
18	5'-CGC(18)	5'-CGC CGG ACA GAA GCA GAA-3'	52.6	5551.7
19	5'-TTC(19)	5'-TTC TGC TTC TGT CCG GCG G-3'	55.4	5777.8
19	5'-CCG(19)	5'-CCG CCG GAC AGA AGC AGA A-3'	55.4	5840.8
20	5'-TTC(20)	5'-TTC TGC TTC TGT CCG GTC GG-3'	55.9	6082.0
20	5'-CCG(20)	5'-CCG ACC GGA CAG AAG CAG AA-3'	55.9	6154.1

2.2.3.2 ssPS-ODNs

The ssPS-ODNs and their complementary strands were purchased from Integrated DNA Technologies, Iowa, USA. All ssPS-ODNs were synthesised with 100 nmol starting synthesis scale, and purified and de-salted with PAGE purification. Table 2.4 contains the sequences of the ssPS-ODNs and their relative T_m and M_w. NB: * denotes phosphorothioate bonds in place of phosphodiester bonds (i.e., replacement by a sulphur atom for a non-bridging oxygen in the phosphate backbone of an oligonucleotide. See Figure 7.1 in Chapter 7 for further details).

Table 2.4. ssPS-ODNs used in this study.

BASE #	CODE	SEQUENCE	T_m (^oC)	M_w (g mol^{-1})
16	5'-TTC*16	5'-T*T*C* T*G*C* T*T*C* T*G*T* C*C*G* G-3'	51.5	5071.1
16	5'-CCG*16	5'-C*C*G* G*A*C* A*G*A* A*G*C* A*G*A* A-3'	51.5	5174.2
18	5'-TTC*18	5'-T*T*C* T*G*C* T*T*C* T*G*T* C*C*G* G*C*G-3'	58.0	5721.6
18	5'-CGC*18	5'-C*G*C* C*G*G* A*C*A* G*A*A* G*C*A* G*A*A-3'	58.0	5824.7

*Represents phosphorothioate backbone

2.3 Methods

This section describes the polymer synthetic methods and characterisation techniques used in this work in the preparation of polymer modified capillary surfaces for CE separation of ODNs and PS-ODNs. The optimised CE methods for normal injection and short-end injection (SEI) analysis of these molecules are detailed herein.

2.3.1 Polymer synthesis

All polymers used in this study were synthesised by either conventional free radical (CFR) or reversible addition-fragmentation chain transfer (RAFT) polymerisation. A brief introduction on each of these mechanisms can be found in Sections 3.3 and 3.4 in Chapter 3. All monomers (see Table 2.1) for this study were purchased with the exception of EPyM which was synthesised as described in Section 2.3.1.1.

2.3.1.1 Ethylpyrrolidine methacrylate monomer synthesis

EPyM was synthesised according to the method described by Gonzalez *et al*. [153]. A solution of methacryloyl chloride (20.12 g, 0.193 mol) in chloroform (37.5 mL) was added drop-wise (over 4 h) with stirring, to a solution of EPy (15.09 g, 0.131 mol) and TEA (18.15 mL) in chloroform (112.5 mL). The reaction was allowed to proceed for a total of 6 h under nitrogen at 0 ^{o}C - 5 ^{o}C in an ice bath then allowed to reach room temperature and left to stir overnight under nitrogen. The reaction mixture was then washed with 5 % w/w NaOH, and dried over anhydrous $MgSO_4$. The solvent was removed by rotary evaporation and the crude EPyM was purified via column chromatography using THF as the eluent and silica gel as the stationary phase. The solvent was again removed by rotary evaporation to yield a brown liquid (24.01 g, 94.41 %). The unwashed, washed, crude and purified products were characterised by ^{1}H nuclear magnetic resonance (NMR) spectroscopy (see Section 3.2.1). The pure EPyM was purged with nitrogen, protected from light and stored at or below 4 ^{o}C to inhibit self-polymerisation.

2.3.1.2 Conventional free radical polymerisation

CFR polymerisation was used to synthesise homopolymers and copolymers to be used as capillary surface modifiers for CE separation of ODNs and PS-ODNs. The general reaction mechanism can be found in Scheme 3.2 in Chapter 3.

2.3.1.2.1 Poly(ethylpyrrolidine methacrylate) homopolymer

Poly(ethylpyrrolidine methacrylate) (PEPyM) homopolymer was synthesised by CFR polymerisation of EPyM (3.186 g, 0.017 mol) in THF (15 mL) using benzoyl peroxide (0.090 g, 0.372 mmol) as the radical initiator. The solution was degassed by nitrogen for 20 min, and heated to 60 ^{o}C - 70 ^{o}C for 49 h. The polymer was precipitated in a large excess of hexane (1 L) and filtered under vacuum to yield a yellow-brown powder (0.0727 g, 2.28 %). The solubility of the homopolymer was investigated using polar protic (water, ethanol), polar aprotic (acetone) and non-polar solvents (hexane) (see Section 3.3.1.1). The PEPyM homopolymer was characterised by ^{1}H NMR and Fourier transform infra-red (FTIR) spectroscopies (see Sections 3.3.1.2 and 3.3.1.3, respectively).

2.3.1.2.2 Poly(methyl methacrylate) homopolymer

Poly(methyl methacrylate) (PMMA) homopolymer was synthesised by CFR polymerisation of MMA (2.808 g, 0.028 mol) in THF (15 mL) using benzoyl peroxide (0.090 g, 0.372 mmol) as the radical initiator. The solution was degassed by nitrogen for 20 min, and heated to 60 ^{o}C for 48 h. The homopolymer was precipitated in a large excess of cold methanol (1 L) and filtered by vacuum to yield a white powder (2.751 g, 97.97 %). The solubility of the homopolymer was investigated using polar protic (water, methanol, ethanol), polar aprotic (acetone, THF) and non-polar solvents (hexane, toluene, chloroform) (see Section 3.3.2.1). The PMMA homopolymer was characterised by ^{1}H NMR and FTIR spectroscopies, and GPC (see Sections 3.3.2.2, 3.3.2.3, and 3.3.2.4, respectively).

2.3.1.2.3 Poly(ethylpyrrolidine methacrylate-co-*methyl methacrylate) random copolymer*

PEPyM-*co*-PMMA (25/75 starting molar ratio) random copolymer was synthesised by CFR copolymerisation of EPyM (4.58 g, 0.025 mol) and MMA (7.51 g, 0.075 mol), using a modified method previously described by Bernal *et al*. [79]. The solution was degassed under nitrogen for 1 h. Copolymerisation was carried out in an oil bath at 60 ^{o}C under nitrogen for 48 h, using benzoyl peroxide (0.36 g, 0.0015 mol) as the radical initiator and THF (100 mL) as the solvent. The copolymer was precipitated in a large excess of hexane (1 L) and filtered under vacuum to yield a pale yellow powder (2.078 g, 17.19 %). The solubility of the copolymer was investigated using polar protic (water, methanol, ethanol), polar aprotic (acetone, THF) and non-polar solvents (hexane, toluene, chloroform) (see Section 3.3.3.1). The CFR PEPyM-*co*-PMMA random copolymer was characterised by ^{1}H NMR and FTIR spectroscopies, and GPC (see Sections 3.3.3.2, 3.3.3.3, and 3.3.3.4, respectively).

2.3.1.2.4 Poly(diethylaminoethyl methacrylate-co-*methyl methacrylate random copolymer*

Poly(diethylaminoethyl methacrylate-*co*-methyl methacrylate) (PDEAEMA-*co*-PMMA) (35/65 starting molar ratio) random copolymer was synthesised by CFR copolymerisation of DEAEMA (4.60 g, 0.025 mol) and MMA (4.68 g, 0.047 mol) in toluene (50 mL) using ACPA (0.030 g, 0.11 mmol) as the radical initiator. The solution was degassed with nitrogen for 1 h, and heated to 60 ^{o}C - 70 ^{o}C for 48 h. The random copolymer was precipitated in hexane and filtered under vacuum to yield a coarse, fibrous, white, gel-like polymer which, once dried, was ground into a powder (4.7971 g, 51.7 %). The solubility of the copolymer was investigated using polar protic (water, methanol, ethanol), polar aprotic (acetone, THF) and non-polar solvents (hexane, toluene, chloroform) (see Section 3.3.4.1). The PDEAEMA-*co*-PMMA random copolymer was characterised by ^{1}H NMR and FTIR spectroscopies, and GPC (see Sections 3.3.4.2, 3.3.4.3, and 3.3.4.4, respectively).

2.3.1.3 Reversible addition-fragmentation chain transfer polymerisation

RAFT polymerisation was used to synthesise macro-RAFT agents from PEPyM and PMMA with a dithiobenzoate-terminated moiety for the preparation of a poly(ethylpyrrolidine methacrylate-*block*-methyl methacrylate) (PEPyM-*b*-PMMA) block copolymer. More details on RAFT polymerisation and the reaction mechanism can be found in Scheme 3.7 in Chapter 3.

2.3.1.3.1 Poly(ethylpyrrolidine methacrylate) homopolymer macro-RAFT agent

The dithiobenzoate-terminated PEPyM homopolymer macro-RAFT agent was synthesised by RAFT polymerisation of EPyM (1.062 g, 0.006 mol) in toluene (10 mL) using ACPA (0.010 g, 0.036 mmol) as the radical initiator and CPDB (0.040 g, 0.180 mmol) as the CTA. The solution was degassed by nitrogen for 15 min, and heated to 70 ^{o}C - 75 ^{o}C for 48 h. Samples (100 µL) were taken for NMR analysis at t = 0 h, 24 h and 48 h. The reaction solutions were cooled to room temperature and the solvent was removed via evaporation under nitrogen. The PEPyM homopolymer macro-RAFT agent was then precipitated in hexane and filtered under vacuum to yield a yellow-brown powder (0.3068 g, 28.89 %). The solubility was investigated using polar protic (water, methanol, ethanol), polar aprotic (acetone, THF) and non-polar solvents (hexane, toluene, chloroform) (see Section 3.4.1.1). The PEPyM homopolymer macro-RAFT agent was characterised by ^{1}H NMR and FTIR spectroscopies, and GPC (see Sections 3.4.1.2, 3.4.1.3, and 3.4.1.4, respectively).

2.3.1.3.2 Poly(methyl methacrylate) homopolymer macro-RAFT agent

The dithiobenzoate-terminated PMMA homopolymer macro-RAFT agent was synthesised by RAFT polymerisation of MMA (1.872 g, 0.042 mol) in DMF (8 mL) using CPDB (0.038 g, 0.18 mmol) as the CTA and ACPA (0.0177 g, 0.063 mmol) as the radical initiator. The solution was degassed with nitrogen for 15 min, and heated to 70 ^{o}C for 48 h. The reaction solution was cooled to room temperature and the solvent was removed via evaporation under nitrogen. The mixture was re-dissolved in a small amount of THF (10 mL) followed by precipitation in cold methanol. The isolated PMMA homopolymer macro-RAFT agent was filtered under vacuum to yield a fine pale pink powder (1.415 g, 75.59 %). The solubility

was investigated using polar protic (water, methanol, ethanol), polar aprotic (acetone, THF) and non-polar solvents (hexane, toluene, chloroform) (see Section 3.4.2.1). The PMMA homopolymer macro-RAFT agent was characterised by ^{1}H NMR and FTIR spectroscopies, and GPC (see Section 3.4.2.2, 3.4.2.3, and 3.4.2.4, respectively). The PMMA homopolymer macro-RAFT agent was used for the chain extension of EPyM monomer for synthesis of a PEPyM-*b*-PMMA block copolymer via RAFT polymerisation (see Section 2.3.1.3.3).

2.3.1.3.2.1 Kinetic study of dithiobenzoate-terminated PMMA homopolymer

The kinetics of RAFT polymerisation of MMA with CPDB in DMF was determined using a predesigned multiple pot method (see Section 3.4.2.5 for characterisation). A reaction batch was prepared from MMA (12.5 mL, 11.7 g, 0.116 mol), CPDB (0.199 g, 0.899 mmol), ACPA (0.059 g, 0.211 mmol) and DMF (50 mL), spiked with toluene (2 mL) as an internal standard. A sample at t = 0 was taken for NMR analysis, after which 5 mL of the batch solution was transferred into 8 separate vials and each was purged with nitrogen for 10 min. The study was performed on a heating plate (60 ^{o}C - 70 ^{o}C) with 8 individual solutions heated for a designated period of time each (1, 4, 8, 12, 18, 24, 36 and 50 h). At the completion of each reaction, a liquid sample (100 μL) was taken for ^{1}H NMR spectroscopy analysis (see Section 3.4.2.5) and the DMF solvent was removed via evaporation under nitrogen. PMMA solutions were redissolved in a small amount of THF (5 mL) followed by precipitation in cold methanol. The isolated PMMA homopolymer macro-RAFT agents were filtered by gravity to yield fine pale pink powders.

2.3.1.3.3 Poly(ethylpyrrolidine methacrylate-b-*methyl methacrylate) block copolymer*

PEPyM-*b*-PMMA block copolymer was synthesised by RAFT polymerisation of the dithiobenzoate-terminated PMMA homopolymer and EPyM monomer. Dithiobenzoate-terminated PMMA (0.112 g, 0.015 mmol) was added to EPyM (0.322 g, 0.0018 mol) in DMF (10 mL) with ACPA (0.0056 g, 0.018 mmol) resulting in a 1/115 molar ratio of polymer to monomer. The solution was degassed for 12 min, and heated to 70 ^{o}C for 48 h. The reaction solution was cooled to room

temperature and the solvent was removed via evaporation under nitrogen. The mixture was redissolved in a small amount of THF (10 mL) followed by precipitation in hexane. The isolated PEPyM-*b*-PMMA was filtered under vacuum to yield a yellow-brown powder (0.164 g, 37.8 %). The solubility of the block copolymer was investigated using polar protic (water, methanol, ethanol), polar aprotic (acetone, THF) and non-polar solvents (hexane, toluene, chloroform) (see Section 3.4.3.1). The PEPyM-*b*-PMMA block copolymer was characterised by ^{1}H NMR and FTIR spectroscopies, and GPC (see Sections 3.4.3.2, 3.4.3.3, and 3.4.3.4, respectively).

2.3.1.4 Sample preparation of polymer solutions for CE coating

All polymer solutions were prepared by dissolving the polymer in either ethanol or acetone containing formic acid (0.83 mM) and aqueous ammonia (0.83 mM) according to Table 2.5. The polymer solutions were used as capillary surface modifiers and/or for surface morphology studies using AFM.

Table 2.5. Preparation of polymer solutions for CE.

Polymer	Concentration (mg mL^{-1})	Solvent
CFR PEPyM-*co*-PMMA	0.2, 0.4, 0.8, 1.0, 1.5, 2.0, 24.4, 40.0	Ethanol
RAFT PEPyM-*b*-PMMA	1, 24.4	Ethanol
CFR PEPyM	1.0	Ethanol
CFR PMMA	1.0	Acetone
RAFT PEPyM	1.0	Acetone
RAFT PMMA	1.0	Acetone
CFR PDEAEMA-*co*-PMMA	1.0	Ethanol

2.3.2 Polymer characterisation techniques

The techniques used to characterise the polymer synthesis and solutions are detailed in the following.

2.3.2.1 Nuclear magnetic resonance spectroscopy

NMR spectroscopy is a useful technique for structural determination of a compound by looking at the absorption of energy by a molecule when placed in a magnetic field [154]. NMR spectroscopy was used in this work to characterise/identify the polymers and confirm the structure and purity.

2.3.2.1.1 Instrumentation and sample preparation

Solution ^{1}H NMR spectroscopy data of all samples were recorded on a 400 MHz Bruker Avance NMR Spectrometer. Solid (5 - 10 mg) and liquid samples (100 µL) were dissolved in either $CDCl_3$ (700 µL) or d6-DMSO (700 µL) and placed in a NMR tube. Chemical shifts (δ) were recorded in ppm and referenced to the solvent peak (7.26 ppm for $CDCl_3$ and 2.50 d6-DMSO). All data were exported into Microsoft Excel (2007 or 2010) for re-plotting.

2.3.2.1.2 Data acquisition

All data were acquired using TopSpin NMR Software (Bruker), and the FIDs were imported into MestRec NMR Software (Mestrelab) for Fourier transforming, solvent referencing and peak integration. The transformed data were exported into Microsoft Excel (2007 or 2010) for re-plotting and further analysis.

2.3.2.2 Fourier transform infrared spectroscopy

FTIR spectroscopy relies on the vibration of bonds at characteristic frequencies to identify functional groups in a molecule and is useful for characterisation of known compounds [154]. It is a complementary technique with other spectroscopic methods and can therefore also be useful for structural determination of unknown compounds. In this work, FTIR spectroscopy was used to confirm the known structure of synthesised polymers.

2.3.2.2.1 Sample preparation

FTIR samples were prepared by thin film on NaCl windows. In order to make thin films, the polymer was dissolved in a minimal amount of chloroform. NaCl windows were first cleaned with ethanol and dried before the polymer/chloroform solution was pipetted onto the window, enough to cover, and allowed to dry. The pipetting process was repeated up to a further 5 times.

2.3.2.2.2 Instrumentation and data acquisition

Samples were analysed on a Thermo Electron FTIR spectrometer (Nicolet Avatar 370 PTGS Model) in % Transmittance mode. A background scan of the chamber was taken before each sample was scanned. Data were collected using EZ Omnic software and exported into Microsoft Excel (2007 or 2010) for re-plotting and analysis.

2.3.2.3 Gel permeation chromatography

GPC is a liquid chromatographic technique similar to HPLC, which has been adapted for polymer characterisation to determine the M_w distributions [155]. Separation is based on the hydrodynamic volumes, in which the larger molecules are eluted first, followed by the smaller [155]. GPC was used in this work to determine the M_w and average number molecular mass (M_n), and hence the polydispersity index (PDI) from Equation 2.1 [156-159].

$$\mathrm{PDI} = \frac{M_w}{M_n}$$

Equation 2.1

The PDI gives a measure of the distribution of M_w in a polymer sample. A value of one (unity) means a completely uniform distribution of M_w indicating that all polymer chains within the sample are the same length [160]. A PDI of one signifies a controlled reaction [161]. As the PDI increases above one, the reaction is said to be less controlled and the polymer chain lengths vary in the sample (broadening of the M_w distribution) [160, 161].

2.3.2.3.1 Sample preparation

Samples for GPC were prepared in acetone (HPLC grade) to a concentration of ~1 mg mL^{-1} and filtered through 0.45 µm syringe filters prior to injection. All samples were stored in the fridge at 4 ^{o}C when not in use.

2.3.2.3.2 Instrumentation and data acquisition

All samples were analysed using a Shimadzu HPLC with a Varian PolarGel™ Organic GPC column (300 mm length, 7.5 mm id) and refractive index detection. Acetone was used as the mobile phase with a flow rate 1 mL min^{-1}. All polymer samples were calibrated against a mixture of four PMMA standards (yellow standard - M_w of 1 000, 13 000, 150 000, 800 000 g mol^{-1}; green standard - M_w of 600, 5 700, 80 000, 470 000 g mol^{-1}) and LC Solutions software was used for data acquisition and analysis.

2.3.2.4 Rheometry

Rheometry is used to study the rheology of the polymers, and for this work it was used to determine the viscosity of the polymers in solution (η), along with the solvent viscosity (η_s). Knowing these, the intrinsic viscosity [η] of the polymer was determined from Equation 1.26 (see Section 1.4.5.2.1), and hence the overlap concentration (c^*) and the polymer radius of gyration (R_p) were calculated from Equations 1.27 (see Section 1.4.5.2.1) and 4.1 (see Section 4.2), respectively.

2.3.2.4.1 Instrumentation and sample preparation

Polymer solutions were prepared according to Section 2.3.1.4. No sample preparation was required for the pure ethanol solutions. Solution viscosity measurements for the CFR PEPyM-*co*-PMMA (1 mg mL^{-1}) polymer solution and a solution of ethanol were recorded using an Advanced Rheometer AR2000 with a Peltier plate, 16 mm, 2^{o} cone, at 30 ^{o}C. Enough of each solution was pipetted (individually) onto the Peltier plate to extend to the cone diameter of ~100 mm.

2.3.2.5 Atomic force microscopy

Atomic force microscopy (AFM) was used to determine whether the polymers were capable of adsorbing from solution onto a silicon (Si) surface and to investigate the morphology of the adsorbed polymers on the surface. It was also used to gain an insight into the adsorption mechanism.

2.3.2.5.1 Sample preparation

Polymer samples for AFM (see Table 2.6) were prepared on either untreated p-type (boron doped, 0.0008 Ω cm - 0.0012 Ω cm) Si wafers (Siltronix, France) or oxidised n-type (phosphorous doped, 0.0008 Ω cm - 0.0012 Ω cm) Si wafers (Siltronix, France). In the case of the oxidised wafers, the oxide layer was prepared overnight by tube furnace treatment at 1000 ^{o}C with water vapour going through the tube. Prior to coating, the wafers were cut into squares (1 cm^2 - 2 cm^2) and sonicated in acetone, cleaned with ethanol, followed by a final rinse with Milli-Q water to remove surface contaminants.

The polymer solutions (100 µL) were either spin-coated onto the Si (both untreated and oxidised) surface at 4000 rpm for 60 s, or spotted onto the surface and allowed to dry for ~2 h. The effect of the washing steps during capillary surface coating preparation (see Section 2.3.3.3) was also investigated on untreated Si wafers. The spin-coated polymer wafers were washed by spin-coating with water (60 µL), Tris-borate (100 mM)/urea (7 M) buffer (100 µL) and a final treatment with Milli-Q water (60 µL) to remove any salt ions to avoid any interference with imaging. The spotted polymer wafers were washed by a rinse with water (60 µL), Tris-borate (100 mM)/urea (7 M) buffer (100 µL) and Milli-Q water (60 µL).

Table 2.6. Silicon wafer treatments with polymer solutions.

Polymer	Conc. (mg mL^{-1})	Wafer type	Coating method	Post-coating surface treatment
CFR PEPyM-*co*-PMMA	1.0	Untreated p-type	Spin-coated	-
CFR PEPyM-*co*-PMMA	1.0	Untreated p-type	Spin-coated	Spin-coat wash
CFR PEPyM-*co*-PMMA	1.0	Untreated p-type	Spotted	-
CFR PEPyM-*co*-PMMA	1.0	Untreated p-type	Spotted	Wash by spotting
CFR PEPyM-*co*-PMMA	0.2, 0.4, 0.8, 1.0, 1.5, 2.0, 24.4, 40.0	Oxidised Si, n-type	Spin-coated	-
CFR PMMA	1.0	Oxidised Si, n-type	Spin-coated	-
CFR PEPyM	1.0	Oxidised Si, n-type	Spin-coated	-
RAFT PMMA	1.0	Oxidised Si, n-type	Spin-coated	-
RAFT PEPyM	1.0	Oxidised Si, n-type	Spin-coated	-
RAFT PEPyM-*b*-PMMA	1.0, 24.4	Oxidised Si, n-type	Spin-coated	-

2.3.2.5.2 Instrumentation and data acquisition

AFM was performed on a Bruker Nanoscope IV Multimode SPM operating in tapping mode in air at ~25 ^{o}C. The cantilevers were NSC15 probes (MikroMasch) with spring constants between 30 N m^{-1} - 60 N m^{-1} and resonant frequencies between 310 kHz - 365 kHz. The amplitude set point was 75 % - 85 % to minimise deformation of the sample. Images were taken with a scan speed of 1.5 lines s^{-1} for 512 lines with 512 pts $line^{-1}$. Nanoscope v5.30r3sr3 was used to acquire data which were subsequently analysed using Nanoscope v6 Analysis offline software. All images were flattened, and 2D and 3D height images were created to investigate morphology. Particle analysis was performed on the height images to investigate changing morphologies. The highlighted regions were then analysed using ImageJ 1.45s software (USA) to calculate the % surface coverage.

2.3.3 Capillary electrophoresis

This section details the ODN and PS-ODN sample preparation, capillary coating methods and the optimised CE methods and instrumentation. CE was used to analyse synthetic oligonucleotides (ODNs and PS-ODNs) on a 30 cm (L_d) capillary with reversed (negative) polarity, as well as on an 8 cm (L_d) capillary utilising SEI at positive polarity. The CE method development can be found in the results and discussion chapters (Chapter 5 for reversed polarity, and Chapters 6 and 7 for the SEI).

2.3.3.1 Preparation and quantitation of ODN and PS-ODN stock solutions

All ssODN (see Table 2.3 in Section 2.2.3.1) and ssPS-ODN (see Table 2.4 in Section 2.2.3.2) stock solutions were prepared by dilution in Milli-Q water (500 µL). Ultraviolet-Visible (UV-Vis) spectrophotometry at 260 nm was used to determine the concentration of the stock solution by a 1 in 100 dilution with Milli-Q water (see Section 2.3.3.1.1). Stock solutions were used to prepare ssODN and ssPS-ODN solutions by further dilution in water. Stock solutions were also used to prepare dsODN and dsPS-ODN solutions according to Section 2.3.3.2.

2.3.3.1.1 UV-Vis spectrophotometry

UV-Vis spectrophotometry is a quantitative technique which detects the absorbance of a molecule in response to excitation of electrons at characteristic wavelengths. DNA has strong absorbance at 260 nm and this was exploited to determine the concentration of ssODNs and ssPS-ODNs solutions. A dual-beam Varian Cary 50 UV-Vis Spectrophotometer (Varian Inc, Melbourne, Australia) and a quartz cuvette (self-masking, 0.5 mL, 10 mm pathlength) were used for the analysis. The instrument was zeroed with Milli-Q water and the simple reads program was used to determine the absorbance of ssODN and ssPS-ODN samples at 260 nm.

2.3.3.2 Preparation of ODN and PS-ODN samples for CE analysis

ODN and PS-ODN solutions for CE analysis were prepared from the stock solutions in water according to the following.

2.3.3.2.1 ODN solutions

dsODN samples were prepared in Milli-Q water (to a final concentration of 18.6 µM) from stock solutions of two complementary ssODNs by heating to above the individual ODN melting temperatures (refer to Table 2.3 in Section 2.2.3.1 for individual T_m) for 20 min then cooling to room temperature (~25 ^oC).

2.3.3.2.2 PS-ODN solutions

dsPS-ODN samples were prepared in Milli-Q water (to a final concentration of 8.5 µM) from stock solutions of two complementary ssPS-ODN by heating to the individual AS-ODN melting temperatures (refer to Table 2.4 in Section 2.2.3.2 for individual T_m) for 20 min then cooling to room temperature (~25 ^oC).

2.3.3.3 Capillary preparation

2.3.3.3.1 Bare capillary activation

Bare fused-silica capillaries (50 µM and 75 µM inner diameter (id)) were cut to size (38 cm L_t, 30 cm L_d) using a capillary scoring wafer. Detection windows were prepared by burning off the polyimide coating. Capillaries were activated by flushing with HCl (1 M) for 10 min, Milli-Q water for 5 min, NaOH (1 M) for 10 min, Milli-Q water for 5 min and Tris-borate (100 mM)/urea (7 M) buffer for 10 min, followed by the application of -131.6 V cm^{-1} for 2 min.

2.3.3.3.2 Preparation of capillary physically adsorbed polymer coatings

Bare fused-silica capillaries (50 µM and 75 µM id) were cut to size (38 cm L_t, 30 cm L_d) using a capillary scoring wafer. Detection windows were prepared by burning off the polyimide coating. Capillaries were first activated by following the procedure described in Section 2.3.3.3.1. To prepare the physically adsorbed coating, the capillaries were flushed with the various fabricated polymer solutions

for 3 min, Milli-Q water for 2 min and Tris-borate (100 mM)/urea (7 M) buffer for 3 min, followed by the application of -131.6 V cm^{-1} for 5 min. Between runs, the capillary was washed with polymer solution for 3 min, Milli-Q water for 2 min and Tris-borate (100 mM)/urea (7 M) buffer for 3 min to regenerate the coating.

2.3.3.4 Reversed polarity

All ODN separations were carried out on an Agilent 3D Capillary Electrophoresis Instrument with diode array UV detection at 260 nm (470 nm was used as a control wavelength) and negative polarity (injection at the cathode and detection at the anode) at -131.6 V cm^{-1} (unless otherwise specified). Analysis was performed on fused-silica capillaries with 363 µm outer diameter (od), 30 cm L_d and 38 cm L_t and either 50 µm or 75 µm id (Agilent Technologies, Australia). The capillaries were coated with polymer solutions after pre-treatment (refer to Section 2.3.3.3). The background electrolyte (BGE) was Tris-borate (100 mM)/urea (7 M) buffer at pH 9.0 (unless otherwise specified). The CE system was set to 30 ^{o}C (unless otherwise specified). Samples were introduced hydrodynamically at 5000 Pa for 6 s, followed by an injection of buffer at 5000 Pa for 4 s.

2.3.3.4.1 EOF determination using a neutral marker

EOF data were determined for bare and coated fused-silica capillaries (75 µm id) by two techniques; a current monitoring system (CMS) (see Section 2.3.3.7) and a neutral marker using the CE system. For the neutral marker determination; the EOF velocities (v_{EOF}) and EOF mobilities (μ_{EOF}) of Tris-borate (100 mM)/urea (7 M) buffer were determined using a buffer/water/acetone (20/75/5 % v/v/v) solution as the neutral marker. This was introduced (in triplicate) hydrodynamically at 5000 Pa for 6 s and separated by a positive or negative applied voltage of 263.2 V cm^{-1} at varying temperatures (15 ^{o}C - 50 ^{o}C, at buffer pH 9) and at varying buffer pH (3 - 11 at 30 ^{o}C) with UV detection at 254 nm. The t_m was used to calculate μ_{EOF} in accordance with Equation 1.11 in Section 1.2.3.3. The repeatability of the coating at each measured temperature and pH was determined from the t_m of the buffer/water/acetone solution (n = 3).

2.3.3.5 Short-end injection

All ODN and PS-ODN separations were carried out on an Agilent 3D Capillary Electrophoresis Instrument with diode array UV detection at 260 nm (470 nm was used as a control wavelength) utilising SEI (injection and detection at the anode) and positive polarity at 263.2 V cm^{-1} (unless otherwise specified). Analysis was performed on fused-silica capillaries with 363 µm od, 8 cm L_d and 38 cm L_t and either 50 µm or 75 µm id, (Agilent Technologies, Australia). The capillaries were coated with polymer solutions after pre-treatment (refer to Section 2.3.3.3). The BGE was Tris-borate (100 mM)/urea (7 M) buffer at pH 9.0 (unless otherwise specified). The CE system was set to 35 ^{o}C (unless otherwise specified). Samples were introduced hydrodynamically at 5000 Pa for 6 s, or by electrokinetic injection at 5 kV for 8 s (unless otherwise specified).

2.3.3.6 Data acquisition

All data were acquired using Agilent ChemStation for CE software (Agilent Technologies, Australia), with automatic peak integration for Gaussian fit, normal tangent skim, and classical baseline correction. Integration and signal data were exported into Microsoft Excel (2007 or 2010) for re-plotting and further analysis.

2.3.3.7 Current monitoring system instrumentation and data acquisition for EOF determination

A CMS was used to measure EOF data of the bare and CFR PEPyM-*co*-PMMA random copolymer coated fused-silica capillaries. The bare and coated capillaries were pre-treated in much the same way as described in Section 2.3.3.3 but with the use of a syringe to force the liquid through instead of using the CE instrument. The CMS consisted of a RS 350/5000 V-25W High Voltage Power Supply (Keithley Instruments Inc., USA) and a 6-11/2 DIGIT Precision Multimeter (Keithley Instruments Inc., USA) to measure the resultant current. Two Tris-borate/urea buffer filled vials (pH 9.0) were connected by a 5 cm fused-silica capillary (75 µm id), with two platinum electrodes completing the circuit (see Figure 2.1).

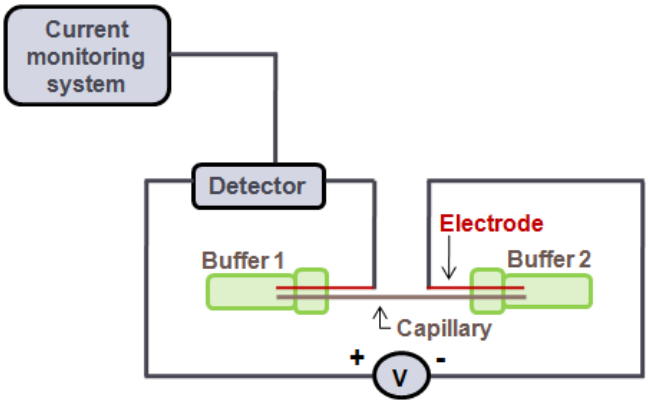

Figure 2.1. Schematic representation of the CMS.

The positive vial contained Tris-borate (20 mM)/urea (1.4 M) buffer, and the negative vial contained Tris-borate (19 mM)/urea (1.3 M) buffer. Labview 8.2 software was used to collect the data. A voltage (60 V cm^{-1} - 100 V cm^{-1}) was applied between the electrodes in the vials driving the flow from the positive to the negative. The time taken for the current to stabilise was used to calculate the EOF velocity (v) according to the Equation 2.2,

$$v = \frac{L_d}{t}$$

Equation 2.2

where t is the time (s) [13]. The μ_{EOF} was then calculated from the v according to the Equation 2.3.

$$\mu_{EOF} = \frac{vL_t}{V}$$

Equation 2.3

3 Polymer synthesis & characterisation

3.1 Synopsis

This chapter describes the synthesis and characterisation of PMMA and PEPyM homopolymers, and PEPyM-co-PMMA and PDEAEMA-co-PMMA random copolymers via CFR polymerisation. The chapter also details the use of RAFT polymerisation to synthesise macro-RAFT CTAs for copolymerisation of a PEPyM-b-PMMA block copolymer. These polymers were used as dynamic coating agents for the CE separations of ODNs and PS-ODNs (see Chapters 5 - 7). Here, the first reported use of RAFT polymerisation to synthesise a block copolymer of EPyM with MMA is described.

3.2 EPyM monomer synthesis

For the synthesis of the CFR PEPyM homopolymer, RAFT PEPyM homopolymer macro-RAFT agent, CFR PEPyM-*co*-PMMA random copolymer, and RAFT PEPyM-*b*-PMMA block copolymer, the synthesis of EPyM monomer was required, as the precursor monomer was not available for purchase. It was therefore synthesised from methacryloyl chloride, EPy and TEA in chloroform according to Scheme 3.1 (refer to Section 2.3.1.1 for the full synthesis method). This scheme shows an esterification reaction in which the acid chloride (methacryloyl chloride) undergoes nucleophilic attack from the EPy via the hydroxyl group. Methacryloyl chloride is extremely reactive and often reacts quite violently with alcohols at room temperature. Therefore the reaction had to be maintained at 0 ^{o}C; this also avoided self-polymerisation of the monomer during synthesis.

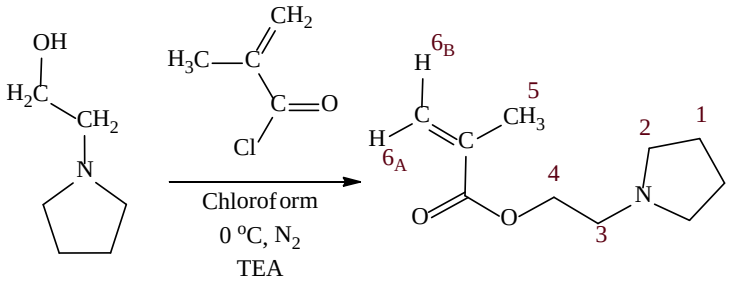

Scheme 3.1. Synthesis of EPyM monomer via esterification.

In methacryloyl chloride the chlorine is an excellent leaving group which, in this reaction, was propelled by the reformation of the carbon to oxygen double bond. This leaves the chlorine free to combine with and remove the proton from the hydroxyl group on the EPy which is observed by the production of a white HCl gas as the by-product. TEA was added to the reaction mixture to quench this HCl by-product [162]. Over the 6 h reaction time, the solution changed from a clear pale yellow to a cloudy brown colour. Washing with aqueous NaOH neutralised any un-reacted HCl to form a salt which was then transferred into the aqueous layer from the chloroform layer. The aqueous layer was then removed and any polymerised material in the organic layer was then removed via column chromatography as it remained adsorbed to the polar stationary phase (silica gel). After purification by column chromatography and solvent evaporation, the resultant EPyM monomer was a brown oily liquid, with typical yields up to 95 %. The crude and purified EPyM were characterised by ^{1}H NMR spectroscopy and tested for purity.

3.2.1 ^{1}H NMR spectroscopy characterisation of EPyM monomer

The EPyM monomer synthesis and purification was monitored using ^{1}H NMR spectroscopy. Figure 3.1(i)-(iv) shows the spectra for the 'unwashed' reaction mixture at t = 6 h, the 'washed' reaction mixture after neutralisation with NaOH, the 'crude' reaction mixture with the solvent removed, and the final 'purified EPyM', respectively. The chemical shifts are shown in Table 3.1.

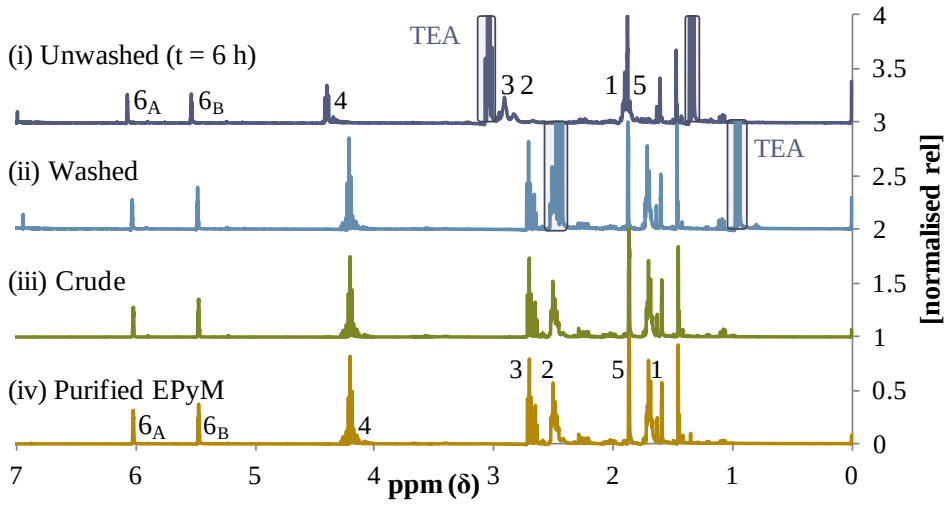

Figure 3.1. ^{1}H NMR spectra for the EPyM monomer synthesis at each stage of the isolation and purification process; unwashed (i), washed (ii), crude (iii), and purified (iv). Data were normalised to the most intense peak in the region of 0 ppm - 7 ppm (excluding the solvent regions).

Table 3.1. ^{1}H NMR peak assignments for the EPyM monomer synthesis at each stage of the isolation and purification process.

*PEAK #	PEAK ASSIGNMENT	CHEMICAL SHIFT (ppm)			
		Unwashed	Washed	Crude	Pure monomer
6_A	C=C**H$_A$**	6.06 - 6.08	6.03 - 6.05	6.02 - 6.03	6.02 - 6.03
6_B	C=C**H$_B$**	5.53 - 5.55	5.48 - 5.50	5.47 - 5.49	5.47 - 5.49
4	C-C**H$_2$**-O	4.37 - 4.42	4.19 - 4.25	4.19 - 4.25	4.18 - 4.24
3	N-C**H$_2$**-C	2.88 - 2.98	2.65 - 2.74	2.65 - 2.73	2.64 - 2.72
2	C-C**H$_2$**-N	2.80 - 2.88	2.49 - 2.54	2.47 - 2.53	2.47 - 2.52
5	C-C**H$_3$**	1.84 - 1.89	1.87 - 1.89	1.86 - 1.88	1.86 - 1.88
1	C-C**H$_2$**-C	1.89 - 1.95	1.68 - 1.74	1.67 - 1.73	1.67 - 1.74

*Peak allocations are shown in Scheme 3.1.

In the unwashed EPyM monomer ^{1}H NMR spectrum (Figure 3.1(i)), the EPyM and TEA chemical shifts had been pushed downfield, meaning the protons were being deshielded. However, once washed (Figure 3.1(ii)) and purified (Figure 3.1(iii)), the chemical shifts moved back upfield due to NaOH neutralisation. TEA was still

present in the washed sample (evidenced by peaks present at ~1 ppm and 2.5 ppm in Figure 3.1(ii)), but was removed during the solvent evaporation. There was little observed difference between the crude (Figure 3.1(iii)) and the pure (Figure 3.1(iv)) product, indicating that the crude EPyM monomer was relatively pure with no observed self-polymerisation during the process. This monomer was thus used for synthesis of CFR PEPyM homopolymer, RAFT PEPyM homopolymer macro-RAFT agent, PEPyM-*co*-PMMA random copolymer and RAFT PEPyM-*b*-PMMA block copolymer. These are covered in the following sections.

3.3 Conventional free radical polymerisation

This section details the CFR synthesis of PEPyM and PMMA homopolymers, and PEPyM-*co*-PMMA and PDEAEMA-*co*-PMMA random copolymers to be used as capillary surface modifiers for ODN and PS-ODN separations. CFR polymerisation is a polymerisation technique that uses radicals to assist in the growth of polymer chains. This reaction requires initiation by a molecule (known as an initiator) which is capable of generating its own radicals and transferring these radicals to the monomer units. CFR polymerisation via vinyl groups is used in this thesis to synthesise homopolymers and random copolymers, and the general mechanism can be seen in Scheme 3.2.

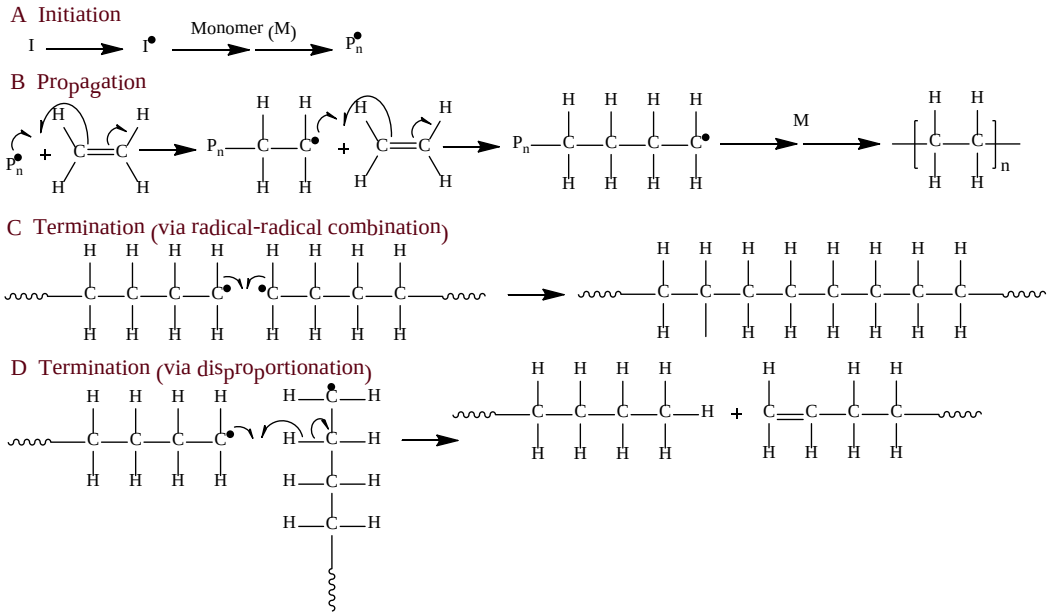

Scheme 3.2. Mechanism for CFR polymerisation via vinyl groups.

The reaction proceeds via a chain mechanism consisting of three mechanistic steps; (1) initiation, (2) propagation, and (3) termination [163]. The initiator undergoes homolytic cleavage by thermal degradation to form radicals, which add across the double bond thus forming an initiator-monomer adduct. This adduct propagates the addition of monomer units to the polymer chain end. Termination occurs via either radical-radical combination (coupling) or disproportionation of two initiator-monomer adducts (the radical on one adduct attacks and removes the β-hydrogen of the neighbouring adduct).

3.3.1 PEPyM homopolymer

PEPyM homopolymer was synthesised by CFR polymerisation of EPyM monomer (previously synthesised in Section 3.2) in THF using benzoyl peroxide as the radical initiator (see Scheme 3.3). Given that the PEPyM homopolymer is hydrophilic due to its weak dipole from the tertiary amine, it is partially polar. Further, the homopolymer also contains an ester group which adds to the polarity. Therefore in order to isolate the PEPyM homopolymer, hexane was used for precipitation. The final product was a yellow-brown powder (2.28 %) (Refer to Section 2.3.1.2.1 for the full synthesis method). The PEPyM was characterised by ^{1}H NMR and FTIR spectroscopies. GPC was not performed due to low yields of the PEPyM homopolymer which was most likely due to an incompatible radical initiator or solvent promoting side-reactions and reducing the monomer conversion [164]. In addition, THF may have formed complexes with the radicals, thereby inhibiting propagation [165, 166].

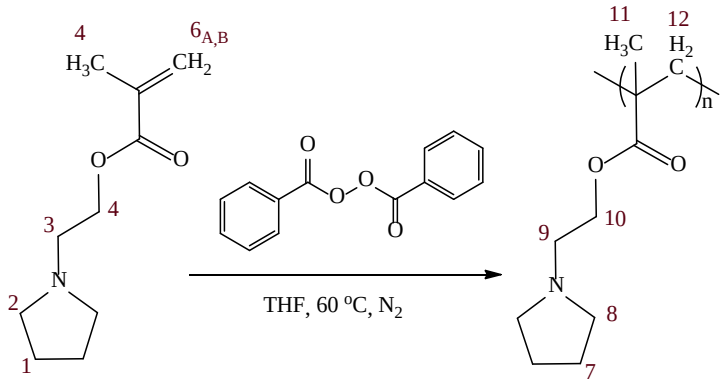

Scheme 3.3. CFR polymerisation of EPyM monomer for synthesis of PEPyM homopolymer.

3.3.1.1 Solubility test of PEPyM homopolymer

After isolation, the PEPyM homopolymer had to be redissolved in order to use it as a dynamic coating for CE capillary modification. Due to obtaining a very low yield of the homopolymer the solubility was only tested using a few solvents of varying polarity, namely acetone, ethanol, water, and hexane. The PEPyM homopolymer was found to have limited solubility in polar protic solvents (such as water and ethanol) as the chains were too large to force their way between molecules in order to disrupt the hydrogen bonding. However, polar aprotic solvents (such as acetone) were capable of dissolving the PEPyM homopolymer. The PEPyM homopolymer did not dissolve in strongly non-polar solvents (hexane), but dissolved slowly in weaker non-polar solvents such as chloroform. Ethanol was therefore used to prepare the PEPyM homopolymer solutions for surface morphology characterisation using AFM (see Section 4.3.1.1) and capillary surface modification (see Section 5.3.4.2).

3.3.1.2 ^{1}H NMR spectroscopy characterisation of PEPyM homopolymer

^{1}H NMR spectroscopy was used to characterise the PEPyM homopolymer at each reaction stage. Figure 3.2(i)-(iii) shows the spectra for the reaction mixture at t = 0 h, t = 48 h, and the isolated PEPyM homopolymer, respectively. The chemical shifts are shown in Table 3.2. Peaks were assigned as per the work of Gonzalez *et al.* [153].

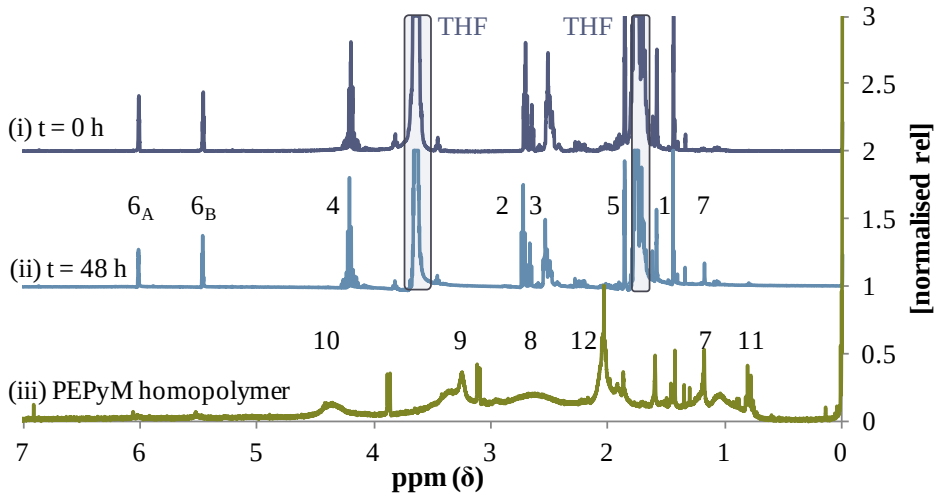

Figure 3.2. ^{1}H NMR spectra for the CFR polymerisation of EPyM monomer at various stages of synthesis of PEPyM homopolymer; t = 0 h (i), t = 48 h (ii), and isolated PEPyM homopolymer (iii). Data were normalised to the most intense peak in the region of 0 ppm - 7 ppm (excluding the solvent regions).

Table 3.2. ^{1}H NMR peak assignments for the CFR polymerisation of EPyM monomer at various stages of synthesis of PEPyM homopolymer.

*PEAK #	PEAK ASSIGNMENT		CHEMICAL SHIFT (ppm) t = 0 h	t = 48 h	Pure polymer
6_A	C=C**H**$_A$	EPyM	6.02 - 6.04	6.02 - 6.04	
6_B	C=C**H**$_B$	EPyM	5.46 - 5.49	5.46 - 5.49	
4	C-C**H**$_2$-O	EPyM	4.16 - 4.29	4.14 - 4.30	
10	C-C**H**$_2$-O	PEPyM			4.19 - 4.60
3	N-C**H**$_2$-C	EPyM	2.64 - 2.74	2.66 - 2.76	
9	N-C**H**$_2$-C	PEPyM			3.18 - 3.52
2	C-C**H**$_2$-N	EPyM	2.46 - 2.55	2.47 - 2.56	
8	C-C**H**$_2$-N	PEPyM			2.40 - 2.90
5	C-C**H**$_3$	EPyM	1.85 - 1.88	1.85 - 1.88	
12	-(C-C**H**$_2$)$_n$	PEPyM			1.84 - 2.14
1	C-C**H**$_2$-C	EPyM	1.67 - 1.74	1.66 - 1.73	
7	C-C**H**$_2$-C	PEPyM		1.17 - 1.19	1.02 - 1.24
11	C-C**H**$_3$	PEPyM		0.78 - 0.82	0.73 - 0.84

*Peak allocations are shown in Scheme 3.3.

At t = 0 h (Figure 3.2(i)), the peaks observed corresponded to EPyM monomer (see Table 3.1) and there were no peaks corresponding to PEPyM, typically observed at the values observed in Table 3.2 ('pure polymer' column); but in particular at ~2 ppm which would be due to the CH_2 groups linking the monomer units (Peak 12 observed in Scheme 3.3). After 48 h of reaction (see Figure 3.2(ii)), some peaks appeared relating to the formation of PEPyM (Peaks 7 and 11), however, these peaks were of very low intensity. The vinyl peaks (6_A and 6_B) (Table 3.2) were still present, although slightly reduced. Once the polymer was isolated (Figure 3.2(iii)), peaks relating to PEPyM were observed and peaks relating to EPyM monomer were diminished, in particular the vinyl peaks between 5.4 ppm and 6 ppm. The homopolymer spectrum (Figure 3.2(iii)) had broader peaks than the corresponding monomer (Figure 3.2(i)) due to a larger number of protons contributing to the resonance peak. There were also a few peaks not associated with the PEPyM homopolymer, and these were most likely trace contaminants. The source, however, was unknown as none of the solvents (hexane, THF), or initiator (benzoyl peroxide) used throughout the process exhibited peaks at these chemical shifts. It was therefore attributed to contaminated deuterated solvent.

^{1}H NMR spectroscopy can be used to observe the tacticity of a polymer in which an isotactic (mm) molecule will have one singlet per unique proton, whereas an atactic molecule will result in multiple peaks (typically doublets for syndiotactic and multiplets for heterotactic) [167]. The stereochemistry/tacticity of the polymer describes the orientation of the repeating units along the polymer chain, and hence the flexibility of the chain. This in turn can affect how the polymer adsorbs onto a surface [168, 169]. It has been observed that a flexible polymer chain can fold or coil onto the surface creating a more uniform layer; whereas a more rigid polymer cannot fold as easily and is more likely to adsorb on the ends, creating a less uniform surface [168, 169]. In general, a polymer can contain both meso (*m*, two identically oriented units in the dyad) and racemo (*r*, 2 units are oppositely oriented) dyads of which the chain can potentially be comprised of *mm* (isotactic), *rr* (syndiotactic), and *mr* (heterotactic) triads (2 adjacent dyads) [167]. Syndiotactic and heterotactic molecules have randomly arranged substituents and are referred to as atactic and, in general, polymers synthesised by free radical polymerisation are atactic. These polymers are more rigid than isotactic polymers due to oppositely oriented units which create steric hindrance. A heterotactic polymer possessing *mr* triads (a mixture of identical and oppositely oriented dyads), has greater flexibility than a syndiotactic polymer (*rr*) with all dyads oppositely oriented. Therefore, the increasing order of flexibility is syndiotactic, heterotactic, and isotactic [168, 169].

From Figure 3.2(iii) it is evident that the isolated PEPyM homopolymer is predominantly heterotactic due to the presence of multiplets [167]. How this affected the surface adsorption is discussed in Chapter 4.

3.3.1.3 FTIR spectroscopy characterisation of PEPyM homopolymer

Figure 3.3 shows an FTIR spectrum of the PEPyM homopolymer. The spectrum shows C-H stretching vibrations (2 bands between 2800 cm^{-1} and 3000 cm^{-1}) and CH_2 bending (~1430 cm^{-1} and very weak peak at ~690 cm^{-1}) corresponding to the CH_2 groups on the EPyM monomer repeating units. CH_3 bending vibrations of the methyl groups were observed at ~1380 cm^{-1}. A C-N stretching vibration between 1230 cm^{-1} and 1250 cm^{-1} confirmed the presence of the *N*-substituted pyrrolidine

ring. Finally, the ester groups were observed as C=O stretching vibrations at ~1720 cm^{-1}, and C-O stretching vibrations between 1100 cm^{-1} and 1150 cm^{-1}. The broad peak between 3100 cm^{-1} and 3650 cm^{-1} can be attributed to the thin film still containing trace amounts of water and thus this vibration is due to hydrogen bonding of the O-H groups.

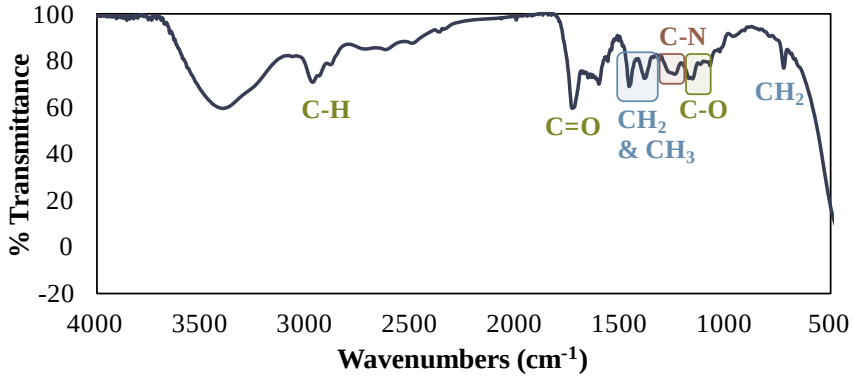

Figure 3.3. FTIR spectrum of PEPyM homopolymer synthesised by CFR polymerisation.

3.3.2 PMMA homopolymer

PMMA homopolymer was synthesised by CFR polymerisation of MMA in THF using benzoyl peroxide as the radical initiator (see Scheme 3.4). Isolation of the polymer yielded a white powder (97.97 %) (Refer to Section 2.3.1.2.2 for the full synthesis method). The PMMA was characterised by ^{1}H NMR and FTIR spectroscopies, and GPC. MMA is a relatively reactive monomer and due to its small, non-bulky size, was easy to polymerise via the vinyl groups. Over time, the reaction mixture increased in viscosity which was an indication of the PMMA homopolymer forming. As the PMMA homopolymer is hydrophobic, the homopolymer was precipitated in cold methanol. PMMA is less capable of hydrogen bonding at high M_w so the use of methanol allows for the unreacted, low M_w monomer to dissolve while the higher M_w polymer can be precipitated out. Carrying out the precipitation in cold solvent ensured complete separation of the monomer from the polymer and this was verified by ^{1}H NMR spectroscopy (Section 3.3.2.2).

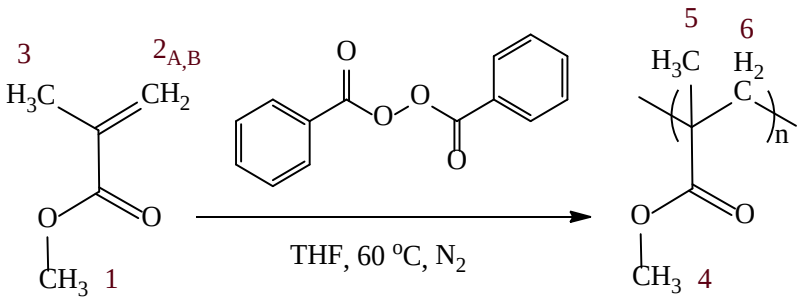

Scheme 3.4. CFR polymerisation of MMA monomer for synthesis of PMMA homopolymer.

3.3.2.1 Solubility test of PMMA homopolymer

After isolation, the PMMA homopolymer had to be redissolved in order to use it as a dynamic coating for the CE capillary modification. PMMA is hydrophobic and relatively non-polar, but it does possess a small dipole moment from the ester group (making it slightly polar) meaning that it will have only limited solubility in both polar aprotic solvents (THF, acetone) and weakly non-polar solvents (toluene, chloroform). However, it was insoluble in polar protic solvents (ethanol, methanol, water) and the strongly non-polar hexane. Therefore, acetone was used to prepare PMMA homopolymer solutions for surface morphology characterisation using AFM (see Section 4.3.1.1) and capillary surface modification (see Section 5.3.4.1).

3.3.2.2 ^{1}H NMR spectroscopy characterisation of PMMA homopolymer

^{1}H NMR spectroscopy was used to investigate the CFR polymerisation of MMA monomer and characterise the final PMMA homopolymer. Figure 3.4(i)-(iii) shows the spectra for the reaction mixture at t = 0 h, t = 48 h, and the isolated PMMA homopolymer, respectively. The chemical shifts are shown in Table 3.3.

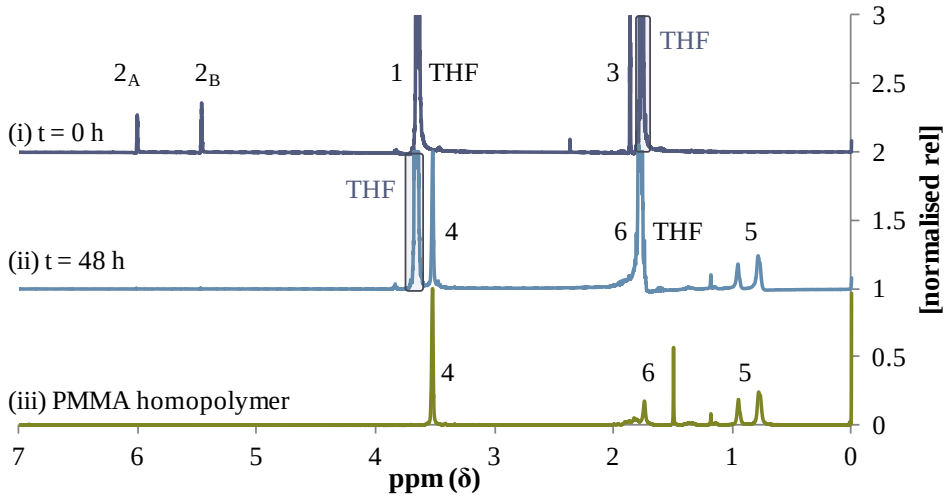

Figure 3.4. ^{1}H NMR spectra for the CFR polymerisation of MMA monomer at various stages of synthesis of PMMA homopolymer; t = 0 h (i), t = 48 h (ii), and isolated homopolymer (iii). Data were normalised to the most intense peak in the region of 0 ppm - 7 ppm (excluding the solvent regions).

Table 3.3. ^{1}H NMR peak assignments for the CFR polymerisation of MMA monomer at various stages of synthesis of PMMA homopolymer.

*PEAK #	PEAK ASSIGNMENT		CHEMICAL SHIFT (ppm) t = 0 h	t = 48 h	Pure polymer
2_A	C=C**H_A**	MMA	6.01 - 6.03		
2_B	C=C**H_B**	MMA	5.47 - 5.49		
1	C**H_3**-O	MMA	~3.67 - 3.68 (behind THF)		
4	C**H_3**-O	PMMA		3.50 -3.56	3.50 - 3.56
3	C-C**H_3**	MMA	1.86 - 1.88		
6	-(C-C**H_2**)$_n$	PMMA		~1.75 (behind THF)	1.70 - 1.92 & 1.49 - 1.51
5	C-C**H_3**	PMMA		0.72 - 1.00	0.90 - 0.99 & 0.73 - 0.83

*Peak allocations are shown in Scheme 3.4.

Figure 3.4(i) shows that at t = 0 h, there were only peaks present for the MMA monomer and THF solvent, indicating that polymerisation had not yet taken place. From Figure 3.4(ii) it can be seen that after 48 h of reaction, the conversion of MMA to PMMA was close to 100 %, as there were no peaks present related to monomer. This was consistent with the 98 % yield achieved upon isolation of PMMA. Once the polymer was isolated (Figure 3.4(iii)), peaks relating only to PMMA were observed indicating high purity (see 'Pure polymer' column in Table

3.3). The peaks between 1.70 ppm and 1.92 ppm (Peak 6) prove the existence of the PMMA homopolymer as they were due to the CH_2 groups linking the repeating monomer units.

A doublet was observed in the aliphatic region (0.5 ppm - 2 ppm) of the isolated PMMA homopolymer (Figure 3.4(iii)) which is due to the tacticity of the polymer [167]. PMMA has been reported to be predominantly syndiotactic and this is represented by the observed doublet peaks. Therefore it is evident from Figure 3.4(iii) that the isolated PMMA homopolymer is predominantly syndiotactic.

3.3.2.3 FTIR spectroscopy characterisation of PMMA homopolymer

Figure 3.5 shows an FTIR spectrum of PMMA homopolymer. The spectrum shows C-H stretching vibrations (2 bands between 2800 cm^{-1} and 3000 cm^{-1}) and CH_2 bending vibrations (730 cm^{-1} - 900 cm^{-1}, and ~1450 cm^{-1}) corresponding to the CH_2 groups connecting MMA repeating units. CH_3 bending vibrations of the methyl and methoxy groups were observed at ~1380 cm^{-1}. The ester groups of the MMA monomer units were observed as C=O stretching vibrations at ~1720 cm^{-1}, and two C-O stretching vibrations between 1100 cm^{-1} and 1150 cm^{-1}. The broad, low intensity peak between 3100 cm^{-1} and 3650 cm^{-1} can be attributed to the thin film still containing trace amounts of water.

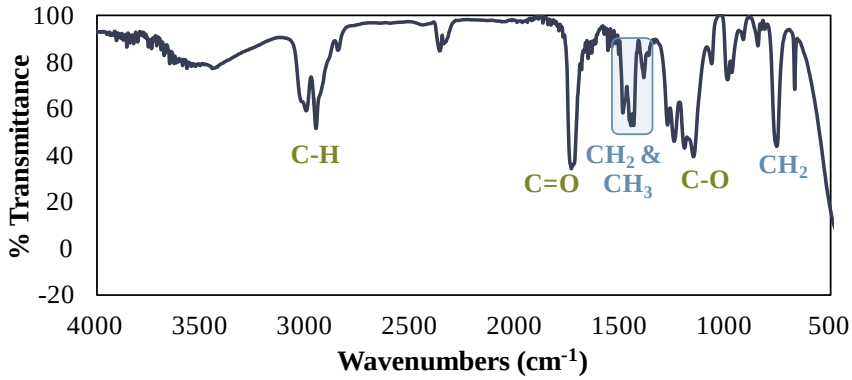

Figure 3.5. FTIR spectrum of PMMA homopolymer synthesised by CFR polymerisation.

3.3.2.4 GPC characterisation of PMMA homopolymer

GPC determined the M_n and M_w of the PMMA homopolymer to be 14 770 g mol^{-1} and 29 272 g mol^{-1}, respectively. The PDI was determined to be 1.98. The PDI was very high, implying that the PMMA was made up of a variety of different polymer

chain lengths. This implied that the reaction was not very controlled and that chain extension occurred randomly.

3.3.3 PEPyM-*co*-PMMA random copolymer

Using a method modified from Bernal *et al*. [79], a PEPyM-*co*-PMMA (25/75 starting molar ratio) random copolymer was synthesised by the CFR copolymerisation of EPyM monomer (synthesised in Section 2.3.1.1 and characterised in Section 3.2) and MMA monomer (see Scheme 3.5). THF was used as the solvent and benzoyl peroxide as the radical initiator. The polymerisation yielded a pale yellow powder (17.19 %) (Refer to Section 2.3.1.2.3 for the full synthesis method). Owing to the fact that the PEPyM-*co*-PMMA random copolymer is both hydrophilic (PEPyM) and hydrophobic (PMMA), isolation of the final product was performed by precipitation in hexane. The PEPyM-*co*-PMMA was then characterised by ^{1}H NMR and FTIR spectroscopies, and GPC.

González *et al.* [153] studied the reactivity of EPyM monomer and MMA monomer during copolymerisation. They discovered that the propagating species ending in EPyM had a greater tendency to react with itself, whereas species ending in MMA preferred to react with the EPyM rather than itself. This behaviour resulted in the formation of random monomer distributions, hence random copolymers are typically formed by the CFR copolymerisation process [153]. Therefore the PEPyM-*co*-PMMA synthesised in the work presented in this thesis should also be random. From Section 4.3 it was observed that the PEPyM units were responsible for adsorption to the surface; therefore, a random distribution of this monomer along the polymer chain should result in a relatively uniform surface.

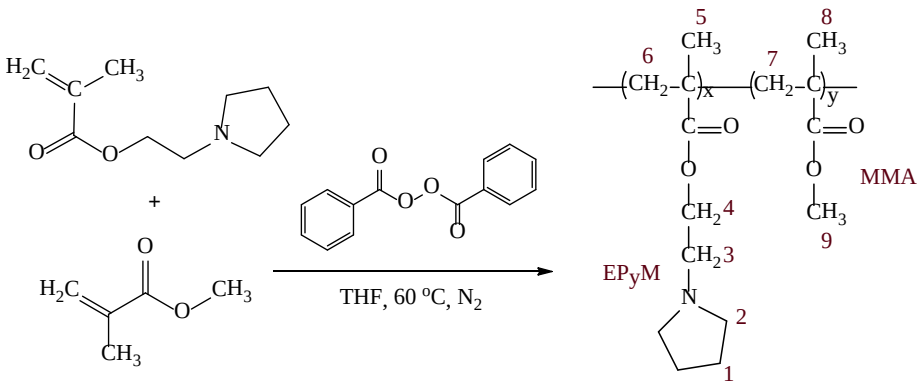

Scheme 3.5. CFR copolymerisation of EPyM monomer and MMA monomer for synthesis of PEPyM-*co*-PMMA random copolymer.

3.3.3.1 Solubility test of PEPyM-co-PMMA random copolymer

After isolation, the PEPyM-*co*-PMMA random copolymer had to be redissolved in order to be used as a dynamic coating for the CE capillary modification. The PEPyM-*co*-PMMA random copolymer was soluble in polar aprotic (THF, acetone), polar protic (ethanol, methanol) and non-polar (chloroform, toluene) solvents (possessed intermediate polar properties). This was due to the PEPyM-*co*-PMMA random copolymer being both hydrophilic and hydrophobic meaning it was insoluble in both strongly polar (water) and non-polar (hexane) solvents; and in these solvents the copolymer solution formed a colloid.

Strong solvents result in less surface adsorption owing to the high copolymer solubility in the solution. Therefore, poor solvents are ideal for preparation of copolymer solutions for surface coatings, as the polymer can more easily adsorb out of solution [54]. Therefore, ethanol was used to prepare the PEPyM-*co*-PMMA random copolymer solution for surface morphology characterisation using AFM (see Section 4.3.1) and capillary surface modification (see Chapters 5, 6 and 7). Furthermore, ethanol was also capable of dissolving the polymer at high concentrations without creating highly viscous solutions which was important in terms of the delivery of the polymer into the capillaries.

3.3.3.2 ^{1}H NMR spectroscopy characterisation of PEPyM-co-PMMA random copolymer

^{1}H NMR spectroscopy was used to characterise the PEPyM-*co*-PMMA random copolymer. Figure 3.6(i)-(iii) shows the spectra for the PEPyM-*co*-PMMA random copolymer, compared to the PEPyM homopolymer, and PMMA homopolymer, respectively. The chemical shifts are shown Table 3.4. Peaks were assigned according to the peak coupling and the work of Bernal *et al.* [79]. For peak assignments of PEPyM homopolymer and PMMA homopolymer refer to Tables 3.2 and 3.3, respectively.

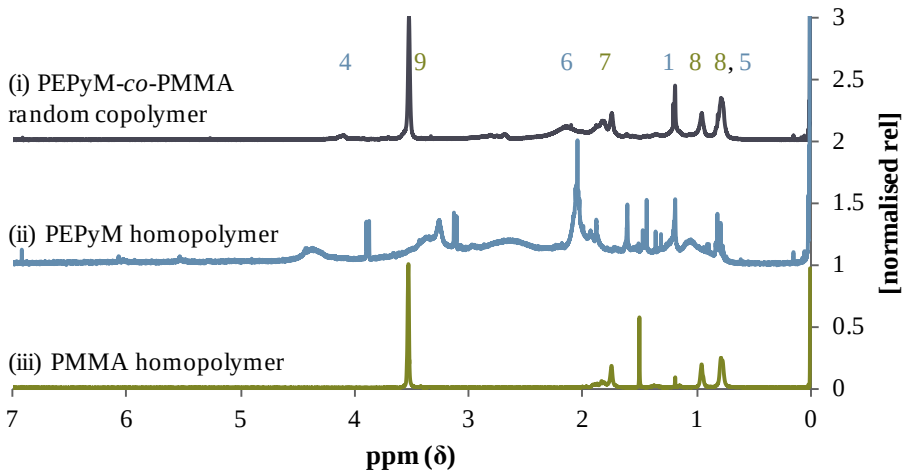

Figure 3.6. ^{1}H NMR spectra of PEPyM-*co*-PMMA random copolymer (i), compared to the PEPyM homopolymer (ii), and PMMA homopolymer (iii), synthesised by CFR polymerisation. Data were normalised to the most intense peak in the region of 0 ppm - 7 ppm.

Table 3.4. ^{1}H NMR peak assignments for the PEPyM-*co*-PMMA random copolymer synthesised by CFR copolymerisation.

*PEAK #	PEAK ASSIGNMENT	CHEMICAL SHIFT (ppm)	
4	C-C**H$_2$**-O	PEPyM	4.07 - 4.20
9	C**H$_3$**-O	PMMA	3.46 - 3.61
3	N-C**H$_2$**-C	PEPyM	2.81 - 2.90
2	C-C**H$_2$**-N	PEPyM	2.66 - 2.82
6	-(C-C**H$_2$**)$_n$	PEPyM	2.00 - 2.32
7	-(C-C**H$_2$**)$_n$	PMMA	1.78 - 1.97
1	C-C**H$_2$**-C	PEPyM	1.16 - 1.24
8	C-C**H$_3$**	PMMA	0.82 - 1.02
5	C-C**H$_3$**	PEPyM	0.70 - 0.82

*Peak allocations are shown in Scheme 3.5.

Isolation of the copolymer yielded a relatively pure product without the presence of either monomers, evidenced by the lack of peaks in the monomer regions, in particular the vinyl region (from 5.4 ppm - 6.1 ppm) (Figure 3.6(i)). Further, the copolymer showed peaks associated with both PMMA homopolymer and PEPyM homopolymer (see Table 3.4), indicating successful copolymerisation. For the copolymer (Figure 3.6(i)), the PEPyM peaks were quite weak in comparison to the PMMA peaks (see Figure 3.6(ii) and (iii)). This was expected given that a smaller quantity of this monomer was used in the synthesis. In addition, peaks 2 and 3 (Table 3.4) were shifted upfield in the copolymer when compared to the homopolymer (see Figure 3.6) meaning that the PEPyM was being shielded by the

electron density of the surrounding molecular orbital. Integration of the PEPyM-*co*-PMMA random copolymer spectrum (using peaks 4 and 9, as peaks 6 and 7 resonated too close together for accurate integration of individual peaks) demonstrated that the ratio of the synthesised PEPyM-*co*-PMMA random copolymer was approximately 21/79. Considering the initial molar ratio was 25/75, this result suggests that under these CFR polymerisation conditions that the MMA monomer was more reactive than the EPyM monomer. This was likely a consequence of using benzoyl peroxide as the radical initiator which preferentially propagated the MMA species owing to a slight incompatibility with the tertiary amines on the EPyM monomer [164, 165].

Interestingly, the peaks present in the aliphatic region (between 0.5 ppm and 2.0 ppm in Figure 3.6(i)) from the PMMA homopolymer were represented by doublets, indicating that the PMMA units in the copolymer were predominantly syndiotactic [167]. The peaks due to the PEPyM were represented mostly by broad singlets, suggesting that copolymerisation with PMMA resulted in predominantly isotactic PEPyM units [167]. This difference in orientation of the PEPyM unit from the homopolymer to the copolymer could potentially result in different surface chemistry for modified capillaries for the separation of ODNs. This was investigated in Chapter 4.

3.3.3.3 FTIR spectroscopy characterisation of PEPyM-co-PMMA random copolymer

Figure 3.7 shows the FTIR spectrum of PEPyM-*co*-PMMA random copolymer. The spectrum shows C-H stretching vibrations (2 bands between 2800 cm^{-1} and 3000 cm^{-1}) and CH_2 bending (~1430 cm^{-1} and a very weak peak at ~690 cm^{-1}) corresponding to the CH_2 groups on the EPyM repeating units and the CH_2 groups connecting the repeating units [79]. CH_3 bending vibrations of the methyl groups on both monomers were observed at ~1380 cm^{-1}. A C-N stretching vibration between 1230 cm^{-1} and 1250 cm^{-1} confirmed the presence of the *N*-substituted pyrrolidine ring. Finally, the ester groups of MMA and EPyM monomers were observed as C=O stretching vibrations at approximately 1720 cm^{-1} and two C-O stretching vibrations between 1100 cm^{-1} - 1150 cm^{-1}. The broad peak at 3100 cm^{-1} - 3650 cm^{-1} can be attributed to the thin film containing trace amounts of water.

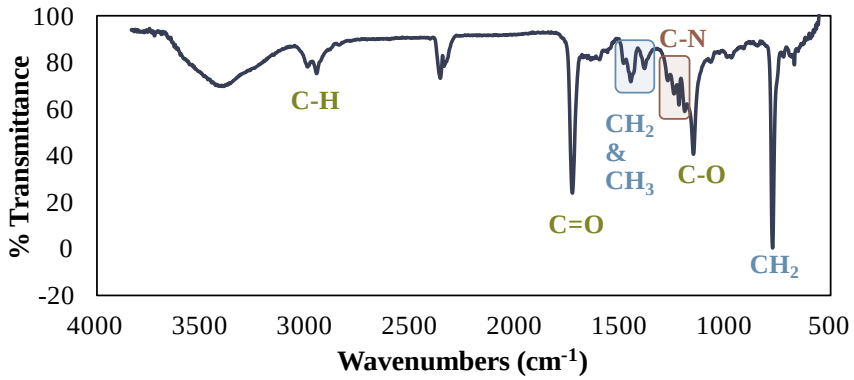

Figure 3.7. FTIR spectrum of PEPyM-*co*-PMMA random copolymer synthesised by CFR polymerisation.

3.3.3.4 GPC characterisation of PEPyM-co-PMMA random copolymer

GPC determined the M_n and M_w of the PEPyM-*co*-PMMA random copolymer to be 11 926 g mol^{-1} and 14 398 g mol^{-1}, respectively. The PDI was determined to be 1.21 which was reasonably low indicating a relatively uniform distribution of polymer chains in the sample. A low PDI is ideal for a capillary surface coating in order to create a uniform layer of polymer; this in turn should enhance the repeatability of the separations. Therefore the PEPyM-*co*-PMMA random copolymer should create an even surface for the separation of ODNs. The approximate distribution of polymer on the surface was investigated on silicon wafers using AFM and it was observed that at low concentrations, the surface roughness was reduced, indicating a uniform surface (see Section 4.3.1.1).

3.3.4 PDEAEMA-*co*-PMMA random copolymerisation

PDEAEMA-*co*-PMMA (35/65 starting molar ratio) random copolymer was synthesised by CFR copolymerisation of DEAEMA monomer and MMA monomer in toluene using ACPA as the radical initiator (see Scheme 3.6). Isolation of the PDEAEMA-*co*-PMMA random copolymer in hexane yielded a fibrous, white, stretchy polymer which shrunk to a hard dense structure when dried (51.7 %) (Refer to Section 2.3.1.2.4 for the full synthesis method). Due to the hard structure of the polymer, it was necessary to grind into a powder for it to be used. The grinding process allowed for a uniform powder to be produced. This was confirmed by the low PDI from the GPC results (see Section 3.3.4.4) which also suggests that the polymer chains remained intact and were not destroyed by the grinding process. The random copolymer was characterised by ^{1}H NMR and FTIR spectroscopies,

and GPC. ACPA was used as the radical initiator instead of benzoyl peroxide, as azo based initiators may prove to be more compatible with the tertiary amine. Hexane was used for the precipitation of the PDEAEMA-*co*-PMMA random copolymer and resulted in a relatively good yield (51.7 %).

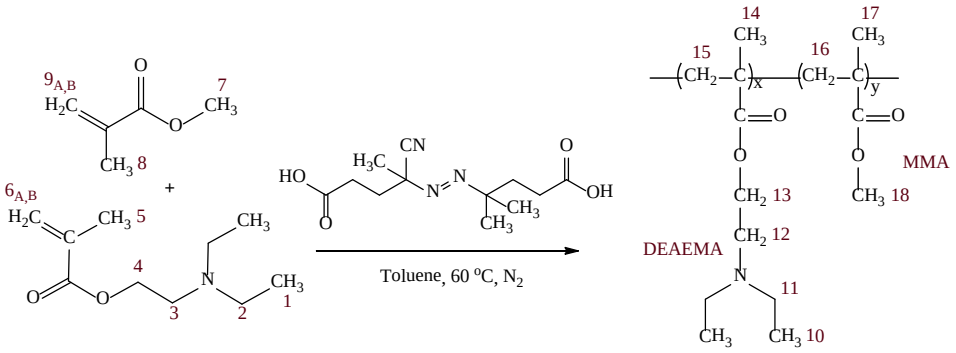

Scheme 3.6. CFR copolymerisation of DEAEMA monomer and MMA monomer for synthesis of PDEAEMA-*co*-PMMA random copolymer.

3.3.4.1 Solubility test of PDEAEMA-co-PMMA random copolymer

After isolation, the PDEAEMA-*co*-PMMA random copolymer was redissolved to be used as a dynamic coating for CE capillary modification. The copolymer exhibited similar solubility properties to the PEPyM-*co*-PMMA random copolymer (Section 3.3.3.1) due to the similar structure. Therefore, the random copolymer was most soluble in polar aprotic solvents (THF, acetone) and exhibited some solubility in weak non-polar (toluene, chloroform) and polar protic (ethanol, methanol) solvents; although it was insoluble in strongly polar water and strongly non-polar hexane. Therefore, ethanol was used to prepare the PDEAEMA-*co*-PMMA random copolymer solution for capillary surface modification (see Section 5.3.4.4).

3.3.4.2 ^{1}H NMR spectroscopy characterisation of PDEAEMA-co-PMMA random copolymer

^{1}H NMR spectroscopy was used to investigate the CFR copolymerisation of DEAEMA monomer and MMA monomer and characterise the resulting PDEAEMA-*co*-PMMA random copolymer product. Figure 3.8(i)-(iii) shows the spectra for the reaction mixture at t = 0 h, t = 48 h, and the isolated PDEAEMA-*co*-PMMA random copolymer, respectively. The chemical shifts are in Table 3.5.

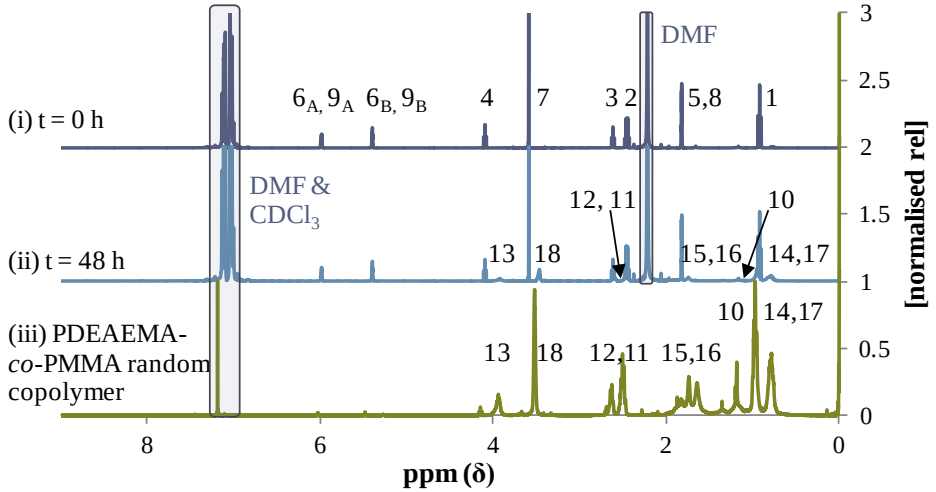

Figure 3.8. ^{1}H NMR spectra of CFR copolymerisation of DEAEMA monomer and MMA monomer at various stages of synthesis of PDEAEMA-*co*-PMMA random copolymer, t = 0 h (i), t = 48 h (ii), and isolated copolymer (iii). Data were normalised to the most intense peak in the region of 0 ppm - 7 ppm (excluding the solvent regions).

Table 3.5. ^{1}H NMR peak assignments for the PDEAEMA-*co*-PMMA random copolymer synthesised by CFR copolymerisation.

*PEAK #	PEAK ASSIGNMENT		CHEMICAL SHIFT (ppm)		
			t = 0 h	t = 48 h	Pure polymer
$6_{A,}\ 9_{A}$	C=C**H**$_{A}$	DEAEMA, MMA	5.98 - 6.02	5.98 - 6.01	
$6_{B,}\ 9_{B}$	C=C**H**$_{B}$	DEAEMA, MMA	5.39 - 5.42	5.39 - 5.42	
4	C-C**H**$_2$-O	DEAEMA	4.08 - 4.12	4.08 - 4.12	
13	C-C**H**$_2$-O	PDEAEMA		3.89 - 4.02	3.89 - 4.02
7	C**H**$_3$-O	MMA	3.59 - 3.61	3.59 - 3.61	
18	C**H**$_3$-O	PMMA		3.44 - 3.52	3.47 - 3.59
3	N-C**H**$_2$-C	DEAEMA	2.60 - 2.64	2.61 - 2.64	
12	N-C**H**$_2$-C	PDEAEMA		2.57 - 2.61	2.60 - 2.72
11	C-C**H**$_2$-N	PDEAEMA		2.49 - 2.53	2.46 - 2.57
2	C-C**H**$_2$-N	DEAEMA	2.43 - 2.49	2.42 - 2.49	
5, 8	C-C**H**$_3$	DEAEMA, MMA	1.81 - 1.84	1.81 - 1.84	
15, 16	-(C-C**H**$_2$)$_n$	PDEAEMA, PMMA		1.70 - 1.78	1.79 - 1.94 & 1.53 - 1.79
10	C**H**$_3$-C	PDEAEMA		0.95 - 1.00	1.11 - 1.23
1	C**H**$_3$-C	DEAEMA	0.90 - 0.95	0.90 - 0.95	
14, 17	C-C**H**$_3$	PDEAEMA, PMMA		0.74 - 0.89	0.89 - 1.04 & 0.69 - 0.88

*Peak allocations are shown in Scheme 3.6.

From Figure 3.8(i) and Table 3.5 it was observed that at t = 0 h, the peaks present corresponded to DEAEMA and MMA monomers only. The aliphatic peaks (observed between 1.81 ppm and 1.84 ppm) and vinyl peaks (between 5.3 ppm and 6.02 ppm) of DEAEMA and MMA monomers resonated together and it was not possible to distinguish the DEAEMA from the MMA in these regions. After 48 h of reaction (Figure 3.8(ii)), there were low intensity peaks present due to the synthesised PDEAEMA-*co*-PMMA random copolymer, but the monomer peaks still dominated the spectrum (refer to 't = 48 h' in Table 3.5). However, integration of the spectrum showed a conversion efficiency of approximately 70 % which was greater than the experimental yield of 51.7 %, presumably due to loss of product during isolation. The spectrum of the isolated PDEAEMA-*co*-PMMA random copolymer (Figure 3.8(iii)) showed very small vinyl peaks from the DEAEMA monomer at ~5.4 ppm - 6.0 ppm indicating that the polymer was not completely isolated from the unreacted monomer. As DEAEMA was not as volatile as the MMA, it was not as easily removed during the evaporation process prior to hexane precipitation. Figure 3.8(iii) showed peaks present from both the PDEAEMA and PMMA (refer to 'pure polymer' in Table 3.5) indicating successful copolymerisation. As was observed with the monomer peaks in Figure 3.8(i), the PDEAEMA and PMMA aliphatic groups resonated together between 0.5 ppm and 2 ppm. Doublets were also observed in this region (0.5 ppm - 2 ppm) for both the PDEAEMA and PMMA indicating that the copolymer was predominantly syndiotactic [47]. Integration of the spectrum (using peaks 4 and 9, Table 3.5) demonstrated that the ratio of the synthesised PDEAEMA-*co*-PMMA random copolymer was approximately 34/66, suggesting that from the starting monomer ratio of 35/65, both monomers had similar reactivities under these conditions.

3.3.4.3 FTIR spectroscopy characterisation of PDEAEMA-co-PMMA random copolymer

Figure 3.9 shows an FTIR spectrum of the PDEAEMA-*co*-PMMA random copolymer. The spectrum shows C-H stretching vibrations (2 bands between 2800 cm^{-1} and 3000 cm^{-1}) and CH_2 bending vibrations (~760 cm^{-1} and ~1430 cm^{-1}) corresponding to the CH_2 groups on the DEAEMA repeating units and the CH_2 groups connecting the repeating units for both the DEAEMA and MMA. CH_3

bending vibrations of the methyl groups on both monomer units were represented by a peak at ~1380 cm^{-1}. A C-N stretching vibration between 1230 cm^{-1} and 1250 cm^{-1} confirmed the presence of the tertiary amine. Finally, the ester groups of the MMA and DEAEMA monomer units were observed as a C=O stretching vibration at ~1720 cm^{-1} and two C-O stretching vibrations between 1100 cm^{-1} and 1150 cm^{-1}.

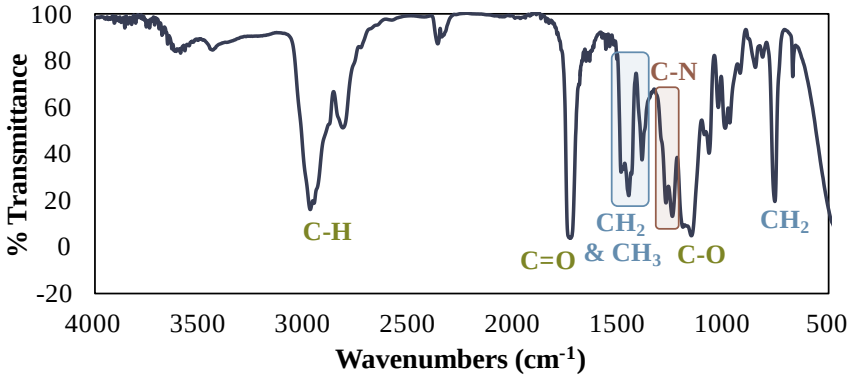

Figure 3.9. FTIR spectrum of PDEAEMA-*co*-PMMA random copolymer synthesised by CFR polymerisation.

3.3.4.4 GPC characterisation of PDEAEMA-co-PMMA random copolymer

GPC determined the M_n and M_w of the PDEAEMA-*co*-PMMA random copolymer to be 16 821 g mol^{-1} and 18 474 g mol^{-1}, respectively. The PDI was determined to be 1.10. The low PDI is indicative of a uniform distribution of polymer chains in the sample which, in turn, when applied to the capillary should create an even polymer surface.

3.4 Reversible addition-fragmentation chain transfer polymerisation

For a more explicitly controlled polymerisation, a 'reversible-deactivation' radical polymerisation technique called RAFT polymerisation can be used [144]. This process is capable of controlling the chain extension of the polymer creating a more even distribution, and thus lowers the PDI of chain-lengths amongst the polymer [144, 170]. RAFT is often carried out in a similar way to conventional free-radical polymerisation, typically employing azo or peroxy thermal initiators, such as ACPA, azo-*bis*-isobutyrylnitrile (AIBN), or benzoyl peroxide *tert*-buty peroxybenzoate [165]. However, the difference lies with the added use of a chain

transfer agent (CTA) to 'control' radical formation [144]. The RAFT mechanism (Scheme 3.7) involves a series of steps (initiation, chain transfer, re-initiation, equilibration and termination) which results in the monomer insertion and growth between the C-S bond of the CTA nearest the R group. The Z group activates the C=S double bond for radical addition, and the R group acts as the leaving group, forming a radical for reinitiation. This process is able to be controlled by trapping the active propagating species into dormant species effectively protecting them from termination reactions [171].

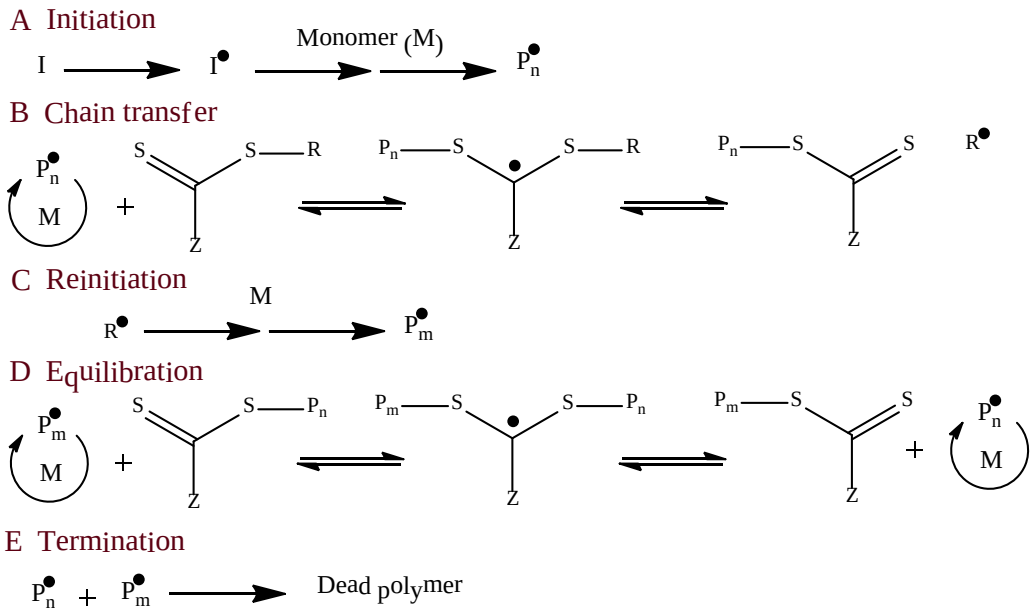

Scheme 3.7. RAFT polymerisation reaction mechanism. Adapted from [171, 172].

RAFT is particularly useful for block copolymerisation and can be performed in heterogeneous media at a wide range of temperatures, making the technique very versatile [172]. RAFT polymerisation of block copolymers is a two-step process (shown in Scheme 3.8) in which one monomer is polymerised first (this is then known as a macro-RAFT agent), followed by the addition of the second monomer with more initiator. The second monomer is grown between the first monomer and the thio group (insertion between the C-S bond of the macro-RAFT agent) [161].

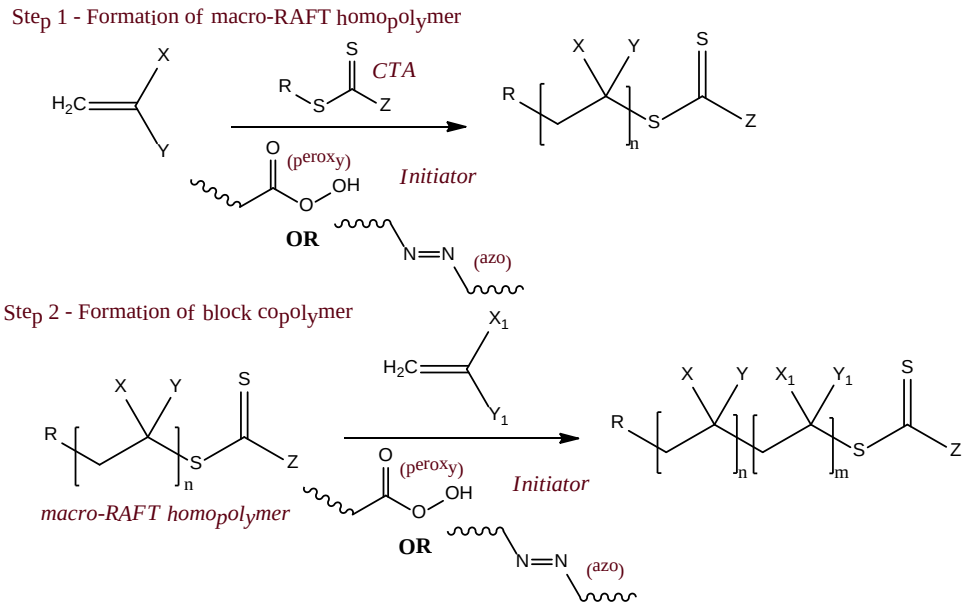

Scheme 3.8. RAFT polymerisation of a block copolymer from a macro-RAFT agent. Adapted from [172].

The following sections detail the synthesis of two different macro-RAFT agents based on homopolymers of PEPyM and PMMA which have a dithiobenzoate-terminated moity (from the CPDB CTA) which can later be used to chain extend with another monomer to form block copolymers. These were then compared for use as the first polymer to form the final block copolymer to be used as a surface modifier for CE analysis of ODNs in this thesis (Chapter 5).

3.4.1 PEPyM homopolymer macro-RAFT agent

A dithiobenzoate-terminated PEPyM macro-RAFT homopolymer was synthesised by RAFT polymerisation of EPyM monomer in toluene using ACPA as the radical initiator and CPDB as the CTA (see Scheme 3.9). Polymerisation of PEPyM homopolymer yielded a yellow-brown powder (27.89 %) which shrunk when dried (Refer to Section 2.3.1.3.1 for the full synthesis method). The PEPyM homopolymer macro-RAFT agent was characterised by ^{1}H NMR and FTIR spectroscopies, and GPC. Given that the CPDB CTA is pink in colour, successful chain extension of the polymer should be observed by the formation of a pink tinged polymer. However, this was not the case, suggesting chain extension was unsuccessful. ^{1}H NMR spectroscopy was used to investigate this (see Section 3.4.1.2).

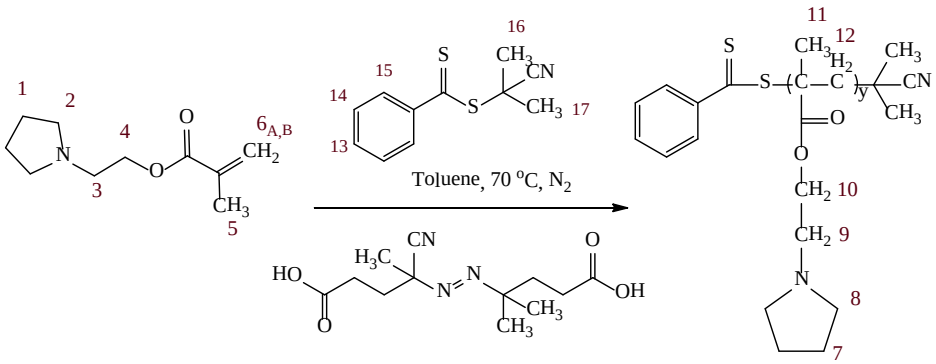

Scheme 3.9. RAFT polymerisation of EPyM for synthesis of a dithiobenzoate-terminated PEPyM homopolymer macro-RAFT agent.

3.4.1.1 Solubility test of PEPyM homopolymer macro-RAFT agent

After isolation, the PEPyM homopolymer macro-RAFT agent had to be redissolved in order to be used as a dynamic coating for the CE capillary modification. Solubility tests showed it possessed very limited solubility. It exhibited partial solubility in polar aprotic solvents (THF, acetone) and weakly non-polar solvents (toluene, chloroform) and was insoluble in polar protic solvents such as water and methanol (except ethanol which resulted in partial solubility) and strongly non-polar (hexane) solvents. Therefore, acetone was used for the preparation of the polymer solutions for surface morphology characterisation using AFM (see Section 4.3.1.1).

3.4.1.2 ^{1}H NMR spectroscopy characterisation of PEPyM homopolymer macro-RAFT agent

^{1}H NMR spectroscopy was used to investigate the RAFT polymerisation of EPyM and characterise the PEPyM homopolymer macro-RAFT agent. Figure 3.10(i)-(iv) shows the spectra for the CPDB CTA, the reaction mixture at t = 0 h, t = 48 h, and the isolated PEPyM homopolymer macro-RAFT agent, respectively. The peak assignments and chemical shifts can be found in Table 3.6.

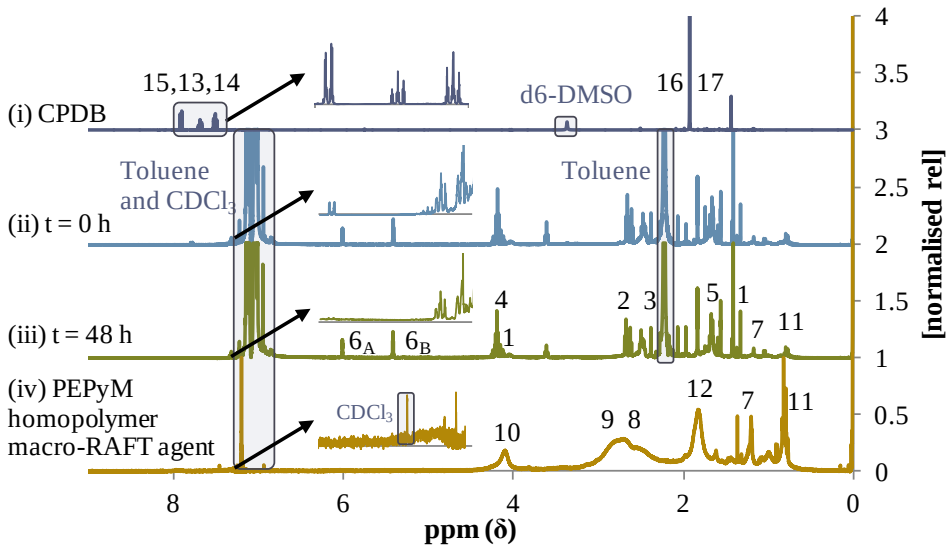

Figure 3.10. ^{1}H NMR spectra for CPDB CTA (i), and RAFT polymerisation of EPyM monomer at various stages of synthesis of PEPyM homopolymer macro-RAFT agent; t = 0 h (ii), t = 48 h (ii), and isolated PEPyM homopolymer macro-RAFT agent (iv). Data were normalised to the most intense peak in the region of 0 ppm - 7 ppm (excluding the solvent regions).

Table 3.6. ^{1}H NMR peak assignments for the RAFT polymerisation of EPyM at various stages of synthesis of PEPyM homopolymer macro-RAFT agent.

*PEAK #	PEAK ASSIGNMENT		CHEMICAL SHIFT (ppm) t = 0 h	t = 48 h	Pure polymer
6_A	C=C**H**$_A$	EPyM	5.99 - 6.01	6.00 - 6.02	
6_B	C=C**H**$_B$	EPyM	5.40 - 5.42	5.41 - 5.42	
4	C-C**H**$_2$-O	EPyM	4.15 - 4.23	4.13 - 4.23	
10	C-C**H**$_2$-O	PEPyM	3.98 - 4.08	3.98 - 4.10	3.92 - 4.38
3	N-C**H**$_2$-C	EPyM	2.59 - 2.67	2.60 - 2.69	
9	N-C**H**$_2$-C	PEPyM			2.62 - 3.08
2	C-C**H**$_2$-N	EPyM	2.42 - 2.51	2.43 - 2.52	
8	C-C**H**$_2$-N	PEPyM			2.28 - 2.61
5	C-C**H**$_3$	EPyM	1.82 - 1.85	1.82 - 1.85	
12	-(C-C**H**$_2$)$_n$	PEPyM			1.73 - 1.94
1	C-C**H**$_2$-C	EPyM	1.62 - 1.70	1.62 - 1.70	
7	C-C**H**$_2$-C	PEPyM	1.15 - 1.21	1.13 - 1.21	1.17 - 1.25
11	C-C**H**$_3$	PEPyM	0.73 - 0.81	0.71 - 0.82	0.76 - 0.85

*Peak allocations are shown in Scheme 3.9.

Figure 3.10(i) is of CPDB which was the CTA used for the RAFT polymerisation. The aromatic protons were represented by doublet peaks between 7.89 ppm and 7.93 ppm, and two sets of triplet peaks at 7.66 ppm - 7.71 ppm, and 7.48 ppm -

7.53 ppm. The methyl groups were represented by peaks at 1.91 ppm - 1.93 ppm, and 1.42 ppm - 1.44 ppm. Figure 3.10(ii) shows some low intensity peaks from polymer in the t = 0 h, owing to self-polymerisation of the monomer during synthesis preparation. Some PEPyM peaks were present at t = 48 h (Figure 3.10(iii)), however, they were very weak (reflected by the relatively low yield). Once the polymer was isolated, all the expected PEPyM polymer peaks were present, and the monomer and solvent peaks were diminished (Figure 3.10(iv)). The polymer exhibited changes in the chemical shift when compared to the monomer and the peaks were broader which was expected. The PEPyM homopolymer macro-RAFT agent exhibited some multiple peaks and some broad singlets in the aliphatic region representative of a heterotactic polymer (differently oriented dyads throughout the polymer chains) (Refer to Section 3.3.2.2 for more details).

For the dithiobenzoate-terminated PEPyM homopolymer to be used as a macro-RAFT agent for the synthesis of a block copolymer with other monomers, the presence of the CTA dithiobenzoate end group needed to be confirmed. If the attachment of the CPDB is insufficient, then the dithiobenzoate-terminated PEPyM homopolymer macro-RAFT agent cannot successfully chain extend successive monomer units. Figure 3.10 shows that the aromatic peaks from the CPDB CTA were present in all three spectra; however the intensity compared to the polymer peaks was reduced over time owing to the growing M_w of the polymer, and the doublet peak could not be distinguished from the noise in the isolated polymer spectrum (Figure 3.10(iii)). These aromatic peaks were represented by weak doublet peaks between 7.80 ppm and 7.76 ppm, and two sets of triplet peaks at 7.29 ppm - 7.35 ppm, and 7.19 ppm - 7.25 ppm for the t = 0 h and t = 48 h; whereas, only the CTA triplet peaks were observed in the isolated PEPyM homopolymer macro-RAFT agent at 7.29 ppm - 7.30 ppm, and 7.24 ppm - 7.25 ppm. The low signal-to-noise in the aromatic region means that it cannot be said with confidence that the PEPyM homopolymer macro-RAFT agent could be used for the successful chain extension of PMMA in the synthesis of a PEPyM-*b*-PMMA block copolymer.

3.4.1.3 FTIR spectroscopy characterisation of PEPyM homopolymer macro-RAFT agent

Figure 3.11 shows an FTIR spectrum of the PEPyM homopolymer macro-RAFT agent. The spectrum shows C-H stretching vibrations at ~2800 cm^{-1} and 3000 cm^{-1} and CH_2 bending vibrations (~1430 cm^{-1} and very weak peak at ~690 cm^{-1}) corresponding to the CH_2 groups on the EPyM repeating units. CH_3 bending vibrations of the methyl groups were observed at ~1380 cm^{-1} and a C-N stretching vibration between 1230 cm^{-1} and 1250 cm^{-1} confirmed the presence of the *N*-substituted pyrrolidine ring. Finally, the ester groups were observed as a C=O stretching vibration at ~1720 cm^{-1} and a C-O stretching vibration at 1100 cm^{-1} - 1150 cm^{-1}. There was no observed stretch at 2250 cm^{-1} indicating the presence of a nitrile (C≡N) from the CPDB CTA, nor any discernable peaks in the region (600 cm^{-1} - 900 cm^{-1}). Therefore, in addition to the ^1H NMR results, the presence of the CTA cannot be confirmed. The broad peak between 3100 cm^{-1} and 3650 cm^{-1} was attributed to the thin film still containing trace amounts of water.

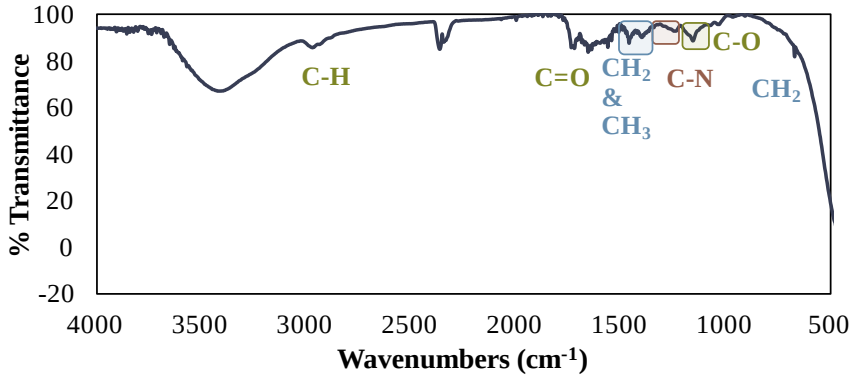

Figure 3.11. FTIR spectrum of PEPyM homopolymer macro-RAFT agent synthesised by RAFT polymerisation.

3.4.1.4 GPC characterisation of PEPyM homopolymer macro-RAFT agent

GPC determined the M_n and M_w of the PEPyM homopolymer macro-RAFT agent to be 14 164 g mol^{-1} and 16 662 g mol^{-1}, respectively. The PDI was determined to be 1.18. According to the GPC results, the PDI was low, indicating relatively uniform chain lengths which are typical for RAFT polymerisation. RAFT polymerisation of EPyM under these conditions resulted in the synthesis of low M_w PEPyM with low polydispersity. Due to the low yield, the PEPyM homopolymer macro-RAFT agent was not used for the chain extension of PMMA in the

formation of PEPyM-*b*-PMMA. In addition, the presence of the dithiobenzoate group could not be confirmed during the characterisation, and given that this group is essential for RAFT polymerisation, the use of the PEPyM macro-RAFT agent for formation of block copolymers was not pursued any further.

3.4.2 PMMA homopolymer macro-RAFT agent

A dithiobenzoate-terminated PMMA homopolymer macro-RAFT agent was synthesised by RAFT polymerisation of MMA monomer in DMF using CPDB as the CTA and ACPA as the radical initiator. The reaction pathway can be seen in Scheme 3.10. The PMMA homopolymer macro-RAFT agent was used for the chain extension of PEPyM in the formation of a PEPyM-*co*-PMMA block copolymer (see Section 3.4.3). Isolation of the PMMA homopolymer macro-RAFT agent yielded a fine pale pink powder (75.59 %) (Refer to Section 2.3.1.3.2 for the full synthesis method). The pink colour was due to the residual CPDB CTA which indicated successful RAFT polymerisation. The PMMA homopolymer macro-RAFT agent was characterised by ^{1}H NMR and FTIR spectroscopies, and GPC.

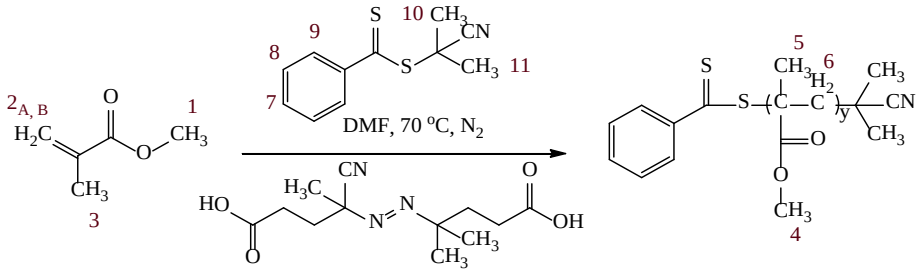

Scheme 3.10. RAFT polymerisation of MMA monomer for synthesis of a dithiobenzoate-terminated PMMA homopolymer macro-RAFT agent.

3.4.2.1 Solubility test of PMMA homopolymer macro-RAFT agent

After isolation, the PMMA homopolymer macro-RAFT agent had to be redissolved in order to be used as a dynamic coating for the CE capillary modification. It exhibited very similar solubility to the PMMA homopolymer synthesised by CFR polymerisation (Section 3.3.2.1), having limited solubility in polar aprotic (THF, acetone, ethanol) and weakly non-polar (toluene, chloroform) solvents. It formed a colloidal suspension in polar protic solvents (ethanol, methanol, water) and was insoluble in strongly non-polar hexane. Therefore, acetone was used to prepare polymer solutions for surface morphology tests using AFM (see Section 4.3.1.1).

3.4.2.2 ^{1}H NMR spectroscopy characterisation of PMMA homopolymer macro-RAFT agent

^{1}H NMR spectroscopy was used to investigate the RAFT polymerisation of MMA monomer and characterise the final PMMA homopolymer macro-RAFT agent. Figure 3.12(i)-(iv) shows the spectra for the reaction mixture at t = 0 h, t = 48 h, t = 48 h after evaporation with nitrogen, and the isolated PMMA homopolymer macro-RAFT agent, respectively. The peak assignments and chemical shifts are shown in Table 3.7.

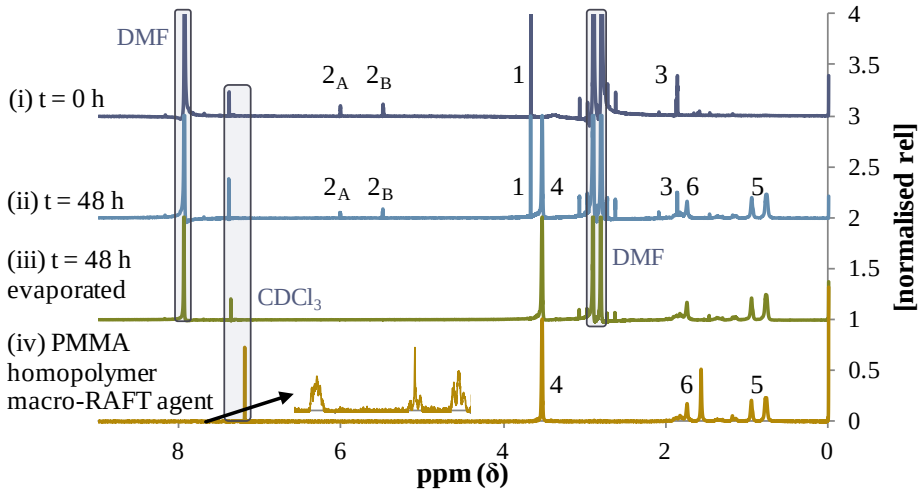

Figure 3.12. ^{1}H NMR spectra for RAFT polymerisation of MMA monomer at various stages of synthesis of PMMA homopolymer macro-RAFT agent; t = 0 h (i), t = 48 h (ii), t = 48 h (reaction solution evaporated) (iii), and isolated PMMA homopolymer macro-RAFT agent (iv). Data were normalised to the most intense peak in the region of 0 ppm - 9 ppm (excluding the solvent regions).

Table 3.7. ^{1}H NMR peak assignments for the RAFT polymerisation of MMA at various stages of synthesis of PMMA homopolymer macro-RAFT agent.

*PEAK #	PEAK ASSIGNMENT		CHEMICAL SHIFT (ppm) t = 0 h	t = 48 h	Pure polymer
2_A	C=C**H**$_A$	MMA	6.01 - 6.03	6.01 - 6.03	
2_B	C=C**H**$_B$	MMA	5.48 - 5.50	5.49 - 5.51	
1	C**H**$_3$-O	MMA	3.67 - 3.68	3.62 - 3.70	
4	C**H**$_3$-O	PMMA	3.51 - 3.56	3.50 - 3.56	3.51 - 3.56
3	C-C**H**$_3$	MMA	1.86 - 1.88	1.86 - 1.88	
6	-(C-C**H**$_2$)$_n$	PMMA		1.72 - 1.92	1.70 - 1.9 & 1.53 - 1.60
5	C-C**H**$_3$	PMMA		0.71 - 1.00	0.91 - 1.00 & 0.72 - 0.84

*Peak allocations are shown in Scheme 3.10.

Figure 3.12(i) shows the spectrum at t = 0 h, and the peaks present corresponded only to MMA monomer and solvent, indicating polymerisation had not yet occurred. After 48 h of reaction (Figure 3.12(ii)), the conversion of MMA monomer to PMMA was ~50 % (from the intensities of the methoxy peak); however the peak intensities are not an accurate indication of polymer conversion, as the actual yield of the isolated PMMA was determined to be 74.7 %. Figure 3.12(iii) shows that evaporation of the reaction mixture by nitrogen removed any remaining MMA monomer due to its high volatility (seen by lack of MMA peaks in the evaporated sample), indicating that this evaporation process can assist in increasing the purity of the final polymer. Figure 3.12(iv) shows that precipitation in methanol yielded a pure PMMA homopolymer macro-RAFT agent. As with the PMMA homopolymer synthesised by CFR polymerisation (Section 3.3.2.2), there were doublets in the aliphatic region (0.5 ppm - 2 ppm) due to the different stereochemistry of the polymer chains. From Figure 3.12 it was evident that the PMMA homopolymer macro-RAFT agent was also predominantly syndiotactic. Although RAFT polymerisation had better control over the chain lengths of polymers (evidenced by the low PDI of 1.18 in Section 3.4.2.4), it did not appear to control the stereochemistry in this case.

For the dithiobenzoate-terminated PMMA homopolymer to be used as a macro-RAFT agent for the synthesis of a block copolymer with EPyM, the presence of the CTA dithiobenzoate end group needed to be confirmed. Figure 3.12(iv) shows successful insertion and chain growth of the PMMA between the R and Z groups of the CPDB evidenced by distinct peaks in the aromatic region. These peaks were observed at 7.78 ppm - 7.84 ppm, 7.42 ppm - 7.47 ppm, and 7.27 ppm - 7.33 ppm, corresponding to peaks 9, 7, and 8, respectively (from Scheme 3.10). In comparison to the spectrum of CPDB (see Figure 10(i)), these peaks were shifted slightly upfield owing to greater shielding by a higher electron density of its surrounding molecular orbital (from being bound to the polymer). These results indicate that the PMMA homopolymer macro-RAFT agent should be capable of chain extending EPyM monomer units for the synthesis of a PEPyM-*b*-PMMA block copolymer (see Section 3.4.3).

3.4.2.3 FTIR spectroscopy characterisation of PMMA homopolymer macro-RAFT agent

Figure 3.13 shows an FTIR spectrum of the PMMA homopolymer macro-RAFT agent. The spectrum shows the C-H stretching vibrations (2 bands between 2800 cm^{-1} and 3000 cm^{-1}) and CH_2 bending vibrations (730 cm^{-1} - 900 cm^{-1}, and ~1450 cm^{-1}) corresponding to the CH_2 groups connecting the MMA repeating units. CH_3 bending vibrations of the methyl and methoxy groups are observed at ~1380 cm^{-1}. The ester groups of the MMA monomer units were observed as C=O stretching vibrations at approximately 1720 cm^{-1} and two C-O stretching vibrations at 1100 cm^{-1} - 1150 cm^{-1}. A broad peak observed between 3100 cm^{-1} and 3650 cm^{-1} arose from the thin film still containing trace amounts of water. There was no observed stretch at 2250 cm^{-1} which would indicate the presence of a nitrile (C≡N) from the CPDB CTA. As ^1H NMR spectroscopy proved the presence of the CTA groups on the polymer, this suggests FTIR spectroscopy was not sensitive enough to detect the small amounts of these groups among the polymer.

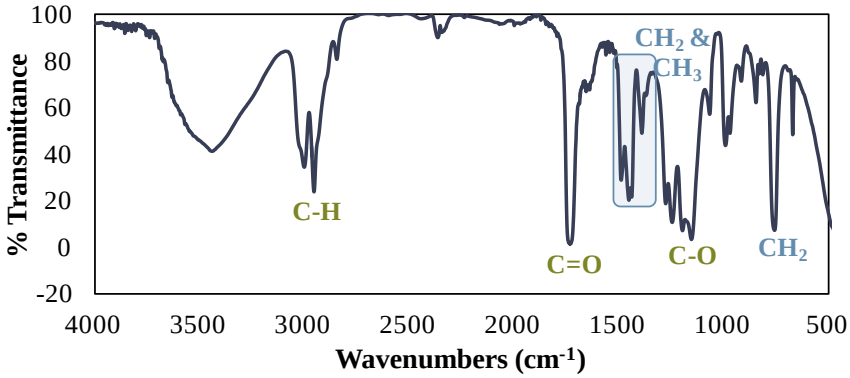

Figure 3.13. FTIR spectrum of PMMA homopolymer macro-RAFT agent synthesised by RAFT polymerisation.

3.4.2.4 GPC characterisation of PMMA homopolymer macro-RAFT agent

GPC determined the M_n and M_w of the PMMA homopolymer macro-RAFT agent to be 7 152 g mol^{-1} and 8 426 g mol^{-1}, respectively. The PDI was determined to be 1.18 which was low indicating that the polymer was relatively uniform in terms of chain length. Clearly, RAFT polymerisation has controlled the chain extension of the polymer creating a more even distribution of chain-lengths amongst the polymer, as expected.

When compared to the PMMA homopolymer synthesised by CFR polymerisation (Section 3.3.2.4), the PDI was much improved (from 1.98 down to 1.18). However, the conversion under the RAFT conditions described here was approximately half that of the CFR PMMA homopolymer with a M_n of 7 152 g mol^{-1} and 14 770 g mol^{-1} for the PMMA homopolymer macro-RAFT agent and CFR PMMA homopolymer, respectively.

3.4.2.5 Kinetic study of PMMA homopolymer macro-RAFT agent

The kinetics of RAFT polymerisation of MMA monomer with CPDB was determined using multiple pot reactions (see Section 2.3.1.3.2.1). A reaction batch was prepared from MMA monomer, CPDB (CTA), ACPA (initiator) and DMF, after which 5 mL of the batch was used for each timed reaction (t = 0, 1, 2, 4, 8, 12, 18, 24, 36, and 50 h). At the completion of each reaction, the polymers were isolated to yield fine pale pink powders. Reaction samples were taken for ^{1}H NMR analysis for each timed reaction prior to precipitation and the resultant spectra can be seen in Figure 3.14.

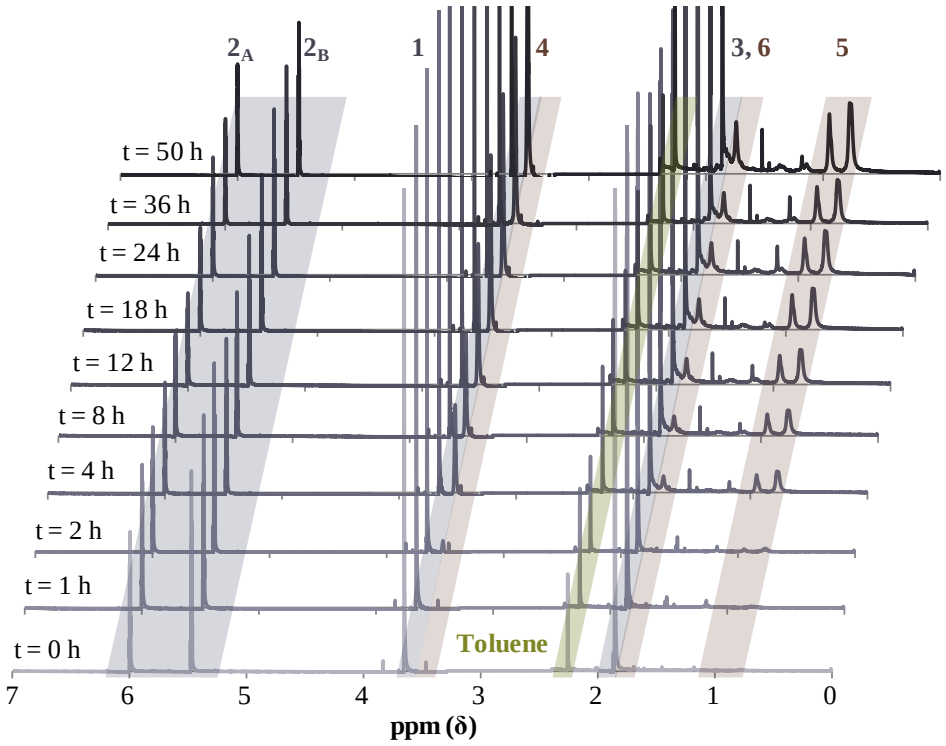

Figure 3.14. ^{1}H NMR spectra for liquid samples from the kinetic study of RAFT polymerisation of MMA. Data were normalised to the largest peak between 0 ppm and 7 ppm (excluding the solvent peaks), and the DMF peaks (2.8 ppm - 3.0 ppm) were removed.

From the ^{1}H NMR spectra in Figure 3.14, it is evident that the polymer peaks did not start forming under these conditions until after ~4 h. Although Figure 3.14 shows that the monomer is being consumed in this time period, no polymer was isolated after 1 h or 2 h. After 4 h, the polymer peaks began to appear (~3.50 ppm - 3.60 ppm , 1.70 ppm - 1.95 ppm, and 0.7 ppm - 1 ppm) and increased in intensity with increasing time. The vinyl peaks at ~6 ppm (Vinyl 2_A from Scheme 3.10) and 5.5 ppm (Vinyl 2_B) decreased over time as the monomer was being converted to polymer. The % conversion was calculated from the ratio of the monomer peaks with time according to Equation 3.1,

$$\% \text{ conversion} = \left(\frac{[M_o] - [M]}{[M_o]}\right) \times 100$$

Equation 3.1

where $[M_o]$ is the integration value from the vinyl monomer peak at t = 0 h and $[M]$ is the integration value from the vinyl monomer peak at t = *n* h. Figure 3.15A shows the plot of % conversion against time (left axis). For a polymerisation reaction to be considered living/controlled, it must follow first order kinetics, therefore a plot of $ln([M_o]/[M])$ against time should follow a linear trend [161] (Figure 3.15A (right axis)). However, it can be seen from Figure 3.15A that although the trend was linear between 0 h and 8 h, the plot deviated from linearity after this time, and began to level out after ~18 h. This coincided with the trend in the mass of the isolated PMMA homopolymer macro-RAFT agents (see Figure 3.15B). This means that after ~8 h, the reaction was not controlled, and after ~12 h an increasing number of polymer chains were undergoing termination reactions (see Scheme 3.7E).

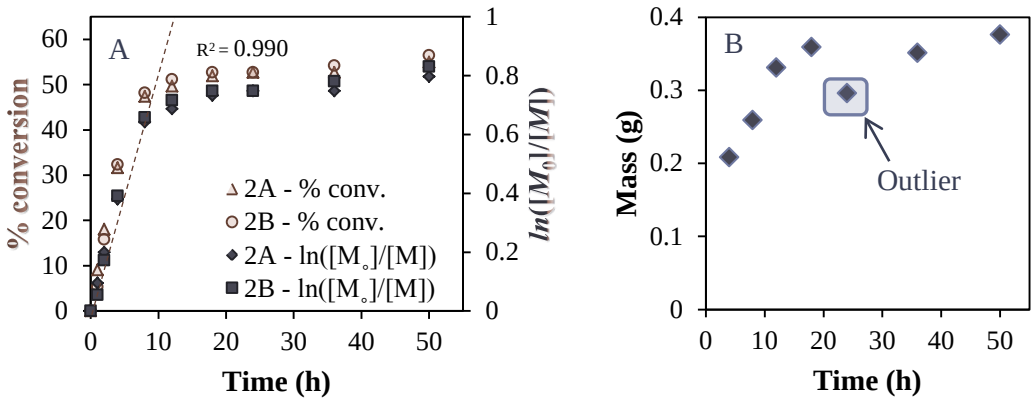

Figure 3.15. Plots of % conversion (left) and $ln([M_o]/[M])$ (right) (from the vinyl peak integration from the ^{1}H NMR spectra) (A), and mass of isolated homopolymer (B), against time.

As synthesis of PMMA homopolymer macro-RAFT agent via RAFT polymerisation was higher yielding with distinct ^{1}H NMR peaks present from the attached CPDB CTA (in comparison to PEPyM homopolymer macro-RAFT agent), this macro-RAFT agent was chosen for the chain extension of PEPyM for the formation of a PEPyM-*b*-PMMA block copolymer.

3.4.3 PEPyM-*b*-PMMA block copolymer

A PEPyM-*b*-PMMA block copolymer was synthesised by RAFT polymerisation of dithiobenzoate-terminated PMMA homopolymer macro-RAFT agent (see Section 3.4.2) and EPyM monomer in DMF with ACPA (Scheme 3.11).

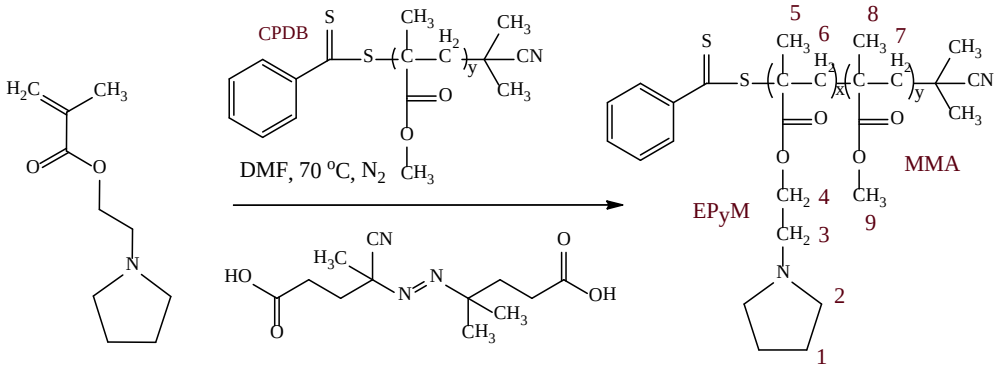

Scheme 3.11. RAFT polymerisation of dithiobenzoate-terminated PMMA homopolymer macro-RAFT agent and EPyM monomer for synthesis of a PEPyM-*b*-PMMA block copolymer.

PMMA was chosen over PEPyM as the macro-RAFT CTA for the chain extension of EPyM in the synthesis of the PEPyM-*b*-PMMA, as it was observed experimentally in this work to be the more reactive monomer (under these conditions) and higher yielding (27.89 % for the PEPyM macro-RAFT agent compared to 75.59 % for PMMA macro-RAFT agent). More importantly, in terms of using this polymer for capillary surface modification, it was preferable to have the PEPyM units grown next to the Z group as this Z group can be removed from the polymer via three different processes. As it has been observed in literature that the C-S bond can become labile (unstable), it is often necessary to replace (or remove) this particular end group., and therefore there are some well established methods in place. Such methods employed include aminolysis [173], radical-induced induction [174] and thermal elimination [172, 175]. The chosen method depends on the desired end group (see Scheme 3.12) [172].

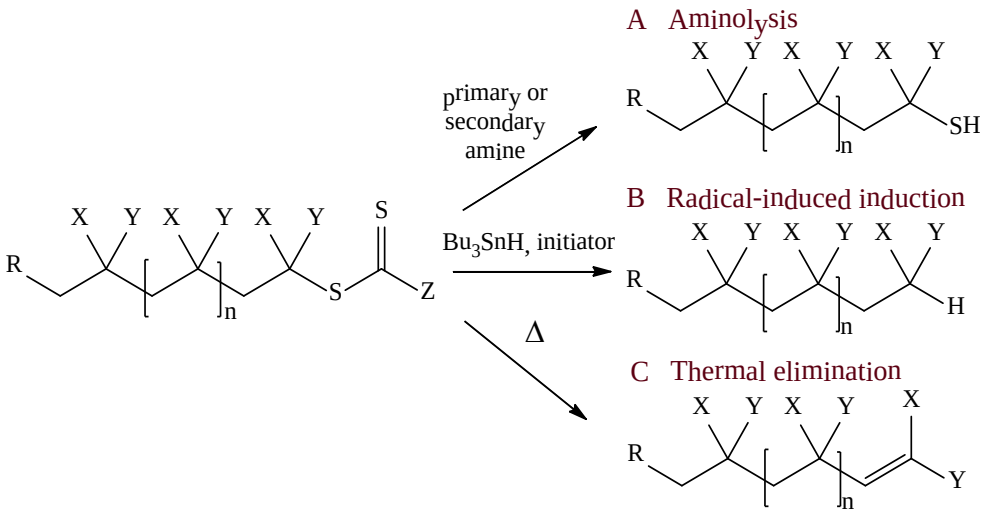

Scheme 3.12. RAFT end-group termination methods (from a macro-RAFT agent homopolymer). Adapted from [172].

Thermal elimination has been used in this thesis to completely remove the dithiobenzoate group (Scheme 3.12C) on the final PEPyM-*b*-PMMA block copolymer, as this resulted in complete exposure of the PEPyM block. Thermal elimination is easily achieved by simply heating the reaction mixture at an elevated temperature (typically 120 ^{o}C - 200 ^{o}C [175]) or simply by prolonged heating. The temperature depends on the end group composition and the ability of the polymer to stabilise the decomposition of the end group [175]. In this work, thermal elimination was achieved by prolonged exposure to heat.

According to Scheme 3.12C, removal of the Z-group (dithiobenzoate moiety) from the polymer exposes more of the PEPyM for adsorption to the capillary surface as it was shown from the surface characterisation (Section 4.3) and from CE separations of ODNs (Section 5.3) that the PEPyM was responsible for adsorption to the surface; whereas the purpose of the PMMA was to enable stabilisation. In addition, CPDB (shown in Scheme 3.11) was chosen as the CTA as it has been reported to be suitable for use with acrylates and is relatively non-bulky [171, 176]. Isolation of the PEPyM-*b*-PMMA block copolymer yielded a yellow-brown powder (37.8 %) (Refer to Section 2.3.1.3.3 for the full synthesis method) which was characterised by ^{1}H NMR and FTIR spectroscopies, and GPC.

*3.4.3.1 Solubility test of PEPyM-*b*-PMMA*

After isolation, the PEPyM-*b*-PMMA block copolymer had to be redissolved in order to be used as a dynamic coating for the CE capillary modification. The block copolymer exhibited only partial solubility in weak non-polar (toluene, chloroform) and polar aprotic (THF, acetone) solvents owing to the relatively non polar PMMA coupled with the RAFT agent which contains a strongly non-polar aromatic group, making the block copolymer less soluble in polar solvents. The slightly polar PEPyM groups allowed for weak solubility in ethanol (polar protic solvent). The copolymer was insoluble in strongly polar (water) and non-polar (hexane) solvents. Therefore, ethanol or acetone was used to prepare the polymer solutions for surface morphology characterisation using AFM (see Section 4.3.1.2) and capillary surface modification (see Section 5.3.4.3).

*3.4.3.2 ^{1}H NMR spectroscopy characterisation of PEPyM-*b*-PMMA*

^{1}H NMR spectroscopy was used to characterise the PEPyM-*b*-PMMA block copolymer. Figure 3.16(i)-(iii) shows the spectra for the PEPyM-*b*-PMMA random copolymer, compared to the PEPyM homopolymer macro-RAFT agent, and PMMA homopolymer macro-RAFT agent, respectively. The chemical shifts are shown in Table 3.8. For peak assignments of PEPyM homopolymer macro-RAFT agent and PMMA homopolymer macro-RAFT agent refer to Tables 3.6 and 3.7, respectively.

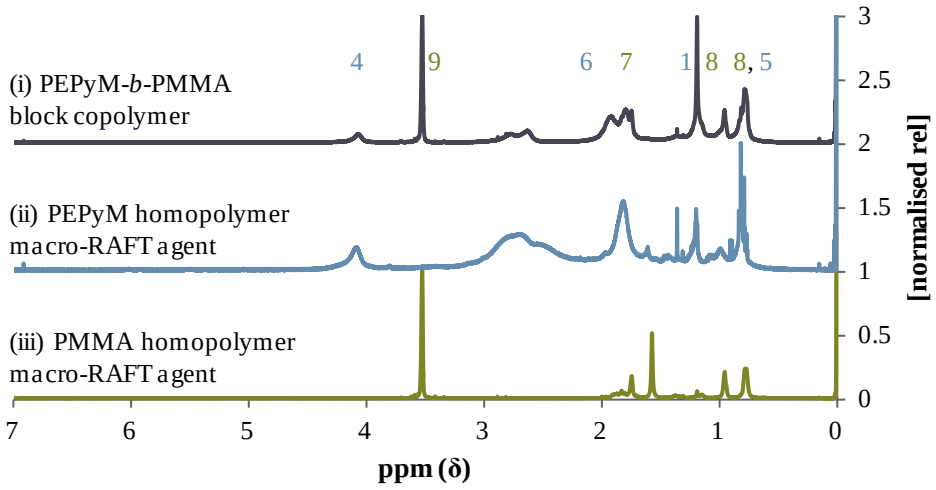

Figure 3.16. ^{1}H NMR spectra of PEPyM-*b*-PMMA block copolymer (i), compared to the PEPyM homopolymer macro-RAFT agent (ii), and PMMA homopolymer macro-RAFT agent (iii), synthesised by RAFT polymerisation. Data were normalised to the most intense peak in the region of 0 ppm - 7 ppm.

Table 3.8. ^{1}H NMR peak assignments for the PEPyM-*b*-PMMA block copolymer synthesised by RAFT copolymerisation.

*PEAK #	PEAK ASSIGNMENT		CHEMICAL SHIFT (ppm)
4	C-C**H**$_2$-O	PEPyM	4.03 - 4.20
9	C**H**$_3$-O	PMMA	3.49 - 3.61
3	N-C**H**$_2$-C	PEPyM	2.72 - 2.92
2	C-C**H**$_2$-N	PEPyM	2.56 - 2.72
6	-(C-C**H**$_2$)$_n$	PEPyM	1.86 - 2.07
7	-(C-C**H**$_2$)$_n$	PMMA	1.72 - 1.86
1	C-C**H**$_2$-C	PEPyM	1.11 - 1.25
8	C-C**H**$_3$	PMMA	0.81 - 1.02
5	C-C**H**$_3$	PEPyM	0.73 - 0.81

*Peak allocations are shown in Scheme 3.11.

Figure 3.16 and Table 3.8 show the presence of both the PMMA (Figure 3.16(ii)) and PEPyM (Figure 3.16(ii)) in the block indicating that the dithiobenzoate-terminated PMMA homopolymer macro-RAFT agent successfully acted as a CTA for the chain extension of the PEPyM, resulting in the formation of the PEPyM-*b*-PMMA block copolymer. The spectrum of the isolated block copolymer (Figure 3.16(i)) was quite similar to the spectrum of the random copolymer synthesised by CFR polymerisation (see Figure 3.6(i)). The main differences are observed as an increase in the intensity of the PEPyM peaks and peaks 6 and 7 (from the CH_2 groups linking the repeating units) resonating closer together as peak 6 (due to PEPyM units) shifted upfield. This was attributed the shielding of the PEPyM in the presence of the CTA. Integration of the spectrum (using peaks 4 and 9) demonstrated that the ratio of the synthesised PEPyM-*b*-PMMA was approximately 30/70. The higher percentage of PEPyM in the block copolymer when compared to the random copolymer was due to improved compatibility with the ACPA initiator under these conditions.

The peaks present in the aliphatic region from the PMMA were represented by doublets indicating that the PMMA units in the copolymer were predominantly syndiotactic; whereas the peaks due to the PEPyM were represented mostly by broad singlets, suggesting that the PEPyM units were predominantly isotactic.

*3.4.3.3 FTIR spectroscopy characterisation of PEPyM-*b*-PMMA*

Figure 3.17 shows an FTIR spectrum of PEPyM-*b*-PMMA block copolymer. The spectrum shows CH_2 bending vibrations (~1430 cm^{-1}) corresponding to the CH_2 groups on the EPyM repeating units and the CH_2 groups connecting repeating units. CH_3 bending vibrations of the methyl groups on both monomer units were observed at ~1380 cm^{-1}. A C-N stretching vibration between 1230 cm^{-1} and 1250 cm^{-1} confirmed the presence of the *N*-substituted pyrrolidine ring. Finally, the ester groups of MMA and EPyM monomer units were observed as C=O stretching vibrations at ~1720 cm^{-1}, and two C-O stretches between 1100 cm^{-1} and 1150 cm^{-1}.

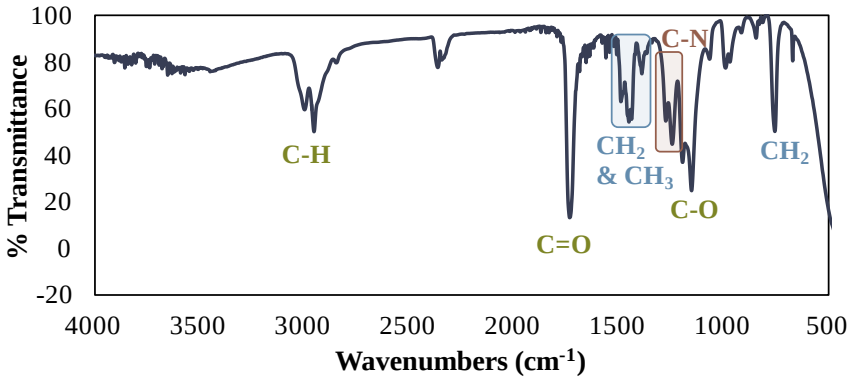

Figure 3.17. FTIR spectrum of PEPyM-*b*-PMMA block copolymer synthesised by RAFT polymerisation.

*3.4.3.4 GPC characterisation of PEPyM-*b*-PMMA*

GPC determined the M_n and M_w of the PEPyM-*b*-PMMA block copolymer to be 7 421 g mol^{-1} and 9 019 g mol^{-1}, respectively. The PDI was determined to be 1.22 which was low, owing to a relatively uniform distribution of chain lengths across the sample. This was consistent with most RAFT polymerisations which have good control of the chain growth.

In comparison to the PEPyM-*co*-PMMA random copolymer synthesised by CFR polymerisation, the PDI (1.21) was very similar with an increased yield (17.19 % and 27.89 % for the random copolymer and the block copolymer, respectively); however, the M_w (14 398 g mol^{-1} for the random copolymer) was reduced (Section 3.3.3.4).

3.5 Concluding remarks

PMMA and PEPyM homopolymers, and PEPyM-*co*-PMMA and PDEAEMA-*co*-PMMA random copolymers, were successfully synthesised by CFR polymerisation. FTIR and ^{1}H NMR spectroscopies confirmed that polymers were produced. ^{1}H NMR spectroscopy in particular was used to determine the tacticity of the CFR polymers. CFR PEPyM and PMMA homopolymers were found to be heterotactic and syndiotactic, respectively. The PMMA units in the CFR PEPyM-*co*-PMMA random copolymer were found to be syndiotactic, whereas the PEPyM units were predominantly isotactic; and the CFR PDEAEMA-*co*-PMMA was observed to be completely syndiotactic. The tacticity can influence the adsorption mechanism to a surface and this was investigated in Chapter 4. Additionally, ^{1}H NMR spectroscopy also determined the final monomer ratio for the CFR PEPyM-*co*-PMMA and CFR PDEAEMA-*co*-PMMA random copolymers to be 21/79 and 34/66, respectively.

GPC results of the polymerisations showed that the CFR polymerisation of MMA was not controlled with a M_n and M_w of 14 770 g ml^{-1} and 29 272 g mol^{-1}, respectively, resulting in a PDI of 1.98 for the PMMA homopolymer. However, the CFR copolymerisation of MMA and EPyM, resulted in the formation of a CFR PEPyM-*co*-PMMA random copolymer via a controlled process shown by a M_n and M_w of 11 926 g mol^{-1} and 14 398 g mol^{-1}, respectively, and a PDI of 1.21. In addition, the CFR copolymerisation of DEAEMA and MMA was also found to be controlled, with a M_n and M_w of 16 821 g mol^{-1} and 18 474 g mol^{-1}, respectively, and a PDI of 1.10.

A comparison was then made between CFR synthesised polymers and RAFT synthesised polymers. RAFRT PMMA and PEPyM homopolymer macro-RAFT agents, and a RAFT PEPyM-*b*-PMMA block copolymer were synthesised via RAFT polymerisation. FTIR and ^{1}H NMR spectroscopies confirmed that the polymers were produced. ^{1}H NMR spectroscopy in particular was used to determine the tacticity of the RAFT polymers. RAFT PEPyM and PMMA homopolymer macro-RAFT agents were heterotactic and syndiotactic, respectively. The PMMA units in the RAFT PEPyM-*b*-PMMA block copolymer were found to

be syndiotactic, whereas the PEPyM units were predominantly isotactic. This shows that the stereochemistry was independent of the polymerisation method, as the same tacticity was observed for both CFR and RAFT polymerisation. ^{1}H NMR spectroscopy also determined the final monomer ratio for the RAFT PEPyM-*b*-PMMA block copolymer to be 30/70.

GPC results showed that, unlike for the CRF method, RAFT polymerisation of MMA to produce a RAFT PMMA homopolymer macro-RAFT agent was a controlled process with a M_n and M_w of 7 152 g mol^{-1} and 8 426 g mol^{-1}, respectively, resulting in a PDI of 1.18. RAFT copolymerisation of this PMMA homopolymer macro-RAFT agent with EPyM monomer, resulted in the formation of a RAFT PEPyM-*b*-PMMA block copolymer again via a controlled process as shown by a M_n and M_w of 7 421 g mol^{-1} and 9 019 g mol^{-1}, respectively and a PDI of 1.22.

RAFT polymerisation is still a relatively new technique and has been shown here to successfully synthesise a RAFT PMMA homopolymer macro-RAFT agent for the chain extension of PEPyM in the formation of a block copolymer of PEPyM-*b*-PMMA. This is the first reported use of RAFT polymerisation for the synthesis of block copolymers containing PEPyM. The process was shown to be controlled for the formation of both homopolymers and block copolymers, which was an improvement on CFR polymerisation.

In the next chapter (Chapter 4), polymer solutions (excluding the PDEAEMA-*co*-PMMA) are deposited onto silicon wafers via spotting or spin-coating and the surfaces characterised via AFM. In the following chapters, these polymers were trialled as capillary surface modifiers for CE separation of ODNs (see Chapter 5 and 6). In particular, the CFR PEPyM-*co*-PMMA random copolymer synthesised by CFR copolymerisation was used for separation of PS-ODNs in Chapter 7.

4 AFM imaging of polymer modified surfaces

4.1 Synopsis

CE of DNA requires surface modification due to the constant mass-to-charge ratio of the DNA molecule. Dynamic coatings are the preferred method due to the wide range of polymers available and simple capillary preparation. These coatings also have the ability to be regenerated and have a higher degree of repeatability. By coating the capillary inner walls, the surface charge, and hence the EOF, can be controlled. In this work, homopolymers and copolymers of EPyM and MMA were used to modify the capillary surface for charge-based separations of ODNs and PS-ODNs in free solution.

*This chapter details the AFM surface characterisation of homopolymers and copolymers of EPyM and MMA (synthesised by CFR and RAFT polymerisation) on untreated and oxidised Si wafers. It was intended from this chapter to gain an insight into the adsorptive properties of the polymers and how this was affected by stereochemistry; and in turn, how this affected the surface coverage and distribution. From the surface morphologies, an adsorption mechanism for the PEPyM-*co*-PMMA random copolymer is proposed herein.*

4.2 Rheological study of a dilute CFR PEPyM-*co*-PMMA random copolymer solution (1 mg mL^{-1})

Rheometry is useful to determine the rheology of a polymer in solution, which describes the orientation and elongation of polymer molecules. It is important to know the rheology of the polymer in a specific solvent for CE separations as this will determine the analyte migration/separation mechanism [98, 120]. For this work, it was important to use a polymer solution that did not cause aggregation and to create an even polymer coating on the capillary surface which would enhance the performance of the coating. The operation of such as polymer coatings in the dilute range (below the c^*) allows for the polymer molecules to be hydrodynamically separated from each other, preventing polymer entanglement and aggregation on the capillary surface during the coating process, providing a uniform layer [115]. Homogeneous capillary surfaces are ideal for CE separations, as rough surfaces have been observed to result in poor separations [12, 177].

To determine the c^* of a polymer in solution, and a polymer radius of gyration (R_p), the intrinsic viscosity [η] of a polymer solution must first be calculated. Equation 1.26 (in Section 1.4.5.2.1) shows that the polymer solution viscosity (η) and the solvent viscosity (η_s) first need to be measured to calculate the [η]. The use of this equation is only applicable in the dilute regime [98], therefore a concentration of 1 mg mL^{-1} polymer in ethanol was initially chosen as it was considered dilute, especially for a low M_w polymer [35, 116]. In this case the CFR PEPyM-*co*-PMMA random copolymer has a M_w of 14 398 g mol^{-1} (see Section 3.3.3.4).

The viscosities of ethanol and the CFR PEPyM-*co*-PMMA random copolymer in ethanol (1 mg mL^{-1}) were determined by rheometry to be 1.69 mPa s^{-1} and 1.79 mPa s^{-1}, respectively (see Section 2.3.2.4). All viscosities were measured at 30 ^{o}C to replicate the temperature used to prepare the polymer coating and analyse the ODNs and PS-ODNs. From these values, [η] was calculated using Equation 1.26 to be 0.062 mL mg^{-1}, and the c^* for the polymer solution (at 30 ^{o}C) was calculated from the [η] to be 2.44 % (24.4 mg mL^{-1}) (see Equation 1.27 in Section 1.4.5.2.1).

Once the c^* was determined, the R_p (see Equation 4.1) for the CFR PEPyM-*co*-PMMA random copolymer was calculated to be 5.2 nm (using M_n, 11 926 g mol^{-1}) and 6.2 nm (using M_w, 14 398 g mol^{-1}).

$$R_p = \sqrt[3]{\left(\frac{[\eta] \times (M_w/N_A)}{6.2}\right)}$$

Equation 4.1

It can be seen from these calculations that 1 mg mL^{-1} was well below the c^* (24.4 mg mL^{-1}), and the small R_p suggests that the polymer chains were not entangled at this concentration.

4.3 Polymer surface morphology studies via atomic force microscopy

AFM is a surface characterisation technique which uses high resolution imaging at the nanoscale [178]. It is used in this work for the determination of surface morphology and topography. AFM works by scanning a tip, attached to a cantilever, across a surface. Deflection of the tip due to surface variations is measured by laser light reflected off the cantilever, and converted into a topographical image by software [177] (see Scheme 4.1). AFM was used to characterise the various polymer surfaces used in this thesis by studying the morphology of the topographical images.

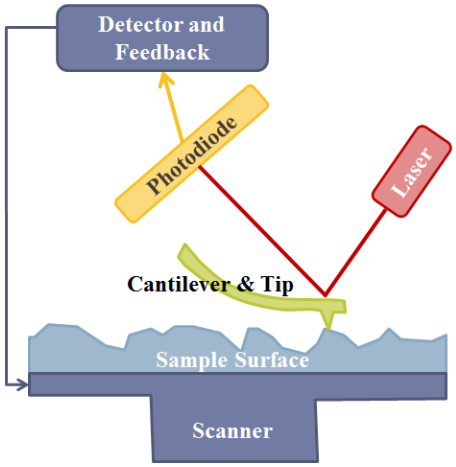

Scheme 4.1. Schematic representation of AFM instrumentation.

4.3.1 AFM imaging of thin films of CFR PEPyM-*co*-PMMA random copolymer deposited on Si wafers

Thin polymer films of CFR PEPyM-*co*-PMMA random copolymer (1 mg mL^{-1}) on untreated Si wafers (see Section 2.3.2.5.1) were prepared via two methods; (1) spotting the polymer solution onto Si wafers and (2) spin-coating the polymer solution onto the Si wafers. Both Si surfaces were prepared from the same polymer solution, and the same volume was applied to each (see Section 2.3.2.5.1 for the procedure).

Figure 4.1A shows a 3D AFM image of the bare Si wafer prior to polymer deposition where the surface roughness RMS was 0.4 nm and the z-height (height in the z-scale range) was 1.4 nm. In the first instance the polymer solution was spotted onto a Si wafer (Figure 4.1B). This resulted in polymer clumping and did not give an even distribution of the polymer on the surface (Figure 4.1B). The surface roughness for this sample was 4.6 nm with a z-height of 12.1 nm, clearly indicating that polymer was deposited using this method. The wafer was then washed by rinsing with Milli-Q water and Tris-borate (100 mM)/urea (7 M) buffer, followed by a final wash with Milli-Q water to remove any deposited salts which would interfere with AFM analysis (see Figure 4.1C). This resulted in a z-height of 10.4 nm and a surface roughness of 5.0 nm. In comparison to the unwashed sample, the z-height was slightly reduced and the roughness was slightly increased. This was attributed to the non-adsorbed polymer being removed from the surface.

An important consideration in polymer deposition is to try and mimic the conditions of how the polymer is introduced into the CE capillary to act as a dynamic coating. This is particularly difficult as in the normal CE process a very high pressure (~94 000 Pa) is applied in order to force the polymer solution through the narrow capillary (50 µm - 75 µm). In an attempt to mimic this process, a spin-coating method was used. Figure 4.1D shows the 3D AFM images of the polymer after spin-coating onto a Si wafer (without subsequent washing). Compared to the spotting method, a far more uniform surface coverage of polymer was observed with a surface roughness RMS of 1.1 nm and a z-height of 4.1 nm. The uniform distribution of the polymer was presumably due to the spinning action used in

creating the thin film. To further replicate conditions of polymer introduction onto a CE capillary whereby any non-adsorbed polymer is removed (by flushing with Milli-Q water and buffer), the spin-coated samples were treated by successive spin coating washes with Milli-Q water, Tris-borate (100 mM)/urea (7 M) buffer, and finally Milli-Q water to remove any deposited salts. From Figure 4.1E it can clearly be seen that the washing steps resulted in an increase in surface roughness (RMS 2.1 nm) implying that along with the removal of non-adsorbed polymer, some of the adsorbed polymer was desorbed from the surface, slightly decreasing the even distribution of the polymer. The z-height of the unwashed sample was 4.1 nm and increased to 7.7 nm after washing.

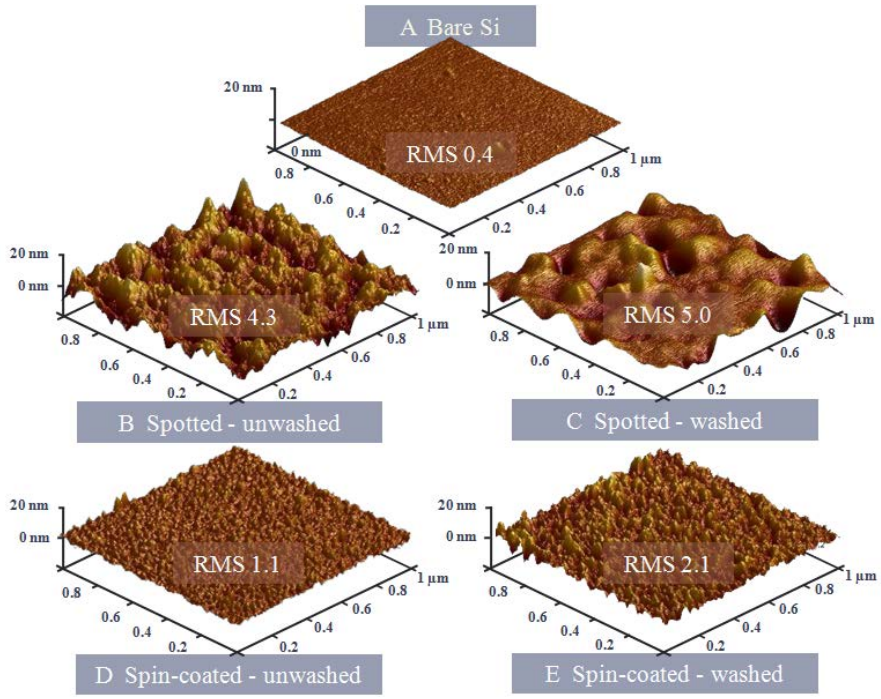

Figure 4.1. 3D AFM images of a bare Si wafer (A), compared to CFR PEPyM-*co*-PMMA random copolymer solution (1 mg mL^{-1}) prepared by spotting (B), followed by washing (C); and prepared by spin-coating (D), followed by washing (E).

4.3.1.1 CFR PEPyM-co-PMMA random copolymer solution concentration study

The dynamics of polymers in solution are governed by the polymer concentration (see Section 1.3.5). Dilute ($c < c^*$) polymer solutions involve the polymer chains being hydrodynamically separated from each other, and as the concentration of polymer in solution is increased, the polymer chains begin to aggregate ($c = c^*$), and entangle ($c > c^*$, semi-dilute) [50, 98, 120, 179]. In order to investigate this,

CFR PEPyM-*co*-PMMA random copolymer solutions were prepared at varying concentration to investigate the effect of concentration on surface coverage and morphology of the adsorbed polymer (see Figure 4.2 for $c < c^*$ solutions). All solutions were spin-coated onto oxidised Si wafers (similar to CE fused silica capillaries) for AFM analysis.

Figure 4.2A shows a 3D AFM image of the bare oxidised Si wafer prior to polymer deposition where the surface roughness RMS was 0.2 nm and the z-height was 0.8 nm. Figure 4.2B-G show the 3D AFM images of CFR PEPyM-*co*-PMMA solutions in the dilute regime and it was observed that as the solution concentration increased from 0.2 mg mL^{-1} to 2.0 mg mL^{-1}, the surface roughness increased linearly from an RMS of 0.8 to 4.7, respectively (see Figure 4.3A). The z-heights also increased, from 3.3 nm for the 0.2 mg mL^{-1}, to 16.3 nm for the 2 mg mL^{-1}. Particle analysis was performed on the particle heights (using NanoScope software) in order to investigate the changing morphology (see Figure 4.3B). Figure 4.3B showed that, in general, the particle heights also increased with increasing concentration, as more polymer was deposited onto the surface.

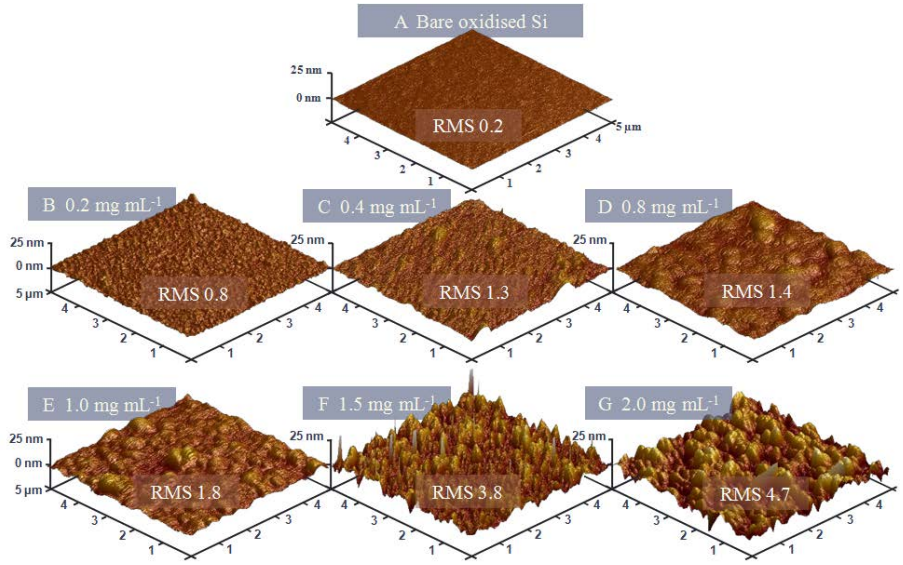

Figure 4.2. 3D AFM images of bare oxidised Si (A), compared to CRF PEPyM-*co*-PMMA random copolymer solutions at varying concentrations (B-G).

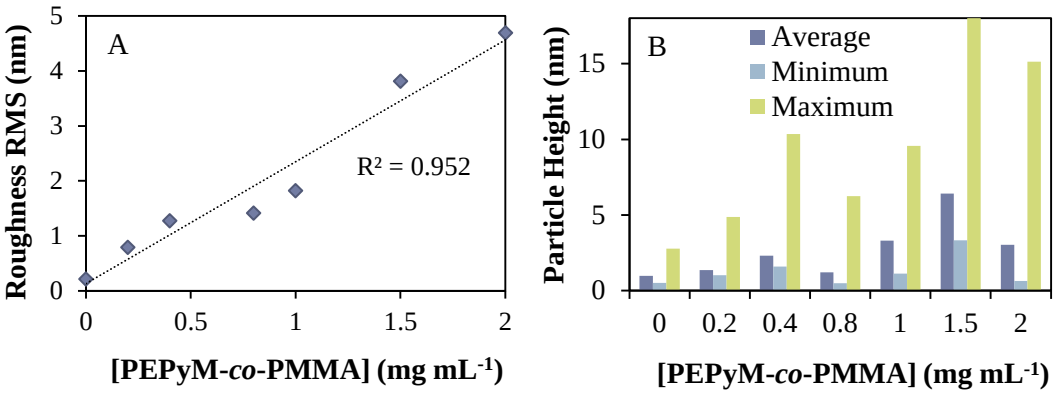

Figure 4.3. Plots of roughness RMS (A), and particle height (B), versus CFR PEPyM-*co*-PMMA random copolymer concentration. Minimum, maximum and average refer to the minimum, maximum and average particle heights, respectively.

Due to the relatively low particle heights, and given the M_w of the CFR PEPyM-*co*-PMMA random copolymer (14 398 g mol^{-1}), it is evident that the polymer chains were folding or coiling and adsorbing onto the surface as individual globules. ^{1}H NMR analysis (see Section 3.3.3.2), showed that the complete polymer was heterotactic. This arose from the analysis that the PMMA component in the copolymer was syndiotactic, which has a fairly rigid conformation; while the PEPyM component was isotactic, which added flexibility to the copolymer. As the PMMA and PEPyM were arranged randomly along the polymer chain, the copolymer was relatively flexible, allowing it to fold or coil. Figure 4.2E appeared to show a complete surface coverage, from an overall increased height compared to the bare surface (Figure 4.2A) with a corresponding low surface roughness (RMS 1.8 nm) and so it was this concentration (1.0 mg mL^{-1}) which was chosen for the dynamic coating of the CE capillary surface.

Figure 4.4A-C shows the 3D AFM images for CFR PEPyM-*co*-PMMA random copolymer solutions at the three different concentration regimes ($c < c^*$, $c = c^*$ and $c > c^*$; see Section 1.3.5.2). The surface roughness again increased with increasing concentration (1.8 nm, 7.4 nm, and 23.5 nm for the 1.0 mg mL^{-1}, 24.4 mg mL^{-1}, and 40.0 mg mL^{-1} solutions, respectively), along with the z-heights (8.0 nm, 25.3 nm, and 75.7 nm for the 1.0 mg mL^{-1}, 24.4 mg mL^{-1}, and 40.0 mg mL^{-1} solutions, respectively). The surface morphologies at the c^* (24.4 mg mL^{-1}) and above the c^* (40.0 mg mL^{-1}) were quite different to the surface for the dilute solutions. The reason for this is the formation of multiple layers along with the aggregation and entanglement of the polymer chains. At the c^* the polymer chains in solution are

said to be coiled and aggregate together, and above the *c**, the chains become entangled creating a mesh. Whilst this was not directly observed in the AFM micrographs, the change in morphology from polymer globules (Figure 4.4A) to a tight aggregation of polymer chains (Figure 4.4B and C) was considered representative of this. The RMS values for the 24.4 mg mL^{-1} and 40.0 mg mL^{-1} solutions were quite high (7.4 nm and 23.5 nm, respectively), and therefore would be detrimental for repeatable CE analysis on capillaries modified with these polymer solutions.

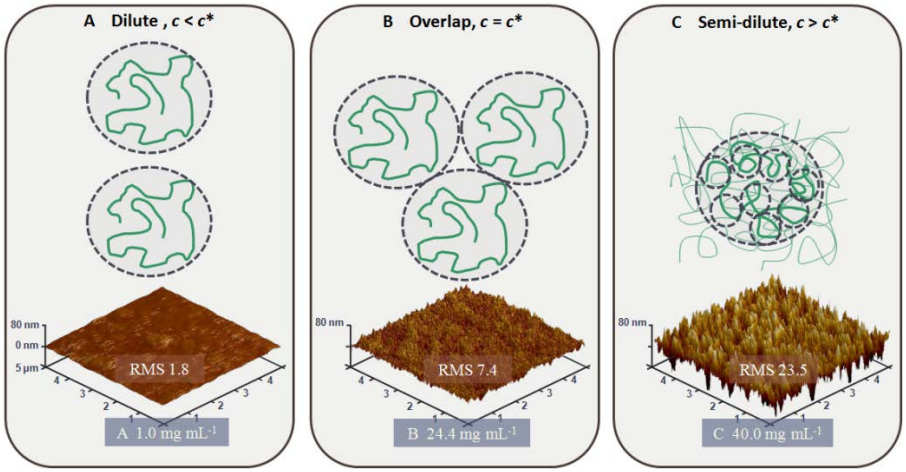

Figure 4.4. 3D AFM images of CFR PEPyM-*co*-PMMA random copolymer solutions at three concentration regimes; dilute regime (1.0 mg mL^{-1}) (A), overlap concentration regime (24.4 mg mL^{-1}) (B), and semi-dilute (entangled) regime (40.0 mg mL^{-1}) (C).

4.3.2 CFR versus RAFT polymer solutions

This section compares the different surface morphologies obtained from homopolymer (Section 4.3.2.1) and copolymer (Section 4.3.2.2) solutions synthesised by CFR and RAFT polymerisation. Polymer solutions of CFR PEPyM and PMMA homopolymers, and RAFT PEPyM and PMMA homopolymer macro-RAFT agents were prepared (1.0 mg mL^{-1}) and their adsorptive properties were compared. Furthermore, the physical adsorptions from polymer solutions of CFR PEPyM-*co*-PMMA (1.0 mg mL^{-1} and 24.4 mg mL^{-1}) were compared to polymer solutions of RAFT PEPyM-*b*-PMMA (1.0 mg mL^{-1} and 24.4 mg mL^{-1}). It was found that surface morphology and coverage was related to polymer tacticity and stereochemistry, and in the case of the RAFT polymers, the presence of the CTA end groups.

4.3.2.1 CFR and RAFT homopolymers of PMMA and PEPyM

The different CFR PEPyM and PMMA homopolymer surfaces and RAFT PEPyM and PMMA homopolymer macro-RAFT agent surfaces were analysed by AFM to gain an insight into the adsorption mechanisms of the polymers onto oxidised Si surfaces similar to CE fused silica capillaries.

Figure 4.5A-D shows 3D AFM images of the CFR PMMA homopolymer (Figure 4.5A) compared to the RAFT PMMA homopolymer macro-RAFT agent (Figure 4.5B); and CFR PEPyM homopolymer (Figure 4.5C) compared to RAFT PEPyM homopolymer macro-RAFT agent (Figure 4.5D). It can be seen from comparison of Figures 4.5A and C, to Figures 4.5B and D that the RAFT PMMA and PEPyM homopolymer macro-RAFT agents had a lower surface coverage than the CFR PMMA and PEPyM homopolymers. This was most likely due to the presence of the RAFT end groups on the homopolymers inhibiting the adsorption to the surface. The CFR PMMA homopolymer (Figure 4.5A) and the RAFT PMMA homopolymer macro-RAFT agent (Figure 4.5B) appeared to adsorb at the chain ends, forming bundles on the surface. Therefore, by looking at the image z-heights (131.7 nm for the CFR PMMA homopolymer, and 50.4 nm for the RAFT PMMA homopolymer macro-RAFT agent), one can gain an insight into the chain lengths of the homopolymers. The CFR PMMA (Figure 4.5A) consisted of many longer chains of polymer surrounded by shorter chains. The high surface roughness (RMS 25.9 nm) demonstrates the non-uniform chain lengths and surface coverage. This was consistent with the high PDI (1.98) and M_w (14 770 g mol^{-1}) determined by GPC (see Section 3.3.2.4). The RAFT PMMA homopolymer macro-RAFT agent (Figure 4.5B) exhibited lower z-heights (due to smaller M_w of 7 152 g mol^{-1}) and reduced surface coverage when compared to the CFR PMMA homopolymer. The surface roughness was decreased (RMS 6.43 nm) owing to a more uniform distribution of polymer chain lengths. This uniformity was reflected in GPC data, which gave a PDI of 1.18 (see Section 3.4.2.4). In this study, a high surface roughness was a direct result of a low surface coverage, therefore, it was more practical to compare the surfaces based on their differences in surface coverage.

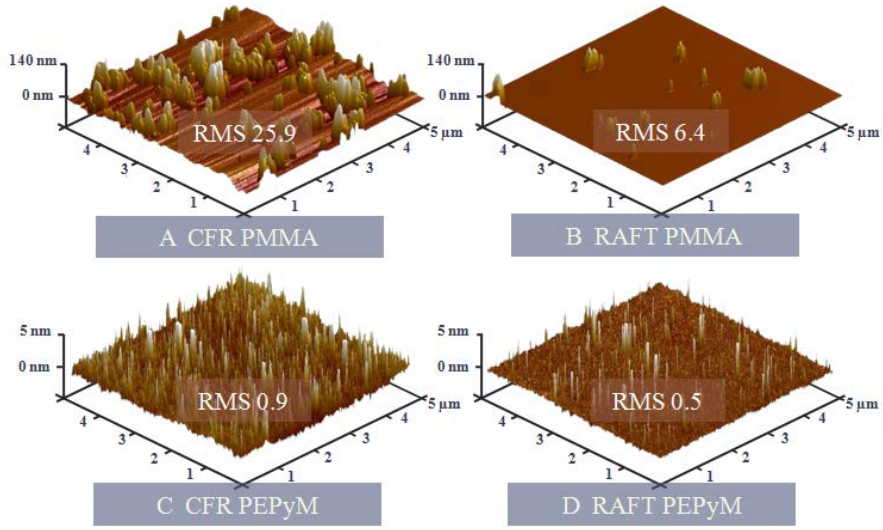

Figure 4.5. 3D AFM images of polymer solutions (1 mg mL^{-1}) of CFR PMMA homopolymer (A), RAFT PMMA homopolymer macro-RAFT agent (B), CFR PEPyM homopolymer (C), and RAFT PEPyM homopolymer macro-RAFT agent (D).

The % surface coverage of the CFR PMMA homopolymer and RAFT PMMA homopolymer macro-RAFT agent (see Figure 4.6A and B) were determined from particle analysis (using NanoScope and ImageJ software) on 2D images, according to Equation 4.2,

$$\%\ \text{surface coverage} = \left(\frac{\text{area of particles in pixels}}{\text{total area of image in pixels}}\right) \times 100$$

Equation 4.2

From Figure 4.5A and B, and Figure 4.6 it was evident that the CFR PMMA homopolymer had a greater surface coverage (19 %) than the RAFT PMMA (2 %).

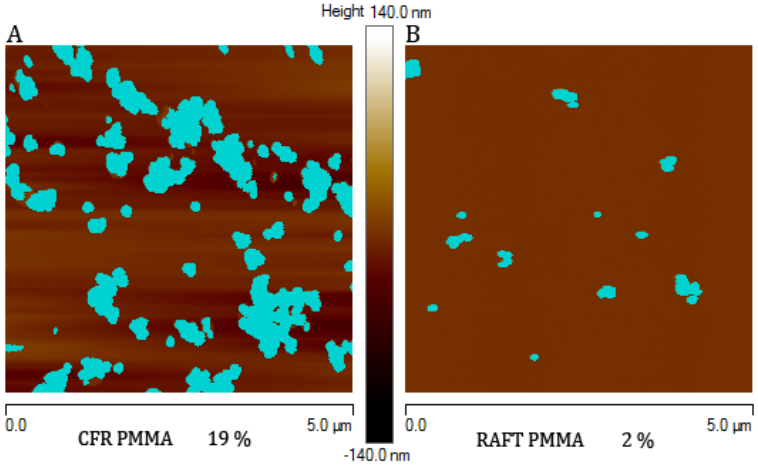

Figure 4.6. 2D AFM images for CFR PMMA homopolymer (A), compared to RAFT PMMA homopolymer macro-RAFT agent (B), showing particle analysis regions in blue.

Figure 4.5C and D showed that the CFR PEPyM homopolymer and the RAFT PEPyM homopolymer macro-RAFT agent did not adsorb at the chain ends (confirmed by the small z-heights of 4.3 nm for CFR PEPyM homopolymer, and 1.6 nm for the RAFT PEPyM homopolymer macro-RAFT agent); rather, a more uniform distribution of polymer was formed across the surface (RMS 0.9 nm for CFR PEPyM homopolymer, and 0.5 nm for RAFT PEPyM homopolymer macro-RAFT agent) which also indicated that the polymer chains were similar in conformation and length. This was confirmed by the low PDI of 1.18 for the PEPyM homopolymer macro-RAFT agent determined by GPC (the PDI for the CFR PEPyM homopolymer was not determined) (see Section 3.4.2.4).

The difference in morphology for the PEPyM and PMMA surfaces was related to the conformation of the polymer chains. From the ^{1}H NMR spectroscopy results (see Sections 3.3.2.2 and 3.4.2.2) it was determined that both CFR PMMA homopolymer and RAFT PMMA homopolymer macro-RAFT agent were predominantly syndiotactic, meaning that the chains were less flexible [180] and therefore less able to fold, hence the formation of erect polymer structures on the surface. Studies on the adsorption of PMMA onto aluminium mirrors (Al-OH surfaces) by Grohens *et al.* [168, 169] found that chain flattening occurred for isotactic PMMA owing to increased flexibility. The authors observed that the number of bound carbonyl groups to the surface was reduced with increasing syndiotacticity, meaning that syndiotactic PMMA did not undergo chain flattening on the aluminium surfaces [168, 169]. On the other hand, the CFR PEPyM homopolymer and RAFT PEPyM homopolymer macro-RAFT agent, were observed from ^{1}H NMR spectroscopy to be predominantly heterotactic (see Sections 3.3.1.2 and 3.4.1.2) resulting in more flexible chains which were able to fold or coil onto the surface [180].

From these surfaces (see Figures 4.5 and 4.6), it was evident that the PMMA did not adsorb as readily to the surface as PEPyM, meaning that it would not effectively reduce the negative charged distribution on the bare fused-silica CE capillaries, and therefore would not effectively eliminate the EOF. The PEPyM, however, created an even polymeric surface which should reduce the negative charge distribution and hence the EOF, and separation of ODNs on this surface

should be achievable. The use of the CFR PMMA and PEPyM homopolymer solutions as a surface coating for the separation of ODNs were investigated in the following chapter (see Sections 5.3.4.1 and Section 5.3.4.2).

4.3.2.2 Comparison of CFR and RAFT copolymers of PEPyM and PMMA surface topographies

The CFR PEPyM-*co*-PMMA random copolymer surface was compared to the RAFT PEPyM-*b*-PMMA block copolymer surface by means of AFM. Polymer solutions (1.0 mg mL^{-1} and 24.4 mg mL^{-1}) were prepared and spin-coated onto oxidised Si wafers. Figure 4.7A-E shows the 3D AFM images comparing the CFR PEPyM-*co*-PMMA random copolymer to the RAFT PEPyM-*b*-PMMA block copolymer, well below the *c** (1.0 mg mL^{-1}) and at the *c** for PEPyM-*co*-PMMA (24.4 mg mL^{-1}).

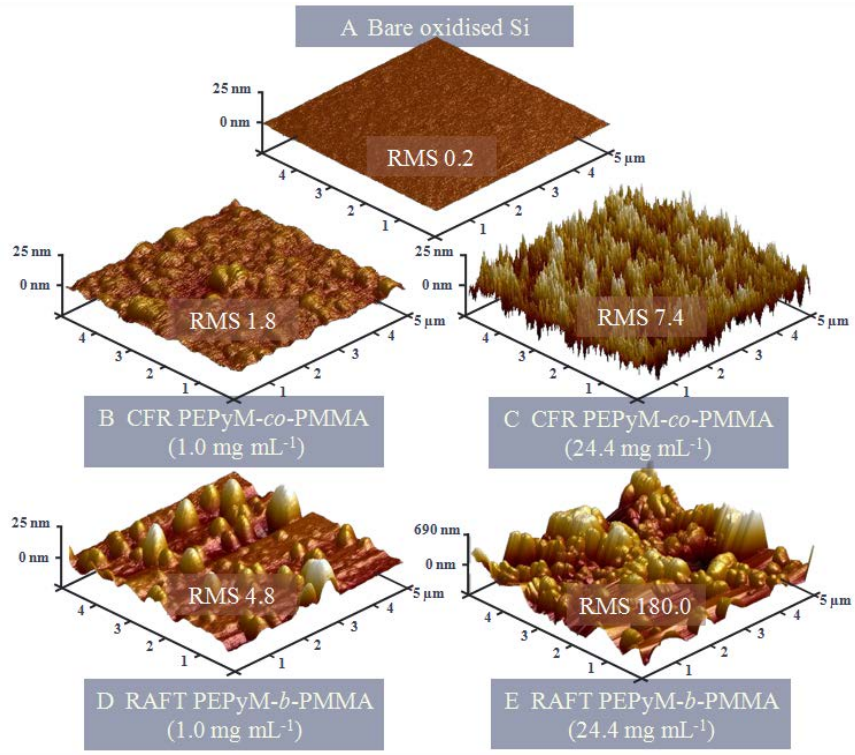

Figure 4.7. 3D AFM images of oxidised bare Si (A); and CFR PEPyM-*co*-PMMA random copolymer solutions at 1.0 mg mL^{-1} (B), and 24.4 mg mL^{-1} (*c**) (C); compared to RAFT PEPyM-*b*-PMMA block copolymer solutions at 1.0 mg mL^{-1} (D), and 24.4 mg mL^{-1} (*c** for CFR PEPyM-*co*-PMMA) (E).

Figure 4.7A shows an AFM image of the bare oxidised Si wafer prior to polymer deposition where the surface roughness RMS was 0.2 nm and the z-height was 0.8 nm. From the surface roughness (RMS of 1.8 nm and 7.4 nm for 1.0 mg mL^{-1} and

24.4 mg mL^{-1}, respectively) and z-heights (8.0 nm and 25.3 nm for 1.0 mg mL^{-1} and 24.4 mg mL^{-1}, respectively) in Figure 4.7B-E, it can be seen that the CFR random copolymer (Figure 4.7B and C) adsorbed evenly on the surface; whereas the RAFT block copolymer (Figure 4.7D and E) formed random aggregates on the surface with increased surface roughness (RMS of 4.8 nm at 1.0 mg mL^{-1}, and 180.0 nm at 24.4 mg mL^{-1}) and z-heights (24.9 nm at 1.0 mg mL^{-1} and 683.6 nm at 24.4 mg mL^{-1}). In addition, the RAFT copolymer solutions resulted in an incomplete surface coverage.

Particle analysis (using NanoScope and ImageJ software) was performed on the 2D AFM images of the RAFT PEPyM-*b*-PMMA block copolymer solutions (see Figure 4.8A and B for the 1.0 mg mL^{-1} and 24.4 mg mL^{-1}, respectively) to determine the % surface coverage according to Equation 4.2. From the particle analysis (Figure 4.8A and B) and Equation 4.2 it was found that the surface coverage of RAFT PEPyM-*b*-PMMA block copolymer solutions were 32 % and 61 % for the 1.0 mg mL^{-1} and 24.4 mg mL^{-1}solutions, respectively. Whilst the surface coverage increased with increasing concentration, even at high concentrations, the block copolymer did not cover the entire surface. The incomplete surface coverage of the RAFT PEPyM-*b*-PMMA block copolymer in comparison to the complete surface coverage of the CFR PEPyM-*co*-PMMA random copolymer (see Figure 4.7B and C), was attributed to the difference in stereochemistry of the polymers.

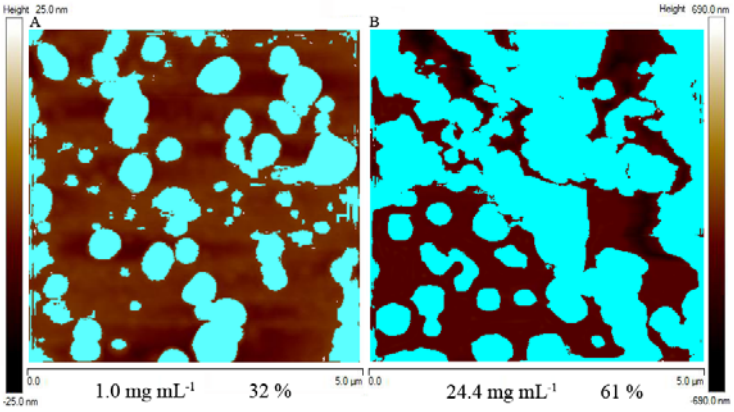

Figure 4.8. 2D AFM images of RAFT PEPyM-*b*-PMMA block copolymer solutions at 1 mg mL^{-1} (A), and 24.4 mg mL^{-1} (B), showing particle analysis regions in blue.

From ^{1}H NMR spectroscopy (see Sections 3.3.3.2 and 3.4.3.2), both the CFR random and RAFT block copolymers were found to be heterotactic (syndiotactic from PMMA and isotactic from PEPyM), and were able to form globules below the

*c** (24.4 mg mL^{-1}); however, owing to the PMMA units present in the block PEPyM-*b*-PMMA, the flexibility was reduced. This decreased flexibility from the PMMA units meant that at high concentrations, rather than entangling, the polymer chains aggregated, further inhibiting polymer folding, leading to the greater peak z-heights observed in Figure 4.5D and E.

From this study, it was found that both copolymers (CFR random PEPyM-*co*-PMMA and RAFT block PEPyM-*b*-PMMA) were capable of adsorbing to the surface by electrostatically shielding some (but not all) of the deprotonated silanol groups on a fused silica CE capillary surface, therefore reducing the negative charge distribution. The use of the CFR PEPyM-*co*-PMMA random copolymer and RAFT PEPyM-*b*-PMMA block copolymer solutions as capillary surface modifiers were investigated for the separation of ODNs in the following chapter (see Section 5.3). Due to the differences in surface morphology/conformation, the observed separation was also shown to be different.

4.4 Adsorption properties of CFR PEPyM-*co*-PMMA random copolymer

The use of copolymer solutions for dynamic coatings means that the polymer can be tailored for optimum performance [52]. Hydrophobic polymers have the ability to displace and replace water molecules from the silanol surface, providing a strongly adsorbed coating [25]. Hydrophilic polymers, on the other hand, are good for modifying the surface charge, but often lack the ability to strongly adsorb to a capillary surface. Combination of both of these properties into one copolymer results in a highly stable modified surface.

The AFM images showed that dilute polymer solutions (1 mg mL^{-1}) of CFR PEPyM-*co*-PMMA created a relatively homogeneous surface to enhance the repeatability and separation of ODNs. Therefore, this polymer was chosen as the main focus for the work presented in this thesis (see Chapters 5, 6 and 7). Copolymers of PEPyM and PMMA are both hydrophilic (EPyM) and hydrophobic (MMA) meaning that they possess good surface adsorptive and shielding properties with the MMA providing stability to the adsorption due to its hydrophobic nature.

The forces involved in physically adsorbed coatings can involve hydrogen bonding, electrostatic interactions, van der Waals forces [90] and hydrophobic interactions [56]. In this case, both the PEPyM and PMMA units have ester groups which are capable of hydrogen bonding to a silanol surface. Although the forces involved with physically adsorbed coatings are well known, the actual mechanisms of attachment are still under speculation [26, 56]. Therefore the AFM experiments were designed to aid in determining the mechanism for the CFR PEPyM-*co*-PMMA adsorption to a silanol surface.

From the 3D AFM images of the CFR homopolymers (Figure 4.5A and C), it was found that the CFR PMMA homopolymer (Figure 4.5A) aggregated in solution and adsorbed onto the surface of the Si wafer on the polymer chain ends forming random bundles, somewhat resembling polymer brushes. The surface coverage was low (19 %) suggesting that the CFR PMMA homopolymer did not readily adsorb to the Si surface. The aggregation of the polymer chains indicated that the attraction between individual CFR PMMA homopolymer chains to each other was greater than the affinity for the surface. On the other hand, the CFR PEPyM homopolymer (Figure 4.5C) was able to adsorb onto the Si surface via potential hydrogen bonding of the carbonyl group to the silanol groups. In addition, the CFR PEPyM homopolymer can provide a positive surface charge to reduce the EOF through the lone pair on the tertiary amine. This lone pair on the CFR PEPyM homopolymer means that it can be easily protonated, providing cationic nature to the polymer which would create a positive surface. In this work, protonation was achieved by addition of formic acid to the polymer solution. A PEPyM-*co*-PMMA random copolymer would possess a combination of the adsorptive qualities described above.

The CFR PEPyM-*co*-PMMA random copolymer and the CFR PMMA and PEPyM homopolymers were used as surface coatings (1 mg mL^{-1}) for the capillary electrophoretic separation of ODNs (see Section 5.3). From the results, it was determined that the PEPyM units were responsible for adsorbing to the surface, and the role of the PMMA units was to stabilise the polymer on the surface by repelling the water molecules that aimed to displace the polymer.

The proposed adsorption mechanism for the PEPyM-*co*-PMMA onto a bare fused-silica surface can be found in Scheme 4.2. According to Zhang *et al*. [26] who used PDMA and PDEA as surface coatings, hydrogen bonds can form between the carbonyl group on the polymer and the silanol groups on the surface. And in the work in this thesis it was found that the PEPyM groups had a greater affinity for the surface and it was therefore through these groups that adsorption was likely to have occurred for the PEPyM-*co*-PMMA random copolymer. Zhang *et al*. [26] also reported that the hydrophobic groups in the PDMA and PDEA moved towards the surface to repel the water molecules in the buffer. In the work herein, the PEPyM units are quite bulky, whereas the PMMA units are relatively small. Therefore the non-adsorbed PMMA can orient itself towards the surface and act as a shield; whereas the non-adsorbed PEPyM can orient itself into the bulk (as shown by Scheme 4.2).

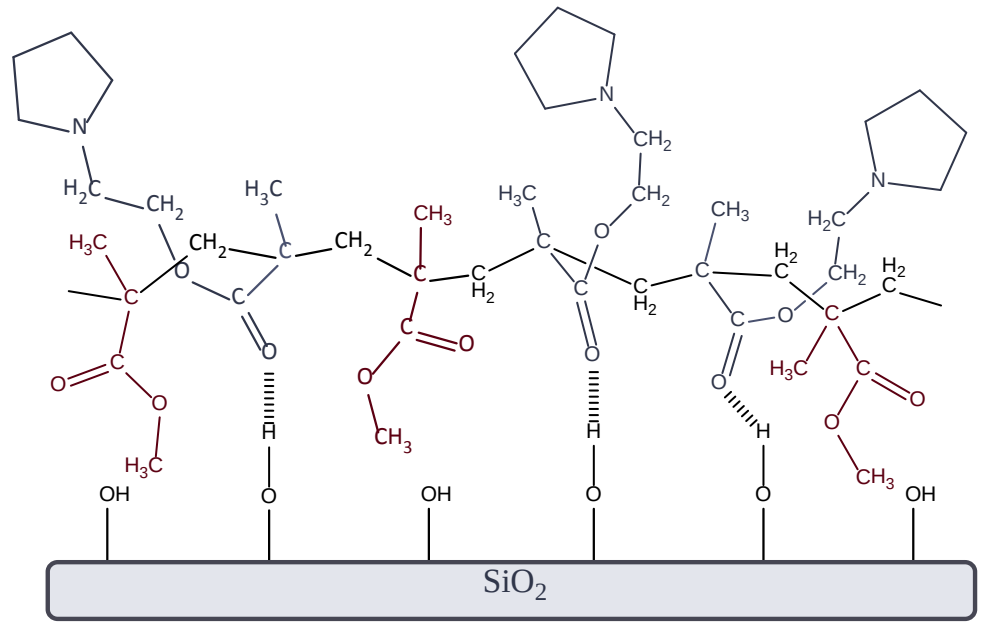

Scheme 4.2. Proposed adsorption mechanism for the CFR PEPyM-*co*-PMMA random copolymer to a silanol surface.

Scheme 4.2 shows that the PEPyM-*co*-PMMA random copolymer is capable of adsorbing to the surface via the carbonyl groups on the PEPyM units and the hydrophobic groups on the PMMA units moved towards the surface releasing their own water of solvation to repel the buffer water molecules hindering them from displacing the adsorbed polymer [26]. The fact that the PEPyM units are arranged in the bulk leaves the *N*-substituted pyrrolidine ring free for ionisation to create a positively charged surface.

4.5 Concluding remarks

Polymer thin films were prepared on Si wafers for the AFM analysis of the topography and hence morphology of the adsorbed polymers. Thin films were prepared by spin-coating in order to replicate the pressure applied to the CE system when coating the inner capillary and the post-coating wash steps resulted in a rougher surface (increased from 1.1 nm for the unwashed surface, to 2.1 nm for the washed surface) with the non-adsorbed polymer being removed from the surface.

The CFR PEPyM-*co*-PMMA random copolymer concentration study showed an increase in surface roughness (from RMS 0.8 nm to 23.5 nm for an increase in concentration from 0.2 mg mL^{-1} to 40.0 mg mL^{-1}) and z-height (from 3.3 nm to 75.7 nm for an increase in concentration from 0.2 mg mL^{-1} to 40.0 mg mL^{-1}) with increasing concentration, with the formation of multiple layers at the *c** (24.4 mg mL^{-1}) and above the *c** (40.0 mg mL^{-1}). It was observed that below the *c**, the dilute CFR PEPyM-*co*-PMMA random copolymer solutions adsorbed to the surface as globules owing to the polymer chains being hydrodynamically separated from one another.

Investigations into homopolymer adsorption found that the CFR PEPyM homopolymer and the RAFT PEPyM homopolymer macro-RAFT agent adsorbed onto the surface as globules from the low surface roughness (RMS 0.9 nm for CFR PEPyM homopolymer, and 0.5 nm for RAFT PEPyM homopolymer macro-RAFT agent) and z-heights (4.3 nm for CFR PEPyM homopolymer, and 1.6 nm for the RAFT PEPyM homopolymer macro-RAFT agent); whereas the CFR PMMA homopolymer and the RAFT PMMA homopolymer macro-RAFT agent adsorbed on the chain ends to form polymer bundles on the surface with reduced surface coverage (RMS 25.9 nm for the CFR PMMA homopolymer, and 6.43 nm for the RAFT PMMA homopolymer macro-RAFT agent) and increased z-heights (131.7 nm for the CFR PMMA homopolymer, and 50.4 nm for the RAFT PMMA homopolymer macro-RAFT agent). The RAFT homopolymer macro-RAFT agents exhibited lower surface coverage due to the inhibition of adsorption by the CTA dithiobenzoate end groups. The different surface morphologies were related to the stereochemistry (and hence flexibility).

The RAFT PEPyM-*b*-PMMA block copolymer solutions resulted in the formation of random aggregates on the surface with reduced surface coverage (32 % and 61 % for the 1.0 mg mL^{-1} and 24.4 mg mL^{-1} solutions, respectively), regardless of concentration. In addition, the surface roughness (RMS of 1.8 nm and 7.4 nm for 1.0 mg mL^{-1} and 24.4 mg mL^{-1}, respectively) and z-heights (8.0 nm and 25.3 nm for 1.0 mg mL^{-1} and 24.4 mg mL^{-1}, respectively) were increased in comparison to the CFR PEPyM-*co*-PMMA random copolymer. The difference in surface morphologies between the random and block copolymers was attributed to the difference in stereochemistry. In terms of CE, a low surface roughness (and hence a uniform surface) is ideal for repeatable separations and enhanced performance [12, 177]; therefore, a 1.0 mg mL^{-1} concentration was chosen for all CE separations (see Chapter 5).

An adsorption mechanism for the CFR PEPyM-*co*-PMMA random copolymer was proposed suggesting that the hydrophilic PEPyM units were responsible for adsorption to the surface via the carbonyl groups, and the hydrophobic PMMA stabilised the attachment. In addition, the PEPyM added cationic nature to the PEPyM-*co*-PMMA copolymer meaning that it could be ionised to create a positive charge and further reduce the EOF for enhanced ODN and PS-ODN mobility.

5 Capillary electrophoretic separation of ODNs

5.1 Synopsis

CE is an attractive technique for the analysis of biomolecules due to its high sensitivity, separation efficiency and reliability [22]. *In particular, there is great interest in the use of CE for the identity and purity of synthetic and therapeutic oligonucleotides. Work described in this thesis focuses on resolving short model dsODNs (16 bp - 20 bp) using CE with the aim to employ the optimised system for PS-ODN separation. To achieve this, dynamic homopolymer and copolymer coatings based on EPyM, MMA and DEAEMA were applied to fused-silica capillaries. The method development is described in the following.*

5.2 CE Method development

5.2.1 PEPyM-*co*-PMMA (21/79) coated capillaries

There are a number of parameters in CE that need to be considered when developing a suitable method for analysis of a specific analyte. It is essential to first consider the properties of the analyte before proceeding too far. In this case, analysis of short fragments of DNA (ODNs). The DNA properties to consider include the negative charge, the acidic nature, and the inflexibility of the strands. During the method development stage in this work, it was also important to consider the buffer composition and pH (as well as organic/ionic modifiers/additives), capillary temperature, applied voltage and the use of and surface modification.

In this work the method initially employed was adapted from Bernal *et al.* [79] for the separation of proteins using a CFR PEPyM-*co*-PMMA random copolymer coating. The PEPyM-*co*-PMMA (21/79) random copolymer was synthesised by CFR polymerisation according to Section 2.3.1.2.3 (refer to Section 3.3.3 for the characterisation) for surface modification and the method was developed with this surface in mind.

As a general rule, while taking into account the analyte properties, following the steps in Scheme 5.1 assists in designing a successful CE method [17]. Each step is defined in the following method development as it applies to this thesis.

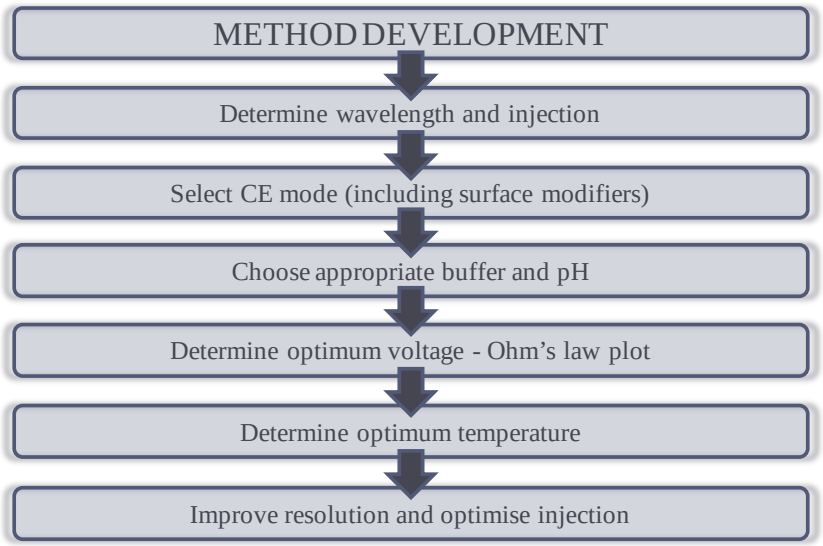

Scheme 5.1. A typical approach for CE method development. Adapted from [17].

5.2.1.1 Wavelength

UV diode array detection (DAD) is capable of detecting analytes at concentrations as low as 1 x 10^{-6} M [15] and while it is not as sensitive as LIF detection (capable of detecting as low as a single molecule), UV detection does not require any enhancement or modification of the analyte with organic or intercalating dyes. A UV scan of ODNs in solution (water) showed a strong absorption at 260 nm, leading to this wavelength being chosen for analysis. A negative control wavelength was also employed at a wavelength in which ODNs do not strongly absorb (470 nm). This control was used to ensure correct peak assignment to the ODNs. The limit of detection (L.O.D) for the optimised system was determined to be 1.04 µM from the equation of the line from the plot of peak area versus height (Figure 5.1).

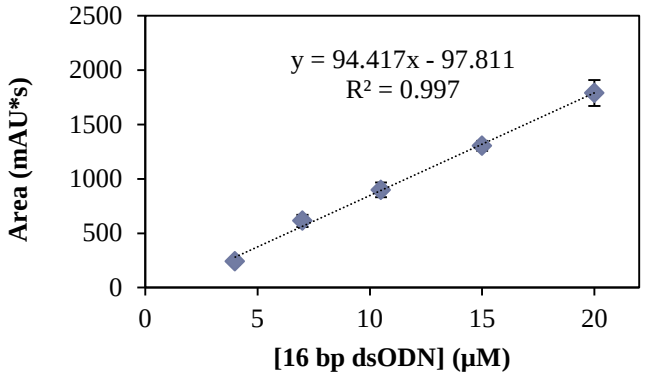

Figure 5.1. Plot of peak area versus 16 bp dsODN concentration to determine the L.O.D. Error bars are ± 1 s_d from n = 3.

5.2.1.2 Injection

The most common injection methods employed in CE are hydrodynamic and electrokinetic injection. Hydrodynamic injection provides high repeatability of injections and it is dependent on instrumental controlled parameters only, whereas electrokinetic injection depends on the analyte apparent mobility (μ_{app}), sample matrix, and EOF at a given voltage. Hydrodynamic injection works by applying a pressure to the injection vial for a pre-determined time, forcing the liquid into the capillary. This method of injection was used in the work presented in this chapter. The approximate injection volumes (v_{int}) of the ODN samples (in water) were calculated from Equation 5.1 to be 0.69 nL and 0.14 nL for a 75 µm and 50 µm capillary, respectively,

$$v_{int} = \pi r^2(\Delta P r^2 t_{int}/(8\eta L_t))$$

Equation 5.1

where r is the capillary inner radius (37.5 x 10^{-4} cm for the 75 µm capillary and 25 x 10^{-4} cm for the 50 µm capillary), ΔP is the change in pressure (5000 Pa), t_{int} is the injection time (6 s), η is the sample viscosity (the viscosity of water (8.9 x 10^{-4} Pa s) was used since the change in viscosity with low concentrations of ODNs was assumed to be negligible), and L_t is the total capillary length (38 cm).

5.2.1.3 Buffer

In order to choose a buffer system for successful separation of a specific analyte, it is important to first consider the physical and chemical properties of the analyte in regards to pKa, solubility, stability and absorbance. Of further importance is the pH and ionic strength of the buffer, along with buffer additives.

5.2.1.3.1 pH

Buffers have a useful pH range [17] which assists in determining a suitable buffer for analysis of a specific analyte. Low pH values will hydrolyse DNA; therefore, it is not useful to use a low pH buffer unless the EOF needs to be decreased or reversed. Likewise at high pH (above 10), DNA can be denatured, thus using a pH between 7 and 9 is ideal. At pH 7, the phosphate groups are strongly negatively charged; therefore it is best to have a pH at or above this value to enhance mobility. A Tris-borate buffer has a useful pH range of 7.9 to 10.1 [17], making it suitable for ODN analysis and hence was the buffer chosen for this study (at pH 9). Tris-borate is commonly used as a DNA separation run buffer as it is proven to increase the negative charge density of the strands by nonspecific binding of the borate ions to the deoxyribose residues [20]. This consequently increases the μ_{app} of the ODNs [105, 181]. Tris-borate is also reported to have a low μ_{app} owing to the borate and Tris base existing in their uncharged forms under acid-base equilibrium [182]. This is advantageous in ODN separations as it results in a slower EOF.

5.2.1.3.2 Ionic strength

An increase in ionic strength results in the compression of the Debye layer, decreasing the zeta potential [18]. The zeta potential is used to describe the diffuse layer, and hence a reduction in this layer results in a reduced EOF. In addition, the reduction in EOF can also be related to the viscosity; as BGE ionic strength increases, so does the viscosity.

The Helmholtz-Smoluchowski equation (Equation 1.9 in Section 1.2.3.2) is used to describe the v_{EOF} [18]; whereas the Smoluchowski equation (Equation 1.6 in Section 1.2.3.2) alone describes the mobility of a charged ion in a charged solution in relation to the EDL, and is applicable to both a migrating analyte and the BGE. Equation 1.2 (Section 1.2.3.1) and Equation 1.6 (Section 1.2.3.2) imply that an increase in the viscosity will result in a decrease in v_{EOF} and μ_{EOF}, effectively decreasing the EOF and, according to Equation 1.7 (Section 1.2.3.2), in free solution electrophoresis this will also decrease the t_m. Increasing the ionic strength may also result in decreased surface-analyte interactions. In addition, changing the ionic strength can also increase the R_s by potentially decreasing analyte-analyte and analyte-buffer interactions [105]. One thing to consider is, increasing the ionic strength also increases the current and hence joule heating, which in turn can reduce the repeatability. For this reason a Tris-borate buffer concentration of 100 mM was chosen for this study which was capable of resolving peaks under low applied voltages, avoiding problems associated with joule heating.

The effect of changing BGE ionic strength on the ODN and PS-ODN mobility was investigated in Chapter 6 and 7, respectively.

5.2.1.3.3 Additives

There are a number of different additives available for CE buffers with a variety of functions, such as organic or inorganic solvents and salts, surfactants and, of course, polymers. In the case of analysis of ODNs, organic salts such as urea are useful to improve the R_s, and modify the EOF.

In this work, urea (7 M) was used to inhibit the formation of secondary structures during electrophoresis [17]. Figure 5.2 shows the analysis of a mixture of 16 bp and 20 bp dsODNs using Tris-borate buffer (100 mM, pH 9) with (Figure 5.2(i)) and without urea (Figure 5.2(i)). Analysis without urea resulted in co-migration of the dsODNs, in comparison to the baseline R_s observed when using a BGE containing urea. A decrease in migration was also observed without urea, indicating ODN-buffer interactions (the formation of ODN-borate complexes which increased the negative charge and hence the μ_{app} [20, 105, 181]). Both these facts verify that the addition of urea successfully inhibited the formation of secondary structures by reducing the ODN-ODN interactions. These types of interactions have previously been reported by Stellwagen & Stellwagen [16, 105] who used ionic salts as buffer additives to control these interactions (see Section 1.4.1.3).

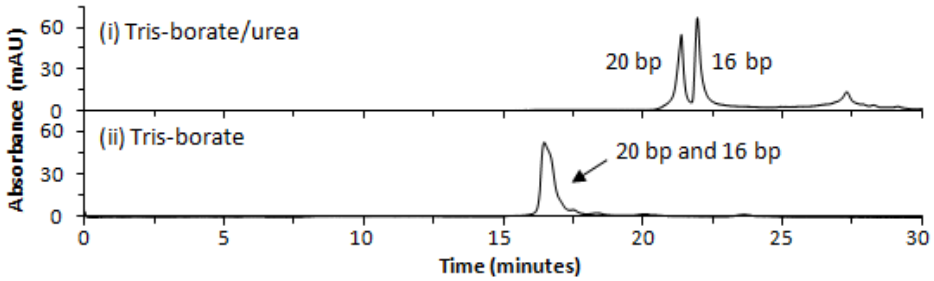

Figure 5.2. CE electropherograms of separation of a mixture of 16 bp and 20 bp dsODNs on a CFR PEPyM-*co*-PMMA random copolymer (21/79) coated fused-silica capillary (30 cm L_d, 38 cm L_t, 75 µm id, 363 µm od) at -131.6 V cm^{-1} with UV detection at 260 nm for 30 min run time. The BGE was Tris-borate (100 mM)/urea (7 M) (i) and Tris-borate (100 mM) (ii) at pH 9.0. Samples were introduced hydrodynamically at 5000 Pa for 6 s.

5.2.1.4 Surface modifiers

Hybrid copolymers were used as surface modifiers to suppress the EOF. For this a copolymer of hydrophilic (EPyM and DEAEMA) and relatively hydrophobic (MMA) monomers were synthesised (see Chapter 2 for synthesis and Chapter 3 for characterisation). In order to provide an even surface coverage, dilute solutions (1 mg mL^{-1} in ethanol or acetone) were used to avoid polymer entanglement. This was discussed further in Chapter 4. The tertiary nitrogen in the EPyM and DEAEMA units adds cationic character to the polymers, with a pKa of approximately 10, meaning that the surface charge has the potential to be pH tuneable.

In this work, it was ideal to reduce (but not eliminate) the EOF, and by modifying the amount of the cationic EPyM monomer in the polymer, the surface charge can be regulated, and hence, the EOF. This has been previously reported for EPyM [79, 80]. While this property is useful for efficient EOF elimination, a highly positively charged surface would promote strong ODN-surface interactions and band-broadening, and it was therefore necessary to use a smaller ratio of EPyM. A 21/79 ratio was effective at reducing the EOF by shielding the surface to a suitable degree to allow enhanced R_s of strands.

5.2.1.5 Ohm's Plot

Ohm's law was used to determine the optimum voltage to avoid joule heating for the Tris-borate (100 mM)/urea (7 M) buffer by plotting current versus applied voltage (see Figure 5.3). Data for the plot were obtained by applying each voltage for 30 s and recording the stabilised current with a 30 s wait period in between each applied voltage. Joule heating was indicated by the plot deviating from linearity, which was caused by the lack of heat dissipation through the capillary walls which is detrimental to the repeatability of the analysis.

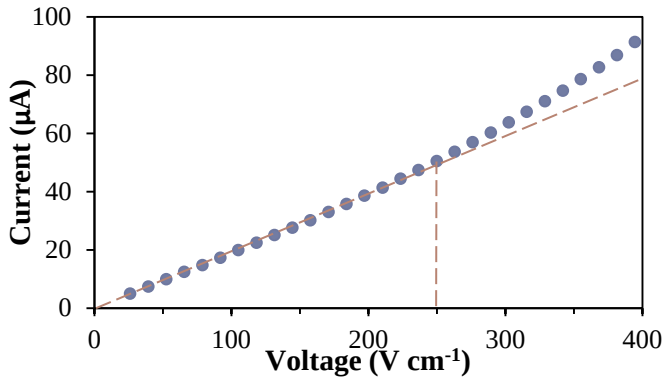

Figure 5.3. Ohm's plot of current versus voltage at 30 °C for the Tris-borate (100 mM)/urea (7 M) buffer at pH 9 on a CFR PEPyM-*co*-PMMA random copolymer (21/79) coated fused-silica capillary (30 cm L_d, 38 cm L_t, 75 µm id, 363 µm od).

From Figure 5.3, it is evident that the effective voltage range is between 0 V cm^{-1} and 250 V cm^{-1} as after this point the plot deviated from linearity. This implied the buffer was no longer capable of overcoming joule heating after 250 V cm^{-1}. The effect of voltage on the R_s of 16 bp and 20 bp dsODN mixtures was investigated and discussed in Section 5.2.1.7.

5.2.1.6 EOF velocity and EOF mobilities

The v_{EOF} and μ_{EOF} governs the migration of the analyte in the system. According to Equation 1.10 (Section 1.2.3.3), in order to determine the overall electrophoretic mobility (μ_{obs}) of the ODNs, the EOF mobility must be evaluated. The EOF of the Tris-borate (100 mM)/urea (7 M) buffer was determined using a CMS and also by use of a neutral marker on the CE instrument; and the two methods were compared. The EOF mobilities were investigated on both bare fused-silica capillaries, and fused silica capillaries coated with CFR PEPyM-*co*-PMMA random copolymer (synthesised by CFR copolymerisation according to Section 2.4.1.2.3) to ascertain the effectiveness of the coating to suppress the EOF.

5.2.1.6.1 Current monitoring system

The v_{EOF} and μ_{EOF} of the Tris-borate (100 mM)/urea (7 M) buffer were determined for coated and uncoated capillaries using a CMS. For an uncoated fused-silica capillary at basic pH the EOF was cathodic due to the large negative charge density along the capillary surface. Replacing some of the silanol groups with copolymer reduced the number of deprotonated silanol groups and reduced (but did not remove) this negative charge distribution indicating the shielding effect of the copolymer. The v_{EOF} and μ_{EOF} values for a bare fused-silica capillary and for a CFR PEPyM-*co*-PMMA random copolymer coated capillary at applied voltages of 60 V cm^{-1}, 80 V cm^{-1} and 100 V cm^{-1} can be found in Table 5.1 along with the associated error (standard deviation (s_d)) and repeatability (represented by % relative standard deviation (% RSD)).

These results indicated that the EOF was suppressed with the CFR PEPyM-*co*-PMMA random copolymer coated capillary and this suppression was independent of voltage. A decrease in μ_{EOF} values (for 100 V cm^{-1}) from 30.6 x 10^{-9} m^2 V^{-1} s^{-1} to 28.1 x 10^{-9} m^2 V^{-1} s^{-1} (total suppression of 8.11 %) with the coating indicated the polymer was shielding the capillary [80]. Figure 5.4 showed that an increase in v_{EOF} was observed with increasing applied voltage which was expected as increasing the voltage increases the current, and hence increases buffer ion movement.

Table 5.1. Calculation of v_{EOF} and μ_{EOF} for a bare fused-silica capillary compared to a CFR PEPyM-*co*-PMMA random copolymer (21/79) coated fused-silica capillary using a CMS.

	Bared fused-silica capillary				PEPyM-*co*-PMMA coated capillary				Magnitude of EOF suppression
Voltage ($V\ cm^{-1}$)	v_{EOF} x 10^{-4} ($m\ s^{-1}$)	μ_{EOF} x 10^{-9} ($m^2\ V^{-1}\ s^{-1}$)	s_d (x 10^{-9}) (n = 3)	RSD (%)	v_{EOF} x 10^{-4} ($m\ s^{-1}$)	μ_{EOF} x 10^{-9} ($m^2\ V^{-1}\ s^{-1}$)	s_d x 10^{-9} (n = 3)	RSD (%)	(%)
60	2.05	34.1	1.79	5.23	1.88	31.3	0.68	2.18	8.25
80	2.52	31.5	0.47	1.50	2.32	29.0	2.09	7.22	8.02
100	3.06	30.6	0.52	1.71	2.81	28.1	1.64	5.83	8.11

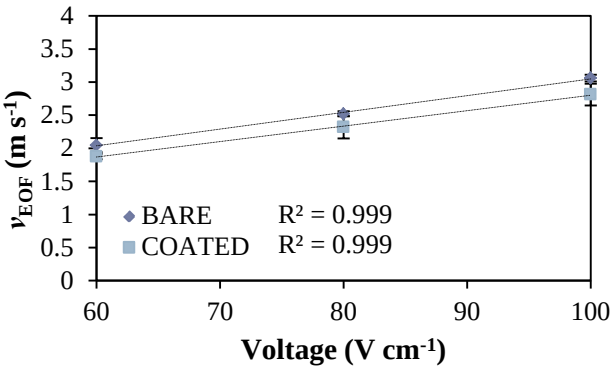

Figure 5.4. Plot of v_{EOF} versus voltage for a bare capillary compared to a capillary coated with CFR PEPyM-*co*-PMMA random copolymer (21/79). Analysis was performed on fused-silica capillaries (5 cm L_t, 75 µm id, 363 µm od). Error bars are ± 1 s_d from n = 3.

Although the μ_{EOF} should be independent of field strength, a slight decreasing trend was observed (see Figure 5.5). However, the error associated with this analysis was quite high (refer to % RSD values in Table 5.1, and the R^2 values and overlapping error bars in Figure 5.5), in particular for the coated capillary, which was detrimental to the accuracy of the analysis. This suggests that the trend is purely a consequence of high systematic error.

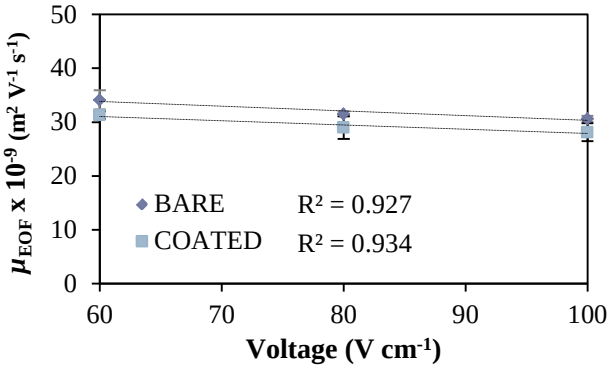

Figure 5.5. Plot of μ_{EOF} versus voltage for a bare capillary compared to a capillary coated with CFR PEPyM-*co*-PMMA random copolymer (21/79). Analysis was performed on fused-silica capillaries (5 cm L_t, 75 µm id, 363 µm od). Error bars are ± 1 s_d from n = 3.

This high degree of error was due to the experiment operating in an uncontrolled environment. The CMS was not temperature controlled and it was therefore not possible to investigate the effect of temperature on the μ_{EOF}. In addition, it had no cooling system in place to assist in heat dissipation and hence was susceptible to joule heating. The EOF data obtained from the CMS cannot be directly compared to the electrophoretic mobilities of the ODNs owing to the different operating conditions and capillary preparation. Therefore, a neutral marker was employed for the use on the CE system to determine the EOF mobilities for direct comparison.

5.2.1.6.2 Neutral marker

The v_{EOF} and μ_{EOF} of the Tris-borate (100 mM)/urea (7 M) buffer were also determined for CFR PEPyM-*co*-PMMA random copolymer coated and bare fused-silica capillaries at varying capillary temperatures (15 ^{o}C - 50 ^{o}C) and buffer pH (3 - 11) using a buffer/water/acetone (20/75/5 % v/v/v) solution as a neutral marker. The neutral marker was used due to its uncharged nature and hence the migration is solely dependent on the bulk flow (EOF) through the capillary. Acetone was chosen as the neutral marker as it is readily available and not easily dissociated or ionised under typical CE conditions.

5.2.1.6.2.1 Temperature study

Figure 5.6 displays the CE electropherograms of the neutral marker at varying temperatures for the bare capillary compared to the coated capillary. From these plots, it is evident that the two capillary surfaces provided significantly different v_{EOF} under the same conditions. The t_m decreased with increasing temperature for both the bare and the coated capillaries.

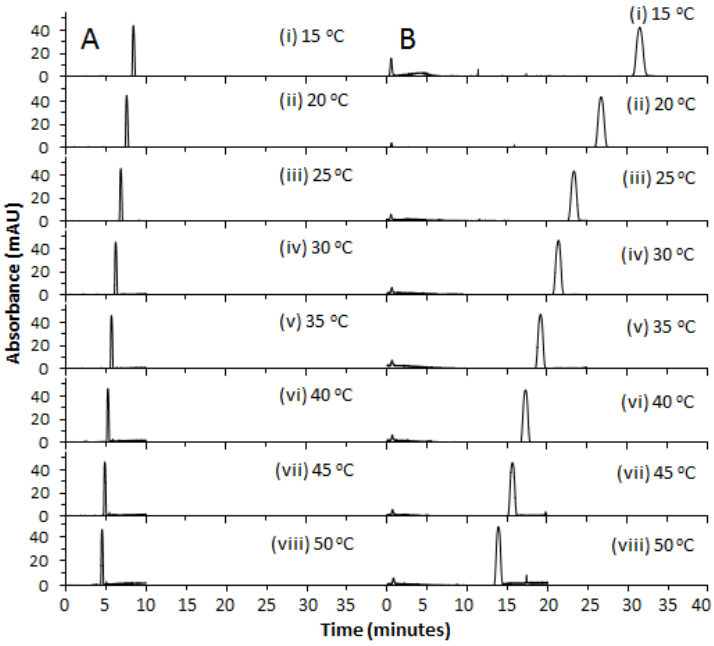

Figure 5.6. CE electropherograms of separation of the buffer/water/acetone neutral marker (20/75/5) on a bare capillary (A), compared to a CFR PEPyM-*co*-PMMA random copolymer (21/79) coated capillary (B), at varying temperatures (i)-(viii). Separation was performed on fused-silica capillaries (30 cm L_d, 38 cm L_t, 75 µm id, 363 µm od) at 263.2 V cm^{-1} with UV detection at 254 nm for 40 min run time. The BGE was Tris-borate (100 mM)/urea (7 M). Samples were introduced hydrodynamically at 5000 Pa for 6 s.

A plot of t_m versus temperature (see Figure 5.7) indicated that the decreasing trend was logarithmic (R^2 values of 0.996 and 0.999 for the bare and coated capillaries, respectively). This was confirmed from a plot of the natural log of t_m versus temperature which exhibited R^2 values of 0.997 and 0.998 for linear regression of the bare and coated capillaries, respectively (the plot of the natural log of t_m versus temperature can be found in Figure 10.1 in Appendix A). The neutral marker on the coated capillary experienced a different migration pattern with respect to temperature than the bare capillary. An increase in temperature increased the EOF by decreasing the buffer viscosity, and at lower temperatures, the coating was more effective at shielding the surface charge.

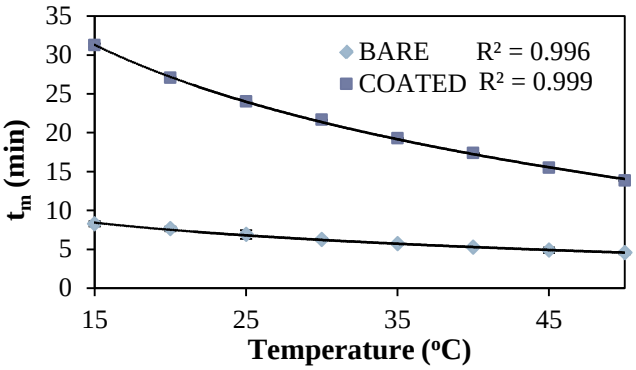

Figure 5.7. Plot of t_m of the neutral marker versus temperature for a bare capillary compared to a capillary coated with CFR PEPyM-*co*-PMMA random copolymer (21/79). Separation was performed on fused-silica capillaries (30 cm L_d, 38 cm L_t, 75 µm id, 363 µm od). Error bars are ± 1 s_d from n = 3.

The t_m is not a good measure of mobility as it does not take into account the EOF, capillary length and voltage. The μ_{EOF} is a much more accurate measure of EOF and can easily be calculated from the t_m of a neutral marker, applied voltage, L_d and L_t according to Equation 1.9 (Section 1.2.3.3). The v_{EOF} of the buffer was also determined but it is important to keep in mind that it is voltage dependent, and does not give an accurate measure of the EOF. The velocities at 263.2 V cm^{-1} were calculated from the μ_{EOF} according to Equation 5.2,

$$v_{EOF} = \frac{\mu_{EOF} V}{L_t}$$

Equation 5.2

where V is the voltage. However, the v_{EOF} was more simply calculated according to Equation 5.3 using the t_m of the neutral marker and the L_d of the capillary.

$$\nu = \frac{L_d}{t_m}$$

Equation 5.3

The calculated ν_{EOF} and μ_{EOF} values for a bare fused-silica capillary and the CFR PEPyM-*co*-PMMA random copolymer coated capillary at varying temperatures and a positive applied voltage of 263.2 V cm^{-1} can be found in Table 5.2. Analysis was performed in triplicate with acceptable % RSD values for both the bare and coated capillaries. The magnitude of suppression was calculated from Equation 5.4.

$$\% \text{ suppression} = \left(\frac{\mu_{EOF}^{bare} - \mu_{EOF}^{coated}}{\mu_{EOF}^{bare}}\right) \times 100$$

Equation 5.4

In accordance with the results from the CMS, the results using the neutral marker indicated that the EOF was suppressed with the CFR PEPyM-*co*-PMMA random copolymer coated capillary, with the EOF being cathodic in both cases. This again indicated the effective shielding of the surface charge by the polymer as it replaced the silanol groups. The cathodic flow (although reduced) for the coated capillaries suggested that at pH 9, not all the negative groups were replaced by the polymer. The large difference in % EOF suppression recorded by the CMS (Table 5.1) and using a neutral marker in the CE (Table 5.2), was due to the different instruments used for the analysis. The error associated with the CMS was large; whereas the error associated with the neutral marker method was minimal, stressing the importance of operating in a controlled environment. The % EOF suppression determined by the CMS was therefore disregarded.

Table 5.2. Calculation of v_{EOF} and μ_{EOF} at varying temperatures for a bare fused-silica capillary compared to a CFR PEPyM-*co*-PMMA random copolymer (21/79) coated fused-silica capillary using the buffer/water/acetone (20/75/5) neutral marker.

Bare fused-silica capillary						PEPyM-*co*-PMMA coated capillary					Magnitude of EOF Suppression
Temp. (^oC)	t_m (min)	v_{EOF} x 10^{-4} (m s^{-1})	μ_{EOF} x 10^{-9} (m^2 V^{-1} s^{-1})	s_d x 10^{-9} (n = 3)	RSD (%)	t_m (min)	v_{EOF} x 10^{-4} (m s^{-1})	μ_{EOF} x 10^{-9} (m^2 V^{-1} s^{-1})	s_d x 10^{-9} (n = 3)	RSD (%)	(%)
15	8.27	6.04	23.0	0.62	2.72	31.25	1.60	6.1	0. 65	1.06	73.53
20	7.63	6.55	24.9	0.22	0.90	27.06	1.85	7.0	0. 76	1.08	71.80
25	6.89	7.25	27.6	0.20	0.74	23.98	2.09	7.9	0.19	2.35	71.26
30	6.26	7.99	30.4	0.25	0.81	21.62	2.31	8.8	0.07	0.83	71.06
35	5.72	8.74	33.2	0.23	0.68	19.26	2.60	9.9	0.05	0.56	70.30
40	5.27	9.49	36.1	0.18	0.68	17.37	2.88	10.9	0.03	0.56	69.67
45	4.88	10.25	38.9	0.22	0.57	15.46	3.23	12.3	0.28	2.30	68.44
50	4.55	10.99	41.8	0.18	0.43	13.82	3.62	13.8	0.17	1.21	67.09

As was expected, the v_{EOF} and μ_{EOF} increased with increasing temperature (see Figure 5.8) as increasing the temperature decreased the buffer viscosity which, in accordance with Equation 1.6 (Section 1.2.3.2), increased the mobility. This increase followed a linear trend with a R^2 value of 0.998 and 0.991 for the bare and coated capillaries, respectively, indicating a high degree of accuracy in the results.

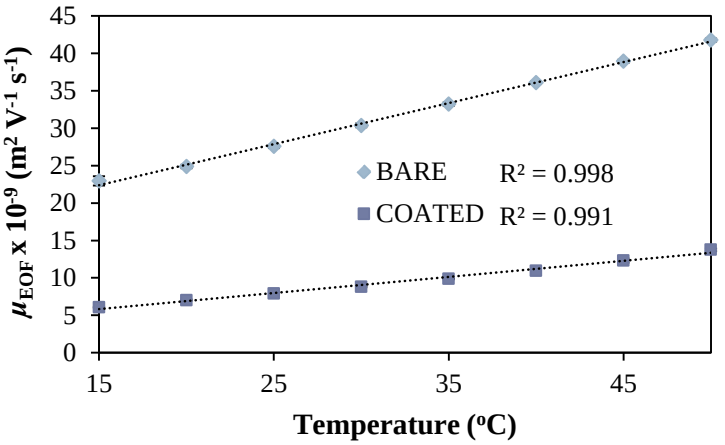

Figure 5.8. Plot of μ_{EOF} versus temperature for a bare capillary compared to a capillary coated with CFR PEPyM-*co*-PMMA random copolymer (21/79). Separation was performed on fused-silica capillaries (30 cm L_d, 38 cm L_t, 75 µm id, 363 µm od). Error bars are ± 1 s_d from n = 3.

A Student's *t*-test was used to compare the sets of data obtained for the mobilities on the bare and coated capillaries (see Table 5.3). Statistical analysis in this case was used to reject the null hypothesis that the mean mobilities from both capillaries were not different. This was done by comparing individual differences according to Equation 5.5,

$$t_{calc} = \frac{\bar{d}}{s_d}\sqrt{n}$$

Equation 5.5

where $\bar{d}$ is the mean difference between the temperature datasets from the two capillaries, s_d is the standard deviation of the mean difference, and n represents the number of datasets. The value of t_{calc} was compared to the values of the Student's *t*-test found in Table 5.4.

Table 5.3. Calculation of t_{calc} for the Student's *t*-test.

Temp. (°C)	μ_{EOF} x 10^{-9} (m^2 V^{-1} s^{-1})		
	Bare	Coated	Difference
15	23.0	6.1	16.9
20	24.9	7.0	17.9
25	27.6	7.9	19.7
30	30.4	8.8	21.6
35	33.2	9.9	23.3
40	36.1	10.9	25.2
45	38.9	12.3	26.6
50	41.8	13.8	28.0
		$\bar{d}$	22.4
		s_d	4.1
		t_{calc}	15.6

Table 5.4. *t*-distribution values.

Degrees of	Confidence level (%)								
freedom	75	90	95	97.5	99	99.5	99.75	99.9	99.95
1	1.000	3.078	6.314	12.706	31.821	63.656	127.321	318.289	636.578
2	0.816	1.886	2.920	4.303	6.965	9.925	14.089	22.328	31.600
3	0.765	1.638	2.353	3.182	4.541	5.841	7.453	10.214	12.924
4	0.741	1.533	2.312	2.776	3.747	4.604	5.598	7.173	8.61
5	0.727	1.476	2.015	2.571	3.365	4.032	4.773	5.894	6.869
6	0.718	1.440	1.943	2.447	3.143	3.707	4.317	5.208	5.959
7	0.711	1.415	1.895	2.365	2.998	3.499	4.029	4.785	5.408
8	0.706	1.397	1.860	2.306	2.896	3.355	3.833	4.501	5.041
9	0.703	1.383	1.833	2.262	2.821	3.250	3.690	4.297	4.781

The Student's *t*-test showed a statistical difference between the bare fused-silica and the coated fused-silica capillary at a 99.95 % confidence level and 7 degrees of freedom (t_{calc} 15.6 > t_{table} 5.4).

The results for the bare fused-silica capillary were moderately lower than those of Bernal *et al.* [79] who used both a bare fused-silica and a CFR PEPyM-*co*-PMMA random copolymer (25/75) coated capillary (30 cm L_d, 50 µm id, 363 µm od) at 30 °C, pH 9.0 and 540.5 V cm^{-1} to obtain μ_{EOF} of ~41 x 10^{-9} m^2 V^{-1} s^{-1} and ~23 x 10^{-9} m^2 V^{-1} s^{-1}, respectively. This difference was likely due to varying polymer

composition and concentration, along with a different BGE and hence different ionic strengths. A further comparison with work by Erny *et al.* [80] who used a PEPyM-*co*-PDMA coated capillary (30 cm L_d, 50 µm id, 363 µm od) at 30 ^{o}C, pH 9.0 and 540.5 V cm^{-1} also showed comparable results between 10 x 10^{-9} m^2 V^{-1} s^{-1} and 25 x 10^{-9} m^2 V^{-1} s^{-1}.

5.2.1.6.2.2 pH study

The v_{EOF} and μ_{EOF} of the Tris-borate (100 mM)/urea (7 M) buffer were also determined for coated and bare capillaries at 30 ^{o}C and varying buffer pH (3 - 11), using the buffer/water/acetone (20/75/5 % v/v/v) solution as a neutral marker. Figure 5.9 displays the CE electropherograms of the neutral marker at varying pH for the bare capillary compared to the coated capillary. Results were not obtained for pH 3 for the bare capillary after allowing the run to proceed for 60 min, thus suggesting that the use of the low pH buffer on the bare capillary created an EOF that was negligible. Data were also not obtained for pH 7 on the coated capillary. Analysis was performed at this pH at both positive and negative polarity for a total run time of 80 min with no peaks detected. Therefore it was concluded that at pH 7 on the coated capillary, the EOF was negligible. At pH values lower than 7, analysis required the use of negative polarity to obtain peaks, meaning that the EOF had been completely reversed.

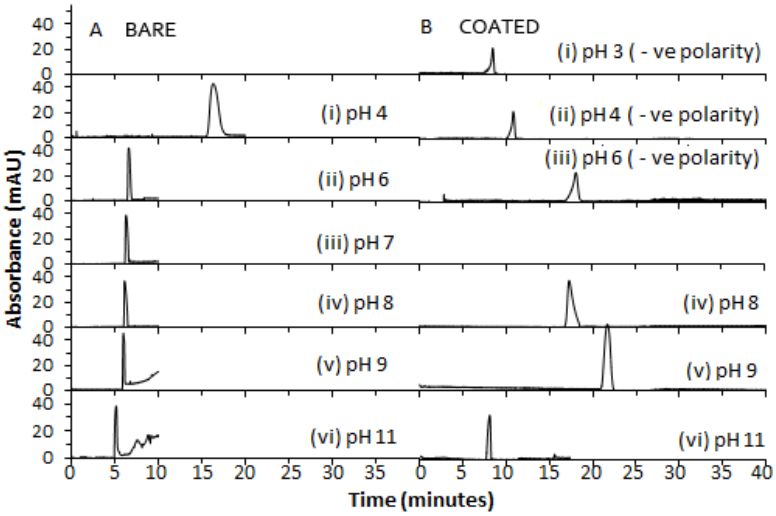

Figure 5.9. CE electropherograms of separation of the buffer/water/acetone neutral marker (20/75/5) on a bare capillary (A), compared to a CFR PEPyM-*co*-PMMA random copolymer (21/79) coated capillary (B), at varying pH (i)-(vi). Separation was performed on fused-silica capillaries (30 cm L_d, 38 cm L_t, 75 µm id, 363 µm od) at 263.2 V cm^{-1} (basic pH) and -263.2 V cm^{-1} (acidic pH) with UV detection at 254 nm for 60 min run time. The BGE was Tris-borate (100 mM)/urea (7 M). Samples were introduced hydrodynamically at 5000 Pa for 6 s.

The v_{EOF} and μ_{EOF} values were calculated at each pH value and the percentage difference between the two coatings was determined from Equation 5.4 (represented by magnitude of suppression). These values can be found in Table 5.5.

The results presented in Table 5.5 indicate that the EOF was suppressed at all pH values. A Student's *t*-test was also performed on this data using the same method described in Section 5.2.1.6.2.1. The Student's *t*-test showed a statistical difference between the bare fused-silica and the coated fused-silica capillary at a 99.75 % confidence level and 4 degrees of freedom (t_{calc} 6.0 > t_{table} 5.6).

Table 5.5. Calculation of v_{EOF} and μ_{EOF} at varying pH for a bare fused-silica capillary compared to a CFR PEPyM-*co*-PMMA random copolymer (21/79) coated fused-silica capillary using the buffer/water/acetone (20/75/5) neutral marker.

	Bare fused-silica capillary					PEPyM-*co*-PMMA coated capillary					Magnitude of EOF Suppression
pH	t_m (min)	v_{EOF} x 10^{-4} ($m\ s^{-1}$)	μ_{EOF} x 10^{-9} ($m^2\ V^{-1}\ s^{-1}$)	s_d x 10^{-9} (n = 3)	RSD (%)	t_m (min)	v x 10^{-4} ($m\ s^{-1}$)	μ_{EOF} x 10^{-9} ($m^2\ V^{-1}\ s^{-1}$)	s_d x 10^{-9} (n = 3)	RSD (%)	(%)
3						-8.43	-5.93	-22.5	0.06	0.27	
4	17.42	2.87	10.9	0.92	8.39	-10.83	-4.62	-17.5	0.04	0.20	260.85
6	6.71	7.46	28.3	0.53	1.85	-18.48	-2.71	-10.3	0.35	3.43	136.29
7	6.18	8.09	30.7	0.85	2.76						
8	6.04	8.28	31.4	0.57	1.81	17.32	2.89	11.0	0.57	5.23	65.12
9	6.00	8.34	31.7	0.07	0.23	21.69	2.30	8.8	0.01	0.13	72.35
11	5.13	9.75	37.0	1.12	3.02	8.19	6.10	23.2	0.42	1.83	37.38

* The negative sign denotes separation at negative polarity and hence an anodic flow

EOF data are better represented visually as a plot; therefore, Figure 5.10 shows the plot of μ_{EOF} versus pH at 30 ^{o}C for the bare fused-silica capillary compared to the CFR PEPyM-*co*-PMMA random copolymer coated capillary. It can be seen from this plot that for all pH values on the bare fused-silica capillary, the EOF was cathodic with a reduction in μ_{EOF} with a decrease in pH (from 37.0 x 10^{-9} m^2 V^{-1} s^{-1} to 10.9 x 10^{-9} m^2 V^{-1} s^{-1}). This was due to the surface being protonated resulting in a relatively positive surface charge. Not only did the CFR PEPyM-*co*-PMMA random copolymer coated capillary show a greater reduction in μ_{EOF} with decreasing pH (when compared to the bare capillary), it also exhibited a reversal in the EOF from cathodic (23 x 10^{-9} m^2 V^{-1} s^{-1} at pH 11) to anodic (-23 x 10^{-9} m^2 V^{-1} s^{-1} at pH 3) with an almost zero EOF theorised to occur around pH 7 (data not obtained due to very small EOF, however, the plot crosses the x-axis at this pH).

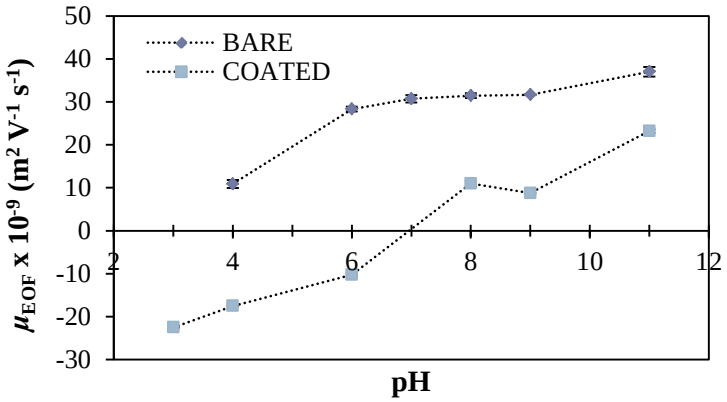

Figure 5.10. Plot of μ_{EOF} versus pH for a bare capillary compared to a capillary coated with CFR PEPyM-*co*-PMMA random copolymer (21/79). Separation was performed on fused-silica capillaries (30 cm L_d, 38 cm L_t, 75 µm id, 363 µm od). Error bars are ± 1 s_d from n = 3.

The CFR PEPyM-*co*-PMMA random copolymer is cationic in nature and, when adsorbed to the surface, it replaced some silanol groups effectively shielding the capillary. At low pH the polymer groups dominated the charge creating a positive surface and hence an anodic EOF. At high pH, however, the remaining negative silanol groups predominated and the EOF, whilst reduced, remained cathodic.

While a reversal in EOF would increase the μ_{app} of the dsODNs (their migration would both be anodic) it would likely decrease the R_s of the different strands in the mixture as the residence time would decrease. In addition, using a low pH would likely result in protonation of the ODN strands, potentially neutralising the

negative charge [183], implying that the μ_{app} of the ODNs would depend more on the EOF. In contrast, the use of high pH would result in denaturation of the strands [184] which should be avoided.

It is necessary to consider the separation mechanism when choosing an appropriate EOF. In this work, the polymer was used as an EOF suppressant, and separation was based on migration in free solution, coupled with surface ion-pairing. In dilute polymer solutions it is common to use uncoated capillaries as the EOF can assist in enhancing the R_s by increasing the residence time on the capillary [119]. Traditionally, for separations in free solution it is preferable to have a negligible EOF in order to determine the physical and chemical properties of ODNs using CE [8, 20, 93]. Taking these points into consideration, a pH of 9 was chosen for analysis with the CFR PEPyM-*co*-PMMA random copolymer coating as it showed sufficient EOF suppression without harsh conditions.

5.2.2 Optimisation of ODN separation on PEPyM-*co*-PMMA (21/79) coated capillaries

DNA strands above ~170 bp are considered to be free draining molecules and cannot be separated in free solution electrophoresis. On the other hand, shorter strands (less than ~170 bp) exhibit mobilities in free solution that increase with increasing bp length. To enable separation of short strands in free solution, it is necessary to reduce or remove the EOF by surface modification with polymers either physically adsorbed or covalently attached to the surface.

Dynamic (physically adsorbed) coatings are preferred over static (covalently attached) coatings due to the ease of use and regeneration, along with the wide range of polymers available which are not limited by covalent surface attachment chemistry. To date, a wide range of polymers have been physically adsorbed onto a CE capillary in order to modulate the surface charge and hydrophobicity, such as linear polyacrylamide (LPA) [37, 56], poly(dimethylacrylamide) (PDMA) [26, 54, 56], poly(diethylacrylamide) (PDEA) [26, 56], poly(vinyl pyrrolidone) (PVP) [53], and poly(ethylene oxide) (PEO) [36, 90, 185]. These types of coatings have been used extensively for the separation of ssDNA [52-55, 66] and large fragments of

dsDNA [26, 52, 53, 56]. However there is a significant gap in the literature regarding the analysis of short fragments of dsDNA and ODNs using physically adsorbed polymer coatings, with much of the research having been focussed on dynamic coatings with the polymer in the running buffer.

This section describes the use of a physically adsorbed coating of CFR PEPyM-*co*-PMMA random copolymer (21/79 ratio, 14 398 g mol^{-1}) on a bare fused-silica capillary for the separation of synthetic ODNs (16 bp - 20 bp) in free solution. The CFR PEPyM-*co*-PMMA random copolymer coating was shown to suppress the EOF at all pH values and temperatures analysed, with a total suppression on 72 % at 30 ^{o}C and pH 9. With a much more simplified CE method, under cathodic flow and basic conditions (pH 9.0), separation of dsODNs between 16 bp and 20 bp was achieved without the need for sieving solutions or high polymer concentrations. Results show that 1 bp R_s was achieved with good peak R_s between 1.5 and 1.6 (with partial R_s of 16 bp and 17 bp), and t_m repeatability (n = 3) of ODN mixtures between 0.3 and 1.9 % and individual solutions between 0.3 and 0.9 %. Well resolved peaks were achieved using a low negative applied voltage (-131.6 V cm^{-1}) at 30 ^{o}C using a Tris-borate (100 mM)/urea (7 M) buffer at pH 9.0 and UV detection at 260 nm. EOF mobility studies showed that the CFR PEPyM-*co*-PMMA random copolymer coating was effective at reducing the EOF under these conditions. Interestingly, it was observed that the smaller dsODN fragments were retained to a larger extent on the polymer coated capillary than the larger fragments, and thus the dsODN eluted in the order of 20 bp to 16 bp. It was proposed that this was due to a combination of the free solution mobility and the stronger ODN-pyridyl screening of the smaller fragments charge coupled with the low M_w of the dilute polymer on the surface.

5.2.2.1 Effect of voltage on ODN separation

The voltage dependence on the separation of the ODNs on a CFR PEPyM-*co*-PMMA random copolymer coated capillary (30 cm L_d) was determined using a dsODN (18.6 µM) mixture of 16 bp and 20 bp (refer to Table 2.1 in Section 2.2.3.1 for ODN sequences). The t_m, R_s, separation efficiency (N) and peak shape were used to determine the optimum voltages for separation of the mixture. The R_s was calculated from Equation 5.6,

$$R_s = (2ln2)^{1/2}\left(\frac{t_{m2} - t_{m1}}{W_{h1} + W_{h2}}\right)$$

Equation 5.6

where W_h is the peak width at half height. The separation efficiency was calculated from Equation 5.7.

$$N = 5.54\left(\frac{t_m}{W_h}\right)^2$$

Equation 5.7

The voltage was tested in 0.5 kV increments, from 5 kV to 15 kV. All other parameters were kept constant. Figure 5.11 (i)-(xii) shows the electropherograms for injections of dsODNs at varying voltages, Figure 5.12 shows plots of voltage versus t_m, W_h, R_s, N, velocity (v), and observed electrophoretic mobility (μ_{obs}). The μ_{obs} was calculated from Equation 1.12 in Section 1.2.3.3 using the calculated μ_{app} and the mean μ_{EOF} from the EOF temperature and pH study at 30 ^{o}C and a pH of 9 ($8.8 \pm 0.02 \times 10^{-9}$ m^2 V^{-1} s^{-1}). The migration and mobility data can be found in Table 10.1 in Appendix A.

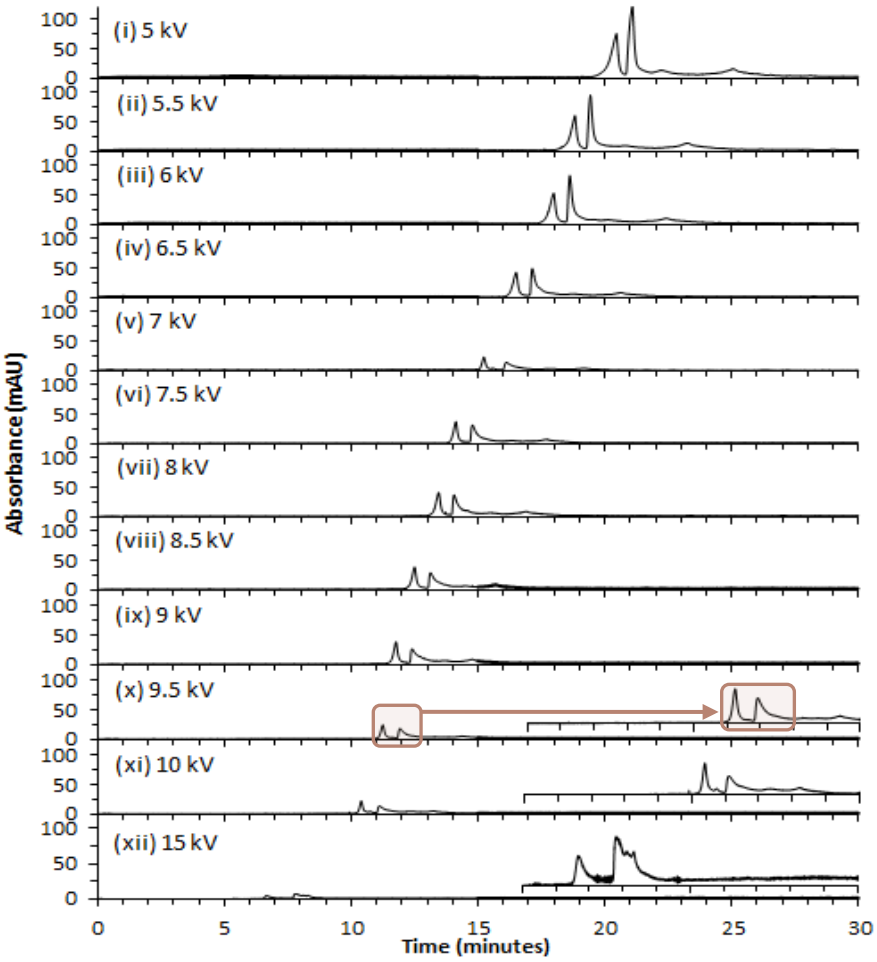

Figure 5.11. CE electropherograms of a mixture of 16 bp and 20 bp dsODNs (18.6 µM) at varying voltages (i)-(xii), using a CFR PEPyM-*co*-PMMA random copolymer (21/79) coated fused-silica capillary (30 cm L_d, 38 cm L_t, 75 µm id, 363 µm od). Separation was performed at 30 °C with UV detection at 260 nm for 30 min run time. The BGE was Tris-borate (100 mM)/urea (7 M) at pH 9.0. Samples were introduced hydrodynamically at 5000 Pa for 6 s.

As can be seen from Figure 5.11 and Figure 5.12A, the t_m decreased with increasing voltage for both strands. A power trend-line was fitted to the curve with R^2 values above 0.995 for both strands. An increase in voltage led to a change in the peak heights (reduced) and shapes, with non-Gaussian peaks observed after approximately 7 kV. Figure 5.12 showed that the W_h and N decreased with increasing voltage, leading to sharper peaks, with increased R_s [17]. The v increased with increasing voltage owing to the greater current applied by the higher voltage; however, there was no obvious trend for μ_{obs} as this was independent of the applied voltage.

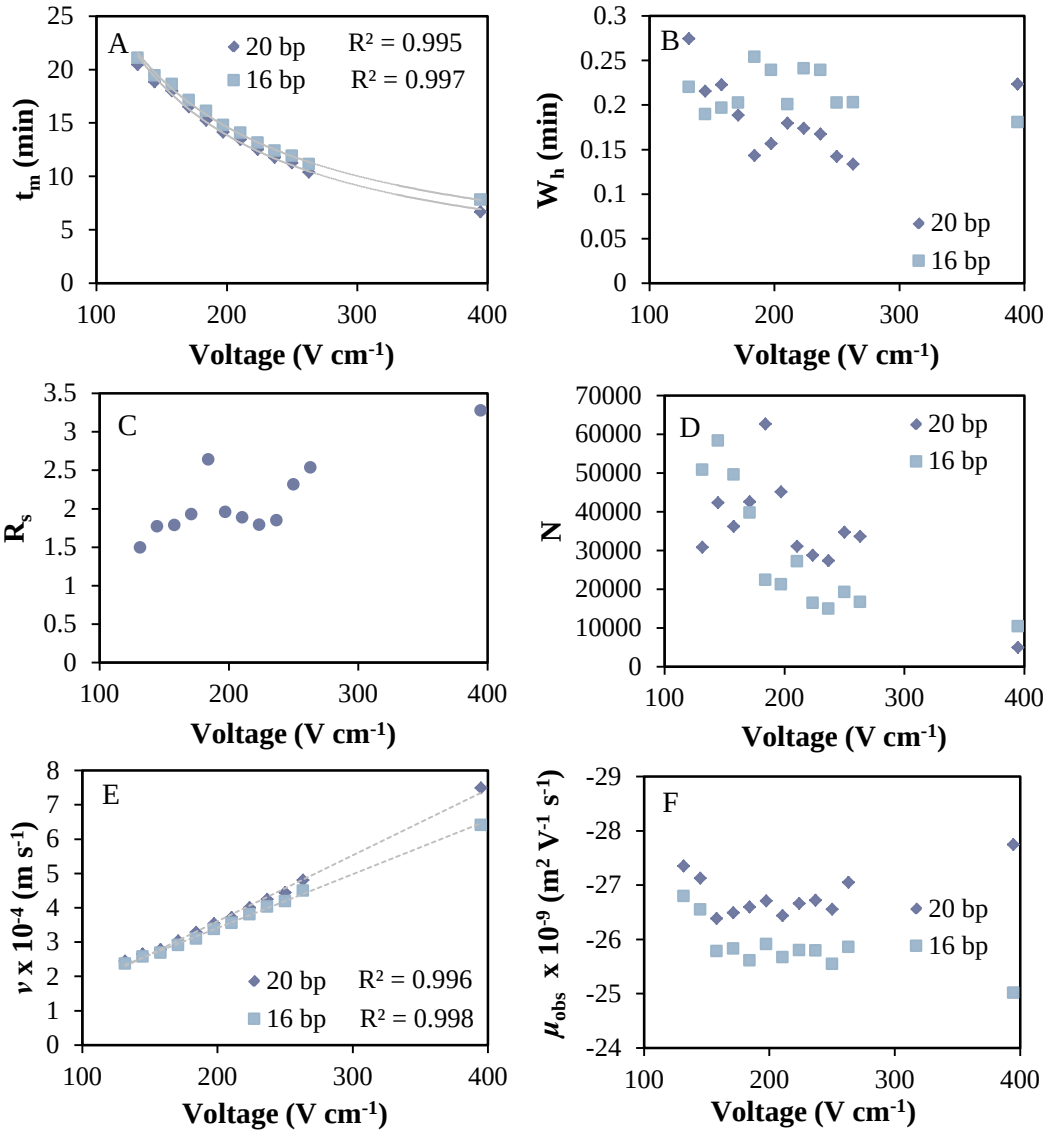

Figure 5.12. Plots of t_m (A), W_h (B), R_s (C), N (D), ν (E), and μ_{obs} (F), versus voltage for separation of 16 bp and 20 bp dsODNs (18.6 µM) on a CFR PEPyM-*co*-PMMA random copolymer (21/79) coated capillary (30 cm L_d, 38 cm L_t, 75 µm id, 363 µm od).

The use of higher voltages increased the current in the capillaries which in turn increased joule heating. In general, as the capillary heats up, the repeatability of the surface and hence the results suffer. For ODN analysis, this should be avoided as a build-up of excess heat can potentially denature or degrade the short strands. Although the R_s was improved with increasing voltages, low voltages still achieved well resolved peaks, thereby avoiding any of the heating problems associated with higher voltages. These results indicate that under these conditions the optimum voltages for enhanced separation with Gaussian peaks and improved signal-to-noise was between 5 and 7 kV. Therefore, it was this range of voltages used for all following separations in this chapter.

5.2.2.2 Effect of temperature on ODN separation

The temperature dependence on the separation of the ODNs on a CFR PEPyM-*co*-PMMA random copolymer coated capillary (30 cm L_d) was determined using a dsODN (18.6 µM) mixture of 16 bp and 20 bp. The t_m, R_s and peak shape were used to determine the optimum temperature for separation of the mixture. The temperature was tested in 5 ^oC increments, from 15 ^oC to 50 ^oC. All other parameters were kept constant. Figure 5.13(i)-(viii) shows the electropherograms for injections of dsODNs at temperatures between 15 ^oC and 50 ^oC. R_s and t_m for all temperatures can be found in Table 10.2 in Appendix A, along with the N, v, μ_{app} and μ_{obs}.

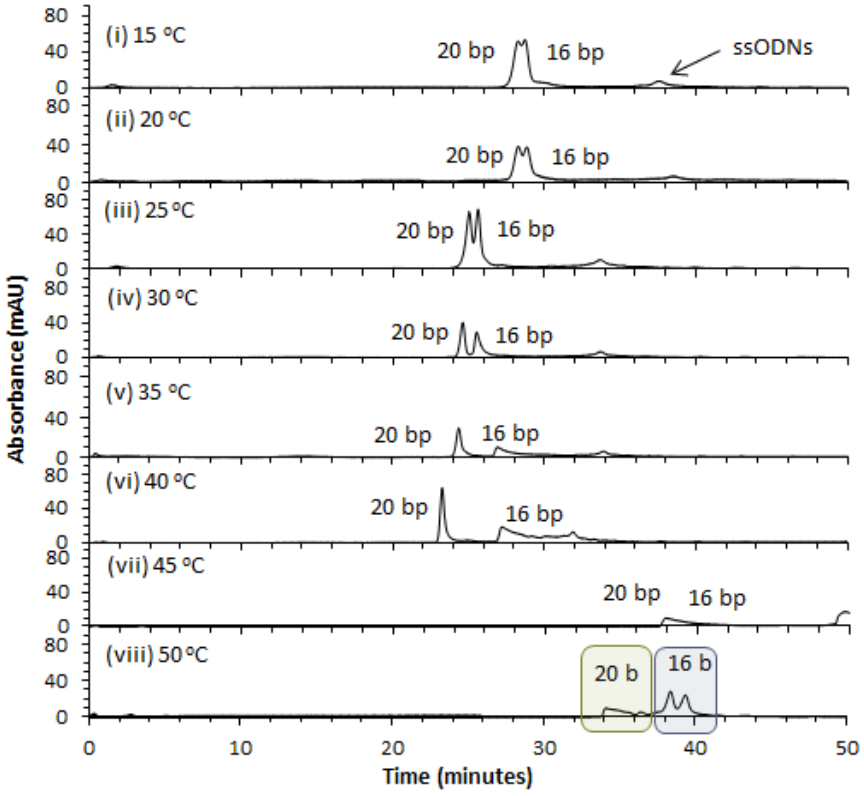

Figure 5.13. CE electropherograms of a mixture of 16 bp and 20 bp dsODNs (18.6 µM) at varying temperatures (i)-(viii), using a CFR PEPyM-*co*-PMMA random copolymer (21/79) coated fused-silica capillary (30 cm L_d, 38 cm L_t, 75 µm id, 363 µm od). Separation was performed at -131.6 V cm^{-1} with UV detection at 260 nm for 50 min run time. The BGE was Tris-borate (100 mM)/urea (7 M). Samples were introduced hydrodynamically at 5000 Pa for 6 s.

At 15 ^oC the 16 bp and 20 bp dsODNs migrated close to each other with an R_s of 0.71, with the 20 bp peak detected first (28.29 min) followed by the 16 bp peak (28.74 min). The smaller peak at 37.59 min was due to residual ssODNs (Figure 5.13(i)). An increase in temperature to 20 ^oC (Figure 5.13(ii)) increased the R_s to

0.80 and resulted in a slight shift in the t_m to 28.83 min for the 16 bp peak. By increasing the temperature to 25 ^oC (Figure 5.13(iii)), the R_s of the two peaks increased to 1.06 and the t_m decreased to 25.04 min and 25.64 min for the 20 bp and 16 bp, respectively. At 30 ^oC (Figure 5.13(iv)) the R_s increased to 1.71 and the t_m further decreased to 24.62 min and 25.54 min for the 20 bp and 16 bp, respectively. At 35 ^oC, the peak shapes became deformed (Figure 5.13(v)). This was due to denaturing and degradation of the strands. The first peak at 24.36 min was due to the 20 bp dsODN, which seemed to be so far unaffected by the higher temperature. However, the 16 bp peak at 26.89 min decreased in size and the peak shape was poor. The R_s for these peaks was 4.30. The same can be said for analysis at 40 ^oC (Figure 5.13(vi)) with the 20 bp peak at 23.27 min and 16 bp (poorly shaped) at 27.21 min, with a peak R_s of 7.50. At 45 ^oC (assumed to be exceeding the ODN melting temperatures (T_m)) there was further degradation and deformation of the dsODN strands (Figure 5.13(vii)). The two peaks were barely resolved (R_s = 0.32) with a t_m of 37.88 min and 37.96 min, respectively. Figure 5.13(viii) showed that 50 ^oC was too high for the ODNs as this was most likely above the melting temperatures (see Table 2.2 in Section 2.2.3.1). The strands appeared to be denatured and hence migrated in their ss forms resulting in 4 partially resolved peaks (R_s of 1.3 and 4.0 for 20 b and 16 b strands, respectively) with t_m between 34.09 min and 39.36 min.

By examining plots of temperature versus t_m (Figure 5.14A) it was evident that t_m decreased for the 20 bp peak with increasing temperature between 15 ^oC and 40 ^oC, and once exceeding 40 ^oC, the t_m increased due to the strands denaturing. The 16 bp peak, however, showed a slightly different trend. Owing to the smaller strand length, the T_m is lower, meaning that these strands should denature sooner than the 20 bp strands. Therefore, a decreasing trend for t_m for 16 bp was observed for increasing temperature until 35 ^oC in which the trend was reversed. The R_s was increased with increasing temperature up to 40 ^oC until both strands became partially denatured (see Figure 5.14C). By elevating the temperature, the t_m was reduced, owing to a weakening of the ion-pair interactions between the dsODNs and the polymer surface, meaning that the dsODNs were retained less. However, once the temperature exceeded 40 ^oC and the dsODNs were denatured, they migrated as single strands which were observed to have a lower mobility than their

ds counterparts (see Figure 5.23). It was concluded that 30 °C was the optimum temperature for the separation of the dsODN mixture on the CFR PEPyM-*co*-PMMA random copolymer coated capillary due to the superior R_s (1.71), peak shape (symmetric) and t_m (24.57 min and 25.47 min).

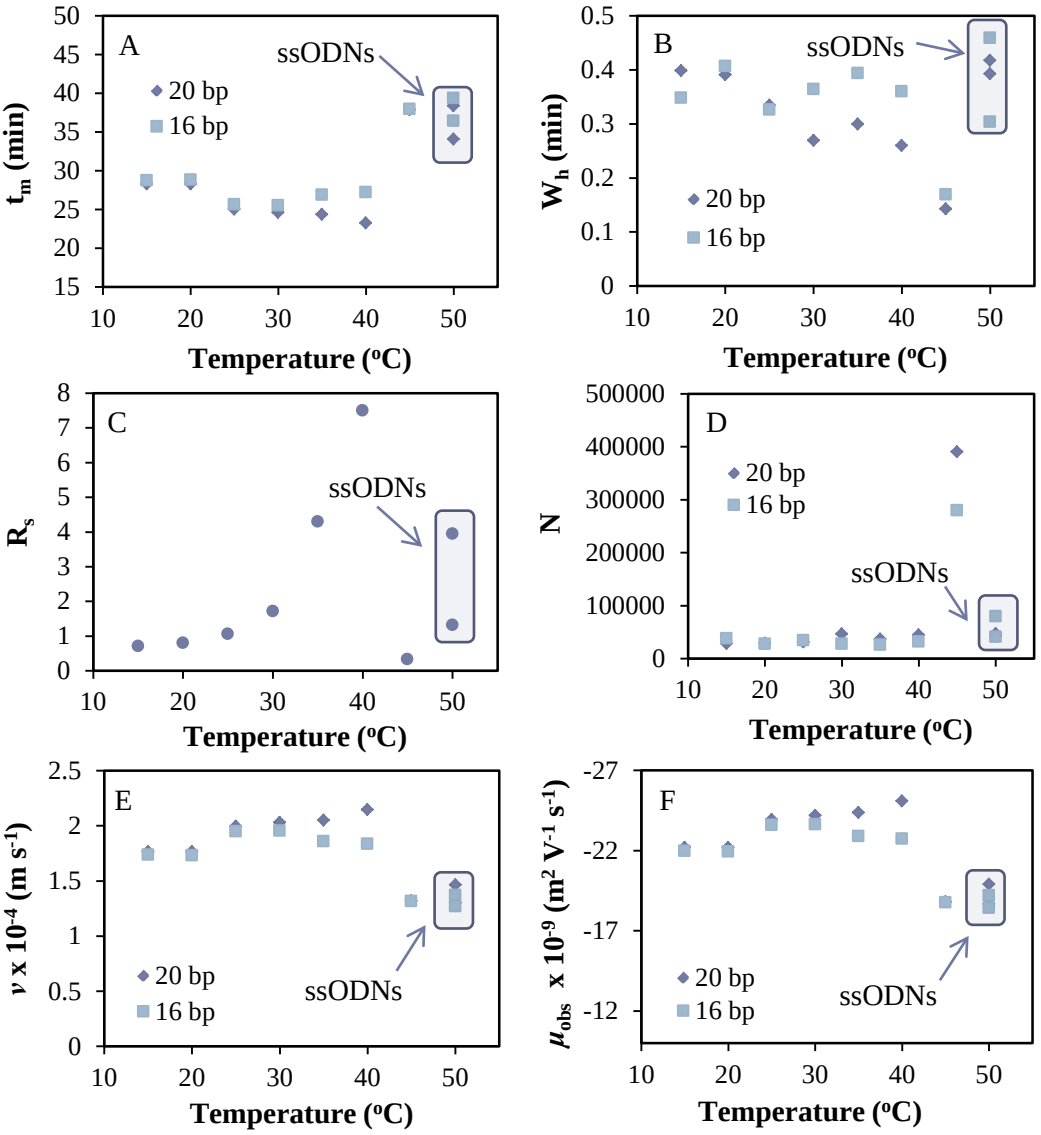

Figure 5.14. Plots of t_m (A), W_h (B), R_s (C), N (D), ν (E), and μ_{obs} (F), versus temperature for separation of 16 bp and 20 bp dsODNs (18.6 µM) using a CFR PEPyM-*co*-PMMA random copolymer (21/79) coated fused-silica capillary (30 cm L_d, 38 cm L_t, 75 µm id, 363 µm od).

5.2.2.3 Coating repeatability study

The repeatability of the coating for migration of the 16 bp and 20 bp dsODN mixture was determined by modifying the pre-conditioning steps on the CFR PEPyM-*co*-PMMA random copolymer treated surface. The effects of no between-run conditioning (the capillary was not flushed between runs, nor was the coating

regenerated), buffer conditioning (refers to flushing with buffer between runs to remove any remaining analyte and replenish the buffer ions in the capillary), and polymer regeneration (between runs, the coating was regenerated and the capillary was re-filled with buffer) were investigated from the repeatability of the t_m.

5.2.2.3.1 Effect of no between-run conditioning

The effect of no between-run conditioning on 8 repetitive injections of a 16 bp and 20 bp dsODN (18.6 μM) mixture was investigated on a new fused-silica capillary activated and coated with CFR PEPyM-*co*-PMMA random copolymer according to Section 2.3.3.3. The results from this investigation are represented by Table 5.6 and Figure 5.15 and the CE electropherograms are found in Figure 10.2 in Appendix A.

Table 5.6. Calculation of mean t_m, R_s, μ_{app}, and μ_{obs} for 8 injections of a 16 bp and 20 bp dsODN mixture with no between-run conditioning on a CFR PEPyM-*co*-PMMA random copolymer (21/79) coated fused-silica capillary.

Peak (bp)	t_m (min)	W_h (min)	R_s	μ_{app} x 10^{-9} ($m^2 V^{-1} s^{-1}$)*	s_d x 10^{-9} (n = 8)	RSD (%)	μ_{obs} x 10^{-9} ($m^2 V^{-1} s^{-1}$)*
20	19.69	0.28	1.34	-19.3	0.83	4.29	-28.1
16	20.24	0.21		-18.8	0.82	4.36	-27.6

*The negative sign denotes an anodic mobility

Figure 5.15A immediately showed that the coating was not repeatable as t_m decreased from run to run. A decrease in t_m (and hence an increase in μ_{app} and μ_{obs}) cannot be explained by surface instability, because an unstable surface would result in an increase in cathodic EOF as the polymer is displaced from the surface, thereby increasing the t_m. This trend was best explained by the fact that the polymer became more stable over time which is not a desirable quality for repeatability. It is also necessary to condition the capillary between runs to avoid any contamination from un-eluted species and remove any species that may have temporarily adhered to the surface. Table 5.6 shows the mean values for the t_m and calculated μ_{app} and its associated % RSD. The W_h (Figure 5.15B) showed no observable trend suggesting that any surface-analyte interactions were consistent from run to run, although the R_s (Figure 5.15B) of the 16 bp and 20 bp peaks decreased with each injection which was attributed to the increasing mobility.

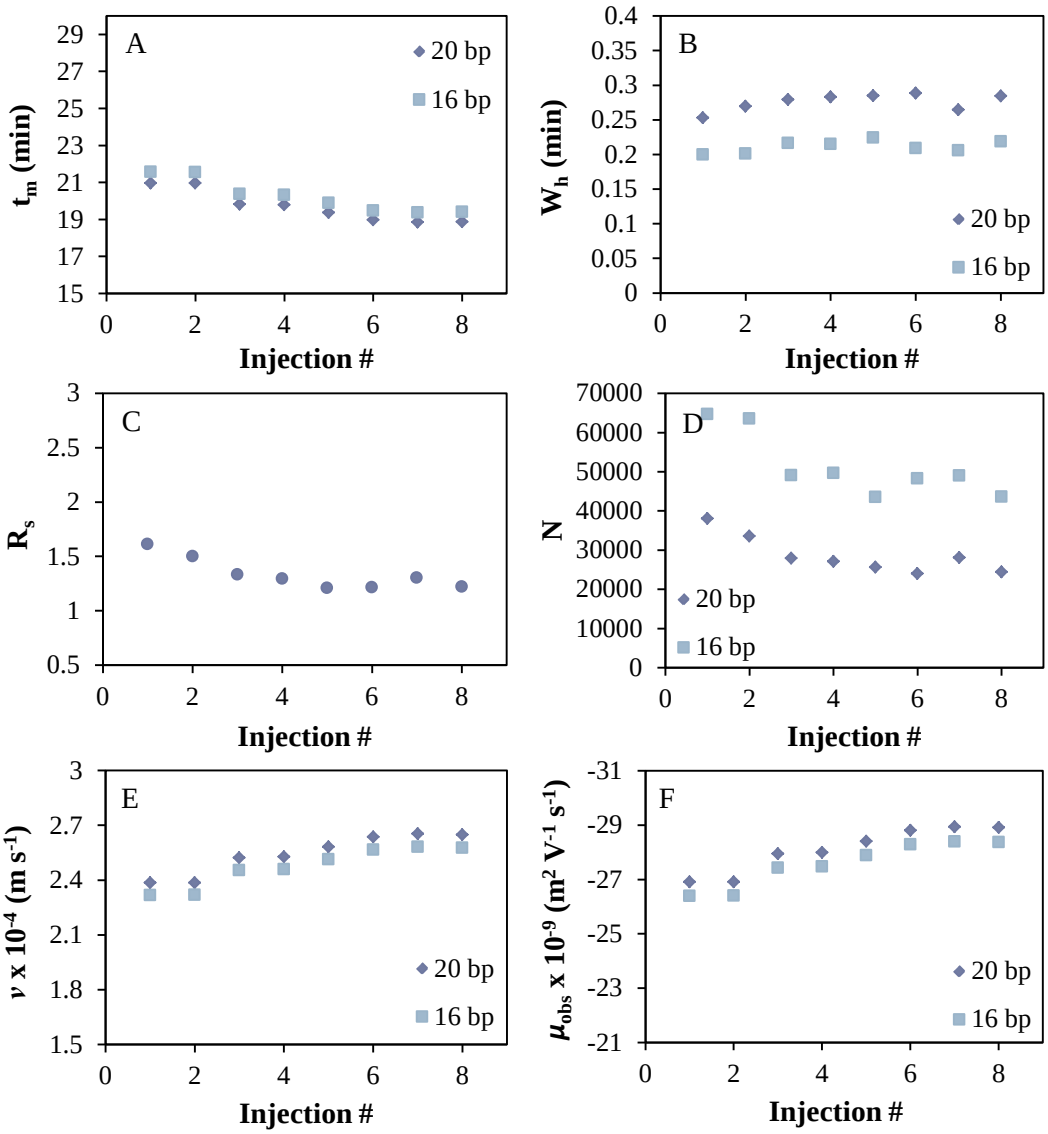

Figure 5.15. Plots of t_m (A), W_h (B), R_s (C), N (D), v (E), and μ_{obs} (F), versus injection # for the separation of 16 bp and 20 bp dsODNs (18.6 µM) on a CFR PEPyM-*co*-PMMA random copolymer (21/79) coated fused-silica capillary (30 cm L_d, 38 cm L_t, 75 µm id, 363 µm od). The capillary was not conditioned between runs.

5.2.2.3.2 Effect of between-run buffer conditioning

The effect of flushing with buffer (without polymer) for 2 min between each run was investigated on repetitive injections of 16 bp and 20 bp dsODN mixture using a new activated and CFR PEPyM-*co*-PMMA random copolymer coated fused-silica capillary (see Section 2.3.3.3). The results from the study are found in Table 5.7 and Figure 5.16, and the CE electropherograms are observed in Figure 10.3 in Appendix A.

Table 5.7. Calculation of mean t_m, R_s, μ_{app}, and μ_{obs} for 8 injections of a 16 bp and 20 bp dsODN mixture with between-run buffer conditioning on a CFR PEPyM-*co*-PMMA random copolymer (21/79) coated fused-silica capillary.

Peak (bp)	t_m (min)	W_h (min)	R_s	μ_{app} x 10^{-9} (m^2 V^{-1} s^{-1})*	s_d x 10^{-9} (n = 8)	RSD (%)	μ_{obs} x 10^{-9} (m^2 V^{-1} s^{-1})*
20	22.74	0.30	2.18	-16.8	1.38	8.22	-25.6
16	23.68	0.21		-16.1	1.38	8.54	-24.9

*The negative sign denotes an anodic mobility

The results for this study contradict the results observed for no between-run conditioning (see Section 5.2.2.3.1). Figure 5.16 showed that the coating was even less repeatable owing to an increased t_m from run to run. The increased t_m (and hence decreased μ_{app} and μ_{obs}) was due to the polymer being displaced from the surface during the conditioning step increasing the cathodic EOF and reducing the mobility of the dsODNs. Table 5.7 shows the mean values for the t_m and calculated μ_{app} and its associated % RSD. The W_h (Figure 5.16B) and R_s between the 16 bp and 20 bp peaks (Figure 5.16B) increased with each injection which was attributed to the decreasing mobility. The next step was to investigate the repeatability of polymer regeneration.

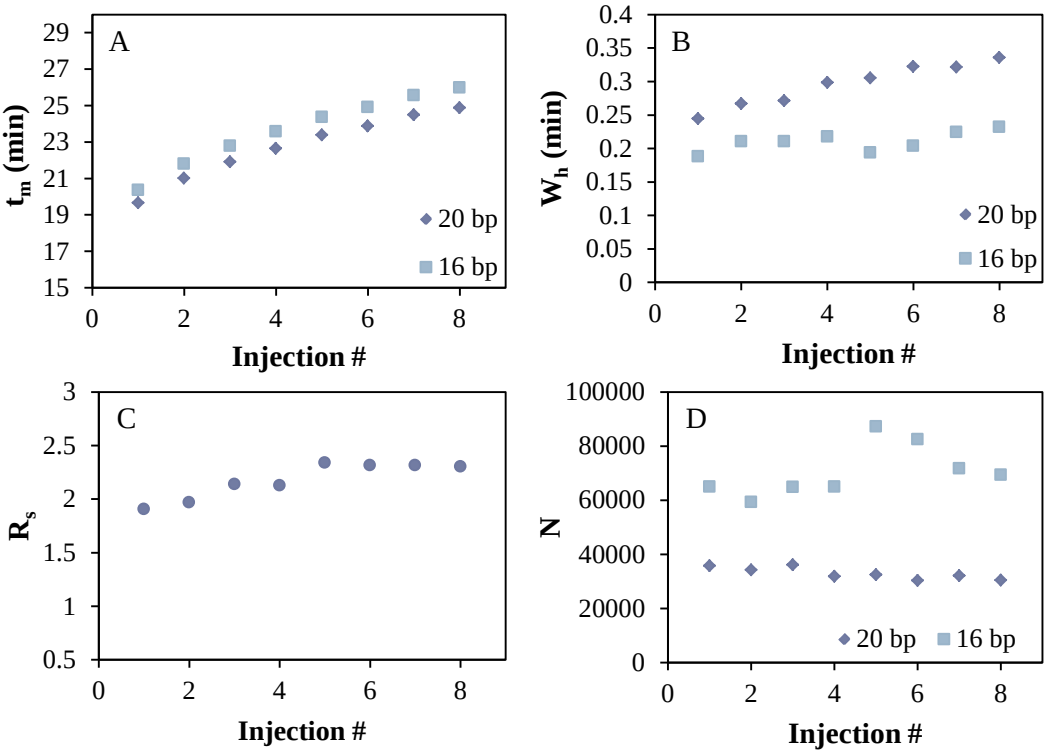

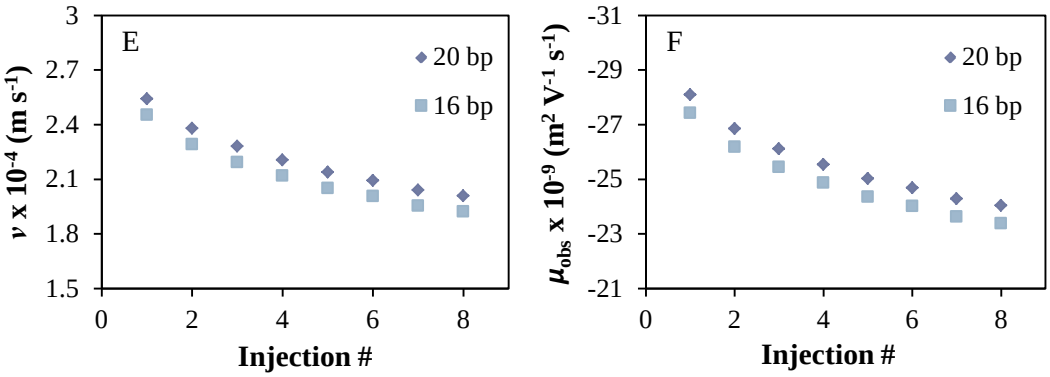

Figure 5.16. Plots of t_m (A), W_h (B), R_s (C), N (D), ν (E), and μ_{obs} (F), versus injection # for separation of 16 bp and 20 bp dsODNs (18.6 µM) on a CFR PEPyM-*co*-PMMA random copolymer (21/79) coated fused-silica capillary (30 cm L_d, 38 cm L_t, 75 µm id, 363 µm od). The capillary was conditioned by flushing with buffer for 2 min between runs.

5.2.2.3.3 Effect of between-run polymer conditioning

The effect of between-run conditioning with polymer solution for 3 min, H_2O for 2 min, and buffer for 3 min was investigated on repetitive injections of 16 bp and 20 bp dsODN mixture using a new activated and CFR PEPyM-*co*-PMMA random copolymer coated fused-silica capillary (see Section 2.3.3.3). The outcome of this investigation is represented by Table 5.8 and Figure 5.17, and the CE electropherograms can be found in Figure 10.4 in Appendix A.

Table 5.8. Calculation of mean t_m, R_s, μ_{app}, and μ_{obs} for 8 injections of a 16 bp and 20 bp dsODN mixture with between-run polymer conditioning on a CFR PEPyM-*co*-PMMA random copolymer (21/79) coated fused-silica capillary.

Peak (bp)	t_m (min)	W_h (min)	R_s	μ_{app} x 10^{-9} (m^2 V^{-1} s^{-1})*	s_d x 10^{-9} (n = 8)	% RSD	μ_{obs} x 10^{-9} (m^2 V^{-1} s^{-1})*
20	21.51	0.23	1.55	-17.7	0.11	0.65	-26.4
16	22.09	0.21		-17.2	0.11	0.63	-26.0

*The negative sign denotes an anodic mobility

It can be seen from the % RSD value in Table 5.8, that the repeatability of the coating using this regeneration method was enhanced. This was further confirmed from the plots in Figure 5.17 which show no real observable trends from run to run.

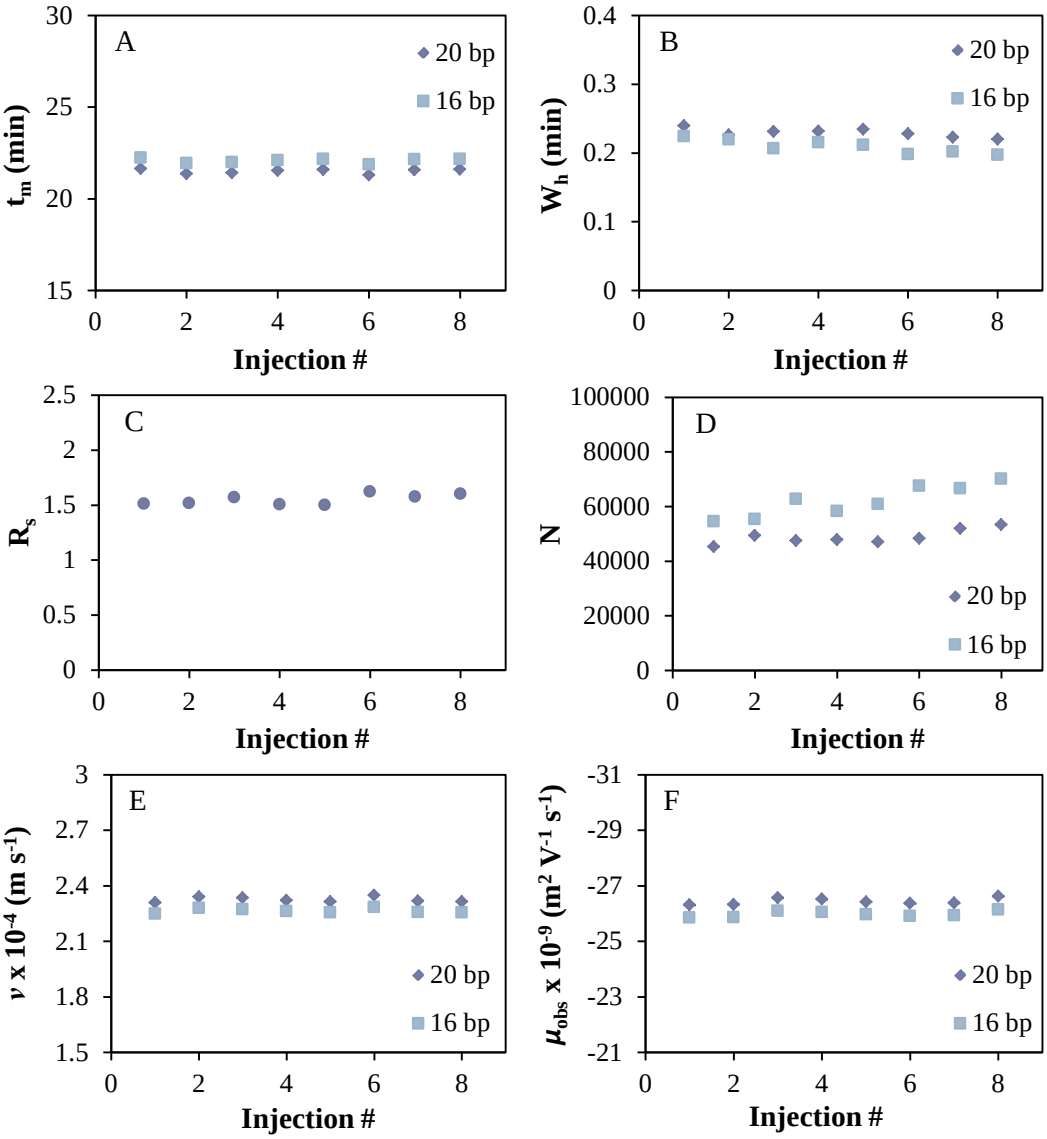

Figure 5.17. Plots of t_m (A), W_h (B), R_s (C), N (D), ν (E), and μ_{obs} (F), versus injection # for the separation of 16 bp and 20 bp dsODNs (18.6 µM) on a CFR PEPyM-*co*-PMMA random copolymer (21/79) coated fused-silica capillary (30 cm L_d, 38 cm L_t, 75 µm id, 363 µm od). The capillary was conditioned between runs by flushing with polymer solution for 3 min, H_2O for 2 min and buffer for 3 min.

It was concluded from the repeatability studies that polymer regeneration was essential for reproducible results. The polymer flushing step was necessary to replace any polymer that was removed from the surface during electrophoresis and the other rinsing steps. The treatment of the capillary with buffer prior to injection was necessary to fill the capillary with ions to carry the charge as the polymer solution alone (prepared in ethanol) would not be suitable.

5.2.2.4 Effect of capillary diameter on ODN separation

The effect of surface-analyte interactions was investigated by decreasing the capillary diameter from a 75 µm CFR PEPyM-*co*-PMMA random copolymer coated fused-silica capillary to a 50 µm capillary. A 16 bp and 20 bp dsODN (18.6 µM) mixture was investigated for diameter related effects on the t_m (and hence *v,* and μ_{app}), R_s, N, peak shape, height and W_h, and the % RSD (see Figure 5.19). Figure 5.18 shows the CE electropherograms comparing the separation of the ODN mixture on both capillaries.

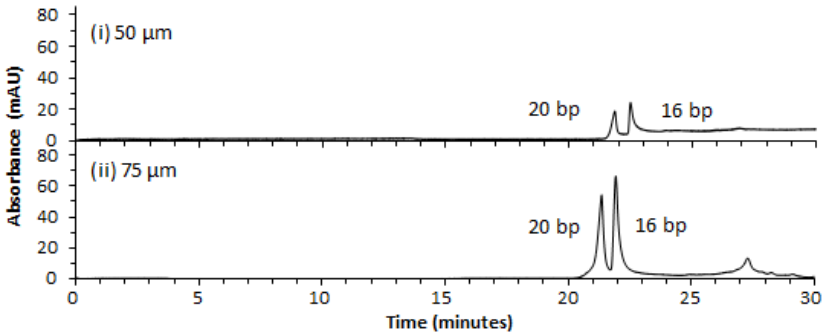

Figure 5.18. CE electropherograms of a mixture of 16 bp and 20 bp dsODNs (18.6 µM) using different capillary diameters. Separation was performed on CFR PEPyM-*co*-PMMA random copolymer (21/79) coated fused-silica capillaries (30 cm L_d, 38 cm L_t, 363 µm od, (i) 50 µm id, (ii) 75 µm id) at -131.6 V cm^{-1} and 30 °C with UV detection at 260 for 30 min run time. The BGE was Tris-borate (100 mM)/urea (7 M). Samples were introduced hydrodynamically at 5000 Pa for 6 s.

It can be seen from Figures 5.18 and 5.19 that decreasing the capillary diameter had an effect on the μ_{app} of the dsODNs. By comparing Table 5.9 to Table 5.8, the mean t_m (n = 8) for the 16 bp and 20 bp dsODN mixture increased slightly with a reduction in capillary diameter from 75 µm to 50 µm. However, the R_s was increased from 1.55 for the 75 µm coated capillary to 2.28 for the 50 µm coated capillary indicating a greater interaction of the dsODNs with the CFR PEPyM-*co*-PMMA random copolymer coated capillary surface (Figure 5.19).

Table 5.9. Calculation of mean t_m, R_s and μ_{app} for 8 injections of 16 bp and 20 bp dsODN mixture on a CFR PEPyM-*co*-PMMA random copolymer (21/79) coated fused-silica capillary (50 µm).

Peak (bp)	t_m (min)	W_h (min)	R_s	μ_{app} x 10^{-9} (m^2 V^{-1} s^{-1})*	s_d x 10^{-9} (n = 8)	% RSD
20	21.53	0.16	2.29	-17.7	0.49	2.77
16	22.19	0.18		-17.1	0.53	3.06

*The negative sign denotes an anodic mobility

Furthermore, Figure 5.18 showed that the peak symmetry differed for both capillaries with the 75 µm capillary giving rise to relatively symmetrical peaks whereas a 50 µm capillary gave rise to peaks that were asymmetric with peak tailing, presumably a result of greater surface-analyte interactions, and subsequent resistance to mass transfer. The reductions in height and W_h were due to a lower volume of sample injected (as according to Equation 5.1, hydrodynamic injection volume is dependent on the capillary inner radius) which, along with increased surface-analyte interactions, also contributed to the increased R_s.

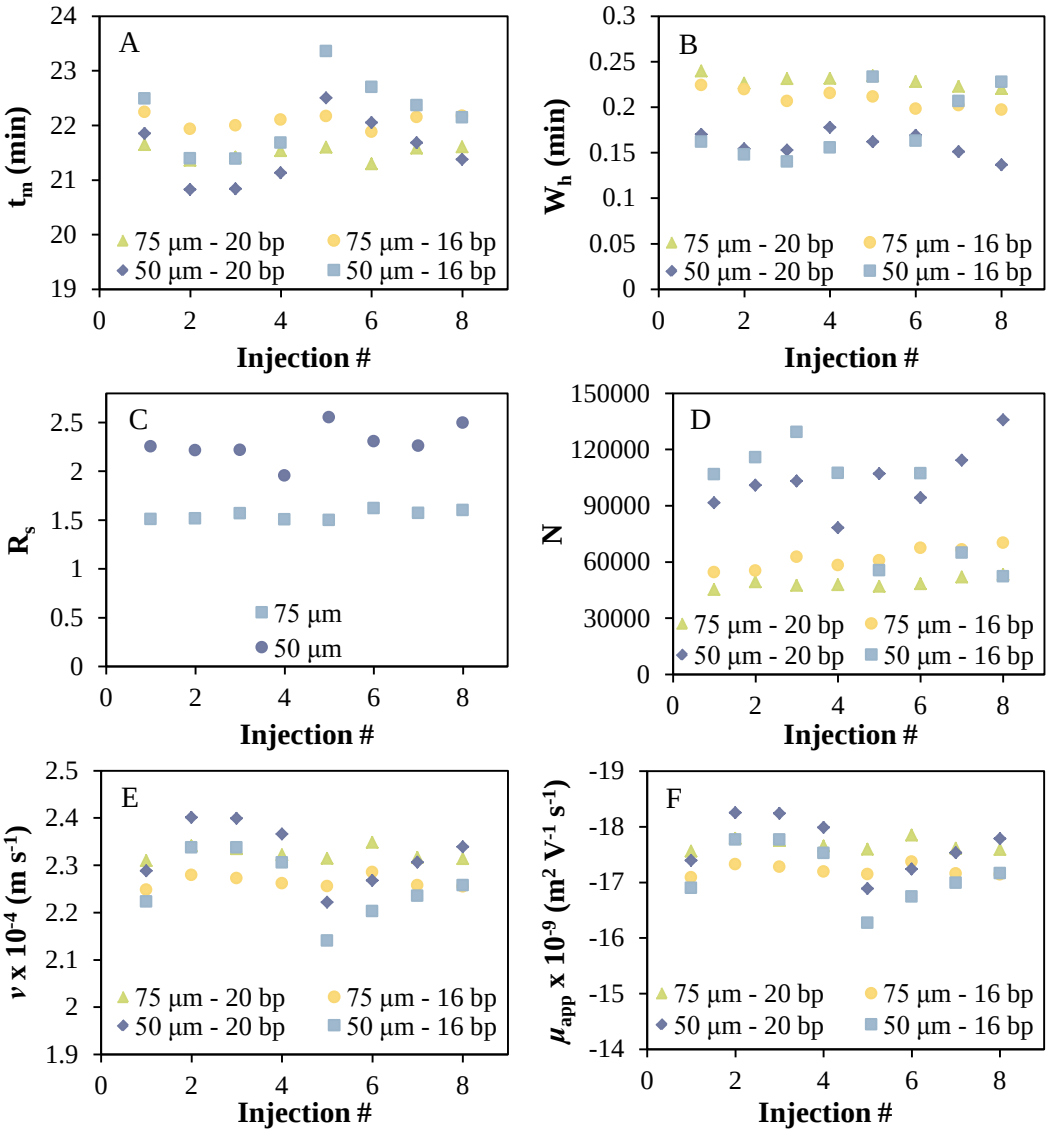

Figure 5.19. Plots of t_m (A), W_h (B), R_s (C), N (D), ν (E), and μ_{app} (F), versus injection # for the separation of 16 bp and 20 bp dsODNs (18.6 µM) on CFR PEPyM-*co*-PMMA random copolymer (21/79) coated fused-silica capillaries (30 cm L_d, 38 cm L_t, 363 µm od) with 50 µm or 75 µm id.

The repeatability of the coating was determined from the ODN t_m for both capillary diameters. The t_m % RSD (n = 8) of the 50 µm capillary in Table 5.9 were poor in comparison to the 75 µm capillary (Table 5.8), again indicating a stronger surface-analyte interaction with the 50 µm capillary (see Figure 10.5 in Appendix A for the CE electropherograms of the 8 injections on the 50 µm capillary). The 75 µm capillary was used for the remainder of the work (unless otherwise specified) owing to Gaussian peak shapes and improved repeatability, signal-to-noise, and t_m.

5.2.2.5 Control runs

Analysis of ODN mixtures was also performed on bare fused-silica capillaries to demonstrate the necessity to coat the capillaries. Additionally, control runs of Milli-Q water and Tris-borate (100 mM)/urea (7 M) buffer were performed on the CFR PEPyM-*co*-PMMA random copolymer coated capillary to identify any peaks related to these species.

5.2.2.5.1 Bare fused-silica capillaries

Bare fused-silica capillaries were activated according to the method described in Section 2.3.3.3.1. Analysis on the bare capillary was performed using individual solutions of 16 bp, 18 bp, 19 bp and 20 bp dsODNs, and mixtures of 16 bp and 18 bp, 16 bp and 19 bp, and 16 bp and 20 bp dsODNs. Figure 5.20 shows the dsODN separation on the bare capillary.

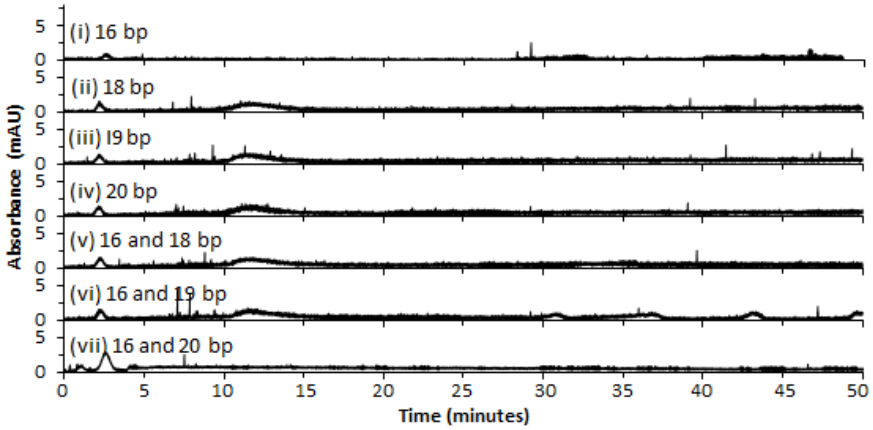

Figure 5.20. CE electropherograms of individual solutions of 16 bp (i), 18 bp (ii), 19 bp (iii), and 20 bp (iv), dsODNs (18.6 µM); and dsODN mixtures (18.6 µM) of 16 bp and 18 bp (v), 16 bp and 19 bp (vi), and 16 bp and 20 bp (vii). Separation was performed on a bare fused-silica capillary (30 cm L_d, 38 cm L_t, 75 µm id, 363 µm od) at -131.6 V cm^{-1} and 30 ^{o}C with UV detection at 260 for 50 min run time. The BGE was Tris-borate (100 mM)/urea (7 M). Samples were introduced hydrodynamically at 5000 Pa for 6 s.

In Figure 5.20 there was no detection of the dsODNs in any of the samples, demonstrating the need to coat the capillary surface for successful separation of these negatively charged molecules. The broad low intensity 'peak' between 10 min and 15 min observed in some of the electropherograms was due to an artefact of either the injection or of the buffer itself. This same anomaly was observed in Figure 5.21(i) for an injection of buffer only. In addition, the peak at approximately 2 min was due to equilibration of the running buffer (also observed in the buffer blank runs in Figure 5.21).

5.2.2.5.2 PEPyM-co-PMMA (21/79) coated capillaries

New bare fused-silica capillaries were activated and coated with CFR PEPyM-*co*-PMMA random copolymer according to Section 2.3.3.3.2. After which, they were used in the electrophoresis of Milli-Q water and Tris-borate (100 mM)/urea (7 M) buffer.

5.2.2.5.2.1 Injection of Tris-borate (100 mM)/urea (7 M) buffer

Blank control runs of repetitive injections of Tris-borate (100 mM)/urea (7 M) buffer showed very small peaks at the beginning of the run due to equilibration of the running buffer with the capillary (see Figure 5.21). Injections of buffer also resulted in downward sloping baselines. Importantly, there are no large peaks detected between 15 min and 25 min which would indicate the presence of ODNs under these conditions. It can therefore be concluded that the peaks for ODNs were correctly assigned.

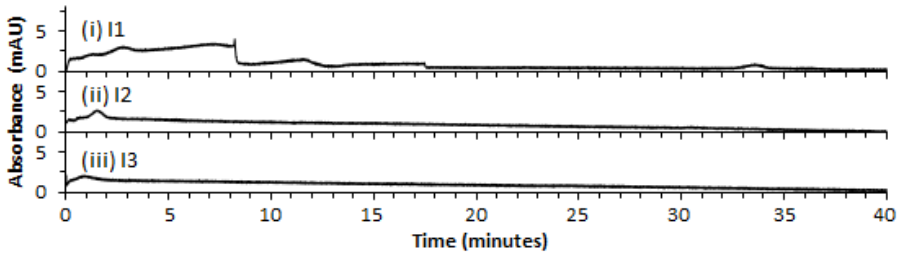

Figure 5.21. CE electropherograms of repetitive injections of Tris-borate (100 mM)/urea (7 M) buffer. Separation was performed on a CFR PEPyM-*co*-PMMA random copolymer (21/79) coated fused-silica capillary (30 cm L_d, 38 cm L_t, 75 µm id, 363 µm od) at -131.6 V cm^{-1} and 30 ^{o}C with UV detection at 260 for 40 min run time. The BGE was Tris-borate (100 mM)/urea (7 M). Samples were introduced hydrodynamically at 5000 Pa for 6 s.

5.2.2.5.2.2 Injection of Milli-Q water

Milli-Q water was used in the preparation of the ODNs; therefore it was necessary to perform blank runs of Milli-Q water to ensure it did not lead to any peaks in the region (15 min - 25 min) in which the ODNs were being detected. Blank control runs of repetitive injections of Milli-Q water (see Figure 5.22) showed very small peaks at the beginning of the run which were due to the running buffer as these peaks were also present in the buffer control runs. These results confirmed the correct identification of the ODN peaks.

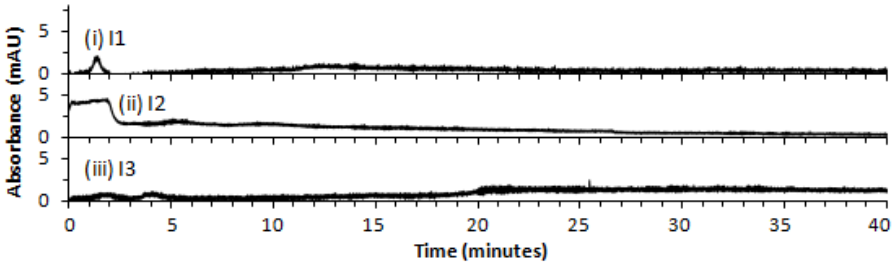

Figure 5.22. CE electropherograms of repetitive injections of Milli-Q water. Separation was performed on a CFR PEPyM-*co*-PMMA random copolymer (21/79) coated fused-silica capillary (30 cm L_d, 38 cm L_t, 75 µm id, 363 µm od) at -131.6 V cm^{-1} and 30 ^oC with UV detection at 260 for 40 min run time. The BGE was Tris-borate (100 mM)/urea (7 M). Samples were introduced hydrodynamically at 5000 Pa for 6 s.

5.3 Optimised separation of ODNs on PEPyM-*co*-PMMA (21/79) coated capillaries

The optimised method developed for analysis of ODNs on CFR PEPyM-*co*-PMMA random copolymer coated capillaries is represented by Scheme 5.2. This method was used for the analysis of ssODNs and dsODNs between 16 bp and 20 bp in length in individual solutions and in mixtures. The mobilities were investigated and the separation mechanism determined. The performance of this coating was compared to coatings of homopolymers of PEPyM and PMMA, and a PEPyM-*b*-PMMA (30/70) block copolymer coating. The performance of the coating was also compared to a similar cationic hybrid random copolymer of PDEAEMA-*co*-PMMA (34/66).

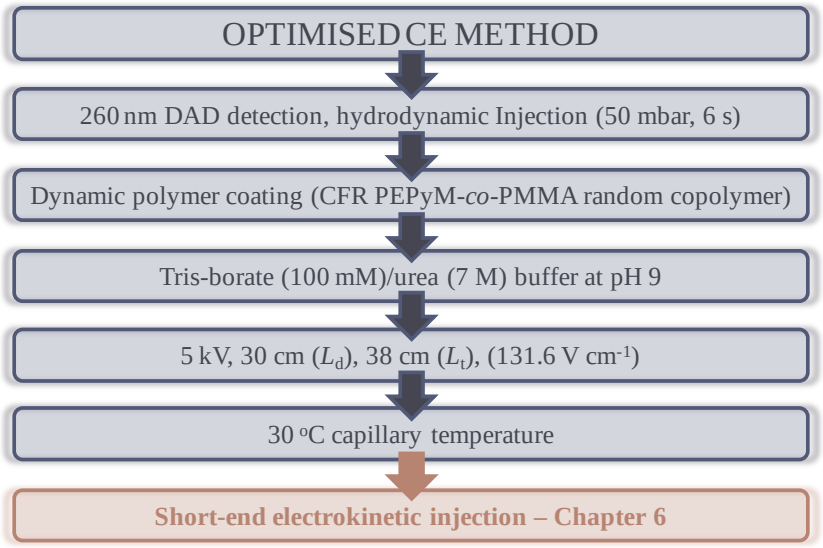

Scheme 5.2. Optimised CE method for analysis of ODNs on CFR PEPyM-*co*-PMMA random copolymer (21/79) capillaries.

5.3.1 Mobility of ssODNs versus dsODNs

The differential separation of ssODNs and dsODNs was investigated using individual solutions (18.6 µM) of 16 b ssODNs, and 16 bp dsODNs. Figure 5.23 shows the CE electropherograms of each injection. The mean t_m, calculated mobilities and % RSD values can be found in Table 5.10.

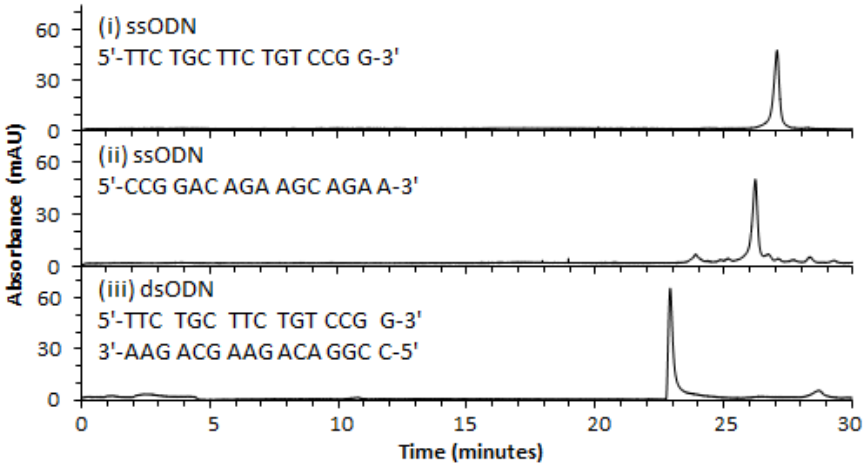

Figure 5.23. CE electropherograms of complementary 16 b ssODNs (18.6 µM) (i)-(ii), and the hybridized 16 bp dsODN (18.6 µM) (iii). Separation was performed on a CFR PEPyM-*co*-PMMA random copolymer (21/79) coated fused-silica capillary (30 cm L_d, 38 cm L_t, 75 µm id, 363 µm od) at -131.6 V cm^{-1} and 30 °C with UV detection at 260 nm for 60 min run time. The BGE was Tris-borate (100 mM)/urea (7 M). Samples were introduced hydrodynamically at 5000 Pa for 6 s.

The electropherograms show that dsODNs had a shorter t_m when compared to the complementary ssODNs indicating that dsODNs possessed a greater resistance to the cathodic flow than the ssODNs. This was attributed to the larger net negative charge on the dsODNs when compared to the ssODNs. The ODNs travelled towards the anode, and were therefore said to have an anodic μ_{app}. From the v_{EOF} and μ_{EOF} data of the polymer coating (Section 5.2.1.6.2) it was found that the flow (at pH 9), although reduced, was still towards the cathode which meant that the ODNs were travelling against the bulk flow of the capillary and the more negatively charged species (in this case dsODNs) could migrate more easily against this cathodic flow. In addition, Madabhushi [54] reported an increase in DNA-surface interactions for ssDNA when compared to dsDNA, and the author attributed this to the exposure of the bases to the coating. An increase in ODN-surface interactions would result in a longer t_m, which was observed in the work presented here. Figure 5.23(iii) also contained a small peak at ~28.7 min, attributed to non-hybridised ssODNs which is a consequence of the sample containing one of the ssODNs in excess.

Table 5.10. Calculation of mean t_m, μ_{app}, μ_{obs} and repeatability for 3 injections of 16 bp dsODN and its complementary ssODNs on a CFR PEPyM-*co*-PMMA random copolymer (21/79) coated fused-silica capillary.

ODN sample	t_m (min)	W_h (min)	N	v x 10^{-4} (m s^{-1})	μ_{app} x 10^{-9} (m^2 V^{-1} s^{-1})*	s_d x 10^{-9} (n = 3)	RSD (%)	μ_{obs} x 10^{-9} (m^2 V^{-1} s^{-1})*
16 b 5'-TTC	30.76	0.28	69864	1.63	-12.4	0.12	0.97	-21.2
16 b 5'-CCG	27.57	0.23	77505	1.81	-13.8	0.10	0.75	-22.6
16 bp	23.03	0.18	87134	2.17	-16.5	0.15	0.92	-23.3

*The negative sign denotes an anodic mobility

It can be seen from Table 5.10 that the mobility was different for each of the complementary ssODN strands suggesting sequence dependent mobilities. This has also been observed for separation of ss and ds oligomers in free solution [8, 146]. Stellwagen & Stellwagen [8] reported that sequences containing A-tracts (consecutive adenine residues in the helix) exhibited slower mobilities due to preferential counterion binding to these regions reducing the charge density of the strand. However, the sequence dependence for the synthetic oligonucleotides used herein was not due to the presence of A-tracts. This is evidenced by the fact that the

lower mobility strand (5'-TTC) did not contain any adenine residues, whereas the higher mobility strand (5'-CCG) contained 2 consecutive adenine residues in the sequence. Therefore, the sequence dependence in this case was related to the exposure of the bases. Under basic conditions, the approximate reported pKa values of thymine, guanine, adenine and cytosine are between 9.9 - 10.5, 9.2 - 9.6, 4.1 - 4.2 and 4.2 - 4.4, respectively [186]. A lower pKa value indicates a higher degree of dissociation and hence a higher negative charge. Of the 16 bases in the 5'-CCG strand, 11 of these are A or C, compared to the 5'-TTC which contained only 5. Therefore the overall charge, and hence the mobility, of the 5'-CCG strand was greater.

5.3.2 Mobility of dsODNs

Individual solutions of 16 bp, 18 bp, 19 bp and 20 bp dsODNs (18.6 µM) were analysed in order to determine the migration order of the dsODN strands (see Figure 5.24). The results were consistent with those obtained previously (see Section 5.3.1) with the strand containing the higher charge density possessing the greater mobility.

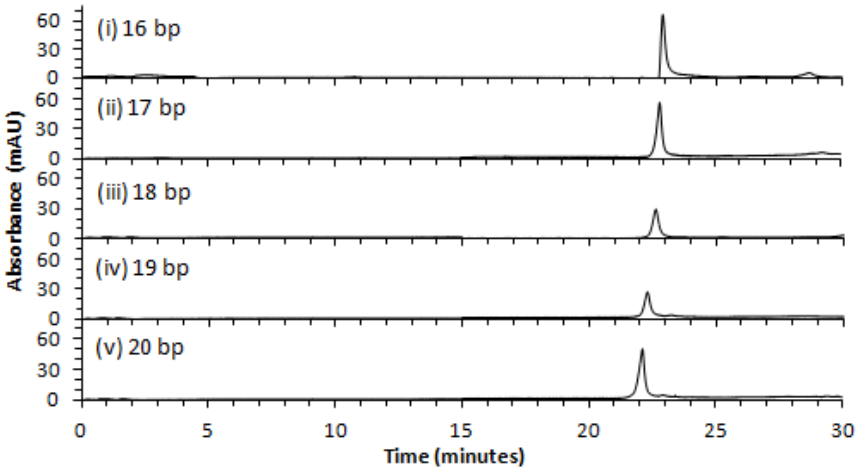

Figure 5.24. CE electropherograms of individual solutions of 16 bp (i), 18 bp (ii), 19 bp (iii), and 20 bp (iv), dsODNs (18.6 µM). Separation was performed on a CFR PEPyM-*co*-PMMA random copolymer (21/79) coated fused-silica capillary (30 cm L_d, 38 cm L_t, 75 µm id, 363 µm od) at -131.6 V cm^{-1} and 30 ^{o}C with UV detection at 260 nm for 30 min run time. The BGE was Tris-borate (100 mM)/urea (7 M). Samples were introduced hydrodynamically at 5000 Pa for 6 s.

The migration order was from largest to smallest with the 20 bp dsODN having the shortest t_m and hence the greatest mobility, followed by 19 bp, 18 bp, 17 bp and finally the 16 bp dsODN, due to the greater overall charge. Linear trends were observed from plots of t_m and μ_{obs} versus bp length (see Figure 5.25).

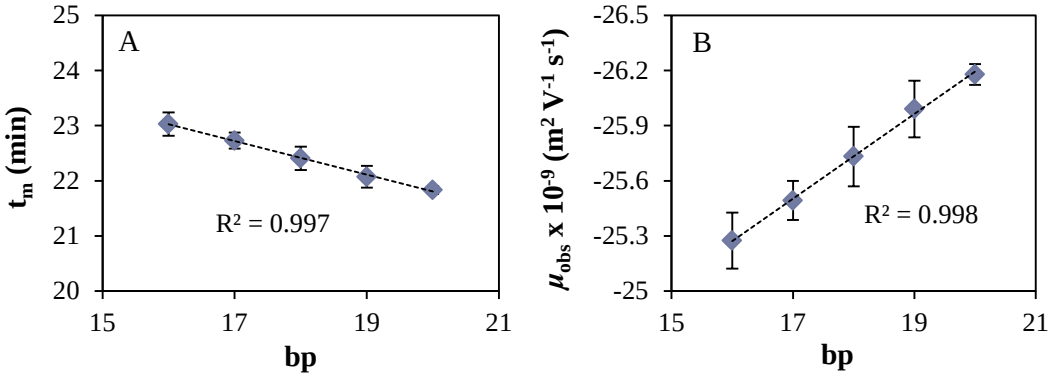

Figure 5.25. Plots of t_m (A), and μ_{obs} (B), versus bp length for separation of individual solutions of dsODNs (18.6 µM) on a CFR PEPyM-*co*-PMMA random copolymer (21/79) coated fused-silica capillary (30 cm L_d, 38 cm L_t, 75 µm id, 363 µm od). Error bars are ± 1 s_d from n = 3.

The repeatability of the individual dsODN solutions and their calculated μ_{app} and μ_{obs} are listed in Table 5.11. As already demonstrated in the method development, the repeatability of the coating for ODN separations was acceptable (below 1 %).

Table 5.11. Calculation of mean t_m, μ_{app}, μ_{obs} and repeatability for 3 injections of individual dsODN solutions on a CFR PEPyM-*co*-PMMA random copolymer (21/79) coated fused-silica capillary.

dsODN sample	t_m (min)	W_h (min)	N	v x 10^{-4} (m s^{-1})	μ_{app} x 10^{-9} (m^2 V^{-1} s^{-1})*	s_d x 10^{-9} (n = 3)	RSD (%)	μ_{obs} x 10^{-9} (m^2 V^{-1} s^{-1})*
16 bp	23.03	0.18	87134	2.17	-16.5	0.15	0.92	-23.3
17 bp	22.73	0.20	70195	2.20	-16.7	0.11	0.64	-25.5
18 bp	22.41	0.23	54003	2.23	-17.0	0.16	0.95	-25.7
19 bp	22.07	0.22	63296	2.27	-17.2	0.15	0.90	-26.0
20 bp	21.83	0.24	54787	2.29	-17.4	0.06	0.32	-26.2

*The negative sign denotes an anodic mobility

In most CE separations of DNA using polymer solutions, it is found that the shorter strands have a greater mobility than longer strands due to the sieving abilities of the polymer. However, none of these mechanisms can be applied to the work presented here as separation was not performed with sieving media. A study on low M_w

polymer solutions by Zhu *et al.* [37] proposed that the inverse relationship of t_m to bp length was due to the globular structure of the low M_w polymer combined with the rod-like structure of the short DNA strands. The migration of the short-strands was dependent on their interactions with the polymer and how readily they could diffuse through the matrix. Essentially, the system behaved similarly to size-exclusion chromatography, in which the shorter strands were more likely to be trapped in the polymer pores [37]. The order of elution reported here can be partly explained by this mechanism because the CFR PEPyM-*co*-PMMA random copolymer (~14 398 g mol^{-1}) concentration (1 mg mL^{-1}) was well below the *c** and hence the polymer coils were hydrodynamically isolated from each other [34, 35, 37, 50, 98, 120]. However, for the method herein, due to the fact that the polymer was confined to the capillary surface and not acting as a sieving media, pores were unlikely to form. Therefore, it is proposed that the shorter negatively charged dsODNs were screened more via ion-pairing with the positively charged polymer coating than longer strands, and hence interacted with the capillary surface to a greater extent under the same applied voltage (see Scheme 5.3). Thus the lower negative charge combined with the smaller molecule size reduced the migration against the cathodic flow.

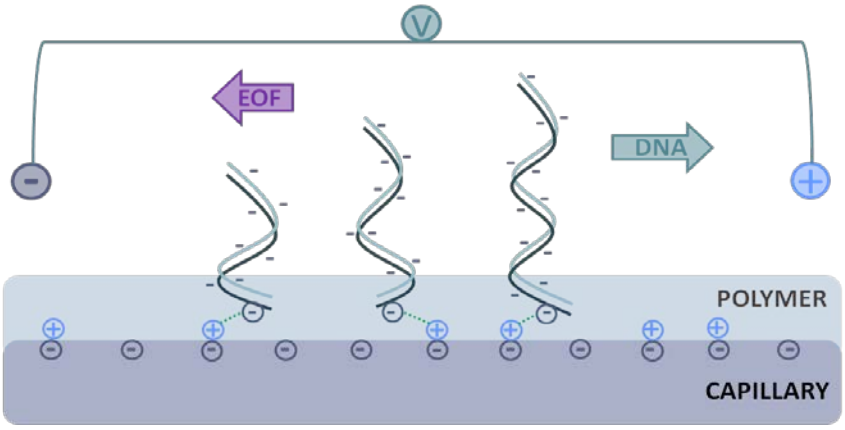

Scheme 5.3. Proposed ODN migration mechanism through the CFR PEPyM-*co*-PMMA random copolymer (21/79) coated fused-silica capillary in free solution.

Furthermore, a study by Stellwagen & Stellwagen [8] investigated the free solution mobility of DNA, and found that for shorter strands (less than 170 bp) the t_m was inversely proportional to bp length. This is in concordance with the work presented here, suggesting that the mechanism was also based on the free solution mobility of ODNs (see Section 1.4.1). Further research into free solution mobility [20, 21, 93,

94, 100, 187] indicated that the migration trend was due, in short, to the conformation of the DNA strands, hydrodynamic coupling between monomer subunits, and electrolyte friction [20, 93, 96]. The rod-like conformation of the shorter strands meant that counterion condensation did not occur and the mobility increased with increasing M_w due to hydrodynamic coupling between subunits [101]. In addition, shorter strands are said to experience solvent friction more than larger strands owing, again, to the rod-like structure.

5.3.3 Separation of ODN mixtures

Figure 5.26 shows the electropherograms for the separation of mixtures of dsODNs. Mixtures were prepared containing (i) 16 bp and 17 bp, (ii) 16 bp and 18 bp, (iii) 16 bp and 19 bp, and (iv) 16 bp and 20 bp dsODNs.

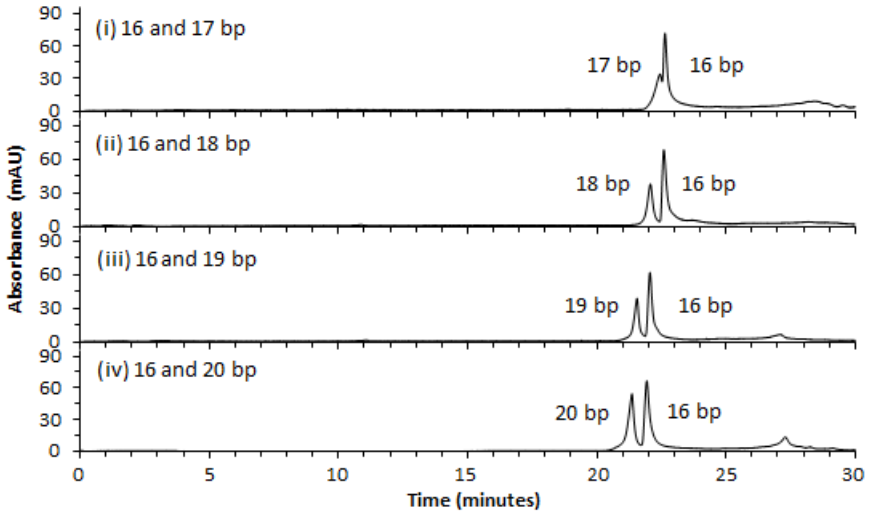

Figure 5.26. CE electropherograms of a mixture of 16 bp dsODNs (18.6 µM) containing 17 bp (i), 18 bp (ii), 19 bp (iii), and 20 bp (iv), dsODNs (18.6 µM). Separation was performed on a CFR PEPyM-*co*-PMMA random copolymer (21/79) coated fused-silica capillary (30 cm L_d, 38 cm L_t, 75 µm id, 363 µm od) at -131.6 V cm^{-1} and 30 ^{o}C with UV detection at 260 nm for 30 min run time. The BGE was Tris-borate (100 mM)/urea (7 M). Samples were introduced hydrodynamically at 5000 Pa for 6 s.

Consistent with earlier results, the t_m for the separations decreased with increasing bp length, with the 20 bp dsODN mixture having the fastest t_m. The plots of R_s and t_m versus bp length (Figure 5.27) demonstrated an increase in both R_s and μ_{obs} with increasing bp length owing to the separation of dsODNs in free solution. One disadvantage of electrophoresis, is that it results in greater peak areas for slower moving analytes [20] and this was evident from the results presented here. This is due to the difference in velocity of the analyte zone as they pass the detector.

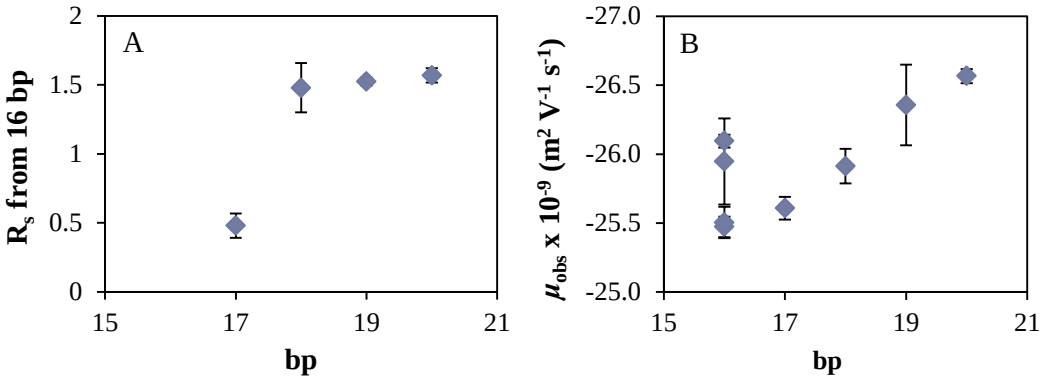

Figure 5.27. Plots of R_s from 16 bp (A), and μ_{obs} (B), versus bp length for separation of dsODN mixtures (18.6 µM) on a CFR PEPyM-*co*-PMMA random copolymer (21/79) coated fused-silica capillary (30 cm L_d, 38 cm L_t, 75 µm id, 363 µm od). Error bars are ± 1 s_d from n = 3.

As was expected from the results obtained for the individual solutions, the electropherograms show that (with the exception of the 16 bp and 17 bp mixture) each of the dsODN strands were separated with near baseline R_s (for R_s values refer to Table 5.12). This analysis showed that the CFR PEPyM-*co*-PMMA random copolymer coating and the coating procedure was sufficient for separation of dsODNs with 1 - 4 bp difference.

As illustrated in Figure 5.27B and Table 5.12, the μ_{obs} of the 16 bp strand was not consistent within each mixture (peaks in the electropherograms were not additive). This was a strong indication of ODN-ODN interactions occurring between the different complementary double strands as they migrated, as well as ODN-buffer interactions [105]. It was also likely that there was competition between the different strands for the surface during migration. These interactions were investigated by altering the BGE ionic strength, and by use of a 16 bp strand (denoted by CAT strand) with a sequence non-complementary to the 17 b, 18 b, 19 b and 20 b ODN strands used in this study, and the results can be found in Chapter 6.

Table 5.12. Calculation of mean t_m, μ_{app}, μ_{obs} and repeatability for 3 injections of dsODN mixtures on a CFR PEPyM-*co*-PMMA random copolymer (21/79) coated fused-silica capillary.

dsODN mixture	Peak (bp)	t_m (min)	W_h (min)	R_s	N	v x 10^{-4} (m s^{-1})	μ_{app} x 10^{-9} (m^2 V^{-1} s^{-1})*	s_d x 10^{-9} (n = 3)	RSD (%)	μ_{obs} x 10^{-9} (m^2 V^{-1} s^{-1})*
17 & 16 bp	17	22.57	0.22	0.48	59120	2.22	-16.8	0.08	0.49	-25.6
	16	22.75	0.23		53989	2.20	-16.7	0.07	0.44	-25.5
18 & 16 bp	18	22.17	0.22	1.48	55567	2.26	-17.1	0.13	0.73	-25.9
	16	22.71	0.21		65417	2.20	-16.7	0.11	0.69	-25.5
19 & 16 bp	19	21.61	0.20	1.52	64616	2.31	-17.6	0.29	1.67	-26.4
	16	22.13	0.20		68698	2.26	-17.2	0.31	1.82	-25.9
20 & 16 bp	20	21.36	0.23	1.57	48446	2.34	-17.8	0.05	0.41	-26.6
	16	21.94	0.21		61543	2.28	-17.3	0.05	0.39	-26.1

*The negative sign denotes an anodic mobility

5.3.4 Comparison to other polymer surfaces

The separation of ODNs on the CFR PEPyM-*co*-PMMA random copolymer (random copolymer) coated capillaries was compared to surfaces of the CFR PMMA homopolymer and CFR PEPyM homopolymer to investigate the adsorption and separation mechanisms. The PEPyM-*co*-PMMA and its homopolymers were all synthesised by CFR polymerisation. Separation was also compared to the use of a RAFT PEPyM-*b*-PMMA block copolymer coated capillary (synthesised by RAFT polymerisation) to investigate the significance of using random versus block copolymers. Finally, ODN separation was investigated on a similar cationic copolymer to the CFR PEPyM-*co*-PMMA random copolymer, that being a CFR PDEAEMA-*co*-PMMA random copolymer (synthesised by CFR copolymerisation). For the synthesis, structures, and characterisation of these polymers, refer to Chapters 2 and 3.

5.3.4.1 PMMA coated capillaries

A new capillary was activated according to the procedure described in Section 2.3.3.3.1. After which, the capillary was treated with a CFR PMMA (29 272 g mol^{-1}) homopolymer solution (1 mg mL^{-1} in acetone) according to Section 2.3.3.3.2. The coating was tested with injections of ODN mixtures of 16 bp and 18 bp, 16 bp and 19 bp, and 16 bp and 20 bp (see Figure 5.28).

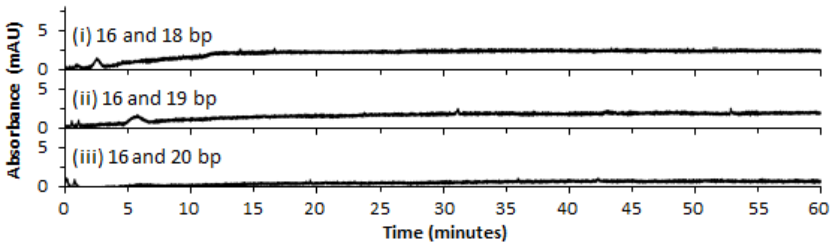

Figure 5.28. CE electropherograms of dsODNs mixtures (18.6 µM) of 16 bp and 18 bp (i), 16 bp and 19 bp (ii), and 16 bp and 20 bp (iii). Separation was performed on a CFR PMMA homopolymer coated fused-silica capillary (30 cm L_d, 38 cm L_t, 75 µm id, 363 µm od) at -131.6 V cm^{-1} and 30 ^{o}C with UV detection at 260 nm for 60 min run time. The BGE was Tris-borate (100 mM)/urea (7 M). Samples were introduced hydrodynamically at 5000 Pa for 6 s.

From Figure 5.28 it was evident that the CFR PMMA homopolymer coating was not capable of resolving the ODN mixtures. This was either due to the CFR PMMA homopolymer not sufficiently adsorbing to the surface, or any adsorbed polymer was not capable of modifying the surface charge and hence not reducing the EOF.

For a coating to be effective at reducing the EOF, it needs to be able to alter the EDL, shielding the surface. If the polymer does not evenly coat the surface, then the negative silanol groups will dominate the charge distribution and provide a strong cathodic EOF. In order to determine whether the CFR PMMA homopolymer was capable of adsorbing to a silanol surface, a CFR PMMA homopolymer polymer solution was spin-coated onto silicon wafers and analysed by AFM. The results (see Chapter 4) indicated that the CFR PMMA homopolymer aggregated in solution and created a highly disordered and uneven surface by adsorbing in random bundles with a surface coverage of only ~19 %. Therefore, the large number of remaining negative silanol groups were not shielded by the polymer and the EDL formed resulted in a strong cathodic EOF.

5.3.4.2 PEPyM coated capillaries

A new capillary was first activated and then coated with a CFR PEPyM (M_w not determined) homopolymer solution (1 mg mL^{-1} in ethanol) according to the procedure described in Section 2.3.3.3. The coating was tested with injections of individual 16 bp, 18 bp, 19 bp and 20 bp dsODNs, and dsODN mixtures of 16 bp and 18 bp, 16 bp and 19 bp, and 16 bp and 20 bp (see Figures 5.29 and 5.30 for the electropherograms and the trend plots, respectively; and Table 10.3 in Appendix A for the mobility and R_s calculations).

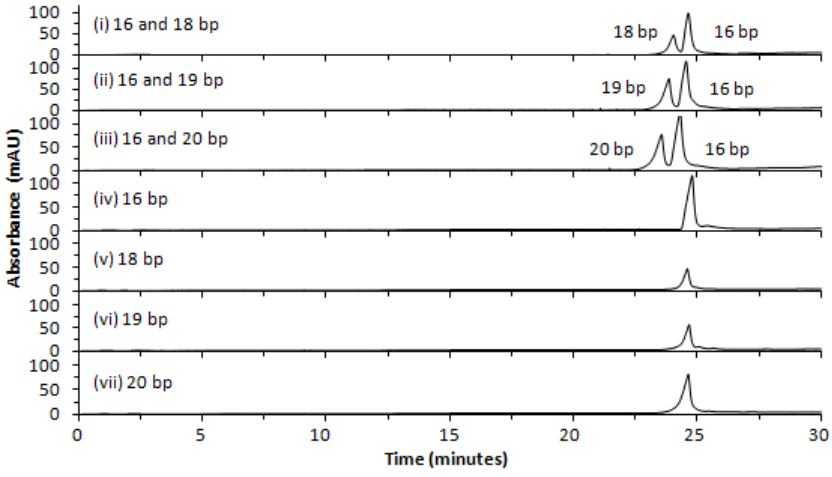

Figure 5.29. CE electropherograms of a mixture of 16 bp dsODNs (18.6 µM) containing 18 bp (i), 19 bp (ii), and 20 bp (iii), dsODNs (18.6 µM) and individual solutions of 16 bp (iv), 18 bp (v), 19 bp (vi), and 20 bp (vii) dsODNs (18.6 µM). Separation was performed on a CFR PEPyM homopolymer coated fused-silica capillary (30 cm L_d, 38 cm L_t, 75 µm id, 363 µm od) at -131.6 V cm^{-1} and 30 °C with UV detection at 260 nm for 30 min run time. The BGE was Tris-borate (100 mM)/urea (7 M). Samples were introduced hydrodynamically at 5000 Pa for 6 s.

From Figures 5.29 and 5.30 it was observed that the migration order was from largest to smallest, in accordance with the CFR PEPyM-*co*-PMMA random copolymer coating, again indicating that migration was based on the free solution mobility of the dsODNs. Figure 5.30 shows a comparison of the CFR PEPyM homopolymer coating to the CFR PEPyM-*co*-PMMA random copolymer for the dsODN mixtures and individual solutions. The trends were similar for both surfaces suggesting that the PEPyM units were responsible for most of the surface chemistry. The repeatability (see Table 10.3 in Appendix A) of the CFR PEPyM homopolymer surface was poorer than for the random copolymer surface, owing to the lack of PMMA units for stabilisation. The mobility and the resolving power were also decreased for the CFR PEPyM homopolymer meaning that the PMMA units played a part in the shielding of the surface charge from generating a strong EOF. This was attributed to the hydrophobic nature of the PMMA which repelled the solvated ions from the surface, thereby reducing the EOF. In addition, the peak shapes were non-Gaussian and appeared to skew to the right (fronted), suggesting stronger interactions with the surface.

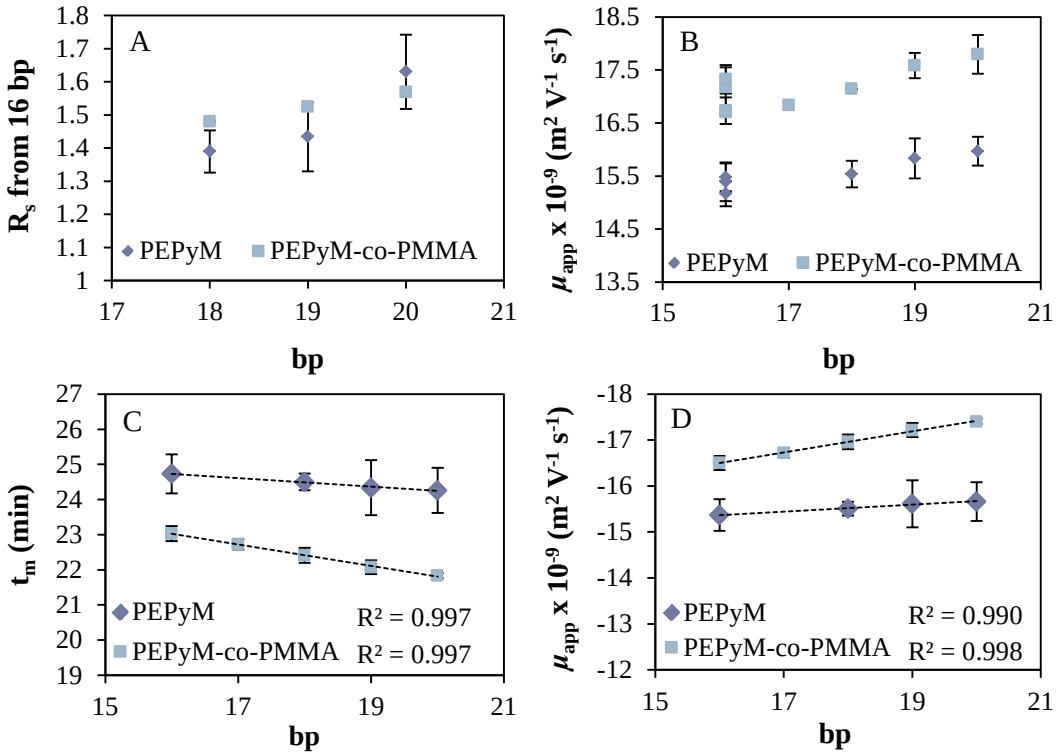

Figure 5.30. Plots of R_s from 16 bp (A), and μ_{app} (B), versus bp length for separation of dsODN mixtures (18.6 µM); and t_m (C), and μ_{app} (D), versus bp length for separation of individual solutions of dsODNs (18.6 µM) on a CFR PEPyM homopolymer coated capillary compared to a CFR PEPyM-*co*-PMMA random copolymer (21/79) coated capillary. Separation was performed on fused-silica capillaries (30 cm L_d, 38 cm L_t, 75 µm id, 363 µm od). Error bars are ± 1 s_d from n = 3.

As with the PEPyM-*co*-PMMA random copolymer surface, the t_m of the mixtures did not coincide with the t_m of the individual solutions indicating strong analyte-analyte interactions. This deduction was further supported by the change in t_m of the 16 bp strand within each mixture.

5.3.4.3 PEPyM-b-PMMA (30/70) coated capillaries

A new capillary was first activated and then coated with a RAFT PEPyM-*b*-PMMA (9 019 g mol^{-1}) block copolymer solution (1 mg mL^{-1} in ethanol) according to the procedure described in Section 2.3.3.3. The coating was initially tested with injections of individual solutions and mixtures of 16 bp and 20 bp dsODNs (see Figure 5.31).

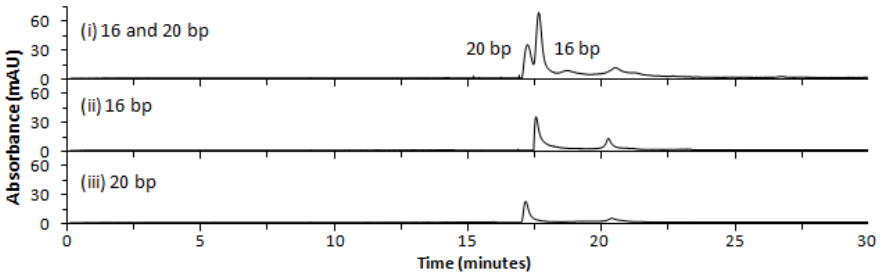

Figure 5.31. CE electropherograms of a mixture of 16 bp and 20 bp dsODNs (18.6 µM) (i), and individual solutions of 16 bp (ii), and 20 bp (iii), dsODNs (18.6 µM). Separation was performed on a RAFT PEPyM-*b*-PMMA block copolymer (30/70) coated fused-silica capillary (30 cm L_d, 38 cm L_t, 75 µm id, 363 µm od) at -131.6 V cm^{-1} and 30 °C with UV detection at 260 nm for 30 min run time. The BGE was Tris-borate (100 mM)/urea (7 M). Samples were introduced hydrodynamically at 5000 Pa for 6 s.

As seen in Figure 5.31, the migration order of the dsODNs was from largest to smallest in agreement with the results obtained for the random copolymer and the homopolymers synthesised by CFR polymerisation. The mean t_m, μ_{app} and R_s of the 16 bp and 20 bp dsODN mixture are found in Table 5.13, along with the % RSD.

Table 5.13. Calculation of mean t_m, R_s, μ_{app} and repeatability for 3 injections of 16 bp and 20 bp dsODN mixture on a RAFT PEPyM-*b*-PMMA block copolymer (30/70) coated fused-silica capillary (75 µm id).

Peak (bp)	t_m (min)	W_h (min)	R_s	μ_{app} x 10^{-9} ($m^2 V^{-1} s^{-1}$)*	s_d x 10^{-9} (n = 3)	RSD (%)
20	17.50	0.21	1.14	-21.7	0.48	2.19
16	17.96	0.26		-21.2	0.52	2.46

*The negative sign denotes an anodic mobility

From Table 5.13, it can be seen that the repeatability of the RAFT PEPyM-*b*-PMMA block copolymer suffered in comparison to the CFR PEPyM-*co*-PMMA random copolymer (see Table 5.11), suggesting that the polymer did not remain adsorbed to the surface resulting in an increased t_m from run to run. The block copolymer adsorbed more weakly to the surface due to the hydrophilic units and hydrophobic units being in blocks, meaning that the PMMA units were less able to stabilise the surface. As the polymer was removed, the surface was no longer being shielded and the negatively charged silanol groups dominated the surface charge. This resulted in an increase in the cathodic EOF and hence a reduction in the dsODN mobility (Figure 5.32A). A slight increase in R_s was also observed owing to the reduced μ_{app} meaning that the ODNs spent more time in the capillary.

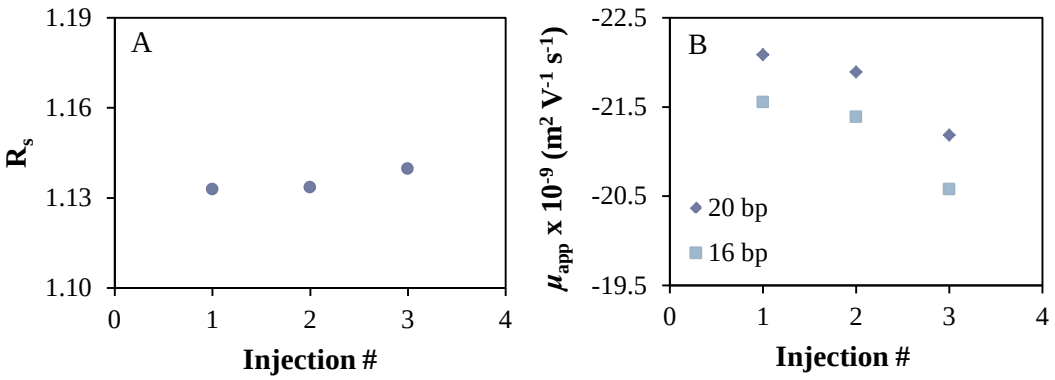

Figure 5.32. Plots of R_s (A), and μ_{app} (B), versus injection # for the separation of 16 bp and 20 bp dsODNs (18.6 µM) on a RAFT PEPyM-*b*-PMMA block copolymer (30/70) coated fused-silica capillary (30 cm L_d, 38 cm L_t, 75 µm id, 363 µm od).

In comparison to the random copolymer, the R_s was reduced by approximately 27 % which was related to a reduction in t_m and different surface interactions. From the AFM images (see Figure 4.7 in Section 4.3.1.2) it was observed that the block copolymer resulted in a lower surface coverage, with the formation of bundles with increased heights (compared to the random copolymer) owing to the aggregated polymer being less coiled and hence more rigid. Given that the surface was very different to the random copolymer surface, which was more uniform, the interactions between the dsODNs and the surface are much more random.

The reduced t_m observed (when the coating was freshly prepared) in comparison to the random copolymer were due to the initial shielding ability from the increased bulk of the block copolymer. The hydrophobic nature of the bulk (from the PMMA

units) initially prevented the generation of a strong EOF from the formation of the EDL; however, the PMMA units could not stabilise the surface for more than a few runs.

From the capillary id study on the CFR PEPyM-*co*-PMMA random copolymer coated capillary (Section 5.2.2.4), it was observed that a decrease in id resulted in an improved R_s with the consequence of reducing the signal-to-noise. Therefore, separation of mixtures of 16 bp and 18 bp, 16 bp and 19 bp, and 16 bp and 20 bp, was performed on a RAFT PEPyM-*b*-PMMA block copolymer coated capillary with a 50 µm id (see Figures 5.33 and 5.34 for the electropherograms and trend plots, respectively; and Table 10.4 in Appendix A for calculation of the R_s and μ_{app}).

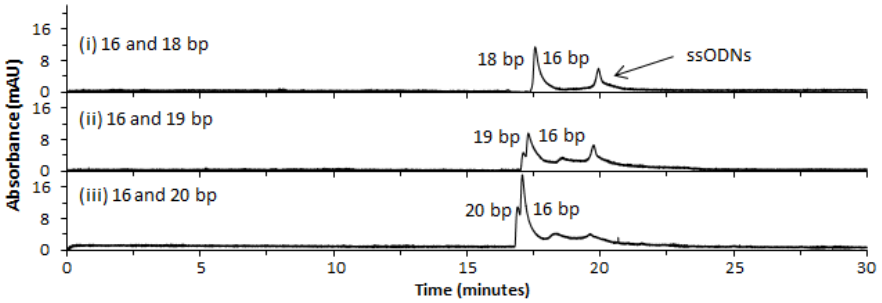

Figure 5.33. CE electropherograms of a mixture of 16 bp dsODNs (18.6 µM) containing 18 bp (i), 19 bp (ii), and 20 bp (iii), dsODNs (18.6 µM). Separation was performed on a RAFT PEPyM-*b*-PMMA block copolymer (30/70) coated fused-silica capillary (30 cm L_d, 38 cm L_t, 50 µm id, 363 µm od) at -131.6 V cm^{-1} and 30 °C with UV detection at 260 nm for 30 min run time. The BGE was Tris-borate (100 mM)/urea (7 M). Samples were introduced hydrodynamically at 5000 Pa for 6 s.

It can be seen from Figures 5.33 and 5.34A that not only was the R_s not improved using a smaller id capillary, it actually decreased. This confirmed that the uneven surface was having more of an effect on the mobility of the ODNs. As the migration order was from largest to smallest, the separation was still based on the free solution mobility; however, it was likely that the bulk of the block copolymer acted as an obstacle, affecting the larger strands to a greater extent, slowing down the migration, and resulting in co-migration of all the fragments. This exemplifies how changing the surface chemistry and conformation can affect the migration of dsODNs.

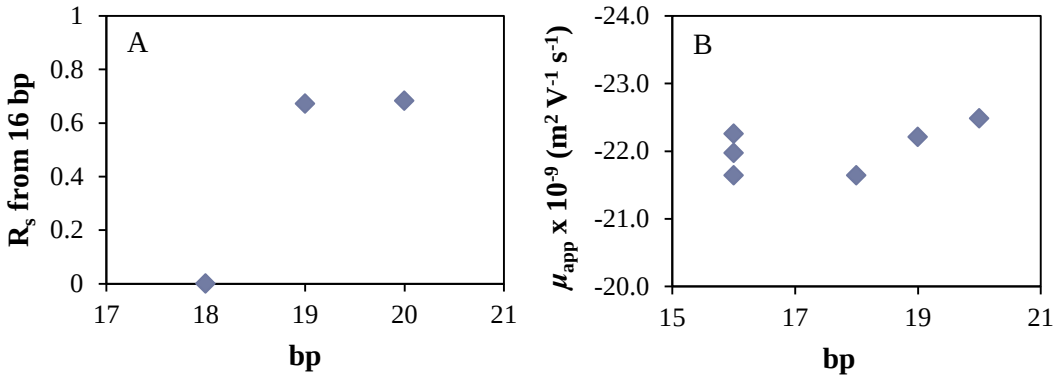

Figure 5.34. Plots of R_s from 16 bp (A), and μ_{app} (B), versus bp length for separation of dsODNs mixtures (18.6 µM) on a RAFT PEPyM-*b*-PMMA block copolymer (30/70) coated fused-silica capillary (30 cm L_d, 38 cm L_t, 50 µm id, 363 µm od).

As was observed with all the polymer surfaces investigated, the t_m of the 16 bp dsODNs changed within each dsODN mixture indicating strong analyte-analyte interactions occurring during electrophoresis.

5.3.4.4 PDEAEMA-co-PMMA (34/66) coated capillaries

A new capillary was first activated and then coated with a CFR PDEAEMA-*co*-PMMA (18 474 g mol^{-1}) random copolymer solution (1 mg mL^{-1} in ethanol) according to the procedure described in Section 2.3.3.3. The coating was tested with injections of dsODN mixtures of 16 bp and 18 bp, 16 bp and 19 bp, and 16 bp and 20 bp (see Figures 5.35 and 5.36 for the electropherograms trend plots, respectively; and Table 10.5 in Appendix A for calculation of the R_s and μ_{app}).

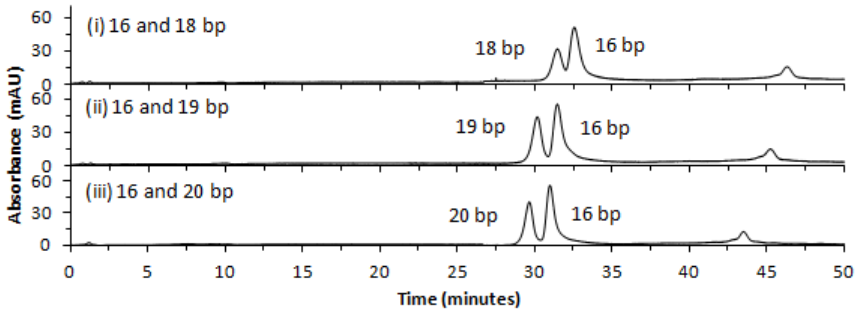

Figure 5.35. CE electropherograms of a mixture of 16 bp dsODNs (18.6 µM) containing 18 bp (i), 19 bp (ii), and 20 bp (iii), dsODNs (18.6 µM). Separation was performed on a CFR PDEAEMA-*co*-PMMA random copolymer (34/66) coated fused-silica capillary (30 cm L_d, 38 cm L_t, 75 µm id, 363 µm od) at -131.6 V cm^{-1} and 30 °C with UV detection at 260 nm for 50 min run time. The BGE was Tris-borate (100 mM)/urea (7 M). Samples were introduced hydrodynamically at 5000 Pa for 6 s.

It can be seen from Figure 5.35 that the migration order of the dsODNs was again from largest to smallest in agreement with the results obtained for all the polymer

coatings, and that the migration is based on the free solution mobility of the dsODNs. Figure 5.36 showed that the R_s increased with increasing bp difference and the μ_{app} increased with increasing bp size. The t_m of the 16 bp dsODNs changed within each dsODN mixture indicating strong analyte-analyte interactions occurring during electrophoresis on the CFR PDEAEMA-*co*-PMMA random copolymer coated capillary.

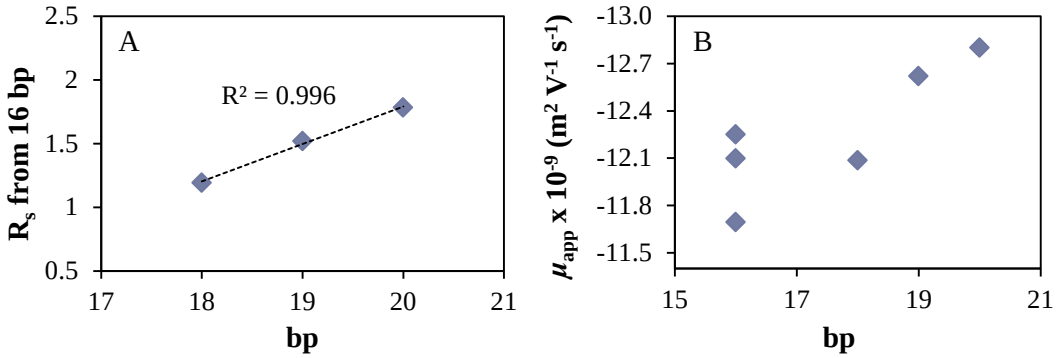

Figure 5.36. Plots of R_s from 16 bp (A), and μ_{app} (B), versus bp length for separation dsODN mixtures (18.6 µM) on a CFR PDEAEMA-*co*-PMMA random copolymer (34/66) coated fused-silica capillary (30 cm L_d, 38 cm L_t, 75 µm id, 363 µm od).

The repeatability of the CFR PDEAEMA-*co*-PMMA random copolymer coating was determined by repetitive injections of 16 bp and 20 bp dsODN mixtures and the results are represented in Table 5.14 and Figure 5.37.

Table 5.14. Calculation of mean t_m, R_s and μ_{app} for 5 injections of a 16 bp and 20 bp dsODN mixture on a CFR PDEAEMA-*co*-PMMA random copolymer (34/66) coated fused-silica capillary.

Peak (bp)	t_m (min)	W_h (min)	R_s	μ_{app} x 10^{-9} (m^2 V^{-1} s^{-1})*	s_d x 10^{-9} (n = 5)	RSD (%)
20	32.39	0.46	1.86	-11.8	1.01	8.54
16	33.80	0.44		-11.3	0.94	8.28

*The negative sign denotes an anodic mobility

As with the PEPyM-*b*-PMMA, the repeatability of the CFR PDEAEMA-*co*-PMMA random copolymer coating suffered. The t_m increased and hence the μ_{app} decreased (see Figure 5.37B) with each successive injection proving that the coating was not stable. In an attempt to improve the repeatability of the coating, the between-run conditioning procedure was performed twice and the 16 bp and 20 bp dsODN mixture was re-analysed. The result is represented by injection #5 in Figure

5.37. It can be seen from this injection that a 2x conditioning resulted in a reduction in t_m and hence an increase in μ_{app}. This suggested the CFR PDEAEMA-*co*-PMMA random copolymer did not adsorb to the surface as strongly as the PEPyM-*co*-PMMA and required longer conditioning times to ensure sufficient re-adsorption to the silanol surface.

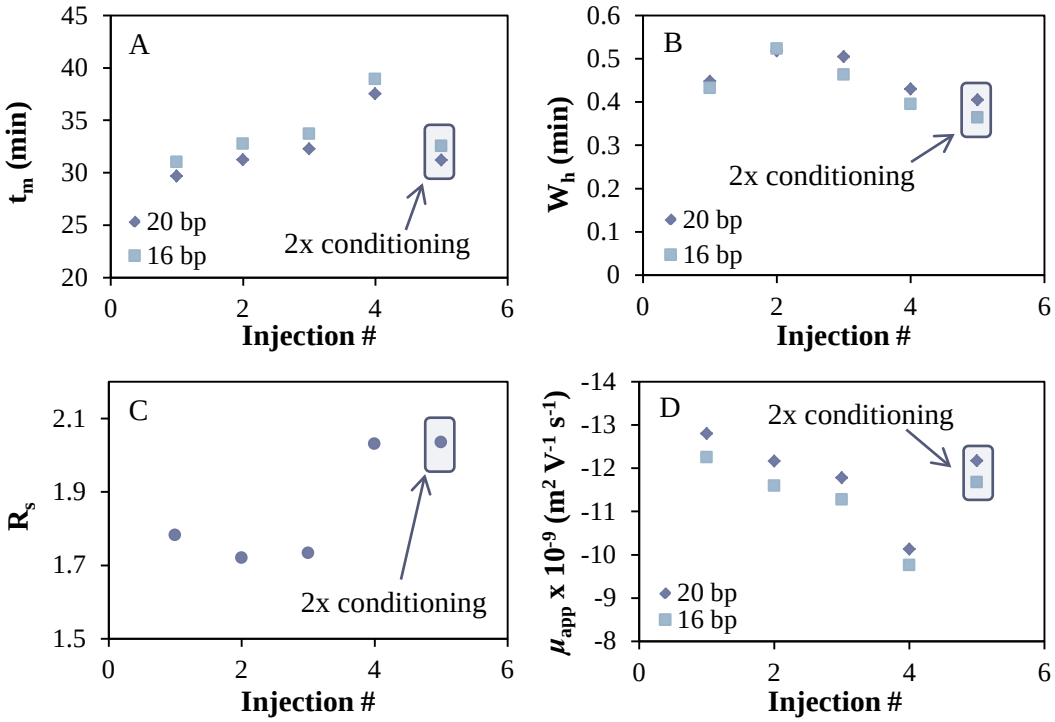

Figure 5.37. Plots of t_m (A), W_h (B), R_s (C), and μ_{app} (D), versus injection # for separation of 16 bp and 20 bp dsODNs (18.6 µM) on a CFR PDEAEMA-*co*-PMMA random copolymer (34/66) coated fused-silica capillary (30 cm L_d, 38 cm L_t, 75 µm id, 363 µm od).

A new method was created replacing the 3 min polymer rinse with a 5 min polymer rinse, and the repeatability was tested on repetitive injections of the 16 bp and 20 bp dsODN mixture (see Table 5.15 and Figure 5.38 for mobility and repeatability data and Figure 10.6 in Appendix A for the electropherograms).

Table 5.15. Calculation of mean t_m, R_s and μ_{app} for 3 injections of a 16 bp and 20 bp dsODN mixture on a CFR PDEAEMA-*co*-PMMA random copolymer (34/66) coated fused-silica capillary.

Peak (bp)	t_m (min)	W_h (min)	R_s	μ_{app} x 10^{-9} (m^2 V^{-1} s^{-1})*	s_d x 10^{-9} (n = 3)	RSD (%)
20	33.86	0.62	1.60	-11.2	0.23	2.09
16	35.52	0.60		-10.7	0.18	1.65

*The negative sign denotes an anodic mobility

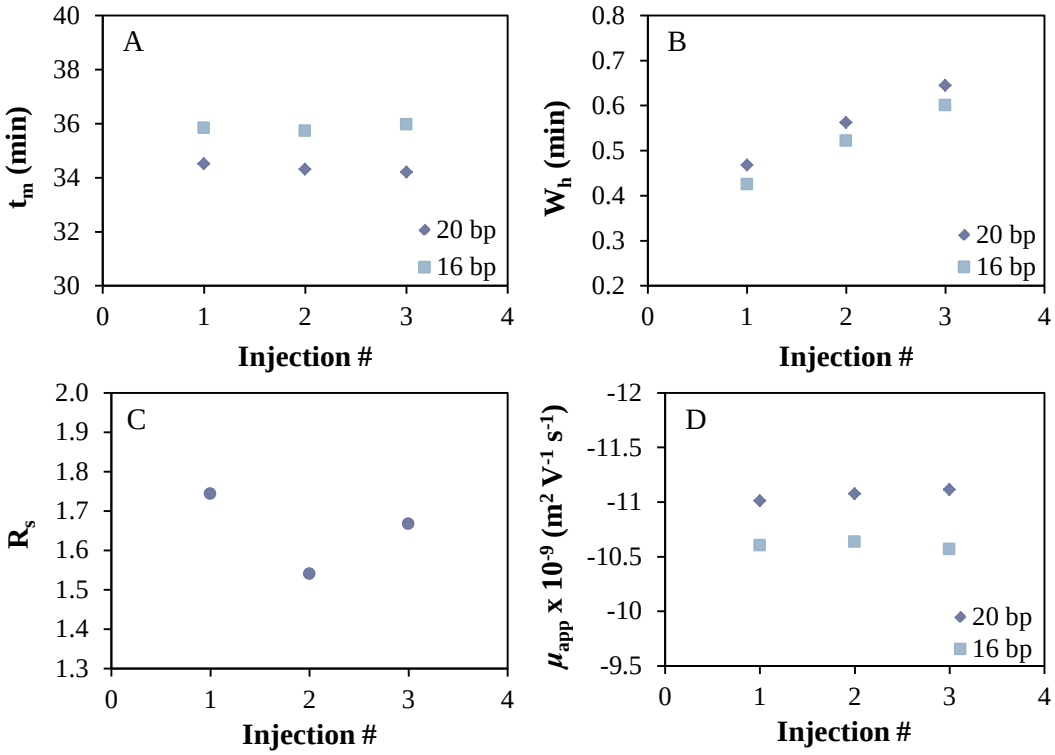

Figure 5.38. Plots of t_m (A), W_h (B), R_s (C), and μ_{app} (D), versus injection # for the separation of 16 bp and 20 bp dsODNs (18.6 µM) on a CFR PDEAEMA-*co*-PMMA random copolymer (34/66) coated fused-silica capillary (30 cm L_d, 38 cm L_t, 75 µm id, 363 µm od).

It can be seen from Table 5.15 and Figure 5.38 that the longer polymer conditioning improved the repeatability by providing a more stable surface; however, the increasing W_h and slightly decreasing t_m suggested that the conditioning resulted in increased interactions with the surface attributed to over-conditioning (application of excess polymer on the surface). Therefore, it was concluded that the initial CFR PDEAEMA-*co*-PMMA random copolymer coating required longer conditioning than the CFR PEPyM-*co*-PMMA random copolymer, although the between-run conditioning time of 3 min was suitable for regeneration. The t_m (and hence μ_{app}) were poor in comparison to the CFR PEPyM-*co*-PMMA random copolymer indicating less shielding of the surface and hence a greater cathodic EOF. Owing to reduced % RSD and μ_{app}, the CFR PDEAEMA-*co*-PMMA random copolymer coating was not pursued any further.

5.4 Concluding remarks

This chapter investigated the effectiveness of polymer surfaces based on hybrid random and block copolymers synthesised from hydrophilic and hydrophobic monomers. Free solution electrophoretic separation of ODNs was achieved by suppressing the EOF by use of the polymer surface coatings. The PEPyM-*co*-PMMA random copolymer synthesised by CFR copolymerisation suppressed the EOF to a greater extent than the PDEAEMA-*co*-PMMA random copolymer (also synthesised by CFR copolymerisation); and the RAFT PEPyM-*b*-PMMA block copolymer synthesised by RAFT polymerisation resulted in a shorter t_m, with the detriment of reduced peak R_s. Interestingly, the CFR PEPyM homopolymer coating demonstrated similar results (with poorer repeatability) to the CFR PEPyM-*co*-PMMA random copolymer coating, suggesting that the PEPyM units were the key contributor to the EOF suppression. The improved repeatability of the copolymer was due to the hydrophobic PMMA units which stabilised the adsorption of copolymer onto the surface. Separation on a CFR PMMA homopolymer coated capillary did not allow for the detection of ODNs suggesting that either the adsorbed CFR PMMA homopolymer was not able to suppress the EOF, or the CFR PMMA homopolymer was not adsorbed to the surface. It was observed from Chapter 4 that the latter was the case, leading to insufficient EOF suppression.

Short chain dsODNs ranging from 16 bp to 20 bp were separated down to 1 bp R_s (partial R_s of 16 bp and 17 bp strand) on a fused-silica capillary coated with CFR PEPyM-*co*-PMMA random copolymer physically adsorbed onto the surface. The CFR PEPyM-*co*-PMMA random copolymer surface was shown to suppress the EOF by ~72 % using a Tris-borate (100 mM)/urea (7 M) buffer at pH 9 and 30 ^{o}C. Separation in free solution was possible on the coated capillary due to the reduction in the negative charge distribution by the polymer. This led to a reduction in the cathodic EOF, and to the screening of the negatively charged dsODNs by the positive charges on the coated surface, meaning that smaller ODN fragments were retained more strongly by the capillary. Hence, the migration order was from largest to smallest. The μ_{obs} of the 16 bp strand did not appear to be consistent within each mixture owing to ODN-ODN interactions occurring between the different complementary double strands as they migrated. Additionally, there may

potentially have been competition between the different strands for the surface during migration along with ODN-buffer interactions. Further investigations into these interactions and potential sequence dependence of separation can be found in Chapter 6.

One advantage of these types of coatings is the ease of preparation. The initial CFR PEPyM-*co*-PMMA random copolymer coating was achieved within 1 h, affording a greatly reduced capillary preparation time. Repetitive injections (with coating regeneration between runs) indicated the lifetime of the coating to be in excess of 70 runs. The efficiency of the dsODN mixture separations was between 48 000 and 70 000 theoretical plates. In addition, the optimised method operated within the lower voltage range (-5 kV) which placed less stress on the capillary and the system and thus increased lifetime and repeatability. The R_s, and improvement thereof of these short strands may prove to be of great importance in future analysis of the purity and content of therapeutic ODNs for pharmaceutical development (see Chapter 7 for the investigation into the separation of PS-ODNs for purity determination).

6 Short-end injection CE analysis of ODNs

6.1 Synopsis

*This chapter describes the use of SEI for the capillary electrophoretic analysis of synthetic ODNs on a fused-silica capillary (8 cm L_d, 38 cm L_t) coated with PEPyM-*co*-PMMA random copolymer (21/79) synthesised by CFR polymerisation. The dependence of ODN sequence on the free solution mobility was investigated. Furthermore, the effect of the sequence and ionic strength on the ODN-ODN and ODN-buffer interactions was explored. SEI was used to reduce the analysis time of the method, and R_s of dsODN mixtures on the shorter column indicates the potential for the method to be applied to microfluidic devices.*

6.2 Method development

This section details the method development for short-end analysis of ssODNs and dsODNs. SEI on the Agilent CE system used throughout this thesis involves injection at the detection end (cathode) which reduces the detection length to 8 cm. In this work, a positive polarity was applied (instead of a negative polarity) so the negatively charged DNA migrated towards the positive electrode (anode), past the detector (see Scheme 6.1). It is important to understand that the injection end is still the cathode, and that the separation via SEI CE essentially uses the same mechanism as that described in Chapter 5, just along a shorter distance.

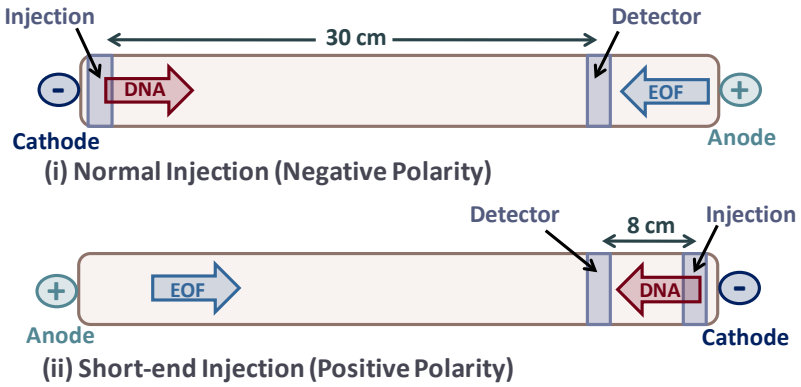

Scheme 6.1. Schematic representation of normal injection (negative polarity) (i), compared to short-end injection utilising a positive polarity (ii).

The first step in developing the method for SEI was to employ the same parameters used for the optimised 'normal injection' method (refer to Scheme 5.2 in Section 5.3). After which, it was clear that although R_s of dsODN mixtures was possible using hydrodynamic injection, this method of injection did not allow for sensitive enough detection (low signal-to-noise), and therefore electrokinetic injection (EKI) was utilised and optimised.

6.2.1 Hydrodynamic injection

Hydrodynamic injection was employed for the work described in Chapter 5 due to its high associated repeatability [17]. The volume of sample injected was a factor of the capillary radius and length, the solution viscosity, the change in pressure, and the time in which the pressure is applied (see Equation 5.1 in Section 5.2.1.2). Hydrodynamic injection proved to be suitable for CE analysis on the 30 cm (L_d) column and therefore it was employed initially for SEI CE analysis.

6.2.1.1 Effect of voltage on ODN separation

The voltage dependence on the separation of the ODNs on a CFR PEPyM-*co*-PMMA random copolymer (21/79, 1 mg mL^{-1}, 14 398 g mol^{-1}) coated capillary (8 cm L_d) was determined using a dsODN (18.6 µM) mixture of 16 bp and 20 bp. The t_m, R_s and peak shape were used to determine the optimum voltages for separation of the mixture. The voltage was tested in 0.5 kV increments, from 1 kV to 7.5 kV. All other parameters were kept constant. Figure 6.1 shows the electropherograms for injections of dsODNs at varying voltages. The migration and mobility data can be found in Table 10.6 in Appendix B.

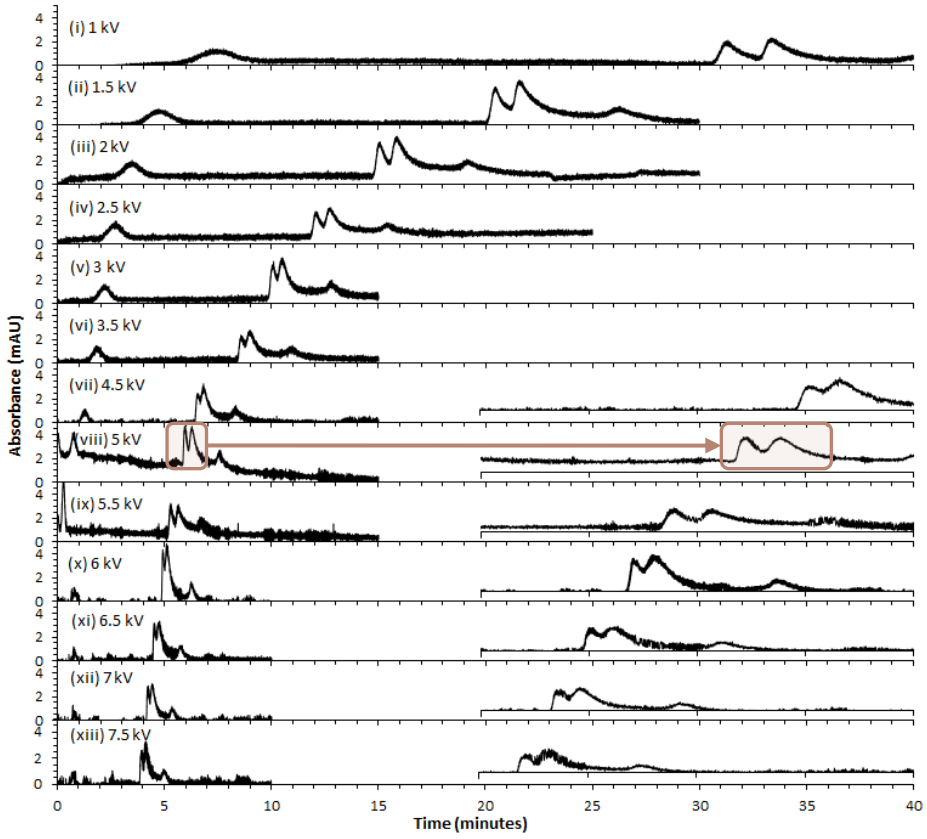

Figure 6.1. CE electropherograms of a mixture of 16 bp and 20 bp dsODNs (18.6 µM) at varying voltages (i)-(xiii), using a CFR PEPyM-*co*-PMMA random copolymer (21/79) coated capillary (the insets show a zoom of the peak region). Separation was performed on a fused-silica capillary (8 cm L_d, 38 cm L_t, 75 µm id, 363 µm od) at 30 °C with UV detection at 260 nm for 40 min run time. The BGE was Tris-borate (100 mM)/urea (7 M) at pH 9.0. Samples were introduced hydrodynamically at 5000 Pa for 6 s.

Figures 6.1 and 6.2A show that the t_m decreased with increasing voltage for both the 16 bp and 20 bp strands. A power trend-line was fitted to the curve with R^2 values above 0.998 for both strands. An increase in voltage led to shaper peaks with reduced W_h (Figure 6.2B) and decreased R_s (Figure 6.2C). When compared to the results obtained using normal injection (Section 5.2.2.1), the trend in R_s was the

reverse. This was due to the decreased residence time of the ODNs meaning that they were not being affected by the capillary heating up, which would normally reduce the interactions between the migrating strands and potentially result in degradation. N was observed to decrease slightly for the 16 bp strand, with no apparent trend for the 20 bp strand (Figure 6.2D). The *v* increased linearly with increasing voltage owing to the greater current applied by the higher voltage (Figure 6.2E); and there was a slight increasing trend observed for the μ_{app} at lower applied voltages (26.3 V cm^{-1} - 65.8 V cm^{-1}) which was attributed to equilibration of the capillary with buffer (Figure 6.2F). The effective voltage range for hydrodynamic SEI was determined to be between 92.1 V cm^{-1} and 144.7 V cm^{-1}.

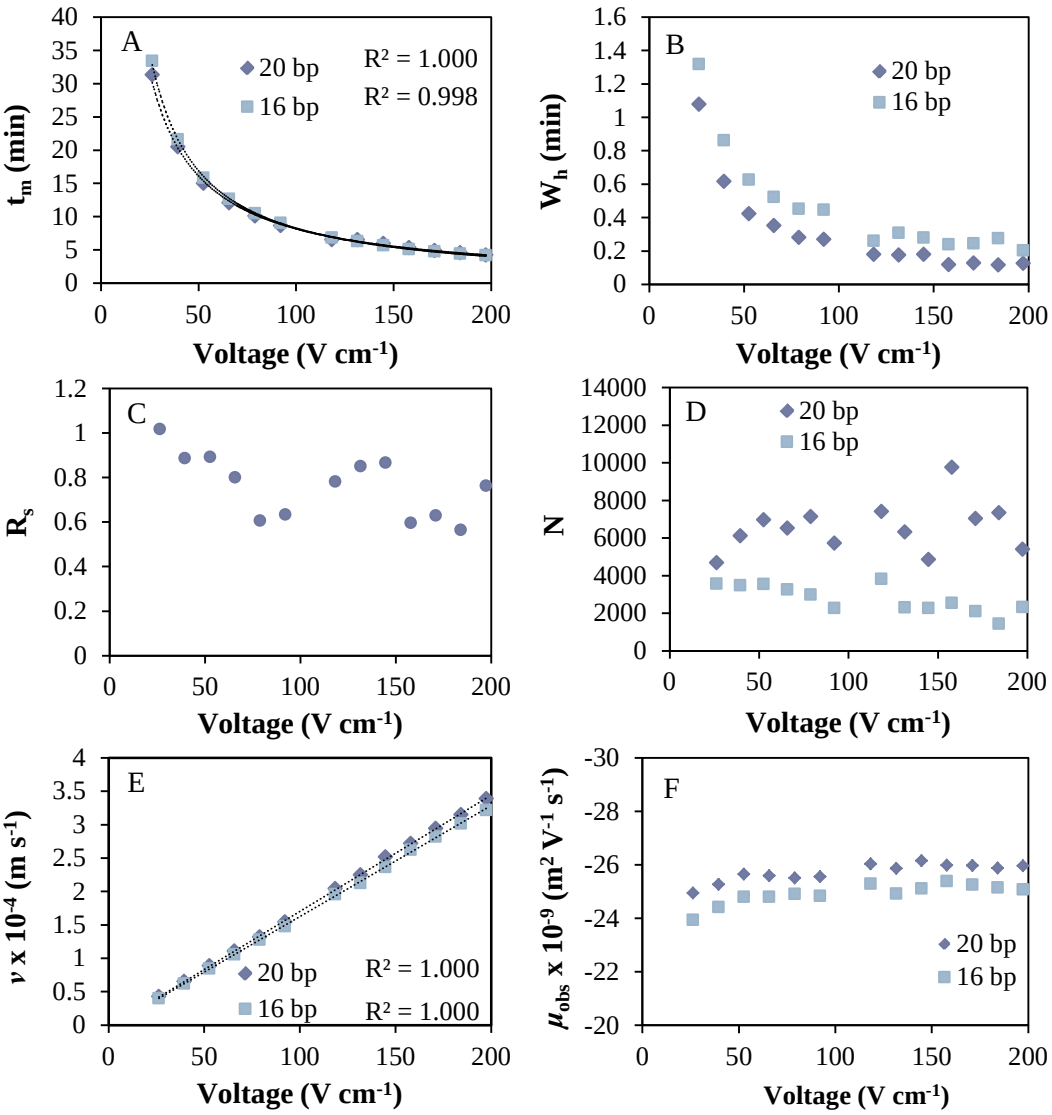

Figure 6.2. Plots of t_m (A), W_h (B), R_s (C), N (D), *v* (E), and μ_{obs} (F), versus voltage for separation of 16 bp and 20 bp dsODNs (18.6 µM) on a CFR PEPyM-*co*-PMMA random copolymer (21/79) coated fused-silica capillary (8 cm L_d, 38 cm L_t, 75 µm id, 363 µm od).

Owing to a decreased residence time of the ODNs and analysis time, joule-heating did not present a problem as the short time period restricted the amount of heat built up in the capillary. Any heating that occurred was sufficiently dissipated through the capillary walls. Therefore, the use of higher voltages and/or temperatures can be afforded for SEI analysis of ODNs.

6.2.1.2 Effect of temperature on ODN separation

The temperature dependence on the separation of the ODNs on a CFR PEPyM-*co*-PMMA random copolymer (1 mg mL^{-1}, 14 398 g mol^{-1}) coated capillary (8 cm L_d) was determined using a dsODN (18.6 µM) mixture of 16 bp and 20 bp. The t_m, R_s and peak shape were used to determine the optimum temperature for separation of the mixture using hydrodynamic injection. The temperature was tested in 5 ^oC increments, from 15 ^oC to 50 ^oC. All other parameters were kept constant. Figure 6.3(i)-(viii) shows the electropherograms for injections of dsODNs at varying temperature. The migration and mobility data can be found in Table 10.7 in Appendix B.

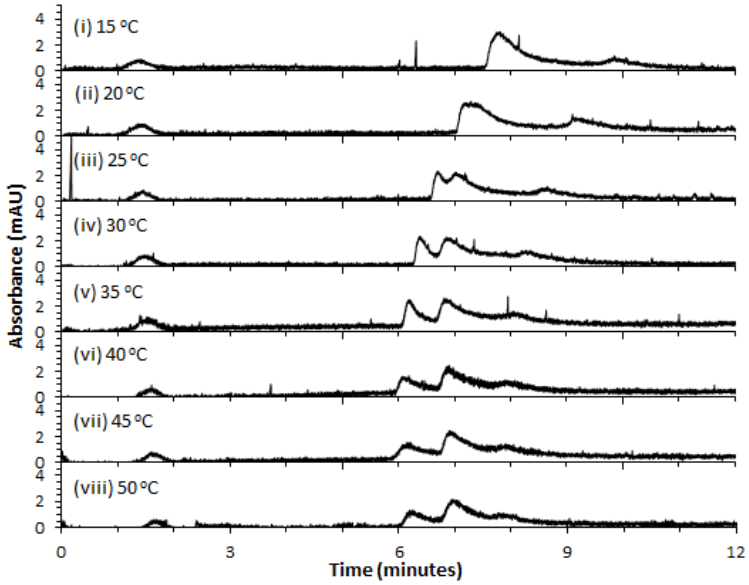

Figure 6.3. CE electropherograms of a mixture of 16 bp and 20 bp dsODNs (18.6 µM) at varying temperatures (i)-(viii), using a CFR PEPyM-*co*-PMMA random copolymer (21/79) coated fused-silica capillary (8 cm L_d, 38 L_t, 75 µm id, 363 µm od). Separation was performed at 131.6 V cm^{-1} with UV detection at 260 nm for 12 min run time. The BGE was Tris-borate (100 mM)/urea (7 M) at pH 9.0. Samples were introduced hydrodynamically at 5000 Pa for 6 s.

At 15 ^oC the 16 bp and 20 bp dsODNs co-migrated at 7.81 min and were unresolved (Figure 6.3 (i)). The smaller peak at ~10 min was due to residual

ssODNs. An increase in temperature to 20 ^{o}C (Figure 6.3(ii)) still resulted in co-migration of the strands with t_m of 7.37 min and 7.42 min for the 20 bp and 16 bp, respectively. The R_s was 0.15 and peak tailing was observed. By increasing the temperature to 25 ^{o}C (Figure 6.3 (iii)), the R_s of the two peaks increased to 1.13 and the t_m further decreased to 6.78 min and 7.11 min for the 20 bp and 16 bp, respectively. At 30 ^{o}C (Figure 6.3(iv)) the R_s increased to 1.65 with a decrease in t_m to 6.44 min and 6.95 min for the 20 bp and 16 bp, respectively. At 35 ^{o}C, the t_m decreased to 6.21 min and 6.91 min with an increase in R_s to 2.55 (Figure 6.3(vi)). An increase in temperature to 40 ^{o}C resulted in reduced signal-to-noise and increased peak tailing (Figure 6.3(vi)). In addition, the ssODNs in the mixture began to co-migrate with the dsODNs. The t_m was 6.07 min and 6.90 min for the 20 bp and 16 bp, respectively, with an R_s of 2.80. After 45 ^{o}C (Figure 6.3(vii)), the t_m of the strands began to increase again (6.17 min for the 20 bp strand, and 7.01 min for the 16 bp strand) with a decrease in R_s to 2.36. At 50 ^{o}C (Figure 6.3(vii)), the dsODN peaks were observed at 6.21 min and 6.95 min for the 20 bp and 16 bp strand, respectively, with an R_s of 2.53. The residual ssODNs were observed at ~7.5 min - 8.5 min. In comparison to the results obtained using normal injection on a 30 cm L_d capillary (see Section 5.2.2.2), denaturation/degradation of the strands was not as evident due to the decreased residence time of the strands.

By examining plots of temperature versus t_m (Figure 6.4A) it was seen that t_m decreased for both the 20 bp and 16 bp peaks with increasing temperature between 15 ^{o}C and 40 ^{o}C, and once exceeding 40 ^{o}C, the t_m increased due to potential degradation of the strands, although they do not appear to be denaturing. Figure 6.4C shows that the R_s was increased with increasing temperature up to 40 ^{o}C. It is likely that the higher temperature was restricting the formation of borate-ODN complexes; therefore reducing the negative charge on the ODN backbone in comparison to lower temperatures, causing a slower mobility for both the 20 bp and 16 bp strands and the R_s to level off. Figures 6.4E and F show that the ν and μ_{app} increased with increasing temperature between 15 ^{o}C and 40 ^{o}C, after which it plateaued. From this analysis it was evident that the optimum temperatures for enhanced separation of ODN mixtures on the CFR PEPyM-*co*-PMMA random copolymer coated capillary using short-end hydrodynamic injection was between 30 ^{o}C and 40 ^{o}C.

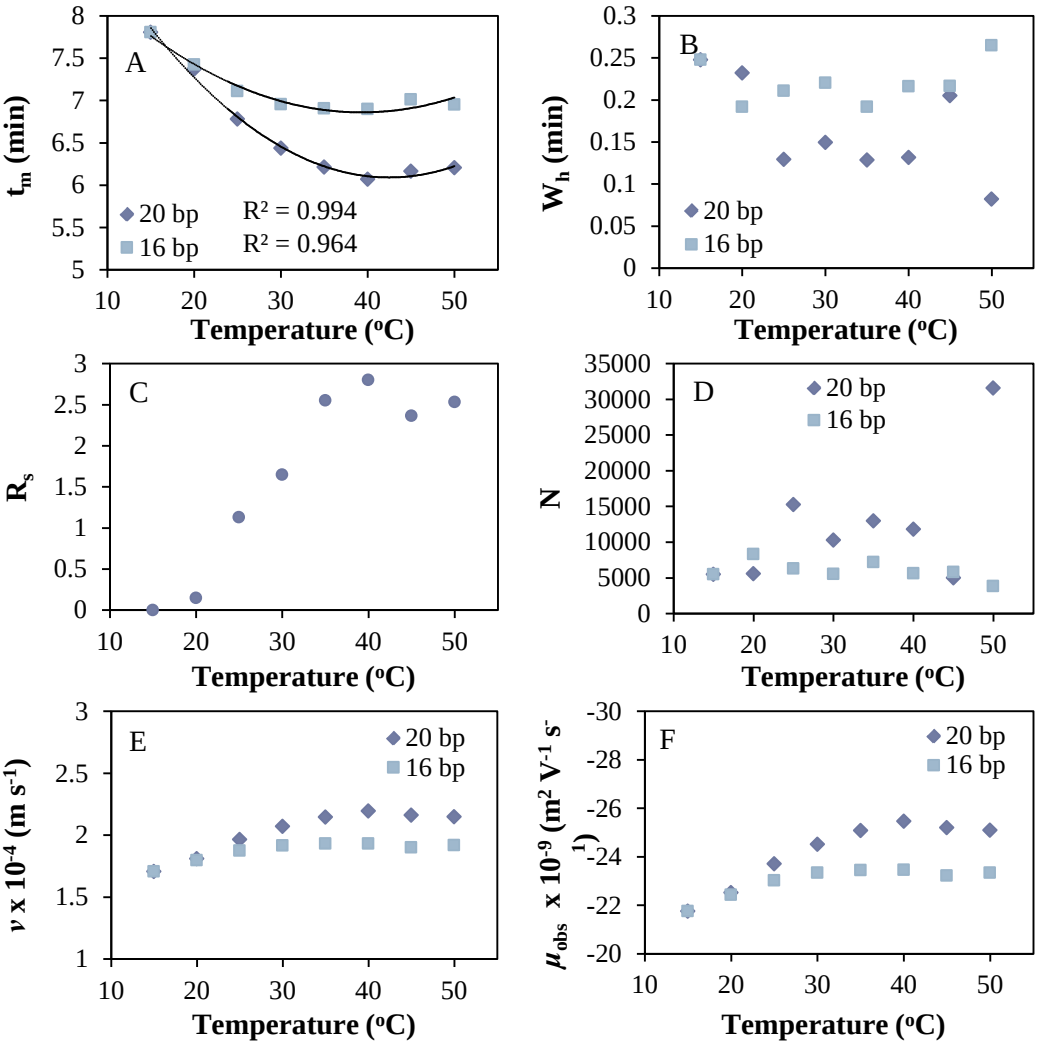

Figure 6.4. Plots of t_m (A), W_h (B), R_s (C), N (D), ν (E), and μ_{obs} (F), versus temperature for separation of 16 bp and 20 bp dsODNs (18.6 µM) at varying temperatures using a CFR PEPyM-*co*-PMMA random copolymer (21/79) coated fused-silica capillary (8 cm L_d, 38 cm L_t, 75 µm id, 363 µm od).

6.2.1.3 Sequence dependence

The sequences for the 17 bp, 18 bp, 19, bp and 20 bp are all extensions of the 16 bp sequence (see Table 2.3 in Section 2.2.3.1). Consequently, during migration ODN-ODN interactions may be occurring which would decrease the R_s. The fact that the mobilities for the 16 bp peak in different mixtures were not additive (see Section 5.3.3) is indicative of ODN-ODN interactions [16, 105]. In addition, analysis of ssODNs was shown to exhibit sequence dependence mobilities (Section 5.3.1) which has also been observed in the literature [8, 20] and therefore may also occur for dsODNs. Therefore, the sequence dependence and ODN-ODN interactions were investigated on a CFR PEPyM-*co*-PMMA random copolymer (1 mg mL^{-1}, 14 398 g mol^{-1}) coated capillary using mixtures containing a 16 bp strand consisting of

a sequence non-complementary to the other double strands in the dsODN mixtures. The CE electropherograms and trend plots can be found in Figures 6.5 and 6.6, respectively, and the R_s and mobility calculations are in Table 10.9 in Appendix B. The non-complementary 16 bp strand (hybridised from 5'-CAT(16) and 5'-GCT(16) ssODNs) was referred to as '16-CAT' and the 16 bp complementary sequence was referred to as '16-COMP' (this is the 16 bp strand that has been used throughout this thesis hybridised from 5'-TTC(16) and 5'-CCG(16) ssODNs). The sequences can be found in Table 2.3 in Section 2.2.3.1.

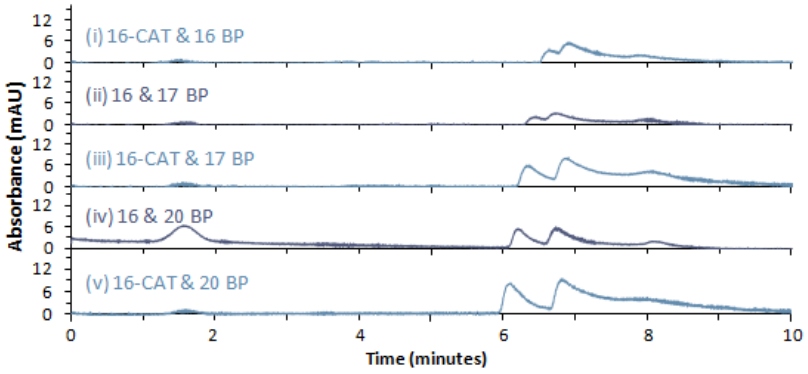

Figure 6.5. CE electropherograms of mixtures of 16-COMP bp and 16-CAT bp (i), 16-COMP bp and 17 bp (ii), 16-CAT bp and 17 bp (iii), 16-COMP bp and 20 bp (iv), and 16-CAT bp and 20 bp (v), dsODNs (18.6 µM) using a CFR PEPyM-*co*-PMMA random copolymer (21/79) coated fused-silica capillary (8 cm L_d, 38 cm L_t, 75 µm id, 363 µm od). Separation was performed at 131.6 V cm^{-1} and 35 ^{o}C with UV detection at 260 nm for 10 min run time. The BGE was Tris-borate (100 mM)/urea (7M) at pH 9.0. Samples were introduced hydrodynamically at 5000 Pa for 6 s.

From Figures 6.5 and 6.6A, it can be seen that the t_m decreased with increasing bp length, leading to a v (Figure 6.6E) and μ_{obs} (Figure 6.6F) that increased with increasing size. From all the CE results it was evident that the overall charge of the molecule was responsible for the migration trends, rather than the molecular size, which explains this observed trend. Therefore there should be no difference in the mobility of strands of equal bp length containing different sequences. However, this was clearly not the case, as the 16-CAT bp dsODN was shown to have a slightly slower mobility (see Figure 10.7 and Table 10.8 in Appendix B). The M_w of the 16-COMP bp dsODN is 9763.5 g mol^{-1}, whereas the M_w of the 16-CAT bp dsODN is 9762.5 g mol^{-1}, differing only by one atomic mass unit. Therefore it cannot be said with confidence that the difference in mobility is related to the size, given that free solution mobility has been shown to be independent of mass [8, 16, 20, 93, 95, 96, 146]. Therefore, the slight difference in mobility must be related to the base sequence in the strand.

From Figure 6.6C, it was observed that the 16-CAT bp mixtures had increased R_s when compared to the 16-COMP bp mixtures, due to decreased interactions, as well as different sequences. The method was also capable of partially resolving (R_s = 0.56) the 16-CAT bp strand from the 16-COMP bp. As with the 16-COMP mixtures, the 16-CAT bp strand was not additive (did not exhibit the same t_m) in each of the mixtures. It is also likely that there was still competition between the strands for the surface. The 17 bp and 20 bp peaks were also not additive between mixture with the 16-CAT bp and 16-COMP bp strands, suggesting that the interactions were different. Additionally, the 17 bp and 20 bp dsODNs had faster mobilities when mixed with 16-CAT bp dsODNs, again indicating decreased interactions with the non-complementary strands.

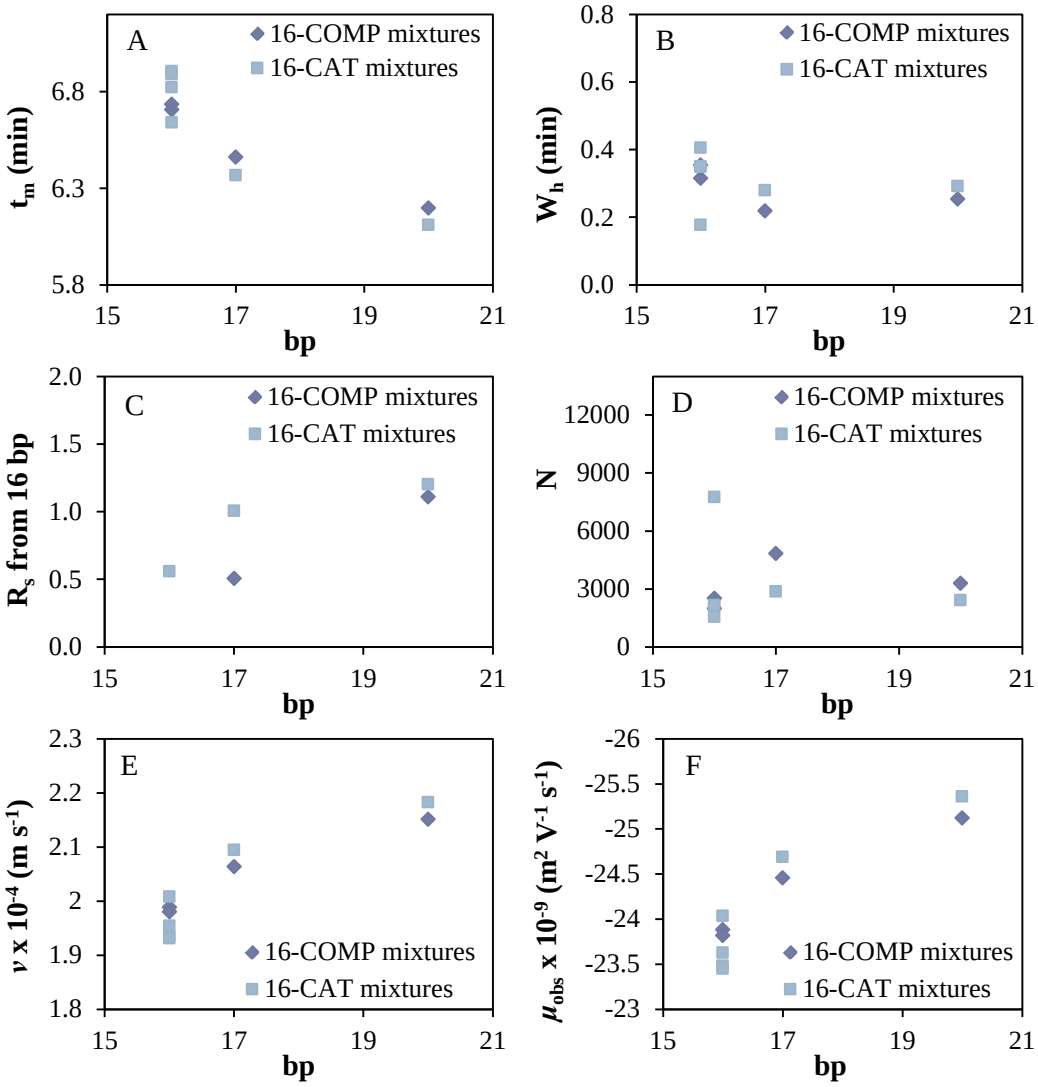

Figure 6.6. Plots of t_m (A), W_h (B), R_s (C), N (D), ν (E), and μ_{obs} (F), versus temperature for separation of dsODN (18.6 µM) mixtures containing sequences that are complementary (16-COMP mixtures), and mixtures containing sequences that are non-complementary (16-CAT mixtures) using a CFR PEPyM-*co*-PMMA random copolymer (21/79) coated fused-silica capillary (8 cm L_d, 38 cm L_t, 75 µm id, 363 µm od).

From the results obtained using hydrodynamic injection, it was evident that the signal-to-noise was poor and the method was not very sensitive.. Additionally, the peak shapes were non-Gaussian and very broad which reduces the efficiency of the separation. Hydrodynamic injection works by applying a pressure to force the analyte in solution into the capillary meaning that the amount detected was highly dependent on the concentration of the analyte in the sample; alternatively, EKI uses an applied voltage to inject the sample resulting in more of the charged analyte being injected (providing it possesses a greater μ_{ep} than the solvent). Therefore EKI was utilised for the separation of ODNs.

6.2.2 Electrokinetic injection

From the voltage and temperature studies using hydrodynamic injection, there was a need to improve the signal-to-noise of the analysis and the peak shapes. This reduced sensitivity was most likely due to a sample loading problem, coupled with the shorter detection length. The method of sample injection used for the 'normal analysis' was hydrodynamic injection. This is because the amount of sample introduced each time should be consistent and independent of a number of factors, such as differing electrophoretic mobilities of the solvent and analyte.

On the other hand, EKI is highly dependent on the mobilities of the analyte and the EOF [17]. This can be advantageous if the analyte has the greater μ_{ep}. In this work, the ODNs were prepared in water and exhibited the greater mobility. Therefore using this type of injection should increase the loading of the analyte from the sample into the capillary. The approximate volume introduced from EKI can be calculated from Equation 6.1 [17],

$$\mathrm{v_{int}} = \pi r^2 (\mu_{\mathrm{app}}) \mathrm{V_{inj}} \frac{\mathrm{t_{int}}}{L_{\mathrm{t}}}$$

Equation 6.1

where V_{inj} is the injection voltage and t_{int} is the injection time. For the optimised method (EKI of 5 kV for 8 s, 38 cm capillary, 37.5 µm radius), the v_{int} for the dsODNs were calculated from Equation 6.1 and can be found in Table 6.1.

Table 6.1. Calculation of the v_{int} for the EKI (5 kV, 8 s) of dsODN mixtures.

dsODN sample	Peak (bp)	μ_{app} x 10^{-9} ($m^2 V^{-1} s^{-1}$)	v_{int} (nL)
16 bp and 16-CAT bp	16	-16.35	7.60
	16-CAT	-15.87	7.38
17 bp and 16-COMP bp	17	-17.02	7.92
	16-COMP	-16.55	7.70
17 bp and 16-CAT bp	17	-17.08	7.94
	16-CAT	-16.02	7.45
18 bp and 16-COMP bp	18	-17.38	8.08
	16-COMP	-16.28	7.57
18 bp and 16-CAT bp	20	-17.45	8.12
	16-CAT	-16.15	7.51
19 bp and 16-COMP bp	19	-17.47	8.12
	16-COMP	-16.33	7.59
19 bp and 16-CAT bp	20	-17.69	8.23
	16-CAT	-16.36	7.61
20 bp and 16-COMP bp	20	-17.72	8.24
	16-COMP	-16.37	7.61
20 bp and 16-CAT bp	20	-17.81	8.28
	16-CAT	-16.31	7.59

*The negative sign denotes an anodic mobility

Table 6.1 shows that the v_{int} was increased ~10-fold using EKI when compared to hydrodynamic injection (see Section 5.2.1.2). It was observed during analysis with hydrodynamic injection that joule heating was negligible due to the shorter analysis time and the use of a higher temperature and/or voltage could be easily afforded to improve the R_s and t_m. The method was optimised for separation efficiency on CFR PEPyM-*co*-PMMA random copolymer coated capillaries (1 mg mL^{-1}, 14 398 g mol^{-1}) in regards to analysis time and peak R_s by investigating the EKI voltage and time, the capillary temperature, and the separation voltage. Once these parameters were optimised, the method was used to analyse therapeutic PS-ODNs (Chapter 7).

6.2.2.1 Injection conditions

As can be seen from Equation 6.1, the v_{int} is dependent on the V_{inj} and t_{int}, therefore it was necessary to investigate these parameters on the EKI of ODNs. Figure 6.7 shows the CE electropherograms of SEI analysis of a mixture of 16 bp and 20 bp dsODNs introduced electrokinetically at varying V_{inj} and t_{int}. The migration and mobility data can be found in Table 10.10 in Appendix B.

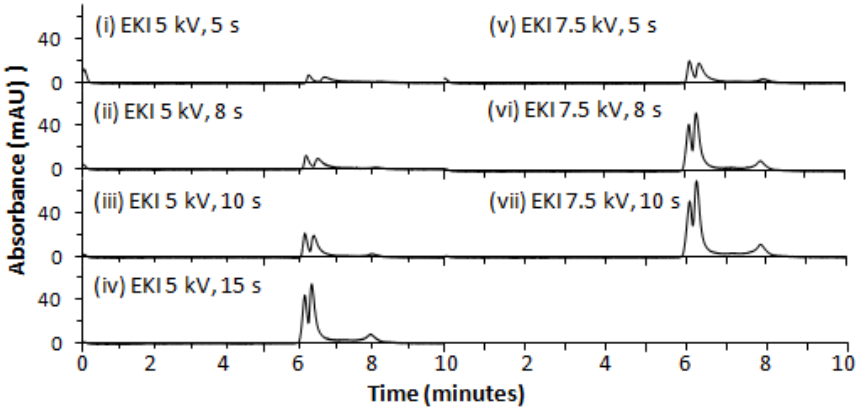

Figure 6.7. CE electropherograms of a mixture of 16 bp and 20 bp dsODNs (18.6 µM) introduced using EKI at 5 kV for 5 s (i), 8 s (ii), 10 s (iii), and 15 s (iv); and EKI at 7.5 kV for 5 s (v), 8 s (vi), and 10 s (vii). Separation was performed on a CFR PEPyM-*co*-PMMA random copolymer (21/79) coated fused-silica capillary (8 cm L_d, 38 cm L_t, 75 µm id, 363 µm od) at 131.6 V cm^{-1} and 35 °C with UV detection at 260 nm for 10 min run time. The BGE was Tris-borate (100 mM)/urea (7 M) at pH 9.0.

In accordance with Equation 6.1, Figure 6.7 shows that increasing the V_{inj} and t_{int} increased the v_{int}, evidenced by the increasing peak heights. The effect of varying V_{inj} and t_{int} on the differential migration of the dsODN mixture is shown by Figure 6.8. The t_m decreased with increasing V_{inj} and t_{int} (Figure 6.8A), meaning that the v (Figure 6.8G) and μ_{obs} (Figure 6.8H) increased with increasing V_{inj} and t_{int}. These trends were less pronounced for the 20 bp dsODN. Figure 6.8B shows that the W_h decreased with increasing V_{inj} but did not exhibit a trend with changing t_{int} (except for the 16 bp peak at a V_{inj} of 5 kV). Importantly the R_s decreased with increasing V_{inj} and t_{int} (Figure 6.8C) due to an increase in v_{int} evidenced by the increasing peak area (Figure 6.8E) and height (Figure 6.8F). Finally, Figure 6.8D shows that the N increased with an increase in V_{inj}, with no real trend in t_{int}. From this study, a V_{inj} of 5 kV and t_{int} of 8 s were chosen as the EKI conditions owing to the improved R_s.

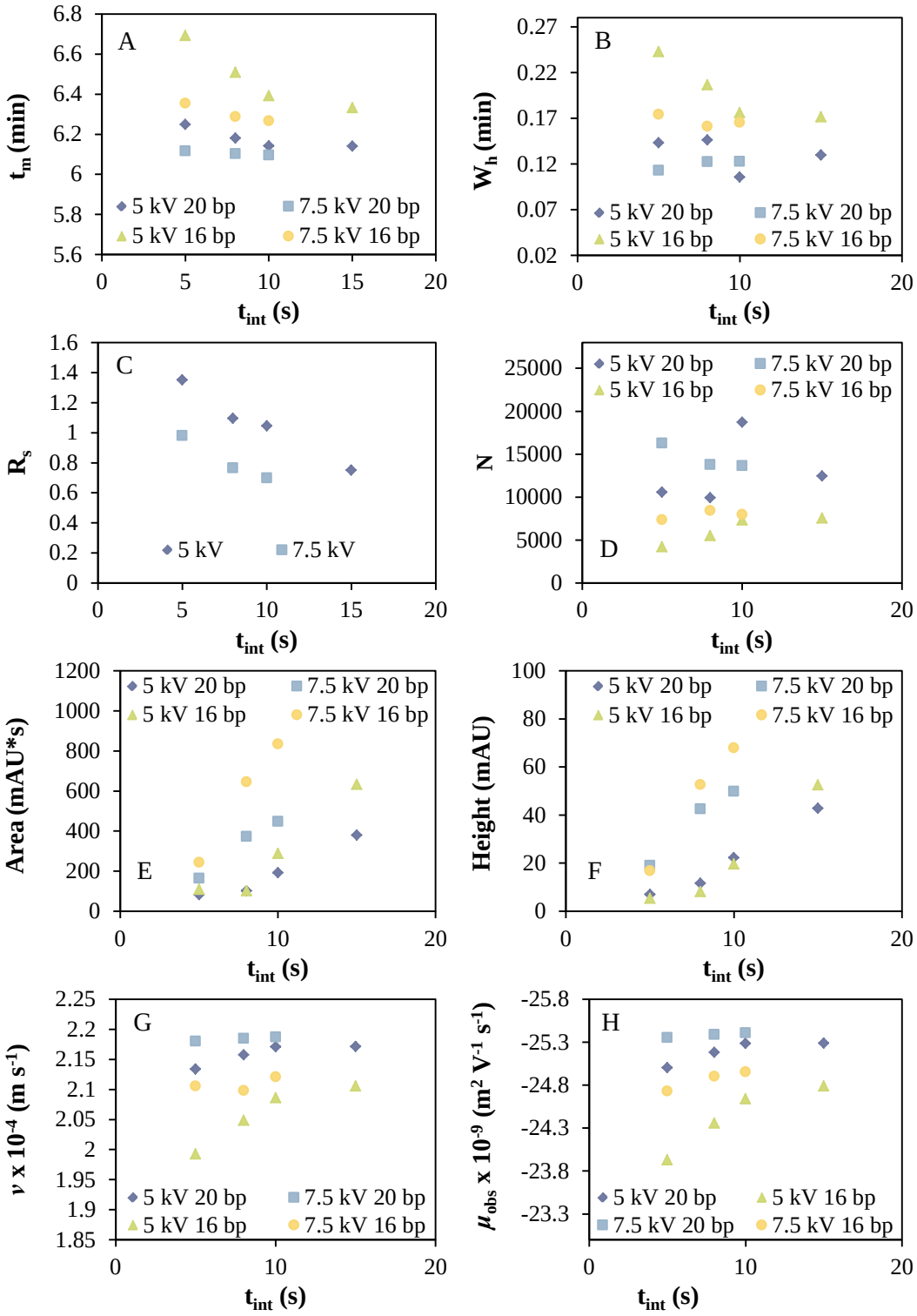

Figure 6.8. Plots of t_m (A), W_h (B), R_s (C), N (D), peak area (E), peak height (F), ν (g), and μ_{obs} (H), versus voltage for separation of 16 bp and 20 bp dsODNs (18.6 µM) at 35 °C on a CFR PEPyM-*co*-PMMA random copolymer (21/79) coated fused-silica capillary (8 cm L_d, 38 cm L_t, 75 µm id, 363 µm od) using EKI.

6.2.2.2 Effect of voltage on ODN separation

The voltage dependence on the separation of the ODNs on a CFR PEPyM-*co*-PMMA random copolymer (1 mg mL^{-1}, 14 398 g mol^{-1}) coated capillary (8 cm L_d) was determined at 35 ^oC and 40 ^oC using a dsODN (18.6 µM) mixture of 16 bp and 20 bp and EKI of 5 kV for 8 s. The t_m, peak R_s, and peak shape were used to determine the optimum voltages for separation of the mixture. The voltage was tested in 0.5 kV increments, from 1 kV to 10 kV, and 2.5 kV increments til 15 kV. Figures 6.9 and 6.10 display the electropherograms at varying voltages for injections of a mixture of 16 bp and 20 bp dsODNs at 35 ^oC and 40 ^oC, respectively. The migration and mobility data can be found in Tables 10.11 and 10.12 in Appendix B.

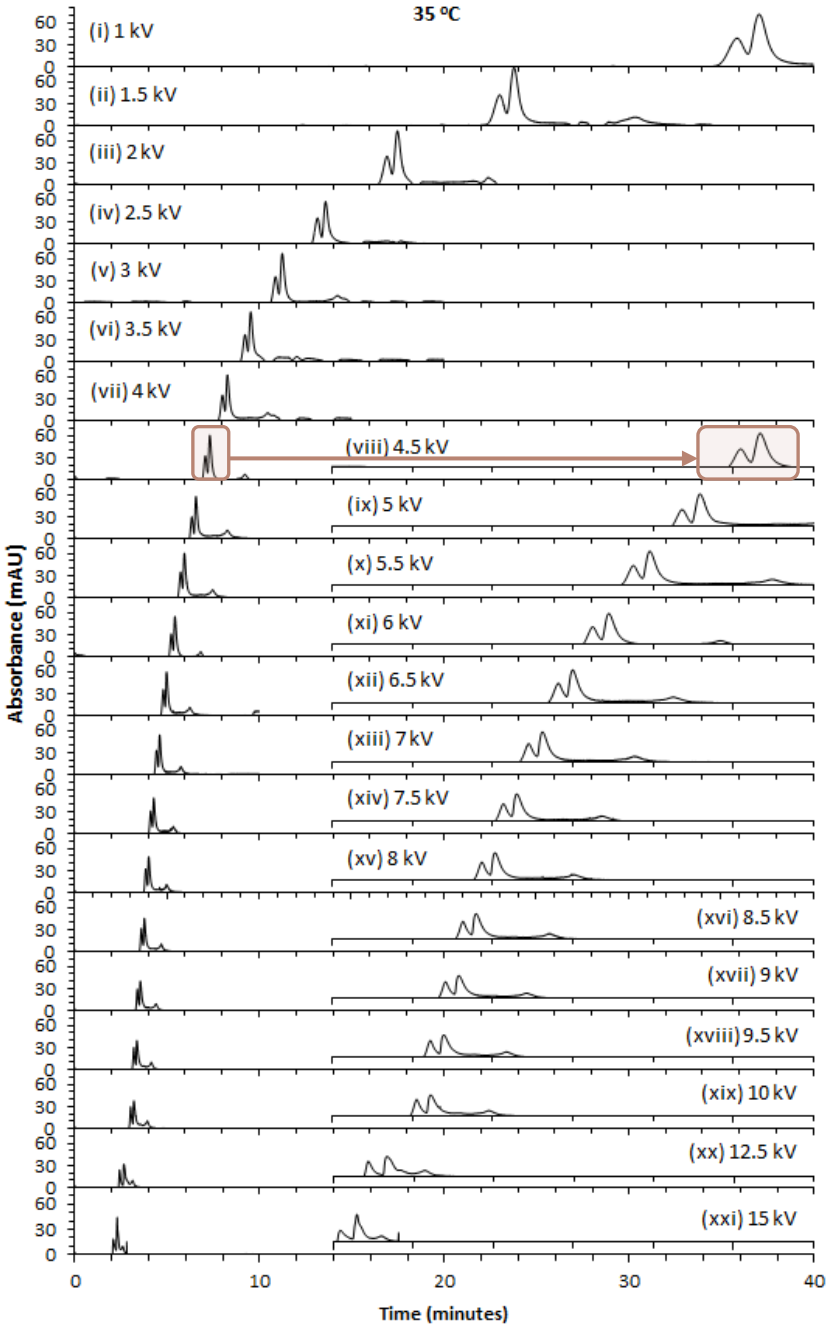

Figure 6.9. CE electropherograms of a mixture of 16 bp and 20 bp dsODNs (18.6 µM) (i)-(xxi) at varying voltages (the insets show a zoom of the peak region). Separation was performed on a CFR PEPyM-*co*-PMMA random copolymer (21/79) coated fused-silica capillary (8 cm L_d, 38 cm L_t, 75 µm id, 363 µm od) at 35 °C with UV detection at 260 nm for 40 min run time. The BGE was Tris-borate (100 mM)/urea (7 M) at pH 9.0. Samples were introduced electrokinetically at 131.6 V cm^{-1} for 8 s.

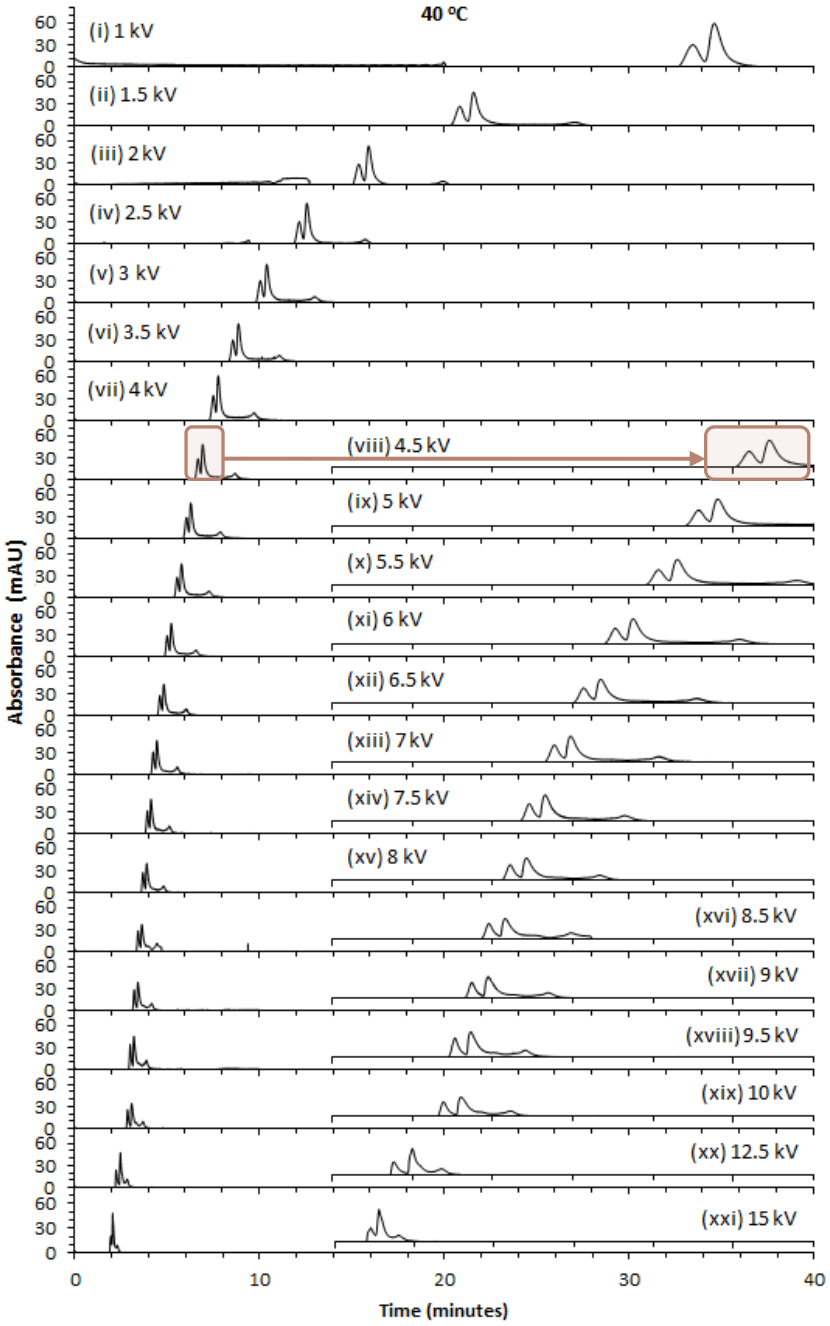

Figure 6.10. CE electropherograms of a mixture of 16 bp and 20 bp dsODNs (18.6 µM) (i)-(xxi) at varying voltages (the insets show a zoom of the peak region). Separation was performed on a CFR PEPyM-*co*-PMMA random copolymer (21/79) coated fused-silica capillary (8 cm L_d, 38 cm L_t, 75 µm id, 363 µm od) at 40 °C with UV detection at 260 nm for 40 min run time. The BGE was Tris-borate (100 mM)/urea (7 M) at pH 9.0. Samples were introduced electrokinetically at 131.6 V cm^{-1} for 8 s.

The trends observed for the voltage study using EKI (Figure 6.11) were very similar to those obtained using hydrodynamic injection (see Figure 6.2). Figures 6.9, 6.10 and 6.11A show that the t_m decreased with increasing voltage for both strands. A power trend-line was fitted to the curve with R^2 values above 0.999 for both strands at 35 ^oC and 40 ^oC. An increase in voltage led to shaper peaks with reduced widths (Figure 6.11B). The R_s (Figure 6.11C) decreased with increasing voltages between 26.3 V cm^{-1} and 171.1 V cm^{-1}, and then began to increase. This observed increase after ~184.2 V cm^{-1} was due to slight joule heating which decreased the interactions between the migrating strands and hence increased the R_s.

At both temperatures, N decreased with increasing voltage for both strands (Figure 6.11D). The v increased linearly with increasing voltage owing to the greater current applied by the higher voltage (Figure 6.11E); and there was a slight increasing trend observed for the μ_{obs} at lower applied voltages (26.3 V cm^{-1} - 65.8 V cm^{-1}) which was attributed to equilibration of the capillary with buffer (Figure 6.11F). Additionally, after 263.2 V cm^{-1}, the peak shapes became non-Gaussian with peak tailing, and the residual ssODNs co-migrated with the dsODNs. This was due to the high voltages heating up the capillary causing the strands to degrade. From this study (by looking at the peak shape, mobility and R_s), the effective voltage range for short-end EKI of ODNS at 35 ^oC and 40 ^oC was between 131.6 V cm^{-1} and 263.2 V cm^{-1}.

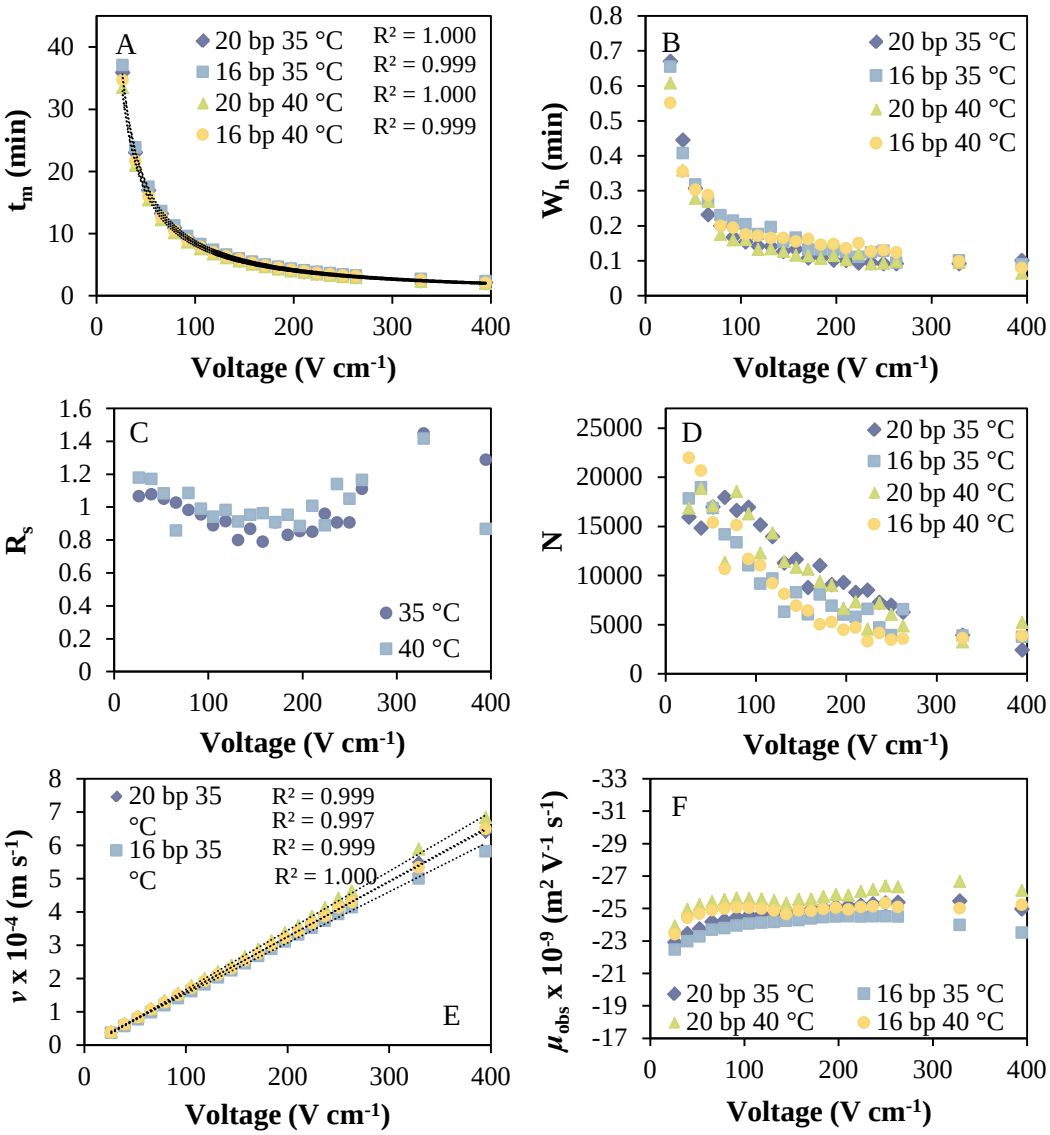

Figure 6.11. Plots of t_m (A), W_h (B), R_s (C), N (D), v (E), and μ_{obs} (F), versus voltage for separation of 16 bp and 20 bp dsODNs (18.6 µM) at 35 °C and 40 °C on a CFR PEPyM-*co*-PMMA random copolymer (21/79) coated fused-silica capillary (8 cm L_d, 38 cm L_t, 75 µm id, 363 µm od) using EKI.

6.2.2.3 Effect of temperature on ODN separation

The temperature dependence on the separation of the ODNs on a CFR PEPyM-*co*-PMMA random copolymer (1 mg mL^{-1}, 14 398 g mol^{-1}) coated capillary (8 cm L_d) with EKI of 5 kV for 8 s, was determined using dsODN (18.6 µM) mixtures of 16 bp and 18 bp, and 16 bp and 20 bp. The t_m, R_s and peak shape were used to determine the optimum temperature for separation of the mixtures using EKI. The temperature was tested in 5 °C increments, from 15 °C to 50 °C. All other parameters were kept constant. Figure 6.12(i)-(viii) shows the electropherograms for injections of dsODNs at varying temperature. The migration and mobility data can be found in Tables 10.13 and 10.14 in Appendix B.

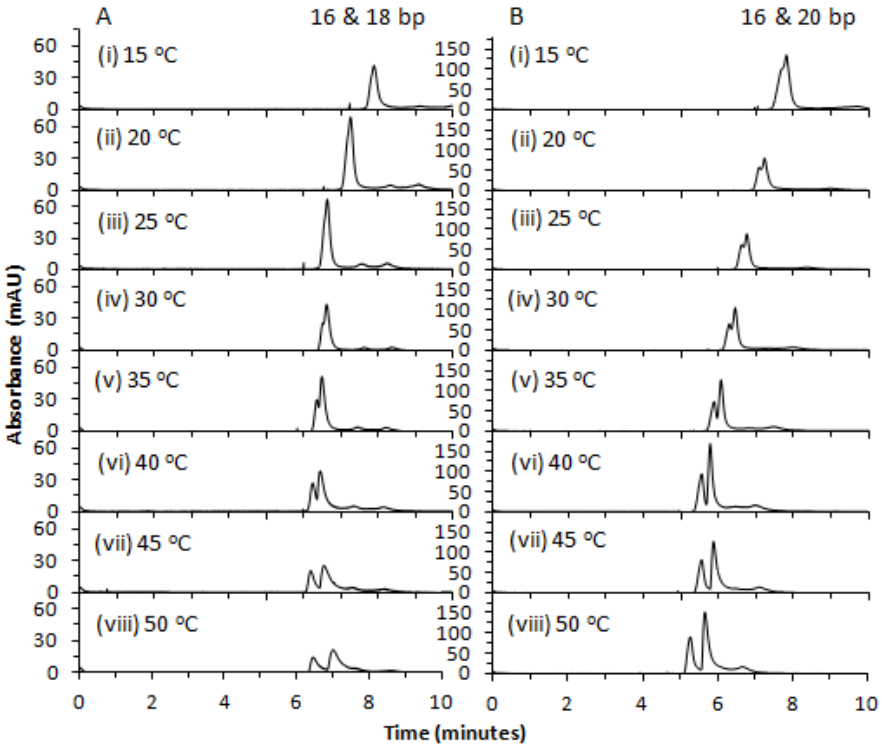

Figure 6.12. CE electropherograms of a mixture of 16 bp and 18 bp (A), and 16 bp and 20 bp (B), dsODNs (18.6 µM) at varying temperatures (i)-(viii), using a CFR PEPyM-*co*-PMMA random copolymer coated fused-silica capillary (8 cm L_d, 38 cm L_t, 75 µm id, 363 µm od). Separation was performed at 131.6 V cm^{-1} with UV detection at 260 nm for 10 min run time. The BGE was Tris-borate (100 mM)/urea (7 M) at pH 9.0. Samples were introduced electrokinetically at 131.6 V cm^{-1} for 8 s.

The trends observed (see Figure 6.13) for the SEI analysis of dsODNs using EKI were very similar to those obtained for the hydrodynamic injections (see Figure 6.4). Co-migration of the strands was observed for both mixtures between 15 °C and 30 °C and the R_s (Figure 6.13(iii)) increased with increasing temperature. It can be seen from Figures 6.12 and 6.13(i), that the t_m decreased between 15 °C and 40 °C, after which, it began to level out. The smaller peaks proceeding the dsODN peaks in Figure 6.12, were due to residual ssODNs, and the t_m of these ssODNs decreased with increasing temperature at a faster rate than the dsODNs until after ~40 °C in which the dsODNs and the ssODNs began to co-migrate. Again, due to the decreased residence time of the strands, denaturation/degradation with increasing temperature was not as evident.

Figure 6.13E and F show that the v and μ_{app} increased with increasing temperature between 15 °C and 40 °C, after which it levelled off. This plateau (and the one observed for the R_s) was most likely due to the restriction of the formation of

borate-ODN complexes at higher temperatures, thereby reducing the overall negative charge in comparison to lower temperatures. From this analysis it was evident that the optimum temperatures for enhanced separation of ODN mixtures on the CFR PEPyM-*co*-PMMA random copolymer coated capillary using short-end EKI was between 35 °C and 40 °C.

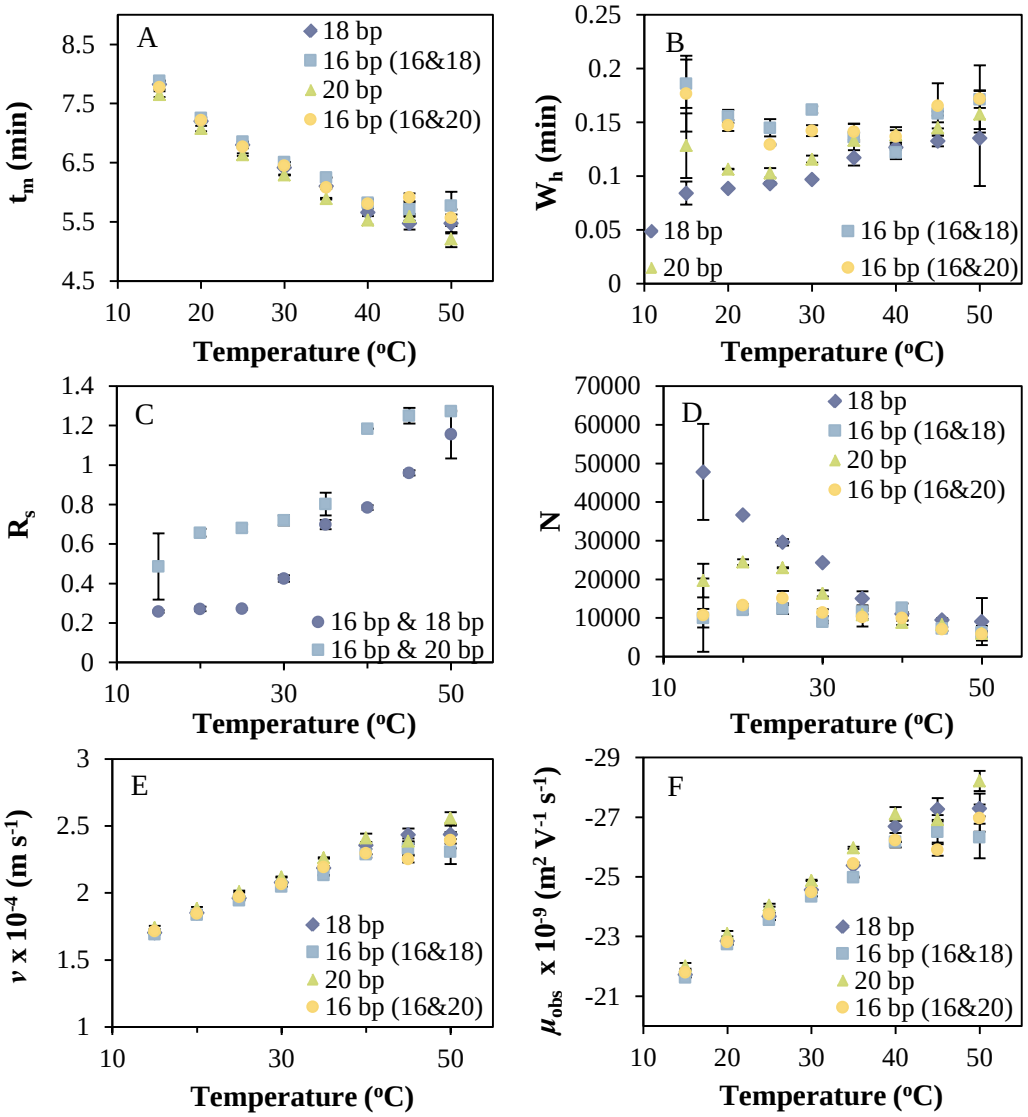

Figure 6.13. Plots of t_m (A), W_h (B), R_s (C), N (D), v (E), and μ_{obs} (F), versus temperature for separation of a mixtures of 16 bp and 18 bp, and 16 and 20 bp dsODNs (18.6 µM) at varying temperatures using a CFR PEPyM-*co*-PMMA random copolymer (21/79) coated fused-silica capillary (8 cm L_d, 38 cm L_t, 75 µm id, 363 µm od) using EKI. Error bars are ± 1 s_d from n = 2.

6.3 Short-end analysis of synthetic oligonucleotides using optimised method

The optimised method developed for SEI analysis of ODNs on CFR PEPyM-*co*-PMMA random copolymer coated capillaries is represented by Scheme 6.2. This method was used for the analysis of dsODNs mixtures between 16 bp and 20 bp. This section further investigates the sequence dependence of the free solution mobility and ODN-ODN interactions of dsODNs. Moreover, the effect of ionic strength on the mobility, ODN-buffer interactions and ODN-ODN interactions was also explored.

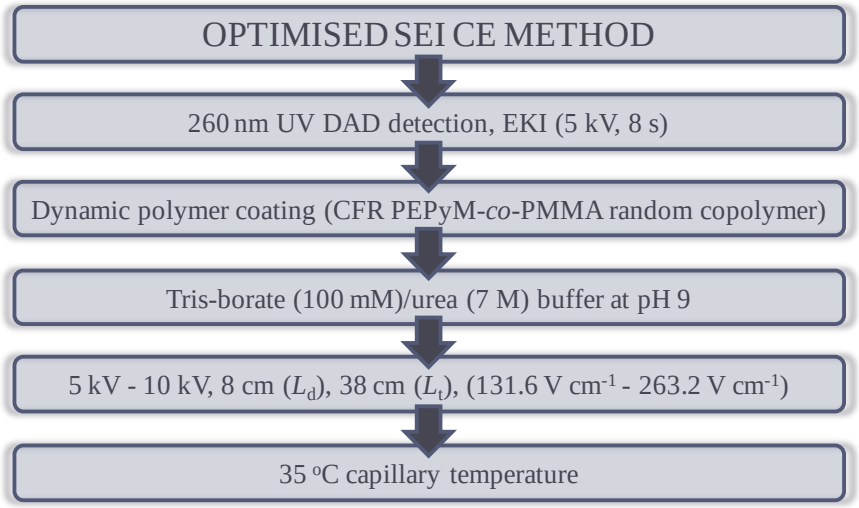

Scheme 6.2. Optimised SEI CE method for analysis of ODNs on CFR PEPyM-*co*-PMMA random copolymer (21/79) capillaries.

6.3.1 Sequence dependence

The sequence dependence and ODN-ODN interactions were also investigated using EKI of mixtures containing a 16 bp strand (16-CAT) consisting of a sequence non-complementary to the other double strands in the dsODN mixtures. The CE electropherograms and trend plots can be found in Figures 6.14 and 6.15, respectively, and the R_s and mobility calculations are in Table 10.15 in Appendix B.

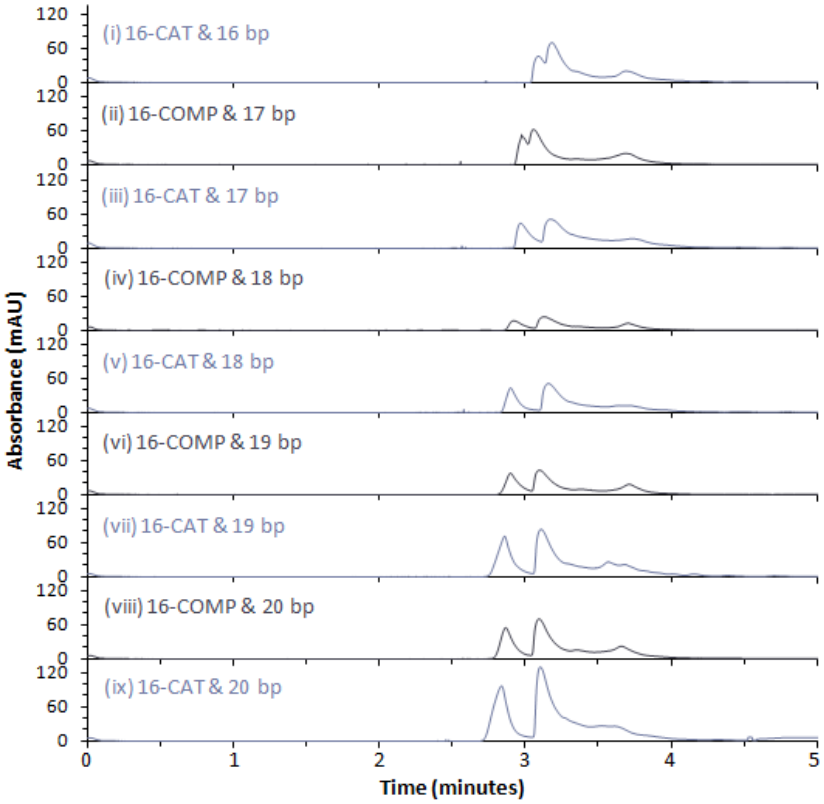

Figure 6.14. CE electropherograms of mixtures of 16-COMP bp and 16-CAT bp (i), 16-COMP bp and 17 bp (ii), 16-CAT bp and 17 bp (iii), 16-COMP bp and 18 bp (iv), 16-CAT and 18 bp (v), 16-COMP bp and 19 bp (vi), 16-CAT bp and 19 bp (vii), 16-COMP bp and 20 bp (viii), and 16-CAT bp and 20 bp (ix) dsODNs (18.6 µM) using a CFR PEPyM-*co*-PMMA random copolymer (21/79) coated fused-silica capillary (8 cm L_d, 38 cm L_t, 75 µm id, 363 µm od). Separation was performed at 263.2 V cm^{-1} and 35 ^oC with UV detection at 260 nm for 12 min run time. The BGE was Tris-borate (100 mM)/urea (7M) at pH 9.0. Samples were introduced electrokinetically at 131.6 V cm^{-1} for 8 s.

The trends observed using EKI were very similar to those observed from the hydrodynamic injection. From Figures 6.14 and 6.15A, it can be seen that the t_m decreased with increasing bp length, leading to a velocity (Figure 6.15E) and mobility (Figure 6.15F) that increased with increasing size. Again, the 16-CAT bp dsODN was shown to have a slightly slower mobility than the 16-COMP bp dsODN. It can be seen from Figure 6.15C that the 16-CAT bp mixtures resulted in increased R_s when compared to the 16-COMP strands due to decreased interactions and different sequences, and the 16-CAT bp and 16-COMP bp mixture was partially resolved (R_s = 0.52). The % improvement in R_s from the 16 bp peak was calculated to be 36.8 %, 16.5 %, 11.8 %, and 4.4 %, for the 17 bp, 18 bp, 19 bp, and 20 bp respectively. Interestingly, the improvement in R_s from the 16 bp peak decreased with increasing bp length suggesting that the sequence dependence mobility may be applicable only to short ODNs.

As with the 16-COMP mixtures, the 16-CAT bp strand was not additive in each of the mixtures due to some interactions still occurring, as well as competition for the surface during migration. The 17 bp, 18 bp, 19 bp and 20 bp peaks were also not additive between mixtures with 16-CAT bp and 16-COMP bp strands suggesting that the interactions were different. The 17 bp, 18 bp, 19 bp and 20 bp dsODNs had faster mobilities when mixed with 16-CAT bp dsODNs, again indicating decreased interactions with the non-complementary strands. This study shows that ODN-ODN interactions were not entirely due to the sequences in the 16-COMP mixtures being the same and that these interactions occurred regardless of sequence. Furthermore, the increase in R_s for the 16-CAT mixtures can also be attributed to the sequence dependent mobility of ODNs in free solution.

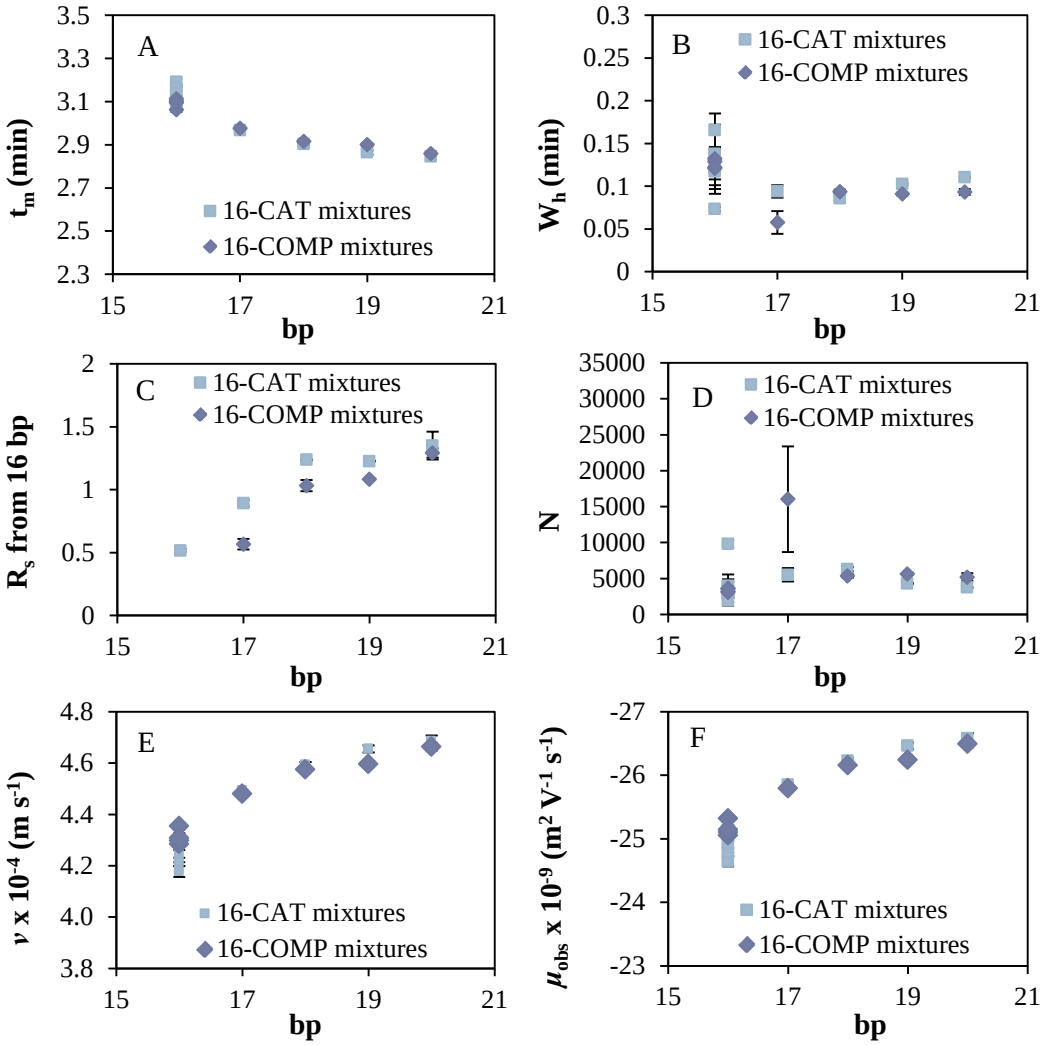

Figure 6.15. Plots of t_m (A), W_h (B), R_s (C), N (D), ν (E), and μ_{obs} (F) versus temperature for separation of dsODN (18.6 µM) mixtures containing sequences that are complementary (16-COMP mixtures), and mixtures containing sequences that are non-complementary (16-CAT mixtures) using a CFR PEPyM-*co*-PMMA random copolymer (21/79) coated fused-silica capillary (8 cm L_d, 38 cm L_t, 75 µm id, 363 µm od) using EKI. Error bars are ± 1 s_d from n = 2.

6.3.2 Effect of ionic strength

It was predicted by Manning [104] and shown experimentally in the literature [16, 93, 105] that the μ_o decreases linearly with the logarithm of ionic strength of the BGE (achieved by increasing the concentration of the BGE). However, the change in mobility upon altering the conductivity of the BGE by the addition of ionic salts is quite different [105]. The effect of ionic strength on the mobility of a mixture of 16 bp and 20 bp dsODNs was investigated by adding Tris-borate (200 mM), and NaCl (in varying amounts) to the BGE. The CE electropherograms can be found in Figure 6.16 and the mobility and R_s calculations are in Table 6.2 for the Tris-borate study and Table 10.16 in Appendix B for the NaCl study.

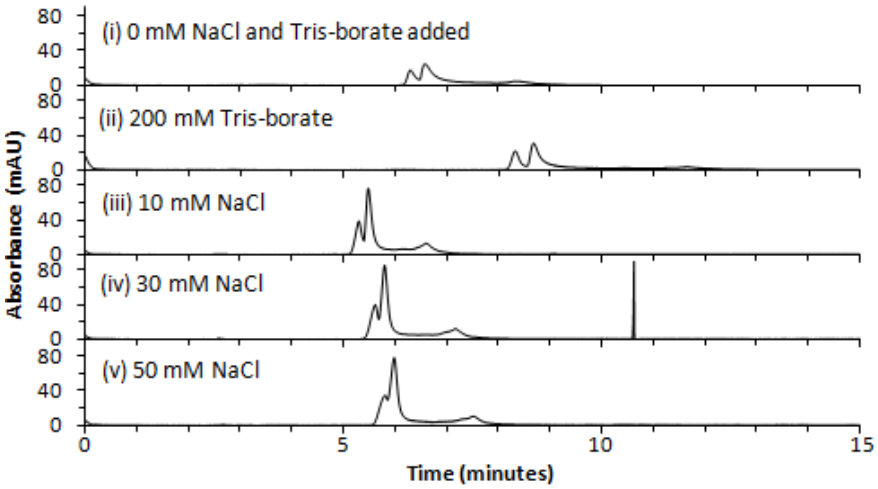

Figure 6.16. CE electropherograms of a mixture of 16 bp and 20 bp dsODNs (18.6 µM) at varying ionic strengths using a CFR PEPyM-*co*-PMMA random copolymer coated fused-silica capillary (8 cm L_d, 38 cm L_t, 75 µm id, 363 µm od). Separation was performed at 35 ^oC and 131.6 V cm^{-1} with UV detection at 260 nm for 15 min run time. The BGE was Tris-borate (100 mM)/urea (7M) at pH 9.0 (i), containing Tris-borate (200 mM) (ii), NaCl (10 mM) (iii), NaCl (30 mM) (iv), and NaCl (50 mM) (v). Samples were introduced electrokinetically at 131.6 V cm^{-1} for 8 s.

From Figure 6.16(i) and (ii) it was observed that addition of Tris-borate (200 mM) to the BGE resulted in an increase in t_m and hence a decrease in mobility. This was due to electrostatic shielding of the ODNs by the surrounding ion atmosphere [16, 105]. Table 6.2 shows that the R_s of the strands increased from 0.94 to 1.27 with the addition of Tris-borate (200 mM) to the BGE attributed to a reduction in ODN-ODN interactions.

Table 6.2. Calculation of R_s and efficiency of the separation of a 16 bp and 20 bp dsODN mixture (18.6 µM) with and without Tris-borate (200 mM) added to the BGE, using a CFR PEPyM-*co*-PMMA random copolymer (21/79) coated fused-silica capillary.

[Tris-borate] added to BGE (mM)	Peak (bp)	t_m (min)	W_h (min)	R_s	N	v x 10^{-4} (m s^{-1})	μ_{app} x 10^{-9} (m^2 V^{-1} s^{-1})
0	20	6.30	0.14	0.94	10929	2.12	-16.09
	16	6.59	0.22		4902	2.02	-15.38
200	20	8.47	0.14	1.27	19279	1.57	-11.97
	16	8.84	0.20		10614	1.51	-11.46

*The negative sign denotes an anodic mobility

However, changing the ionic strength of the BGE by addition of ionic salts (NaCl) to change the conductivity exhibited an entirely different trend. Figure 6.16 shows that addition of NaCl (10 mM) to the BGE resulted in an initial decrease in t_m (Figure 6.16(iii)), which then increased linearly (Figure 6.17A) with increasing amounts of NaCl (Figure 6.16(iii)-(v)).

DNA-buffer electrostatic-based interactions can occur during electrophoresis, in particular for borate ions which are known to form complexes with DNA which increases the mobility. Addition of salts to the BGE results in the dissociation of the DNA-borate complexes, thereby decreasing the mobility [105]. It is evident from Figure 6.16 that as the concentration of NaCl increased, the ODN-buffer interactions were reduced, thus increasing the t_m and hence decreasing the v and μ_{app} (see Figures 6.17E and F). This does not account for the initial decrease in t_m which was attributed to the compression of the EDL from the increase in local viscosity which decreased the EOF and increased the mobility of the ODNs (see Section 5.2.1.3.2 for more details). Interestingly, the W_h (Figure 6.17B) increased as a result of the decreasing R_s (Figure 6.17C). This was a consequence of decreasing ODN-buffer interactions, and a potential increase in ODN-ODN interactions.

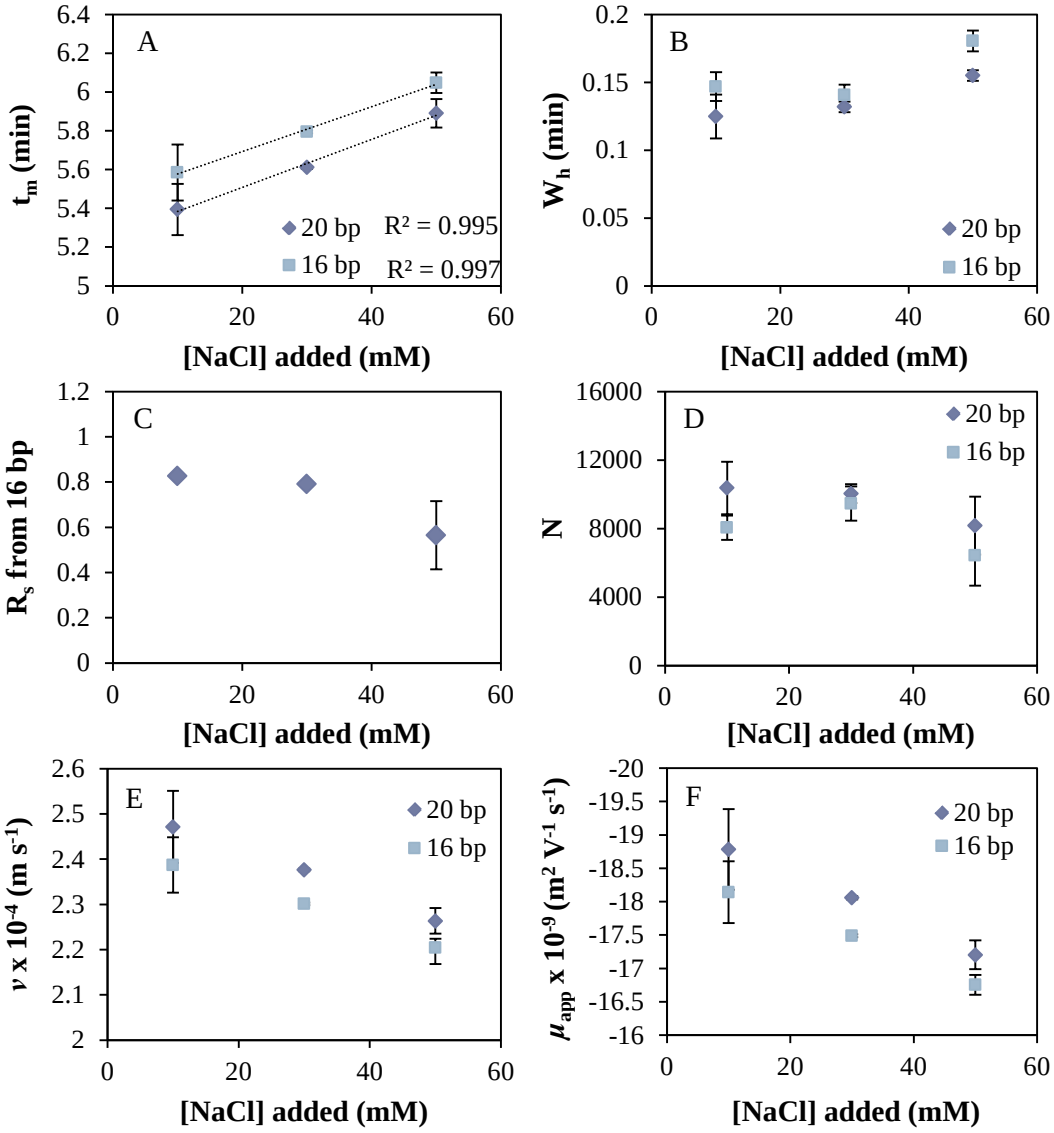

Figure 6.17. Plots of t_m (A), W_h (B), R_s (C), N (D), ν (E), and μ_{obs} (F), versus concentration of NaCl added to the BGE, for separation of 16 bp and 20 bp dsODNs (18.6 µM) on a CFR PEPyM-*co*-PMMA random copolymer (21/79) coated fused-silica capillary (8 cm L_d, 38 cm L_t, 75 µm id, 363 µm od) using EKI. Error bars are ± 1 s_d from n = 3.

6.4 Concluding remarks

This chapter investigated the use of SEI CE analysis for the separation of dsODNs on a CFR PEPyM-*co*-PMMA random copolymer coated capillary (8 cm L_d). Free solution electrophoretic separation of dsODNs was achieved by further optimising the method described in Chapter 5 (see Scheme 5.2 in Section 5.3). It was found that for SEI analysis, hydrodynamic injection resulted in poor signal-to-noise and sensitivity; and by using EKI the signal-to-noise ratio was improved, with an increase in ODN sample loading. Owing to the decreased residence and analysis time of the ODNs, the use of higher voltages and temperatures could be afforded (avoiding joule heating) to improve the R_s and separation efficiency. Short chain dsODNs ranging from 16 bp to 20 bp were separated down to 1 bp R_s (partial R_s of 16 bp and 17 bp strand) using short-end EKI (5 kV, 8 s) on a fused-silica capillary coated with CFR PEPyM-*co*-PMMA random copolymer at 263.2 V cm^{-1} and 35 ^oC.

It was found from using a 16-CAT bp strand (non-complementary to other strands in the mixtures) that the free solution mobility of dsODNs was sequence dependent. The R_s of mixtures containing 16-CAT bp was improved for all mixtures in comparison to the 16-COMP bp mixtures. Moreover, the method was capable of partially resolving a mixture of 16-CAT bp and 16-COMP bp (R_s of 0.52), further proving the sequence dependence. Interestingly, the improvement of R_s from the 16 bp peak decreased with increasing bp length (from 36.8 % for the 17 bp, to only 4.4 % for the 20 bp) suggesting that the sequence dependent mobility is restricted to short chain ODNs.

It was found from comparison of mixtures of the 16-CAT (non-complementary) strand and 16-COMP (complementary) strand that ODN-ODN interactions were sequence independent as the 16 bp peaks were not additive in all mixtures. These ODN-ODN interactions were reduced by increasing the ionic strength with the addition of Tris-borate (200 mM) to the BGE. This was evidenced by an increase in R_s from 0.94 to 1.27 for the 16 bp and 20 bp dsODN mixture (separation voltage was 131.6 V cm^{-1}). An increase in t_m (from 6.30 min to 8.47 min, and 6.59 min to 8.84 min, for the 20 bp and 16 bp, respectively) was also observed due to the

electrostatic shielding of the ODNs by the surrounding ion atmosphere [16, 105]. Changing the ionic strength by altering the BGE conductivity with the addition of NaCl resulted in a different observed mobility trend. The addition of small concentrations of NaCl decreased the t_m to 5.39 min and 5.59 min, for the 20 bp and 16 bp, respectively. This was due to the compression of the EDL from an increase in local viscosity. Further additions of NaCl to the BGE led to a linear increase in t_m as the ODN-buffer interactions were reduced. However, this resulted in a reduction in R_s.

The optimised SEI CE method described in this chapter was shown to be suitable for R_s of short chain dsODNs (16 bp - 20 bp) and may prove to be useful for the separation of short chain PS-ODNs (16* bp - 18* bp) for purity determination (* denotes the presence of a phosphorothioate backbone). This was investigated in the following chapter (Chapter 7).

7 Short-end injection CE analysis of PS-ODNs

7.1 Synopsis

Therapeutic AS-ODNs are ss or ds macromolecules derived from DNA and RNA building blocks with an ideal optimal length for cellular uptake of approximately 20 b [76]. *ss antisense oligonucleotides (ssAS-ODNs) are easily determined by various methods* [73, 75, 151], *however recent pharmaceutical developments of dsAS-ODNs have required new analysis strategies to be developed in order to successfully determine their identity and purity* [67, 188].

*Work herein utilised a CFR PEPyM-*co*-PMMA random copolymer coated capillary for SEI CE analysis of 16* b(p) and 18* b(p) ssPS-ODNs and dsPS-ODNs in free solution. R_s of dsPS-ODNs from ordinary dsODNs was investigated; and the dsPS-ODNs were spiked with ssPS-ODNs to test for purity.*

7.2 Background information and literature

AS-ODNs are short fragments of synthetic ssDNA, generally between 12 b - 50 b [67, 72, 151, 189]. They are a new class of therapeutic compounds isolated in 1978 as ss compounds [190], but it was not until 1998 that the first AS-ODN drug was developed [73]. They are capable of complementary binding to specific gene sequences (ribonucleic acid, RNA) to induce inhibition of gene expression [191] by physically blocking the translation process. The resultant DNA-RNA duplex is susceptible to cellular RNase H activity which cleaves the duplex preventing translation of the RNA [70]. Some AS-ODNs act by a steric blocking mechanism, meaning they are capable of forming strong enough bonds with RNA that nucleases are not needed for blocking or splicing [71]. The ability to easily select a sequence of AS-ODNs complementary to the target is what makes it such an attractive method for therapeutics.

Unfortunately, there is limited use of AS-ODNs in the phosphodiester form (unmodified oligodeoxynucleotides) due to the rapid degradation by intracellular endo- and ex-nucleases typically via 3' to 5' activity. These degradation products can exhibit cytotoxic and antiproliferative effects [72]. Therefore, there has been a lot of work conducted on the modification of the nucleotides to deal with issues associated with toxicity, *in vivo* instability and low cellular uptake [73], leading to the development of three 'generations' of AS-ODNs: (1) PS-ODNs (see Figure 7.1 for structure and base pairing), (2) alkyl modifications to the 2' OH group, and (3) modified phosphate linkages or riboses (phosphorodiamidated morpholino oligomers), and complete modification of the furanose ring in the nucleotide [73]. PS-ODNs are the most common and well-known of the modified AS-ODNs [188] and were therefore used in the work described herein for purity and identification studies using SEI CE analysis.

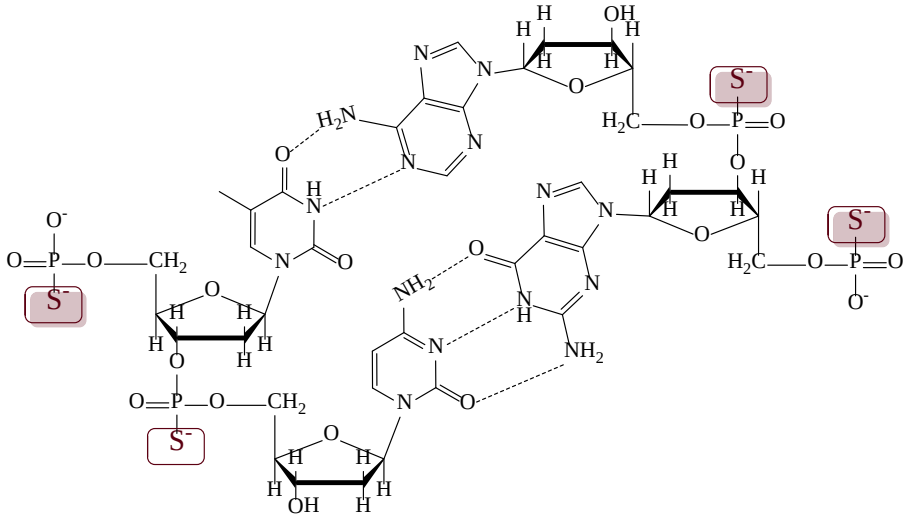

Figure 7.1. Structure and base pairing for PS-ODNs showing the replacement of an oxygen atom for a sulphur atom on the deoxyribose groups.

The latest development of AS-ODNs is now focussing on the use of short chain ds molecules, inspired by the discovery of small interference RNA (siRNA) which are capable of gene suppression with greater efficacy and stability in the ds form over the ss form [188]. Furthermore, recent studies have shown that cellular uptake can be increased by delivery as double-strands [69, 188]. It is for this reason that the work in this thesis has focussed on the separation of dsODNs (and PS-ODNs), rather than ssODNs.

Due to the need to modify the oligodeoxynucleotides, there is the potential for reaction impurities to remain, which need to be identified and removed [188]. In synthetic PS-ODNs (the most commonly used AS-ODNs), impurities include thiation failures (incomplete modification of all repeating units in the one sequence) and more commonly, deletion sequences (failure to add a base) [75]. In addition, Székely *et al.* [67] showed that only some therapeutic ODNs act in their ds form, and the ss form is considered to be an impurity. Therefore it is necessary to have a method in place that is capable of not only separating the ODNs based on the base length, but also separate the ds form from the ss form.

Current methods of AS-ODN analysis include the use of anion exchange chromatography and capillary gel electrophoresis, and more recently, capillary electrophoresis with sieving polymer-buffer solutions. Srivatsa *et al.* [75] have used anion exchange HPLC and CGE as complementary techniques to evaluate

deletion sequences and partial phosphodiester analogs of PS-ODNs of differing lengths (17 bp - 20 bp) and the same base sequences. While anion exchange HPLC was capable of differentiating between the differences in backbone length due to the partial phosphodiester analogs, deletion sequences migrated together as one peak and were unresolved [75]. Whereas polyacrylamide CGE was capable of single b R_s of the deletion sequences but was unable to resolve the phosphorothioate analogs from the phosphodiester analogs [75].

More recent research has focussed on the use sieving polymer-buffer solutions for analysis of AS-ODNs [66, 67]. Enhanced separation of ss and ds AS-ODNs was achieved by Székely *et al.* [67] using a polymer-buffer (Bis-Tris, boric acid containing PEG) sieving media on a PVA pre-coated CE capillary under negative applied voltages. Single b R_s of AS-ODNs between 5 b - 25 b ($p(dT)_{5-25}$) was achieved at 1000 V cm^{-1} using the polymer-buffer containing ACN (~20 % v/v) and PEG (~20 % w/v). As previously stated, some AS-ODNs act only in the ds form, and hence the presence of the ss form indicates impurity. Therefore, the authors spiked a ds drug substance (dsDS, sequence not disclosed due to secrecy reasons) with ssODNs in order to determine if ssODN impurities could be resolved from dsODNs. To maximise the separation of dsDS from the ssODNs, the concentration of PEG in the BGE was decreased to ~6.5 % and R_s was possible using the polymer-buffer at 1000 V cm^{-1}. The authors then went on to investigate whether the dsDS could be resolved from its deletion sequences (n-1, n-2, and n-3) achieving 2 bp R_s as the dsDS could not be resolved from the n-1 deletion sequence.

A suitable CE method for analysis of AS-ODNs should be capable of differentiating between ss and ds AS-ODNs for determining AS-ODN purity, as well as possess the power to resolve ss and ds AS-ODNs down to one b(p).

7.3 CE method development on CFR PEPyM-*co*-PMMA random copolymer (21/79) coated capillaries

Separation of 16* bp and 18* bp dsPS-ODN (8.5 µM) individual solutions and mixtures was tested on CFR PEPyM-*co*-PMMA random copolymer coated capillaries using the short-end EKI method optimised in Chapter 6 (see Scheme 6.2). An interesting study by Astriab-Fisher *et al*. [69] utilised the degradation of unmodified ODNs to assist in the cellular uptake AS-ODNs by delivering the therapeutic oligonucleotide as a duplex (hybrid) between an active ssAS-ODN complementary bound to a shorter and easily degradable ssODN sense strand. This allowed for release of the AS-ODN upon phosphodiesterase degradation to enable it to perform its function [69]. In order to investigate the purity of a ssODN/ssPS-ODN hybrid, a duplex of 16 b ssODN (5'-CCG(16); see Table 2.3 in Section 2.2.3.1) and 18* b ssPS-ODN (5'-TTC*18; see Table 2.4 in Section 2.2.3.2) was formed and analysed. In addition, a sample of the hybrid was spiked with an ordinary 20 bp dsODN and analysed. The CE electropherograms of all samples are shown in Figure 7.2 and the mobility and R_s calculations can be found in Table 7.1.

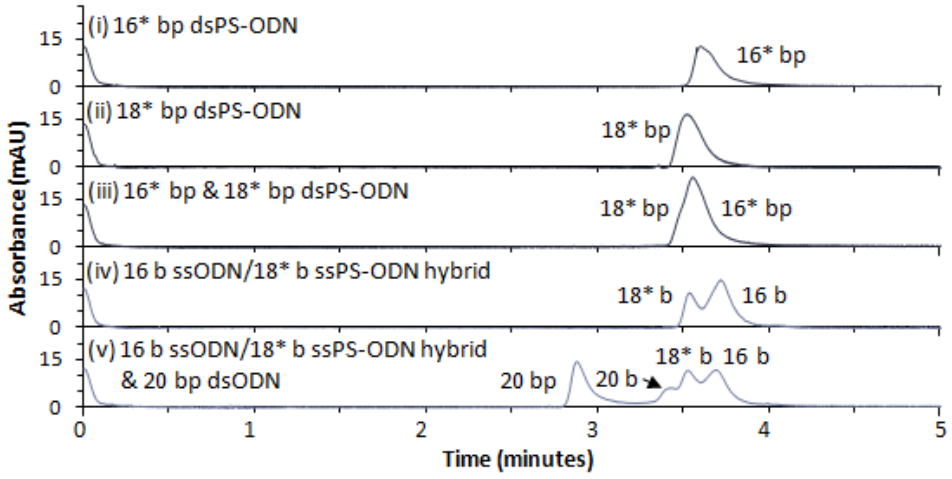

Figure 7.2. CE electropherograms of individual solutions of 16* bp (i), and 18* bp (ii), dsPS-ODNs (8.5 µM); mixture of 16* bp and 18* bp dsPS-ODNs (8.5 µM) (iii); 16 b ssODN/18* b ssPS-ODN hybrid (8.5 µM) (iv); and a mixture of 16 b ssODN/18* b ssPS-ODN hybrid with 20 bp dsODN (8.5 µM) (v). Separation was performed on a CFR PEPyM-*co*-PMMA random copolymer (21/79) coated fused-silica capillary (8 cm L_d, 38 cm L_t, 75 µm id, 363 µm od) at 35 ^{o}C and 263.2 V cm^{-1} with UV detection at 260 nm for 5 min run time. The BGE was Tris-borate (100 mM)/urea (7 M) at pH 9.0. Samples were introduced electrokinetically at 131.6 V cm^{-1} for 8 s.

In comparison to the separation of ODNs (see Section 6.3.1), Figure 7.2 shows that the PS-ODNs exhibited a greater t_m as a result of the sulphur groups on the phosphorothioate backbone (see Figure 7.1). The sulphur has a lower electronegativity than oxygen, therefore reducing the overall negative charge of the molecule [192]. As with the ODNs, the larger fragment (18* bp) had the shorter t_m owing to the greater charge density; therefore the free solution mobility of PS-ODNs was also based on the molecule charge (see Table 7.1 for the mobility data). Figure 7.2(iii) shows that the method was unable to resolve the 16* bp and the 18* bp presumably due to ODN-ODN interactions. These interactions were investigated further by altering the BGE ionic strength (see Section 7.3.2).

It is evident from the two peaks present in Figure 7.2(iv) that the 16 b ODN/18* b PS-ODN hybrid did not fully hybridise. The first peak at 3.54 min was due to the 18* b PS-ODN and the peak at 3.73 min was due to the 16 b dsODN, and the R_s of these peaks is 1.05. Addition of 20 bp dsODN to the hybrid (Figure 7.2(v)) resulted in baseline R_s (3.69) of the 20 bp from the hybrid. Again, the 16 b ODN/18* b PS-ODN hybrid did not fully hybridise with an R_s of 0.89. These results show that the method was capable of separating ODNs from PS-ODNs in the ds and ss form and therefore has the potential to be useful for purity determination of PS-ODNs. However, further method development is required to resolve mixtures of dsPS-ODNs.

Table 7.1. Calculation of R_s and efficiency of separation of PS-ODN and dsODN mixtures (8.5 µM) using a CFR PEPyM-*co*-PMMA random copolymer (21/79) coated fused-silica capillary.

Sample	Peak	t_m (min)	W_h (min)	R_s	N	v x 10^{-4} (m s^{-1})	μ_{app} x 10^{-9} (m^2 V^{-1} s^{-1})	s_d x 10^{-9} (n = 3)	RSD (%)	μ_{obs} x 10^{-9} (m^2 V^{-1} s^{-1})
16* bp	16* bp	3.63	0.13		4108	3.68	-13.98	0.10	0.69	-22.75
18* bp	18* bp	3.55	0.15		2986	3.76	-14.27	0.08	0.54	-23.05
18* bp & 16* bp	18* bp	3.49	0.05	0.28	29246	3.82	-14.52	0.18	1.27	-23.30
	16* bp	3.53	0.14		3333	3.77	-14.34	0.21	1.43	-23.11
5'-TTC*18 b/5'-CCG(16) b	18* b	3.54	0.08	1.05	11236	3.76	-14.30	0.04	0.30	-23.07
	16 b	3.73	0.13		4832	3.58	-13.60	0.02	0.14	-22.37
20 bp with 5'-TTC*18 b/5'-CCG(16) b	20 bp	2.89	0.11	3.69	3719	4.62	-17.55	0.02	0.13	-26.33
	18* b	3.54	0.10	0.89	7532	3.77	-14.33	0.04	0.25	-23.10
	16 b	3.70	0.13		4839	3.60	-13.68	0.03	0.21	-22.46

[#]The negative sign denotes an anodic mobility
*Represents phosphorothioate backbone

7.3.1 Effect of voltage and temperature on PS-ODN separation

From the voltage studies in Sections 6.2.1.1 and 6.2.2.2 on the ODNs it was found that the R_s was increased using low voltages (below ~132 V cm^{-1}) and high voltages (above ~237 V cm^{-1}). Therefore, the effect of decreasing voltage on the R_s of a mixture of 16* bp and 18* bp dsPS-ODNs was investigated. Figure 7.3(i) and (ii) shows the CE electropherograms of analysis at 263.2 V cm^{-1} and 131.6 V cm^{-1}, and the R_s and mobility calculations can be found in Table 7.2.

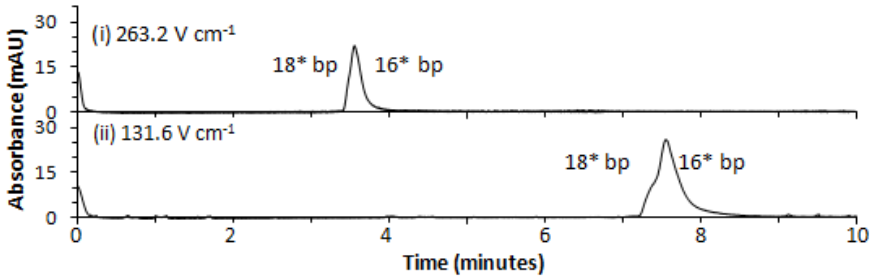

Figure 7.3. CE electropherograms of a mixture of 16* bp and 18* bp dsPS-ODNs (8.5 µM) at 263.2 V cm^{-1} (i), and 131.6 V cm^{-1} (ii), using a CFR PEPyM-*co*-PMMA random copolymer (21/79) coated fused-silica capillary (8 cm L_d, 38 cm L_t, 75 µm id, 363 µm od). Separation was performed at 35 °C with UV detection at 260 nm for 10 min run time. The BGE was Tris-borate (100 mM)/urea (7 M) at pH 9.0. Samples were introduced electrokinetically at 131.6 V cm^{-1} for 8 s.

Figure 7.3 and Table 7.2 show that there was a slight improvement on the R_s from 0.28 to 0.41 for 263.2 V cm^{-1} and 131.6 V cm^{-1}, respectively, with an increase in t_m and a decrease in v. The W_h also increased as the strands began to resolve from each other; however, the 16* bp and 18* bp strands still co-migrated due to ODN-ODN interactions occurring. Therefore, in order to improve the R_s, other avenues needed to be explored, such as capillary temperature and BGE ionic strength.

Table 7.2. Calculation of R_s and efficiency of the separation of 16* bp and 18* bp dsPS-ODNs (8.5 µM) with an applied voltage of 263.2 V cm^{-1} or 131.6 V cm^{-1} using a CFR PEPyM-*co*-PMMA random copolymer (21/79) coated fused-silica capillary (8 cm L_d, 75 µm id).

Voltage ($V\ cm^{-1}$)	Peak (bp)	t_m (min)	W_h (min)	R_s	N	v x 10^{-4} ($m\ s^{-1}$)	μ_{app} x 10^{-9} ($m^2\ V^{-1}\ s^{-1}$)#	μ_{obs} x 10^{-9} ($m^2\ V^{-1}\ s^{-1}$)#
263.2	18*	3.49	0.05	0.28	29334	3.82	-14.52	-23.30
	16*	3.53	0.14		3389	3.77	-14.34	-23.11
131.6	18*	7.41	0.11	0.41	23567	1.80	-13.67	-22.44
	16*	7.55	0.29		3828	1.77	-13.42	-22.19

#The negative sign denotes an anodic mobility *Represents phosphorothioate backbone

From the temperature studies in Sections 6.2.1.2 and 6.2.2.3 on the ODNs it was found that the R_s was improved by increasing the temperature. Therefore, in an attempt to improve the R_s of the 16* bp and 18* bp dsPS-ODNs the effect of increasing temperature was investigated. Figure 7.4(i)-(vi) shows the CE electropherograms at 35 ^oC - 60 ^oC, and the R_s and mobility calculations can be found in Table 10.17 in Appendix B. An applied voltage of 263.2 V cm^{-1} was used for this investigation due to the faster analysis time.

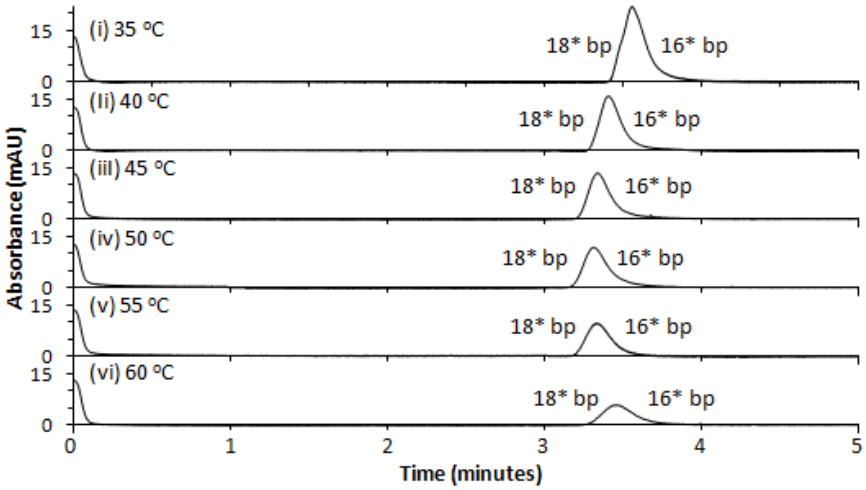

Figure 7.4. CE electropherograms of a mixture of 16* bp and 18* bp dsPS-ODNs (8.5 µM) at varying temperatures (i)-(vi), using a CFR PEPyM-*co*-PMMA random copolymer coated fused-silica capillary (8 cm L_d, 38 cm L_t, 75 µm id, 363 µm od). Separation was performed at 263.2 V cm^{-1} with UV detection at 260 nm for 5 min run time. The BGE was Tris-borate (100 mM)/urea (7 M) at pH 9.0. Samples were introduced electrokinetically at 131.6 V cm^{-1} for 8 s.

From Figure 7.4 and Figure 7.5C it is clear that temperature did not have much of an effect on the R_s, with only a very slight increase. Co-migration of the strands was observed at all temperatures. Unlike the ODNs, denaturation or degradation of the strands did not occur, even at elevated temperatures (50 ^oC - 60 ^oC). This was a result of the decreased residence time, and higher T_m of 51.5 ^oC and 58.0 ^oC for the 16* bp and 18* bp, respectively (see Table 2.4 in Section 2.2.3.2). Figures 7.5E and F show that the v and μ_{obs} first increased between 35 ^oC and 50 ^oC, and then decreased. This decrease in mobility was most likely due to the restriction of the formation of borate-PS-ODN complexes at higher temperatures, thereby reducing the overall negative charge of the PS-ODNs in comparison to lower temperatures. Figure 7.4 also shows that the peak heights decreased with increasing temperature owing to the peaks broadening (observed from the increasing W_h in Figure 7.5B). From this analysis it can be seen that the optimum temperature for separation of the

16* bp and 18* bp dsPS-ODN mixture on the CFR PEPyM-*co*-PMMA random copolymer coated capillary using short-end EKI was between 35 °C and 45 °C; however, changing the temperature did not result in improved R_s of the strands.

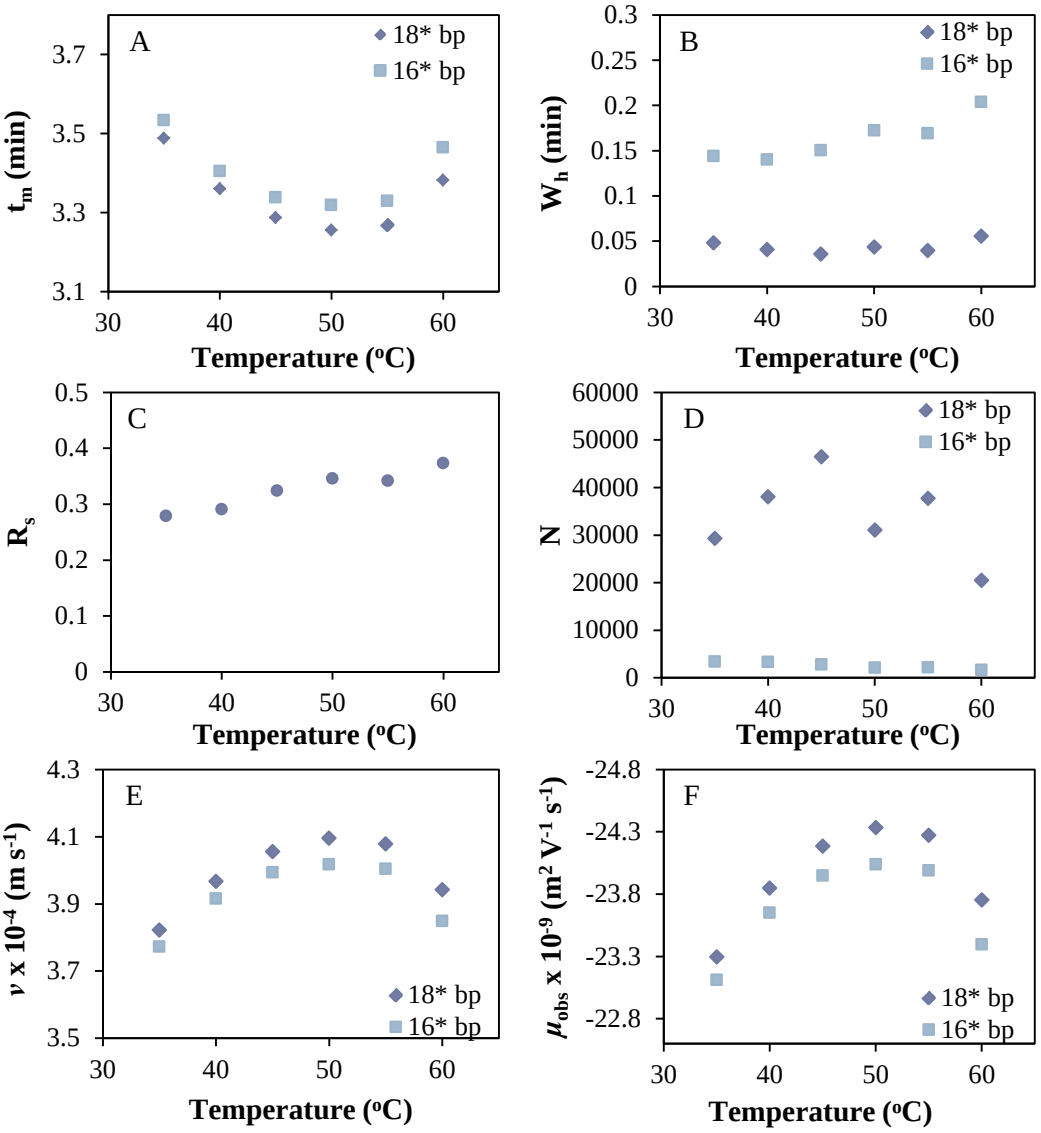

Figure 7.5. Plots of t_m (A), W_h (B), R_s (C), N (D), ν (E), and μ_{obs} (F), versus temperature for separation of a mixture of 16* bp and 18* bp dsPS-ODNs (8.5 µM) at varying temperatures using a CFR PEPyM-*co*-PMMA random copolymer (21/79) coated fused-silica capillary (8 cm L_d, 38 cm L_t, 75 µm id, 363 µm od) using EKI.

7.3.2 Effect of ionic strength on PS-ODN separation

It was shown in Chapter 6 (Section 6.3.2) and in literature that ionic strength of the BGE can affect the R_s and mobility of ODNs by altering ODN-ODN and ODN-buffer interactions, as well as altering the EOF [16, 93, 105]. It was also demonstrated that the ionic strength can be changed by increasing the concentration of the buffer ions, or by altering the conductivity by the addition of ionic salts; and

these two processes produce different results. The effect of ionic strength on the mobility of a mixture of 16* bp and 18* bp dsPS-ODNs was investigated by adding Tris-borate (200 mM), and NaCl (in varying amounts) to the BGE. The CE electropherograms can be found in Figure 7.6 and the mobility and R_s calculations are in Table 7.3 for the Tris-borate study and Table 10.18 in Appendix B for the NaCl study. An applied voltage of 131.6 V cm^{-1} was chosen for direct comparison to the ODN ionic strength study which was also performed at this voltage (see Section 6.3.2).

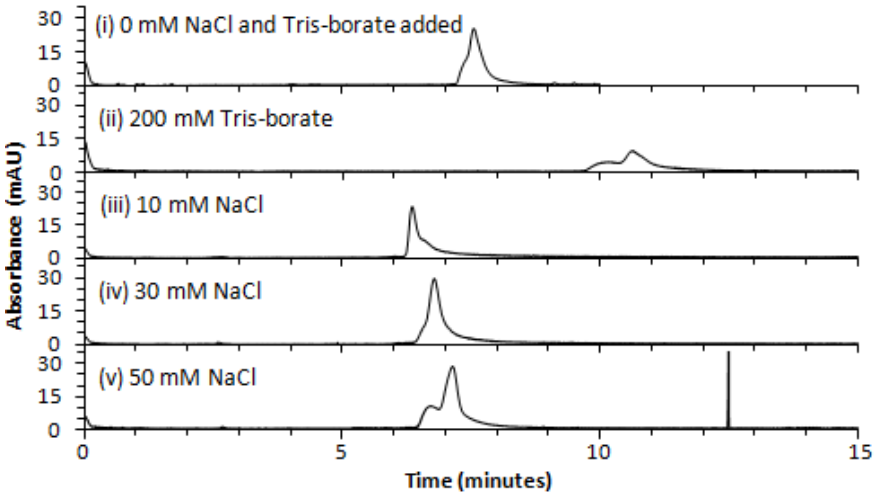

Figure 7.6. CE electropherograms of a mixture of 16* bp and 18* bp dsPS-ODNs (8.5 µM) at varying ionic strengths using a CFR PEPyM-*co*-PMMA random copolymer coated capillary (8 cm L_d, 38 cm L_t, 75 µm id, 363 µm od). Separation was performed at 35 °C and 131.6 V cm^{-1} with UV detection at 260 nm for 15 min run time. The BGE was Tris-borate (100 mM)/urea (7M) at pH 9.0 (i), containing Tris-borate (200 mM) (ii), NaCl (10 mM) (iii), NaCl (30 mM) (iv), and NaCl (50 mM) (v). Samples were introduced electrokinetically at 131.6 V cm^{-1} for 8 s.

From Figure 7.6(i) and (ii) it was clear that addition of Tris-borate (200 mM) to the BGE resulted in an increase in t_m and hence a decrease in mobility. This was also observed for the ODNs (see Section 6.3.2) and was attributed to electrostatic shielding of the PS-ODNs by the surrounding ion atmosphere [16, 105]. Table 7.3 shows that the R_s of the strands increased with the addition of Tris-borate (200 mM) to the BGE attributed to a reduction in ODN-ODN interactions; however it was seen from Figure 7.6(ii) that the peak shapes were quite broad.

Table 7.3. Calculation of R_s and efficiency of the separation of a 16* bp and 18* bp dsPS-ODNs mixture (8.5 µM) with and without Tris-borate (200 mM) added to the BGE, using a CFR PEPyM-*co*-PMMA random copolymer (21/79) coated fused-silica capillary.

[Tris-borate] added to BGE (mM)	Peak (bp)	t_m (min)	W_h (min)	R_s	N	v x 10^{-4} (m s^{-1})	μ_{app} x 10^{-9} (m^2 V^{-1} s^{-1})[#]
0	18*	7.41	0.11	0.41	23567	1.80	-13.67
	16*	7.55	0.29		3828	1.77	-13.42
200	18*	10.24	0.52	0.56	2143	1.30	-9.90
	16*	10.71	0.47		2887	1.24	-9.46

[#]The negative sign denotes an anodic mobility *Represents phosphorothioate backbone

However, changing the ionic strength of the BGE by addition of ionic salts to change the conductivity again exhibited a different trend. Figure 7.6 shows that addition of NaCl (10 mM) to the BGE resulted in an initial decrease in t_m (Figure 7.6(iii)), which then increased linearly (Figure 7.7A) with increasing additions of NaCl (Figure 7.6(iii)-(v)). Addition of NaCl to the BGE resulted in the dissociation of the PS-ODN-borate complexes, thereby increasing the t_m and hence decreasing the v and μ_{obs} (see Figures 7.7E and F) [105]. The initial decrease in t_m was attributed to the compression of the EDL which decreased the EOF, increasing the mobility of the PS-ODNs (see Section 5.2.1.3.2 for more details). Interestingly, the W_h (Figure 7.7B) increased as a result of the changing mobility (Figure 7.7F) and the peak shapes changed (Figure 7.6(iii)-(v)) leading to a change in R_s (Figure 7.7C).

The observed trend in R_s and peak shape was quite different than what was seen for the ODNs (see Section 6.3.2). The addition of NaCl resulted in a decrease in R_s for ODNs; whereas the R_s for the PS-ODNs was improved owing to a decrease in ODN-ODN interactions. Consistent with the results obtained by increasing the concentration of the Tris-borate in BGE, increasing the NaCl concentration resulted in peak broadening, and only partial R_s of the 16* bp and 18* bp dsPS-ODNs was achieved.

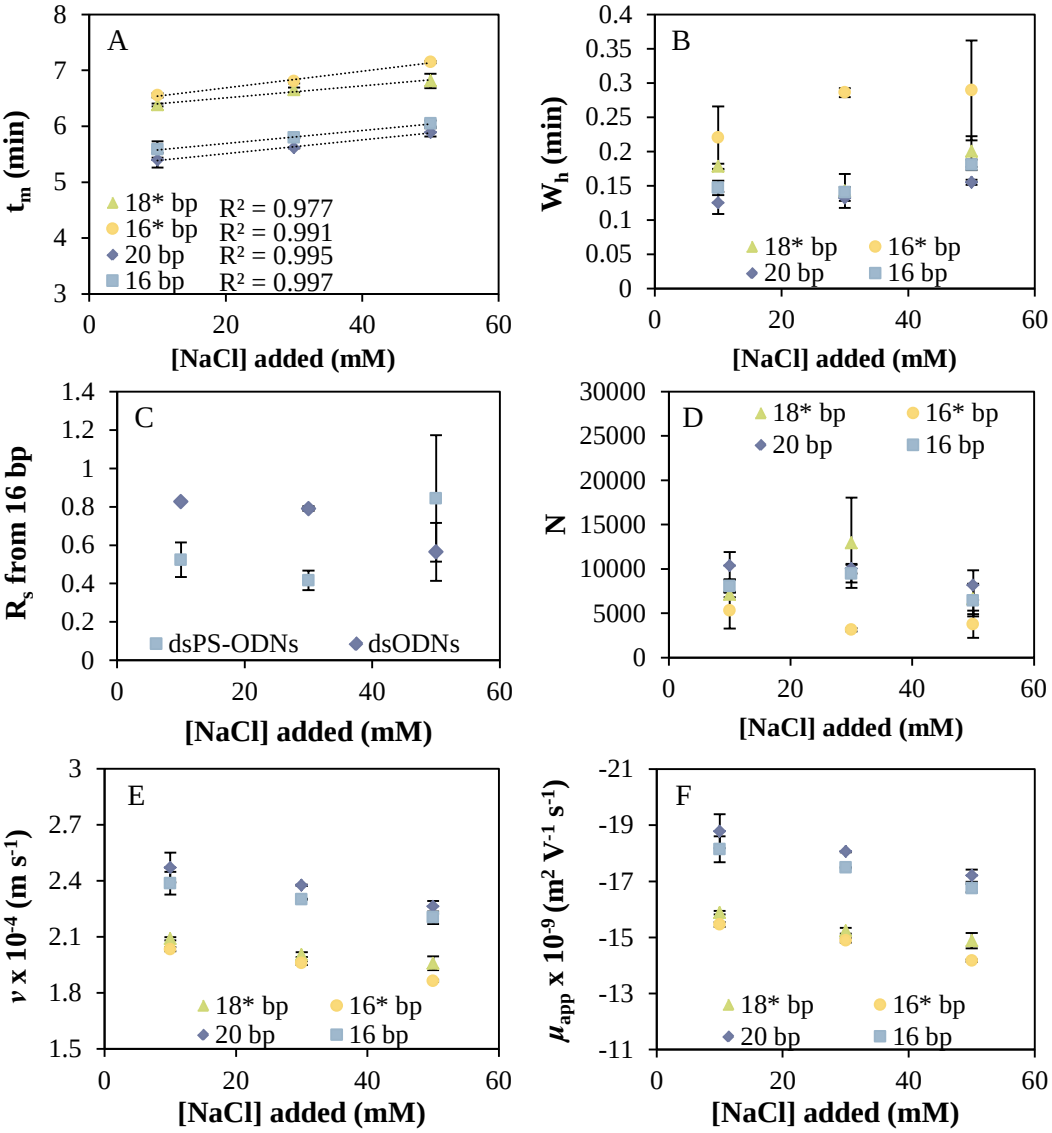

Figure 7.7. Plots of t_m (A), W_h (B), R_s (C), N (D), ν (E), and μ_{app} (F), versus concentration of NaCl added to the BGE, for separation of a mixture of 16* bp and 18* bp dsPS-ODNs (8.5 µM) compared to a mixture of 16 bp and 20 bp dsODNs (18.6 µM) on a CFR PEPyM-*co*-PMMA random copolymer (21/79) coated fused-silica capillary (8 cm L_d, 38 cm L_t, 75 µm id, 363 µm od) using EKI. Error bars are ± 1 s_d from n = 3.

7.3.3 Effect of capillary diameter on PS-ODN separation

From the capillary id study on the 30 cm (L_d) CFR PEPyM-*co*-PMMA random copolymer coated capillary utilising normal injection and negative polarity (Section 5.2.2.4), it was observed that a decrease in id resulted in an improved R_s. Therefore, separation of PS-ODN and ODN mixtures was performed on a CFR PEPyM-*co*-PMMA random copolymer coated capillary with a 50 µm id. In addition to the samples analysed in Section 7.3, solutions of ssPS-ODNs and a 5'-CCG(16) b ssODN were also prepared to determine their mobilities and identify the peaks in the mixtures; a sample of 16* bp dsPS-ODN (8.5 µM) was spiked with

a 5'-TTC*16 b ssPS-ODN (8.5 µM) to analyse the purity; and finally, a mixture of 16 bp dsODNs and 16* bp dsPS-ODNs was prepared to examine the differential mobilities based on the charge density of the strands. The CE electropherograms are shown in Figure 7.8 and the mobility and R_s calculations can be found in Table 7.4. An applied voltage of 263.2 V cm^{-1} was used to allow for direct comparison to the 75 µm capillary (see Section 7.3).

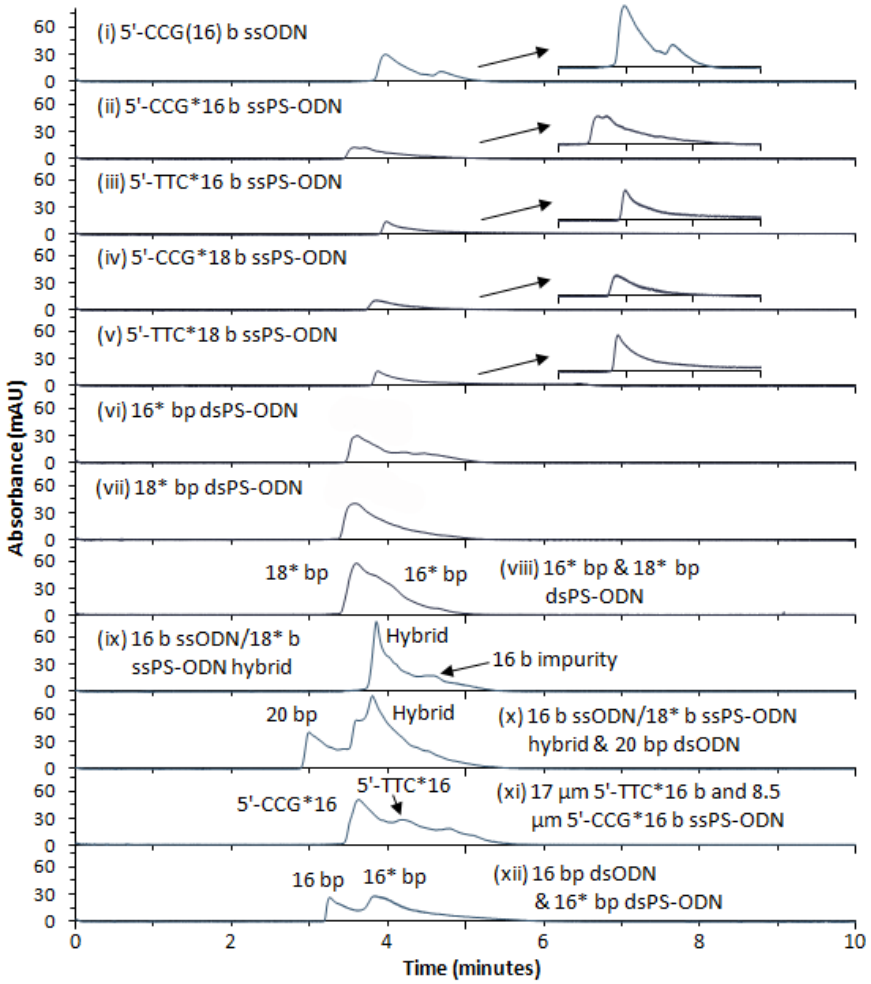

Figure 7.8. CE electropherograms of individual solutions of 5'-CCG(16) b ssODN (i); 5'-CCG*16 b (ii), 5'-TTC*16 b (iii), 5'-CGC*18 b (iv), 5'-TTC*18 b (v), ssPS-ODNs (8.5 µM); 16* bp (vi), and 18* bp (vii), dsPS-ODNs (8.5 µM); a mixture of 16* bp and 18* bp dsPS-ODNs (8.5 µM) (viii); 16 b ssODN/18* b ssPS-ODN hybrid (8.5 µM) (ix); mixture of 16 b ssODN/18* b ssPS-ODN hybrid with 20 bp dsODN (8.5 µM) (x); 5'-TTC*16 b (17 µM) and 5'-CCG*16 b (8.5 µM) ssPS-ODN mixture (xi); and a mixture of 16 bp dsODNs and 16* bp dsPS-ODNs (8.5 µM) (xii). Separation was performed on a CFR PEPyM-*co*-PMMA random copolymer (21/79) coated fused-silica capillary (8 cm L_d, 38 cm L_t, 50 µm id, 363 µm od) at 35 °C and 263.2 V cm^{-1} with UV detection at 260 nm for 10 min run time. The BGE was Tris-borate (100 mM)/urea (7 M) at pH 9.0. Samples were introduced electrokinetically at 131.6 V cm^{-1} for 8 s.

In comparison to the separation of PS-ODNs on the 75 µm capillary (see Section 7.3), Figure 7.8 shows that the PS-ODNs exhibited a greater t_m indicating a greater interaction of the dsPS-ODNs with the CFR PEPyM-*co*-PMMA random copolymer coated capillary surface. The same decrease in μ_{app} was observed for dsODNs (see Section 5.2.2.4). Again, the larger, more negatively charged PS-ODNs exhibited the greater mobility indicating charge-based separation. Interestingly, from Figure 7.8(ii)-(vii) it was observed that the difference in mobilities of the dsPS-ODNs and ssPS-ODNs were not as great as what was seen for the ds and ss ODNs (see Section 5.3.1). Whilst this can be attributed to the reduction in residence time on the shorter capillary, Figure 7.8(i) shows that the 5'-CCG b ssODN had the slowest mobility in comparison to the ssPS-ODNs indicating a reduction in surface-analyte interactions for the ssPS-ODNs. Figure 7.8(ii)-(v) shows that, as with the ODNs, the 5'-CCG* ssPS-ODNs possessed faster mobilities, attributed to the larger overall negative charge from the extra adenine and cytosine bases (refer to Table 2.4 in Section 2.2.3.2 for the sequences).

Figure 7.8(viii) shows that decreasing the capillary diameter did not result in R_s of the 16* bp and the 18* bp, although it was improved very slightly (increased from 0.24 to 0.27 for the 75 µm and 50 µm, respectively). It is evident from the one peak present in Figure 7.8(ix) that the 16 b ODN/18* b PS-ODN hybrid successfully hybridised. The smaller peak at ~4.7 min was due to impurities present in the 5'-CCG(16) b ssODN which was also observed in Figure 7.8(i). This shows that the method was capable of determining ODN impurities in ODN/PS-ODN hybrids. Addition of 20 bp dsODN to the hybrid (Figure 7.8(x)) resulted in baseline R_s (1.29) of the 20 bp from the hybrid. From the electropherogram of the spiked dsPS-ODN mixture (Figure 7.8(xi)) it was seen that ssPS-ODN impurities can be detected in dsPS-ODNs with partial R_s (0.75) achieved. Furthermore, Figure 7.8(xii) shows that dsODNs can be resolved from dsPS-ODNs. These results indicate that the described method is capable of separating ODNs from PS-ODNs in the ds and ss form and therefore has the potential to be useful for purity determination of PS-ODNs. However, it was found that decreasing the capillary diameter did not improve the R_s and further method development is still required to resolve mixtures of dsPS-ODNs.

Table 7.4. Calculation of R_s and efficiency of separation of PS-ODN and ODN mixtures (8.5 µM) using a CFR PEPyM-*co*-PMMA random copolymer (21/79) coated fused-silica capillary.

Sample	Peak	t_m (min)	W_h (min)	R_s	N	v x 10^{-4} (m s^{-1})	μ_{app} x 10^{-9} (m^2 V^{-1} s^{-1})#	s_d x 10^{-9} (n = 3)	RSD (%)	μ_{obs} x 10^{-9} (m^2 V^{-1} s^{-1})#
5'-CCG(16)	5'-CCG(16) b	4.12	0.31	-	964	3.24	-12.31	0.68	5.50	-21.08
5'-CCG*16 b	5'-CCG*16 b	3.72	0.43	-	416	3.59	-13.64	0.63	4.65	-22.41
5'-TTC*16 b	5'-TTC*16 b	3.93	0.23	-	1636	3.39	-12.89	0.23	1.82	-21.66
5'-CGC*18 b	5'-CGC*18 b	3.76	0.26	-	1176	3.54	-13.46	0.30	2.23	-22.23
5'-TTC*18 b	5'-TTC*18 b	3.92	0.18	-	2563	3.40	-12.91	0.44	3.43	-21.69
16* bp	16* bp	3.68	0.31	-	776	3.62	-13.76	0.24	1.75	-22.53
18* bp	18* bp	3.63	0.47	-	325	3.67	-13.95	0.30	2.14	-22.73
18* bp & 16* bp	18* bp	3.72	0.279	0.27	936	3.59	-13.63	0.36	2.68	-22.41
	16* bp	3.88	0.44		436	3.43	-13.05	0.34	2.63	-21.82
5'TTC*18 b & 5'CCG(16) b hybrid	ds hybrid	3.77	0.22	-	1570	3.53	-13.43	0.41	3.07	-22.20
20 bp with 5'TTC*18 b & 5'CCG(16) b hybrid	20 bp	3.11	0.17	1.29	1926	4.28	-16.28	0.56	3.44	-25.05
	ds hybrid	3.85	0.51		318	3.46	-13.15	0.58	4.42	-21.92
5'TTC*16 b (17 µM) & 5'-CCG*16 b (8.5 µM)	16* bp	3.77	0.35	0.75	632	3.54	-13.43	0.50	3.70	-22.21
	5'-TTC*16 b	4.22	0.35		796	3.16	-12.00	0.22	1.79	-20.77
16* bp and 16 bp	16 bp	3.16	0.15	0.99	2634	4.22	-16.03	0.51	3.16	-24.80
	16* bp	3.66	0.45		369	3.64	-13.84	0.49	3.55	-22.61

#The negative sign denotes an anodic mobility
*Represents phosphorothioate backbone

7.4 Concluding remarks

This chapter investigated the use of SEI CE analysis for the separation of dsPS-ODNs in free solution on a CFR PEPyM-*co*-PMMA random copolymer coated capillary (8 cm L_d). It was found that in comparison to the ODNs, the PS-ODNs exhibited slower mobilities due to the reduced electronegativity from the phosphorothioate backbone. However, in accordance with the ODNs, the migration order was from largest to smallest meaning that the migration is based on charge, with the larger, more negatively charged molecules having the greater mobility.

It was observed that on the 75 µm capillary the R_s of 16* bp and 18* bp dsPS-ODNs could not be achieved by altering the applied voltage, nor the capillary temperature. The PS-ODNs underwent greater ODN-ODN interactions than the ordinary ODNs, leading to co-migration. In addition, they possess a higher T_m, meaning that they were more resilient to increasing temperatures and joule heating. Partial R_s was achieved by increasing the ionic strength of the BGE via addition of Tris-borate (200 mM) (R_s = 0.56) or NaCl (50 mM) (R_s = 0.84). Furthermore, it was observed that the 16 b ssODN/18* b ssPS-ODN hybrid did not fully hybridise owing to the two complementary strands having different mobilities (R_s = 1.09). Addition of 20 bp dsODN to the hybrid resulted in baseline R_s (3.69) of the 20 bp from the hybrid, and the complementary ssODN and ssPS-ODNs being partially resolved (R_s of 0.89). An attempt to improve R_s of the dsPS-ODNs using a 50 µm capillary proved to be unsuccessful. Analysis of ssPS-ODNs, dsPS-ODNs spiked with ssPS-ODNs, and a mixture of 16 bp dsODNs and 16* bp dsPS-ODNs indicated that mobility was dependent on sequence and charge, with the greater charged strands exhibiting the greater mobility. This fact allowed for R_s (0.99) of dsPS-ODNs from dsODNs of the same length (16* bp and 16 bp). Additionally, the residual ssPS-ODN in the spiked dsPS-ODN mixture was able to be detected and partially resolved (R_s of 0.75) using this method.

This investigation showed that the method was capable of resolving ODNs from PS-ODNs in the ds and ss form and therefore has the potential for purity determination of PS-ODNs.

8 Conclusions & future perspectives

8.1 Synopsis

The aim of this thesis was to develop a capillary electrophoretic method for the separation, identification and purity determination of synthetic ODNs and PS-ODNs for potential application in microfluidic devices. Optimised separation was achieved in free solution on fused-silica capillaries (8 cm and 30 cm L_d) dynamically coated with a CFR PEPyM-co-PMMA random copolymer. The developed method has the advantage of easy and efficient capillary preparation and regeneration, with extended capillary life-time and enhanced stability under harsh conditions.

From the literature review in Chapter 1 it was found that capillary electrophoretic separation of DNA requires capillary surface modification to reduce and manipulate the EOF and surface-analyte interactions [11, 12, 22, 32, 33]. Large DNA fragments greater than the p_{DNA} are free draining meaning that they exhibit the same μ_{ep} regardless of size. Therefore to enable size separation, sieving media are required to provide obstacles to selectively retard the strands [34, 98, 120, 140]. Conversely, short fragments of DNA smaller than the p_{DNA} are non-free draining and exhibit mobilities in free solution that are dependent on the molecular charge; whereby the smaller, lesser charged DNA have slower mobilities [20, 21, 93]. Operation in free solution requires the suppression of the EOF to enhance the mobilities of the DNA, and in this work this was achieved by using dilute polymer solutions for physical adsorption of polymer confined to the surface. Chapter 2 described the experimental details for the polymer synthesis and characterisation, dynamic polymer solution preparation, and the optimised CE methods for ODN and PS-ODN separation.

Chapters 3 and 4 dealt with the polymer synthesis and characterisation, and surface characterisation. PEPyM and PMMA homopolymers, and PEPyM-*co*-PMMA and PDEAEMA-*co*-PMMA random copolymers were synthesised by CFR polymerisation; and a PMMA homopolymer macro-RAFT agent was synthesised by RAFT polymerisation for the chain extension of PEPyM for the first reported synthesis of a RAFT PEPyM-*b*-PMMA block copolymer. Dilute polymer solutions were prepared for capillary modification via physical adsorption confined to the surface. AFM was used to investigate the adsorptive properties of these polymers onto Si wafers. It was found that the CFR PMMA homopolymer and RAFT PMMA homopolymer macro-RAFT agent adsorbed on the chain ends to form random bundles with low surface coverage (2 % and 19 % for the RAFT and CFR PMMA, respectively); whereas the CFR PEPyM homopolymer, RAFT PEPyM homopolymer macro-RAFT agent and CFR PEPyM-*co*-PMMA random copolymer adsorbed as globules creating a more even surface coverage. Interestingly, the RAFT PEPyM-*b*-PMMA block copolymer resulted in random aggregates and incomplete surface coverage. It was found that the adsorptive properties were governed by the polymer stereochemistry which was defined by the tacticity. ^{1}H NMR spectroscopy (in Chapter 3) determined the polymer tacticity and found that

it was independent of the polymerisation process. From the AFM studies in Chapter 4, it was observed that the PEPyM adsorbed readily to the surface owing to the PEPyM being heterotactic in the CFR and RAFT homopolymers and isotactic in the CFR and RAFT copolymers which added flexibility. On the other hand, the PMMA units in the CFR and RAFT homopolymers and copolymers were found to be syndiotactic. This made the PMMA units in the polymer relatively inflexible. In the case of the CFR random copolymer, these units were randomly formed along the chain meaning that the copolymer was still flexible and able to form globules; whereas, in the RAFT block copolymer, the PMMA units were present in a block thereby reducing the flexibility of the chain causing the polymer to aggregate and adsorb in random bundles. A uniform surface is desirable for repeatable and successful CE separation [12, 177]. The use of these polymers as dynamic physically adsorbed coatings for the separation of ODNs was evaluated in Chapter 5. The results confirmed that homogenous surface coatings provided repeatable and successful detection of ODNs. A dilute CFR PEPyM-*co*-PMMA random copolymer (21/79) solution was shown by both AFM and CE to be the most suitable as it provided an even surface coverage for EOF suppression and repeatable CE analysis of ODNs and PS-ODNs. An adsorption mechanism for this copolymer was proposed suggesting that the hydrophilic PEPyM units adsorbed to the surface via the carbonyl groups and the hydrophobic PMMA units stabilised this attachment.

Chapter 5 showed that enhanced CE separation of dsODNs and ssODNs ranging from 16 bp - 20 bp (containing the same 16 base sequence) was achieved in free solution on capillaries dynamically coated with CFR PEPyM-*co*-PMMA random copolymer (21/79). The random copolymer surface was shown to suppress the EOF by ~72 % using a Tris-borate (100 mM)/urea (7 M) buffer at pH 9 and 30 ^{o}C. This was due to a compression of the EDL, and the shielding of the surface by the adsorbed polymer, allowing for charge-based separation in free solution with the larger, higher charged strands exhibiting greater mobilities. The method was optimised on 30 cm (L_d) capillaries allowing for 1 bp R_s (between 1.48 and 1.57) of dsODN mixtures with partial R_s (0.48) of the 16 bp and 17 bp strand. The observed co-migration of strands was due to ODN-ODN interactions occurring during electrophoresis which was likely a consequence of using mixtures with the same 16

b sequence. The fact that the mobilities for the 16 bp peak in different mixtures were not additive is indicative of ODN-ODN interactions [105]. These interactions were investigated in Chapter 6 on 8 cm (L_d) capillaries using short-end EKI of mixtures containing a 16 bp strand consisting of a sequence non-complementary to the other double strands in the dsODN mixtures. The R_s of mixtures was improved by up to 37 % using these non-complementary sequences. Moreover, a mixture containing two 16 bp strands of different sequences was partially resolved (R_s of 0.52) indicating that the free solution mobility was sequence dependent.

In Chapter 7, the optimised short-end EKI method was utilised for the separation of PS-ODNs in free solution on CFR PEPyM-*co*-PMMA random copolymer dynamically coated capillaries (8 cm L_d) to determine the content and purity. It was found that the dsPS-ODNs had slower mobilities than ordinary dsODNs due to reduced electronegativity from the phosphorothioate backbone allowing them to be separated from mixtures more readily. This was evidenced by successful R_s (0.99) of dsPS-ODNs from dsODNs of the same length (16* bp and 16 bp). Furthermore, ssPS-ODNs were successfully detected in a spiked dsPS-ODN mixture suggesting the potential for purity determination of PS-ODNs. Unfortunately, dsPS-ODN mixtures were unable to be fully resolved using this method despite changing the capillary temperature or applied voltage owing to stronger ODN-ODN interactions experienced by these strands. Although, changing the ionic strength of the BGE showed potential for improved R_s suggesting that the BGE is the key to successful R_s of PS-ODNs on the PEPyM-*co*-PMMA surface. Therefore further investigation into BGE additives is required to reduce the ODN-ODN interactions. It is also possible that the use of an entirely different buffer system may allow for improved R_s.

The R_s of analytes in CE may be affected by a number of factors (such as BGE, surface charge, temperature, voltage), and each of these can be explored in order to improve the R_s of both the ODNs and the PS-ODNs. This thesis touched on these factors, but further work can be done on the BGE and surface modification. In terms of the BGE, it would be ideal to more thoroughly investigate the ionic strength and conductivity for separation of dsODNs and PS-ODNs, respectively. Furthermore, it would be interesting to explore the use of other traditional

electrophoresis buffers, such as TAE, TBE and TAPS. In addition to changing the ionic strength and/or composition of the BGE (including the use of additives/modifiers), modifying the polymer surface itself, may be worth investigating. The role of the polymer is to control the surface charge, and hence regulate the EOF. Additionally it is used to manipulate the migration of the analyte, whether it be to promote or reduce surface-analyte interactions; therefore changing the polymer composition (in this case, the monomer ratios), should have an effect on the overall surface charge. Further work on the polymer surfaces used in this thesis should involve the investigation of additional and/or different monomers of similar structures, which would change the surface chemistry entirely and possibly improve the R_s. In addition, owing to the fact that there has been no reported use of RAFT polymers as capillary surface modifiers, (in particular, for the separation of DNA), a more in-depth focus should be placed upon the investigation and optimisation of RAFT polymer surfaces.

The described method in this thesis operates in free solution with successful suppression of the EOF and regulation of the surface charge, allowing for charge-based separations. It therefore can be useful for determining the physical properties (such as the diffusion coefficients) of ODNs and PS-ODNs [8]. In addition, R_s of dsODNs was achieved on short 8 cm capillaries with the potential application to microfluidic devices. To achieve this, separation will need to be further optimised for analysis on channels reduced to ~3 cm in length to allow for fast and efficient screening of ODNs.

9 References

[1] Butler, J. M. *Forensic DNA Typing: Biology, Technology and Genetics of STR Markers*; 2nd ed.; Elsevier Academic Press: London, **2005**; pp. 1-659.

[2] McMurray, J. *Organic Chemistry: A Biological Approach*; Thomson Brooks/Cole Thomson Corporation: USA, **2007**; pp. 1-1015.

[3] Robertson, J.; Ross, A.; Burgoyne, L. *DNA in Forensic Science: Theory, Techniques and Applications*; Ellis Horwood Limited: West Sussex, England, **1990**; pp. 1-197.

[4] Viovy, J.-L. *Review of Modern Physics* **2000**, *72*, 813-872.

[5] Watson, J. D.; Crick, F. H. C. *Nature* **1953**, *171*, 737-738.

[6] Kubař, T.; Elstner, M. *The Journal of Physical Chemistry B* **2009**, *113*, 5339.

[7] Shi, X.; Hammond, R. W.; Morris, M. D. *Analytical Chemistry* **1995**, *67*, 1132-1138.

[8] Stellwagen, E.; Stellwagen, N. C. *Electrophoresis* **2002**, *23*, 2794-2803.

[9] Volkel, A. R.; Noolandi, J. *Macromolecules* **1995**, *28*, 8182-8189.

[10] Landers, J. P. *Handbook of Capillary Electrophoresis*; CRC Press, Incorporated: Florida, **1994**; pp. 1-649.

[11] Heller, C. *Electrophoresis* **2001**, *22*, 629-643.

[12] Horvath, J.; Dolník, V. *Electrophoresis* **2001**, *22*, 644-655.

[13] Huang, X.; Doneski, L. J.; Wirth, M. J. *Analytical Chemistry* **1998**, *70*, 4023-4029.

[14] Heiger, D. N. *High Performance Capillary Electrophoresis: An Introduction*; 3rd ed.; Hewlett Packard Company: France, **1997**; pp. 1-136.

[15] Sang, F.; Ren, J. *Journal of Separation Science* **2006**, *29*, 1275-1280.

[16] Stellwagen, E.; Stellwagen, N. C. *Biophysical Journal* **2003**, *84*, 1855-1866.

[17] Landers, J. P. *Handbook of Capillary and Microchip Electrophoresis and Associated Microtechniques*; 3rd ed.; CRC Press: London, New York, **2009**; pp. 1-1567.

[18] Znaleziona, J.; Petr, J.; Knob, R.; Maier, V.; Ševčík, J. *Chromatographia* **2008**, *67*, 5-12.

[19] Cretich, M.; Chiari, M.; Pirri, G.; Crippa, A. *Electrophoresis* **2005**, *26*, 1913-1919.

[20] Stellwagen, N. C.; Gelfi, C.; Righetti, P. G. *Biopolymers* **1997**, *42*, 687-703.

[21] Mohanty, U.; Stellwagen, N. C. *Biopolymers* **1999**, *49*, 209-214.

[22] Kleparník, K.; Bocek, P. *Chemical Reviews* **2007**, *107*, 5279-5317.

[23] Hjertén, S. *Journal of Chromatography* **1985**, *347*, 191-198.

[24] Brüggemann, O.; Freitag, R.; Whitcombe, M.; Vulfson, E. *Journal of Chromatography A* **1997**, *781*, 43-53.

[25] Chiari, M.; Cretich, M.; Damin, F.; Ceriotti, L.; Consonni, R. *Electrophoresis* **2000**, *21*, 909-916.

[26] Zhang, P.; Ren, J. *Analytica Chimica Acta* **2004**, *507*, 179-184.

[27] Cifuentes, A.; Canalejas, P.; Diez-Masa, J. C. *Journal of Chromatography A* **1999**, *830*, 423-438.

[28] Hong, C.; Liguo, S.; Jieke, C. *Wuhan University Journal of Natural Sciences* **1997**, *2*, 363-367.

[29] Barron, A. E.; Sunada, W. M.; Blanch, H. W. *Biotechnology and Bioengineering* **1996**, *52*, 259-270.

[30] Slater, G. W.; Kenward, M.; McCormick, L. C.; Gauthier, M. G. *Current Opinion in Biotechnology* **2003**, *14*, 58-64.

[31] Wan, F.; Zhang, J.; Lau, A.; Tan, S.; Burger, C.; Chu, B. *Electrophoresis* **2008**, *29*, 4704-4713.

[32] Mccord, B.; Hartzell-Baguley, B.; King, S. *Methods in Molecular Biology: Separation of DNA by Capillary Electrophoresis*; P. Schmitt-Kopplin, Ed.; Humana Press Inc.: Totowa, NJ, **2008**; pp. 415-429.

[33] Strege, M.; Lagu, A. *Analytical Chemistry* **1991**, *63*, 1233-1236.

[34] Viovy, J.-L.; Duke, T. *Electrophoresis* **1993**, *14*, 322-329.

[35] Barron, E.; Blanch, H. W.; Soane, D. S. *Electrophoresis* **1994**, *15*, 597-615.

[36] Pereira, F.; Hassard, S.; Hassard, J.; DeMello, A. *Electrophoresis* **2009**, *30*, 2100-2109.

[37] Zhu, J.; Feng, Y.-L. *Journal of Chromatography A* **2005**, *1081*, 19-23.

[38] Chiari, M.; Damin, F.; Melis, A.; Consonni, R. *Electrophoresis* **1998**, *19*, 3154-3159.

[39] Stellwagen, N. C. *Advances in Electrophoresis* **1987**, *1*, 179-228.

[40] Yin, H.-F.; Lux, J. A.; Schomburg, G. *Journal of High Resolution Chromatography* **1990**, *13*, 624-627.

[41] Guttman, A.; Cooke, N. *Analytical Chemistry* **1991**, *63*, 2038-2042.

[42] Cohen, A. S.; Najarian, D. R.; Paulus, A.; Guttman, A.; Smith, J. A.; Karger, B. L. *Proceedings of the National Academy of Sciences of the United States of America* **1988**, *85*, 9660-9663.

[43] Kleemiß, M. H.; Gilges, M.; Schomburg, G. *Electrophoresis* **1993**, *14*, 515-522.

[44] Stellwagen, E.; Lu, Y.; Stellwagen, N. C. *Nucleic Acids Research* **2005**, *33*, 4425-4432.

[45] Butler, J. M.; Buel, E.; Crivellente, F.; McCord, B. R. *Electrophoresis* **2004**, *25*, 1397-1412.

[46] Butler, J. M.; Shen, Y.; McCord, B. R. *Journal of Forensic Sciences* **2003**, *48*, 1054-1064.

[47] Mansfield, E. S.; Robertson, J. M.; Vainer, M.; Isenberg, A. R.; Frazier, R. R.; Ferguson, K.; Chow, S.; Harris, D. W.; Barker, D. L.; Gill, P. D.; Budowle, B.; McCord, B. R. *Electrophoresis* **1998**, *19*, 101-107.

[48] Heiger, D. N.; Cohen, A. S.; Karger, B. L. *Journal of Chromatography* **1990**, *516*, 33-48.

[49] McIntosh, S. L.; Deligeorgiev, T. G.; Gadjev, N. I.; McGown, L. B. *Electrophoresis* **2002**, *23*, 1473-1479.

[50] Braun, B.; Blanch, H. W.; Prausnitz, J. M. *Electrophoresis* **1997**, *18*, 1994-1997.

[51] Chin, A. M.; Colburn, J. C. *American Biotechnology Laboratory, News Edition* **1989**, *7*, 16.

[52] Chu, B.; Ying, Q.; Wang, Y.; Zhang, J. *Macromolecular Symposia* **2005**, *227*, 77-88.

[53] Wang, Q.; Xu, X. *Chinese Chemical Letters* **2003**, *14*, 1278-1280.

[54] Madabhushi, R. S. *Electrophoresis* **1998**, *19*, 224-230.

[55] Zhang, J.; Liang, D.; He, W.; Wan, F.; Ying, Q.; Chu, B. *Electrophoresis* **2005**, *26*, 4449-4455.

[56] Doherty, E. S.; Berglund, K. D.; Buchholz, B. A.; Kourkine, I. V.; Przybycien, T. M.; Tilton, R. D.; Barron, A. E. *Electrophoresis* **2002**, *23*, 2766-2776.

[57] Xu, Y.; Vaidya, B.; Patel, A. B.; Ford, S. M.; McCarley, R. L.; Soper, S. A. *Analytical Chemistry* **2003**, *75*, 2975-2984.

[58] Koutny, L.; Schmalzing, D.; Salas-Solano, O.; El-Difrawy, S.; Adourian, A.; Buonocore, S.; Abbey, K.; McEwan, P.; Matsudaira, P.; Ehrlich, D. *Analytical Chemistry* **2000**, *72*, 3388-3391.

[59] Fung, E. N.; Yeung, E. S. *Analytical Chemistry* **1995**, *67*, 1913-1919.

[60] Luckey, J. A.; Norris, T. B.; Smith, L. M. *The Journal of Physical Chemistry* **1993**, *97*, 3067-3075.

[61] Luckey, J. A.; Smith, L. M. *Analytical Chemistry* **1993**, *65*, 2841-2850.

[62] Hanning, A.; Lindberg, P.; Westberg, J.; Roeraade, J. *Analytical Chemistry* **2000**, *72*, 3423-3430.

[63] Kosobokova, O.; Gavrilov, D. N.; Khozikov, V.; Stepukhovich, A.; Tsupryk, A.; Pan'kov, S.; Somova, O.; Abanshin, N.; Gudkov, G.; Tcherevishnik, M.; Gorfinkel, V. *Electrophoresis* **2007**, *28*, 3890-3900.

[64] Horsman, K. M.; Bienvenue, J. M.; Blasier, K. R.; Landers, J. P. *Journal of Forensic Sciences* **2007**, *52*, 784-799.

[65] Paulus, A.; Ohms, J. *Journal of Chromatography* **1990**, *507*, 113-123.

[66] Li, W.; Ma, Y.; Gan, Z.; Ling, X.; Yang, Z. *Chromatographia* **2011**, *73*, 579-582.

[67] Székely, L.; Kiessig, S.; Schwarz, M. A.; Kálmán, F. *Electrophoresis* **2009**, *30*, 1579-1586.

[68] Christoffersen, R. E. *Nature Biotechnology* **1997**, *15*, 483-484.

[69] Astriab-Fisher, A.; Fisher, M. H.; Juliano, R.; Herdewijn, P. *Biochemical Pharmacology* **2004**, *68*, 403-407.

[70] Weintraub, H. M. *Scientific American* **1990**, *262*, 40-46.

[71] Goodchild, J. *Therapeutic Oligonucleotides: Methods and Protocols*; Goodchild, J., Ed.; Humana Press: NY, USA, **2011**; pp. 1-15.

[72] Dias, N.; Stein, C. A. *Molecular Cancer Therapeutics* **2002**, *1*, 347-355.

[73] Kurreck, J. *European Journal of Biochemistry* **2003**, *270*, 1628-1644.

[74] Kanayama, N.; Takarada, T.; Kimura, A.; Shibata, H.; Maeda, M. *Reactive and Functional Polymers* **2007**, *67*, 1373-1380.

[75] Srivatsa, G. S.; Klopchin, P.; Batt, M.; Feldman, M.; Carlson, R. H.; Cole, D. L. *Journal of Pharmaceutical and Biomedical Analysis* **1997**, *16*, 619-630.

[76] Patil, S. D.; Rhodes, D. G.; Burgess, D. J. *The AAPS Journal* **2005**, *7*, E61-77.

[77] González, N.; Elvira, C.; San Román, J.; Cifuentes, A. *Journal of Chromatography A* **2003**, *1012*, 95-101.

[78] Song, L.; Liu, T.; Liang, D.; Fang, D.; Chu, B. *Electrophoresis* **2001**, *22*, 3688-3698.

[79] Bernal, J.; Rodríguez-Meizoso, I.; Elvira, C.; Ibáñez, E.; Cifuentes, A. *Journal of Chromatography A* **2008**, *1204*, 104-109.

[80] Erny, G. L.; Elvira, C.; San Román, J.; Cifuentes, A. *Electrophoresis* **2006**, *27*, 1041-1049.

[81] Bernal, J.; Sánchez-Hernández, L.; Elvira, C.; Velasco, D.; Ibáñez, E.; Cifuentes, A. *Journal of Separation Science* **2009**, *32*, 605-612.

[82] Guttman, A.; Cohen, A. S.; Heiger, D. N.; Karger, B. L. *Analytical Chemistry* **1990**, *62*, 137-141.

[83] McCormick, R. M. *Analytical Chemistry* **1988**, *60*, 2322-2328.

[84] Cobb, K.; Dolnik, V.; Novotny, M. *Analytical Chemistry* **1990**, *62*, 2478-2483.

[85] Chiari, M.; Nesi, M.; Sandoval, J. E.; Pesek, J. J. *Journal of Chromatography A* **1995**, *717*, 1-13.

[86] Bachmann, S.; Vallant, R.; Bakry, R.; Huck, C. W.; Corradini, D.; Bonn, G. K. *Electrophoresis* **2010**, *31*, 618-629.

[87] García-Cañas, V.; González, R.; Cifuentes, A. *Journal of Agricultural and Food Chemistry* **2002**, *50*, 1016-1021.

[88] Chiari, M.; Cretich, M.; Horvath, J. *Electrophoresis* **2000**, *21*, 1521-1526.

[89] Yang, R.; Wang, Y.; Zhou, D. *Electrophoresis* **2007**, *28*, 3223-3231.

[90] Iki, N.; Yeung, E. S. *Journal of Chromatography A* **1996**, *731*, 273-282.

[91] Hardenborg, E.; Zuberovic, A.; Ullsten, S.; Söderberg, L.; Heldin, E.; Markides, K. E. *Journal of Chromatography A* **2003**, *1003*, 217-221.

[92] Yang, R.; Shi, R.; Peng, S.; Zhou, D.; Liu, H.; Wang, Y. *Electrophoresis* **2008**, *29*, 1460-1466.

[93] Dong, Q.; Stellwagen, E.; Dagle, J. M.; Stellwagen, N. C. *Electrophoresis* **2003**, *24*, 3323-3329.

[94] Allison, S.; Chen, C.; Stigter, D. *Biophysical Journal* **2001**, *81*, 2558-2568.

[95] Cottet, H.; Gareil, P. *Electrophoresis* **2000**, *21*, 1493-1504.

[96] Stellwagen, N. C.; Bossi, A.; Gelfi, C.; Righetti, P. G. *Electrophoresis* **2001**, *22*, 4311-4315.

[97] Ferguson, K. *Metabolism* **1964**, *13*, 985-1002.

[98] Sartori, A.; Barbier, V.; Viovy, J.-L. *Electrophoresis* **2003**, *24*, 421-440.

[99] Frank, S.; Winkler, R. G. *Europhysics Letters* **2008**, *83*, 38004 pp 1-6.

[100] Hoagland, D.; Arvanitidou, E.; Welch, C. *Macromolecules* **1999**, *32*, 6180-6190.

[101] Cottet, H.; Pierre, G.; Theodoly, O.; Williams, C. E. *Electrophoresis* **2000**, *21*, 3529-3540.

[102] Frank, S.; Winkler, R. G. *The Journal of Chemical Physics* **2009**, *131*, 234905 pp 1-8.

[103] Stellwagen, N. C.; Magnusdottir, S.; Gelfi, C.; Righetti, P. G. *Journal of Molecular Biology* **2001**, *305*, 1025-1033.

[104] Manning, G. S. *Journal of Physical Chemistry* **1981**, *85*, 1506-1515.

[105] Stellwagen, E.; Stellwagen, N. C. *Electrophoresis* **2002**, *23*, 1935-1941.

[106] Tietz, D.; Chrambach, A. *Analytical Biochemistry* **1987**, *161*, 395-411.

[107] Ogston, A. *Transactions of the Faraday Society* **1958**, *54*, 1754-1757.

[108] Tietz, D. *Advances in Electrophoresis* **1988**, *2*, 109-164.

[109] Rodbard, D.; Chrambach, A. *Proceedings of the National Academy of Sciences of the United States of America* **1970**, *65*, 970-977.

[110] De Gennes, P. G. *The Journal of Chemical Physics* **1971**, *55*, 572.

[111] Duke, T. A.; Semenov, A.; Viovy, J.-L. *Physical Review Letters* **1992**, *69*, 3260-3263.

[112] Heller, C. *Electrophoresis* **1999**, *20*, 1962-1977.

[113] Viovy, J.-L.; Rubinstein, M.; Colby, R. H. *Macromolecules* **1991**, *24*, 3587-3596.

[114] Read, D. J.; Jagannathan, K.; Likhtman, A. E. *Macromolecules* **2008**, *41*, 6843-6853.

[115] Noguchi, H. *The Journal of Chemical Physics* **2000**, *112*, 9671-9678.

[116] Sunada, W. M.; Blanch, H. W. *Electrophoresis* **1998**, *19*, 3128-3136.

[117] Tietz, D.; Chrambach, A. *Electrophoresis* **1986**, *7*, 241-250.

[118] Viovy, J.-L.; Duke, T. *Physical Review E* **1994**, *49*, 2408-2416.

[119] Stellwagen, N. C.; Stellwagen, E. *Journal of Chromatography A* **2009**, *1216*, 1917-1929.

[120] Grossman, P. D.; Soane, D. S. *Biopolymers* **1991**, *31*, 1221-1228.

[121] Rodbard, D.; Chrambach, A. *Analytical Biochemistry* **1971**,.*40*, 95-134.

[122] Viovy, J.-L.; Duke, T.; Caron, F. *Contemporary Physics* **1992**, *33*, 25-40.

[123] Lunney, J.; Chrambach, A.; Rodbard, D. *Analytical Biochemistry* **1971**, *40*, 158-173.

[124] Serwer, P. *Electrophoresis* **1983**, *4*, 375-382.

[125] Lerman, L. S.; Frisch, H. L. *Biopolymers* **1982**, *21*, 995-997.

[126] Lumpkin, O. J.; Déjardin, P.; Zimm, B. H. *Biopolymers* **1985**, *24*, 1573-1593.

[127] Hervet, H.; Bean, C. P. *Biopolymers* **1987**, *26*, 727-742.

[128] Slater, G. W.; Rousseau, J.; Noolandi, J.; Turmel, C.; Lalande, M. *Biopolymers* **1988**, *27*, 509-524.

[129] Fangman, W. L. *Nucleic Acids Research* **1978**, *5*, 653-666.

[130] Slater, G. W.; Drouin, G. *Electrophoresis* **1992**, *13*, 574-582.

[131] Bustamante, C. *Annual Review of Biophysics and Biophysical Chemistry* **1991**, *20*, 415-446.

[132] Gurrieri, S.; Rizzarelli, E.; Beach, D.; Bustamante, C. *Biochemistry* **1990**, *29*, 3396-3401.

[133] Zhu, M.; Hansen, D. L.; Burd, S.; Gannon, F. *Journal of Chromatography* **1989**, *480*, 311-319.

[134] Bode, H.-J. *FEBS Letters* **1976**, *65*, 56-58.

[135] Pulyaeva, H.; Wheeler, D.; Garner, M. M.; Chrambach, A. *Electrophoresis* **1992**, *13*, 608-614.

[136] Daoud, M.; de Gennes, P. *Journal of Polymer Science: Polymer Physics Edition* **1979**, *17*, 1971-1981.

[137] Broseta, D.; Leibler, L.; Lapp, A.; Strazielle, C. *Europhysics Letters* **1986**, *2*, 733-737.

[138] Peng, S.; Shi, R.; Yang, R.; Zhou, D.; Wang, Y. *Electrophoresis* **2008**, *29*, 4351-4354.

[139] Graessley, W. W. *Advances in Polymer Science* **1982**, *47*, 67-117.

[140] Barron, A. E.; Soane, D. S.; Blanch, H. W. *Journal of Chromatography A* **1993**, *652*, 3-16.

[141] Schwinefus, J. J.; Morris, M. D. *Macromolecules* **1999**, *32*, 3678-3684.

[142] Chiesl, T. N.; Forster, R. E.; Root, B. E.; Larkin, M.; Barron, A. E. *Analytical Chemistry* **2007**, *79*, 7740-7747.

[143] Starkweather, M. E.; Hoagland, D. A.; Muthukumar, M. *Macromolecules* **2000**, *33*, 1245-1253.

[144] Chiefari, J.; Chong, Y. K. B. (Bill); Ercole, F.; Krstina, J.; Jeffery, J.; Le, T. P. T.; Mayadunne, R. T. A.; Meijs, G. F.; Moad, C. L.; Moad, G.; Rizzardo, E.; Thang, S. H. *Macromolecules* **1998**, *31*, 5559-5562.

[145] Hubert, S. J.; Slater, G. W.; Viovy, J.-L. *Macromolecules* **1996**, *29*, 1006-1009.

[146] Stellwagen, N. C.; Magnusdottir, S.; Gelfi, C.; Righetti, P. G. *Biopolymers* **2001**, *58*, 390-397.

[147] Righetti, P. G.; Gelfi, C.; Verzola, B.; Castelletti, L. *Electrophoresis* **2001**, *22*, 603-611.

[148] Yu, S.-B.; Zhou, P.; Feng, A.-R.; Shen, X.-C.; Zhang, Z.-L.; Hu, J.-M. *Analytical and Bioanalytical Chemistry* **2006**, *385*, 730-736.

[149] Cifuentes, A.; Canalejas, P.; Ortega, A.; Carlos, J. *Journal of Chromatography A* **1998**, *823*, 561-571.

[150] Wang, Q.; Xu, X.; Dai, L.-X. *Chinese Journal of Chemistry* **2006**, *24*, 1766-1772.

[151] Khan, K.; Vanschepdael, A.; Hoogmartens, J. *Journal of Chromatography A* **1996**, *742*, 267-274.

[152] Sjödahl, J.; Lindberg, P.; Roeraade, J. *Journal of Separation Science* **2007**, *30*, 104-109.

[153] González, N.; Elvira, C.; San Román, J. *Journal of Polymer Science Part A: Polymer Chemistry* **2003**, *41*, 395-407.

[154] Solomons, G.; Fryhle, C. *Organic Chemistry*; 8th ed.; John Wiley & Sons: USA, **2004**; pp. 386-394.

[155] Vander Heyden, Y.; Popovici, S.-T.; Schoenmakers, P. J. *Journal of Chromatography A* **2003**, *986*, 1-15.

[156] Rogosic, M.; Mencer, H. J.; Gomzi, Z. *European Polymer Journal* **1996**, *32*, 1337-1344.

[157] Sordi, M. L. T.; Riegel, I. C.; Ceschi, M. A.; Müller, A. H. E.; Petzhold, C. L. *European Polymer Journal* **2010**, *46*, 336-344.

[158] Schricker, S.; Palacio, M.; Thirumamagal, B. T. S.; Bhushan, B. *Ultramicroscopy* **2010**, *110*, 639-649.

[159] Baines, F. L.; Billingham, N. C.; Armes, S. P. *Macromolecules* **1996**, *29*, 3416-3420.

[160] Lynd, N.; Meuler, A. J.; Hillmyer, M. *Progress in Polymer Science* **2008**, *33*, 875-893.

[161] Liu, L.; Wu, C.; Zhang, J.; Zhang, M.; Liu, Y.; Wang, X.; Fu, G. *Journal of Polymer Science Part A: Polymer Chemistry* **2008**, *46*, 3294-3305.

[162] Willham, K. A.; Laurent, B. A.; Grayson, S. M. *Tetrahedron Letters* **2008**, *49*, 2091-2094.

[163] Tedder, J. M.; Walton, J. C. *Accounts of Chemical Research* **1976**, *9*, 183-191.

[164] Barner-Kowollik, C. *Handbook of RAFT Polymerization*; WILEY-VCH Verlag GmbH & Co.: Weinheim, Germany, **2008**; pp. 1-543.

[165] Matyjaszewski, K.; Davis, T. P. *Handbook of Radical Polymerization*; Wiley Interscience, John Wiley & Sons: Hoboken, Canada, **2002**; pp. 1-920.

[166] Mayo, F. R. *Journal of the American Chemical Society* **1943**, *65*, 2324-2329.

[167] Mccord, E. F.; Anton, W. L.; Wilczek, L.; Ittel, S. D.; Lissa, T. J.; Raffell, K. D.; Hansen, J. E.; Berge, C. *Macromolecular Symposia* **1994**, *86*, 47-64.

[168] Grohens, Y.; Brogly, M.; Labbe, C.; Schultz, J. *European Polymer Journal* **1997**, *33*, 691-697.

[169] Grohens, Y.; Schultz, J.; Prud'homme, R. E. *International Journal of Adhesion and Adhesives* **1997**, *17*, 163-167.

[170] Moad, G.; Chiefari, J.; Chong, B. Y. K.; Krstina, J.; Mayadunne, R. T. A.; Postma, A.; Rizzardo, E.; Thang, S. H. *Polymer International* **2000**, *49*, 993-1001.

[171] Liu, X.-H.; Li, Y.-G.; Lin, Y.; Li, Y.-S. *Journal of Polymer Science Part A: Polymer Chemistry* **2007**, *45*, 1272-1281.

[172] Moad, G.; Chong, Y. K.; Postma, A.; Rizzardo, E.; Thang, S. H. *Polymer* **2005**, *46*, 8458-8468.

[173] Boyer, C.; Liu, J.; Bulmus, V.; Davis, T. P. *Australian Journal of Chemistry* **2009**, *62*, 830-847.

[174] Chong, Y. K.; Moad, G.; Rizzardo, E.; Thang, S. H. *Macromolecules* **2007**, *40*, 4446-4455.

[175] Willcock, H.; O'Reilly, R. K. *Polymer Chemistry* **2010**, *1*, 149-157.

[176] Favier, A.; Charreyre, M.-T. *Macromolecular Rapid Communications* **2006**, *27*, 653-692.

[177] Cifuentes, A.; Díez-Masa, J. C.; Fritz, J.; Anselmetti, D.; Bruno, A. E. *Analytical Chemistry* **1998**, *70*, 3458-3462.

[178] Binnig, G.; Quate, C. F.; Gerber, C. *Physical Review Letters* **1986**, *56*, 930-933.

[179] Noguchi, H.; Takasu, M. *The Journal of Chemical Physics* **2001**, *114*, 7260-7266.

[180] Ebewele, R. O. *Polymer Science and Technology*; CRC Press: Florida, **2000**; pp. 1-483.

[181] Schwinefus, J. J.; Bloomfield, V. A. *Biopolymers* **2000**, *54*, 572-577.

[182] Scope, R. K. *Protein Purification: Principles and Practice*; Cantor, C. R., Ed.; 3rd ed.; Springer Science & Business Media, LLC: New York, USA, **1994**; pp. 1-383.

[183] Rouzina, I.; Bloomfield, V. A. *Biophysical Journal* **2001**, *80*, 894-900.

[184] Ageno, M.; Dore, E.; Frontali, C. *Biophysical Journal* **1969**, *9*, 1281-1311.

[185] Huang, M.-F.; Huang, C.-C.; Chang, H.-T. *Electrophoresis* **2003**, *24*, 2896-2902.

[186] Verdolino, V.; Cammi, R.; Munk, B. H.; Schlegel, H. B. *Journal of Physical Chemistry B* **2008**, *112*, 16860-16873.

[187] Stellwagen, N.; Gelfi, C.; Righetti, P. G. *Electrophoresis* **2002**, *23*, 167-175.

[188] Jekerle, V.; Kassack, M. U.; Reilly, R. M.; Wiese, M.; Piquette-Miller, M. *Journal of Pharmacy and Pharmaceutical Sciences* **2005**, *8*, 516-527.

[189] Khan, K.; Schepdael, A. Van; Hoogmartens, J. *Journal of Pharmaceutical and Biomedical Analysis* **1996**, *14*, 1101-1105.

[190] Stephenson, M. L.; Zamecnik, P. C. *Proceedings of the National Academy of Sciences of the United States of America* **1978**, *75*, 285-288.

[191] Hélène, C.; Toulmé, J.-J. *Biochimica et Biophysica Acta* **1990**, *1049*, 99-125.

[192] Kotz, J. C.; Treichel, P. M. *Chemistry and Chemical Reactivity*; McDonald, A., Ed.; 5th ed.; Thomson, Brooks/Cole: USA, **2003**; pp. 1-997.

10 Appendices

10.1 Appendix A

This section details the supporting data for capillary electrophoretic separation of ODNs utilising normal injection and negative polarity on 30 cm (L_d) polymer modified capillaries.

10.1.1 EOF temperature study

The v_{EOF} and μ_{EOF} of the Tris-borate (100 mM)/urea (7 M) buffer were determined for PEPyM-*co*-PMMA coated and bare fused-silica capillaries at varying temperatures (15 ^{o}C - 50 ^{o}C) using a buffer/water/acetone (20/75/5 % v/v/v) solution as a neutral marker. The trend in t_m was logarithmic, as shown by the plot of natural log of t_m versus temperature (Figure 10.1).

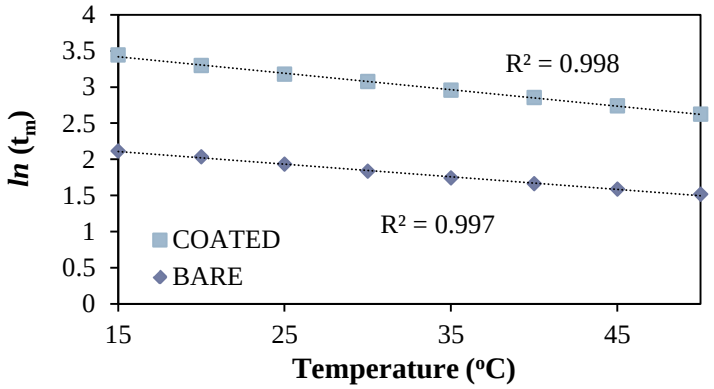

Figure 10.1. Plot of *ln*(t_m) of the neutral marker versus temperature for a bare capillary compared to a capillary coated with CFR PEPyM-*co*-PMMA random copolymer (21/79). Separation was performed on fused-silica capillaries (30 cm L_d, 38 cm L_t, 75 µm id, 363 µm od).

10.1.2 Effect of voltage on ODN separation

The effect of voltage on ODN migration was determined using a 16 bp and 20 bp dsODN mixture. Table 10.1 contains the migration data and the associated mobility and R_s calculations.

Table 10.1. Calculation of R_s and efficiency of the separation of 16 bp and 20 bp dsODNs (18.6 µM) at varying voltages using a CFR PEPyM-*co*-PMMA random copolymer (21/79) coated fused-silica capillary.

Voltage ($V\ cm^{-1}$)	Peak bp	t_m (min)	W_h (min)	R_s	N	v x 10^{-4} ($m\ s^{-1}$)	μ_{app} x 10^{-9} ($m^2\ V^{-1}\ s^{-1}$)*	μ_{obs} x 10^{-9} ($m^2\ V^{-1}\ s^{-1}$)*
131.58	20	20.46	0.27	1.49	30799	2.44	-18.58	-27.35
	16	21.08	0.22		50786	2.37	-18.02	-26.80
144.74	20	18.82	0.22	1.77	42241	2.66	-18.35	-27.13
	16	19.43	0.19		58300	2.57	-17.78	-26.55
157.89	20	17.98	0.22	1.78	36112	2.78	-17.61	-26.38
	16	18.62	0.20		49517	2.69	-17.01	-25.78
171.05	20	16.50	0.19	1.92	42510	3.03	-17.72	-26.49
	16	17.14	0.20		39728	2.92	-17.06	-25.83
184.21	20	15.23	0.14	2.64	62561	3.28	-17.82	-26.60
	16	16.12	0.25		22355	3.10	-16.84	-25.61
197.37	20	14.13	0.16	1.95	45110	3.54	-17.93	-26.71
	16	14.78	0.24		21189	3.38	-17.14	-25.91
210.53	20	13.45	0.18	1.89	31047	3.72	-17.66	-26.44
	16	14.05	0.20		27129	3.56	-16.90	-25.67
223.68	20	12.50	0.17	1.79	28681	4.00	-17.89	-26.66
	16	13.13	0.24		16435	3.81	-17.03	-25.80
236.84	20	11.76	0.17	1.85	27346	4.25	-17.95	-26.72
	16	12.40	0.24		14893	4.03	-17.02	-25.80
250.00	20	11.25	0.14	2.31	34671	4.45	-17.79	-26.56
	16	11.92	0.20		19223	4.19	-16.78	-25.55
263.16	20	10.40	0.13	2.53	33559	4.81	-18.28	-27.05
	16	11.12	0.20		16667	4.50	-17.09	-25.86
394.74	20	6.68	0.22	3.27	4947	7.49	-18.98	-27.75
	16	7.80	0.18		10347	6.41	-16.24	-25.02

*The negative sign denotes an anodic mobility

10.1.3 Effect of temperature on ODN separation

The effect of temperature on ODN migration was determined using a 16 bp and 20 bp dsODN mixture. Table 10.2 contains the migration data and the associated μ_{app} and R_s calculations.

Table 10.2. Calculation of R_s and efficiency of the separation of 16 bp and 20 bp dsODNs (18.6 µM) at varying temperatures using a CFR PEPyM-*co*-PMMA random copolymer (21/79) coated fused-silica capillary.

Temp. (^oC)	Peak	t_m (min)	W_h (min)	R_s	N	v x 10^{-4} (m s^{-1})	μ_{app} x 10^{-9} (m^2 V^{-1} s^{-1})*	μ_{obs} x 10^{-9} (m^2 V^{-1} s^{-1})*
15	20 bp	28.29	0.4	0.71	27902	1.77	-13.43	-22.21
	16 bp	28.74	0.35		37728	1.74	-13.22	-22.00
20	20 bp	28.29	0.39	0.8	29051	1.77	-13.43	-22.20
	16 bp	28.83	0.41		27825	1.73	-13.18	-21.95
25	20 bp	25.04	0.33	1.06	31057	2	-15.17	-23.95
	16 bp	25.64	0.33		34225	1.95	-14.82	-23.60
30	20 bp	24.62	0.27	1.71	46319	2.03	-15.43	-24.21
	16 bp	25.54	0.36		27299	1.96	-14.88	-23.65
35	20 bp	24.36	0.3	4.3	36579	2.05	-15.60	-24.37
	16 bp	26.89	0.39		25809	1.86	-14.13	-22.91
40	20 bp	23.27	0.26	7.5	44484	2.15	-16.33	-25.10
	16 bp	27.21	0.36		31692	1.84	-13.96	-22.74
45	20 bp	37.88	0.14	0.32	390323	1.32	-10.03	-18.81
	16 bp	37.96	0.17		279538	1.32	-10.01	-18.78
50	20 b (5'-CCG)	34.09	0.39	3.95	41824	1.47	-11.15	-19.92
	20 b (5'-TTC)	36.43	0.3		46837	1.37	-10.43	-19.20
	16 b (5'-CCG)	38.39	0.42	1.31	46837	1.3	-9.90	-18.67
	16 b (5'-TTC)	39.36	0.46		40742	1.27	-9.65	-18.43

*The negative sign denotes an anodic mobility

10.1.4 Coating repeatability study

The repeatability of the coating was investigated by modifying the between-run conditioning steps, and the CE electropherograms of repetitive injections of the 16 bp and 20 bp dsODN mixture using three different conditioning methods are represented by Figures 10.2, 10.3 and 10.4.

10.1.4.1 Effect of no between-run conditioning

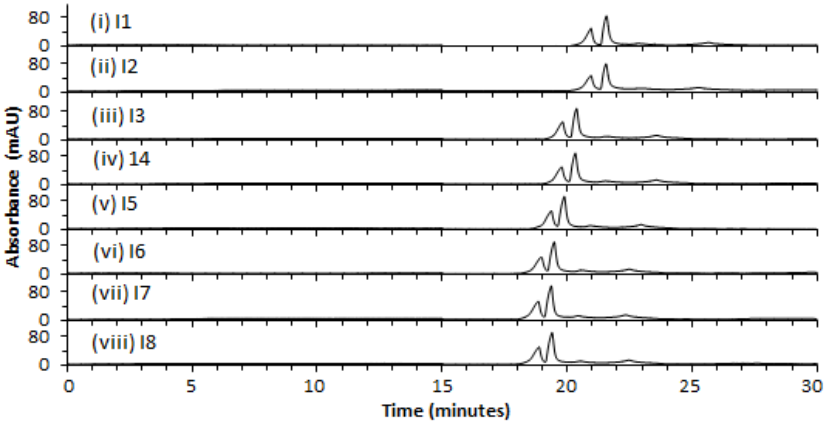

Figure 10.2. CE electropherograms of repetitive injections of a mixture of 16 bp and 20 bp dsODNs (18.6 µM). Separation was performed on a CFR PEPyM-*co*-PMMA random copolymer (21/79) coated fused-silica capillary (30 cm L_d, 38 cm L_t, 75 µm id, 363 µm od) at -131.6 V cm^{-1} and 30 ^oC with UV detection at 260 nm for 30 min run time. The BGE was Tris-borate (100 mM)/urea (7 M). Samples were introduced hydrodynamically at 5000 Pa for 6 s. No conditioning was performed between runs.

10.1.4.2 Effect of between-run buffer conditioning

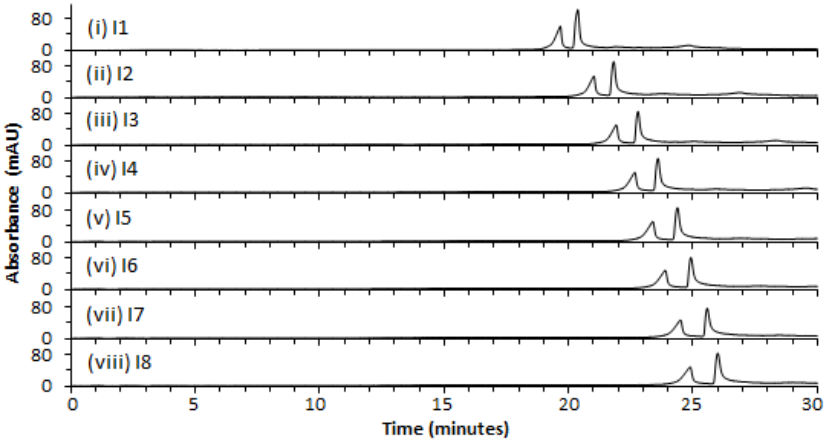

Figure 10.3. CE electropherograms of repetitive injections of a mixture of 16 bp and 20 bp dsODNs (18.6 µM). Separation was performed on a CFR PEPyM-*co*-PMMA random copolymer (21/79) coated fused-silica capillary (30 cm L_d, 38 cm L_t, 75 µm id, 363 µm od) at -131.6 V cm^{-1} and 30 ^oC with UV detection at 260 nm for 30 min run time. The BGE was Tris-borate (100 mM)/urea (7 M). Samples were introduced hydrodynamically at 5000 Pa for 6 s. The capillary was conditioned by flushing with buffer for 2 min between runs.

10.1.4.3 Effect of between-run polymer conditioning

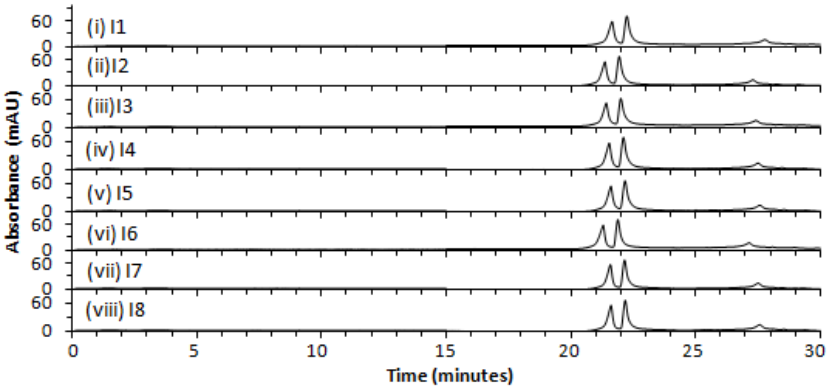

Figure 10.4. CE electropherograms of repetitive injections of a mixture of 16 bp and 20 bp dsODNs (18.6 µM). Separation was performed on a CFR PEPyM-*co*-PMMA random copolymer (21/79) coated fused-silica capillary (30 cm L_d, 38 cm L_t, 75 µm id, 363 µm od) at -131.6 V cm^{-1} and 30 °C with UV detection at 260 nm for 30 min run time. The BGE was Tris-borate (100 mM)/urea (7 M). Samples were introduced hydrodynamically at 5000 Pa for 6 s. The capillary was conditioned between runs by flushing with polymer solution for 3 min, H_2O for 2 min and buffer for 3 min.

10.1.5 Effect of capillary diameter on ODN separation

The repeatability of the 50 µm id capillary was determined by repetitive injections of a mixture of 16 bp and 20 bp dsODNs and compared to the 75 µm id capillary. The resultant CE electropherograms for the 50 µm capillary can be seen in Figure 10.5.

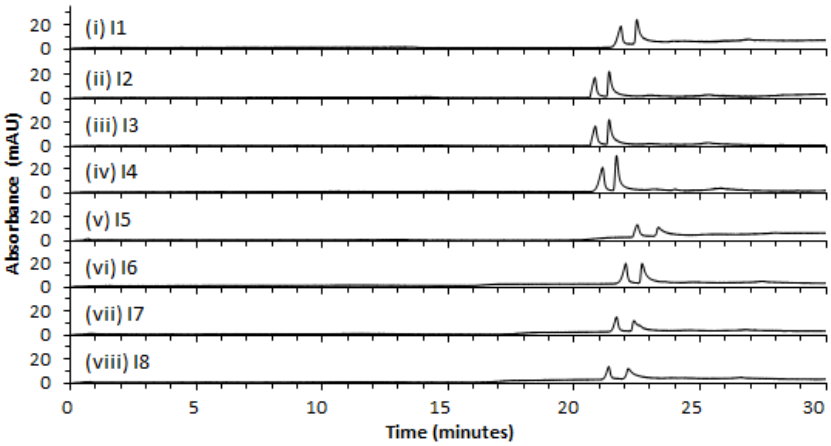

Figure 10.5. CE electropherograms of repetitive injections of a mixture of 16 bp and 20 bp dsODNs (18.6 µM). Separation was performed on a CFR PEPyM-*co*-PMMA random copolymer (21/79) coated fused-silica capillary (30 cm L_d, 38 cm L_t, 50 µm id, 363 µm od) at -131.6 V cm^{-1} and 30 °C with UV detection at 260 nm for 30 min run time. The BGE was Tris-borate (100 mM)/urea (7 M). Samples were introduced hydrodynamically at 5000 Pa for 6 s. The capillary was conditioned between runs by flushing with polymer solution for 3 min, H_2O for 2 min and buffer for 3 min.

10.1.6 PEPyM coated capillaries

A CFR PEPyM homopolymer coated capillary was used to separate dsODN mixtures and individual solutions in order to gain an insight into the separation mechanism and surface chemistry by comparing the results to the PEPyM-*co*-PMMA coated capillary. Table 10.3 displays the migration and repeatability data on a PEPyM coated capillary.

Table 10.3. Calculation of mean t_m, efficiency, R_s and μ_{app} for 3 injections of dsODN mixtures and individual dsODN solutions on a CFR PEPyM homopolymer coated fused-silica capillary (75 µm id).

dsODN sample	Peak (bp)	t_m (min)	W_h (min)	R_s	N	v x 10^{-4} (m s^{-1})	μ_{app} x 10^{-9} (m^2 V^{-1} s^{-1})*	s_d (n = 3)	RSD (%)
18 &	18	24.46	0.27	1.39	46739	2.04	-15.5	0.25	1.62
16 bp	16	25.05	0.24		62304	2.00	-15.2	0.24	1.56
19 &	19	24.00	0.29	1.43	37679	2.08	-15.8	0.38	2.39
16 bp	16	24.69	0.27		44686	2.03	-15.4	0.36	2.36
20 &	20	23.80	0.28	1.63	38841	2.10	-16.0	0.27	1.69
16 bp	16	24.55	0.26		49087	2.04	-15.5	0.26	1.69
16	16	24.73	0.24	-	58165	2.02	-15.4	0.34	2.24
18	18	24.50	0.23	-	64392	2.04	-15.5	0.15	0.97
19	19	24.34	0.26	-	49568	2.05	-15.6	0.51	3.28
20	20	24.26	0.29	-	38755	2.06	-15.7	0.42	2.69

*The negative sign denotes an anodic mobility

10.1.7 PEPyM-*b*-PMMA (30/70) coated capillaries

A RAFT PEPyM-*b*-PMMA block copolymer coated capillary was also used to separate dsODN mixtures to investigate the separation mechanism and surface chemistry by comparing the results to the CFR PEPyM-*co*-PMMA random copolymer coated capillary. Table 10.4 contains the migration and repeatability data on a RAFT PEPyM-*b*-PMMA block copolymer coated capillary.

Table 10.4. Calculation of R_s, efficiency and μ_{app} from the t_m of mixtures of 16 bp and 18 bp, 16 bp and 19 bp, and 16 bp and 20 bp dsODNs on a RAFT PEPyM-*b*-PMMA block copolymer (30/70) coated fused-silica capillary (50 µm id).

dsODN sample	Peak (bp)	t_m (min)	W_h (min)	R_s	N	v x 10^{-4} (m s^{-1})	μ_{app} x 10^{-9} (m^2 V^{-1} s^{-1})
18 & 16 bp	18	17.56	0.27	0.00	54309	2.85	-21.6
	16	17.56	0.24		54309	2.85	-21.6
19 & 16 bp	19	17.11	0.29	0.67	146242	2.92	-22.2
	16	17.30	0.27		35396	2.89	-22.0
20 & 16 bp	20	16.90	0.28	0.68	165855	2.96	-22.5
	16	17.07	0.26		40672	2.93	-22.3

*The negative sign denotes an anodic mobility

10.1.8 PDEAEMA-*co*-PMMA (34/66) coated capillaries

Finally the migration of dsODN mixtures and individual solutions on CFR PEPyM-*co*-PMMA random copolymer coated capillaries were compared to a similar cationic hybrid random copolymer of CFR PDEAMEA-*co*-PMMA. Although both coatings exhibited similar trends, the CFR PDEAEMA-*co*-PMMA random copolymer resulted in a lower efficiency due to broad peaks and longer t_m (observed in Table 10.5).

Table 10.5. Calculation of R_s, efficiency and μ_{app} from the t_m of mixtures of 16 bp and 18 bp, 16 bp and 19 bp, and 16 bp and 20 bp dsODNs on a CFR PDEAEMA-*co*-PMMA random copolymer (34/66) coated fused-silica capillary.

dsODN sample	Peak (bp)	t_m (min)	W_h (min)	R_s	N	v x 10^{-4} (m s^{-1})	μ_{app} x 10^{-9} (m^2 V^{-1} s^{-1})*
18 & 16 bp	18	31.44	0.51	1.19	21157	1.59	-12.1
	16	32.50	0.53		20636	1.54	-11.7
19 & 16 bp	19	30.11	0.49	1.52	20576	1.66	-12.6
	16	31.41	0.51		20687	1.59	-12.1
20 & 16 bp	20	29.69	0.45	1.78	24308	1.68	-12.8
	16	31.02	0.43		28516	1.61	-12.3

*The negative sign denotes an anodic mobility

The repeatability of the optimised method (5 min polymer rinse replaced the 3 min rinse) was determined using the 16 bp and 20 bp dsODN mixture and the resultant electropherograms can be found in Figure 10.6.

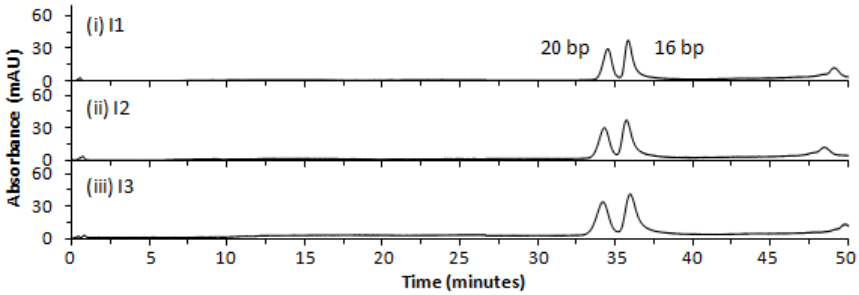

Figure 10.6. CE electropherograms of repetitive injections of a mixture of 16 bp and 20 bp dsODNs (18.6 µM). Separation was performed on a CFR PDEAEMA-*co*-PMMA random copolymer (34/66) coated fused-silica capillary (30 cm L_d, 38 cm L_t, 75 µm id, 363 µm od) at -131.6 V cm^{-1} and 30 ^oC with UV detection at 260 nm for 60 min run time. The BGE was Tris-borate (100 mM)/urea (7 M). Samples were introduced hydrodynamically at 5000 Pa for 6 s. The capillary was conditioned between runs by flushing with polymer solution for 5 min, H_2O for 2 min and buffer for 3 min.

10.2 Appendix B

This section details the supporting data for capillary electrophoretic separation of ODNs and PS-ODNs utilising SEI and positive polarity on 8 cm (L_d) capillaries modified with a CFR PEPyM-*co*-PMMA random copolymer (21/79).

10.2.1 AS-ODNs

10.2.1.1 Hydrodynamic injection

10.2.1.1.1 Voltage study

The effect of voltage on ODN migration using short-end hydrodynamic injection was determined using a 16 bp and 20 bp dsODN mixture. Table 10.6 contains the migration data and the associated mobility and R_s calculations.

Table 10.6. Calculation of R_s and efficiency of the separation of 16 bp and 20 bp dsODNs (18.6 μM) at varying voltages using a CFR PEPyM-*co*-PMMA random copolymer (21/79) coated fused-silica capillary (8 cm L_d).

Voltage ($V\ cm^{-1}$)	Peak (bp)	t_m (min)	W_h (min)	R_s	N	v x 10^{-4} ($m\ s^{-1}$)	μ_{app} x 10^{-9} ($m^2\ V^{-1}\ s^{-1}$)*	μ_{obs} x 10^{-9} ($m^2\ V^{-1}\ s^{-1}$)*
26.32	20	31.34	1.08	1.02	4682	0.43	-16.17	-24.94
	16	33.41	1.32		4682	0.40	-15.17	-23.94
39.47	20	20.48	0.62	0.89	6110	0.65	-16.50	-25.27
	16	21.59	0.86		6110	0.62	-15.64	-24.42
52.63	20	15.01	0.42	0.89	6969	0.89	-16.87	-25.65
	16	15.81	0.62		6969	0.84	-16.03	-24.80
65.79	20	12.05	0.35	0.80	6519	1.11	-16.82	-25.59
	16	12.64	0.52		6519	1.05	-16.03	-24.80
78.95	20	10.09	0.28	0.61	7137	1.32	-16.74	-25.51
	16	10.47	0.45		7137	1.27	-16.13	-24.91
92.11	20	8.63	0.27	0.63	5730	1.55	-16.78	-25.55
	16	9.01	0.45		5730	1.48	-16.06	-24.83
105.26	20	6.54	0.16	0.31	9376	2.04	-19.37	-28.14
	16	6.66	0.31		9376	2.00	-19.01	-27.78
118.42	20	6.53	0.18	0.78	7399	2.04	-17.26	-26.03
	16	6.82	0.26		7399	1.96	-16.52	-25.29
131.58	20	5.93	0.18	0.85	6314	2.25	-17.10	-25.87
	16	6.28	0.31		6314	2.12	-16.14	-24.92
144.74	20	5.30	0.18	0.87	4847	2.52	-17.38	-26.15
	16	5.64	0.28		4847	2.37	-16.34	-25.12
157.89	20	4.91	0.12	0.60	9750	2.72	-17.22	-25.99
	16	5.08	0.24		9750	2.62	-16.61	-25.38
171.05	20	4.53	0.13	0.63	7039	2.94	-17.20	-25.97
	16	4.73	0.24		7039	2.82	-16.48	-25.25
184.21	20	4.23	0.12	0.56	7334	3.15	-17.10	-25.87
	16	4.42	0.28		7334	3.02	-16.38	-25.15
197.37	20	3.93	0.13	0.76	5399	3.39	-17.18	-25.95
	16	4.14	0.20		5399	3.22	-16.30	-25.07

*The negative sign denotes an anodic mobility

10.2.1.1.2 Temperature study

The effect of temperature on ODN migration using short-end hydrodynamic injection was determined using a 16 bp and 20 bp dsODN mixture. Table 10.7 contains the migration data and the associated mobility and R_s calculations.

Table 10.7. Calculation of R_s and efficiency of the separation of 16 bp and 20 bp dsODNs (18.6 µM) at varying temperatures using a CFR PEPyM-*co*-PMMA random copolymer (21/79) coated fused-silica capillary.

Temp. (^oC)	Peak bp	t_m (min)	W_h (min)	R_s	N	v x 10^{-4} (m s^{-1})	μ_{app} x 10^{-9} (m^2 V^{-1} s^{-1})*	μ_{obs} x 10^{-9} (m^2 V^{-1} s^{-1})*
15	20	7.81	0.25	0.00	5504	1.71	-12.98	-21.75
	16	7.81	0.25		5504	1.71	-12.98	-21.75
20	20	7.37	0.23	0.15	5578	1.81	-13.75	-22.52
	16	7.42	0.19		8303	1.80	-13.65	-22.43
25	20	6.78	0.13	1.13	15285	1.97	-14.94	-23.71
	16	7.11	0.21		6295	1.88	-14.26	-23.03
30	20	6.44	0.15	1.65	10277	2.07	-15.74	-24.51
	16	6.95	0.22		5525	1.92	-14.57	-23.34
35	20	6.21	0.13	2.55	12985	2.15	-16.31	-25.08
	16	6.91	0.19		7183	1.93	-14.67	-23.45
40	20	6.07	0.13	2.80	11802	2.20	-16.69	-25.47
	16	6.90	0.22		5647	1.93	-14.69	-23.46
45	20	6.17	0.21	2.36	5010	2.16	-16.44	-25.21
	16	7.01	0.22		5805	1.90	-14.45	-23.23
50	20	6.21	0.08	2.53	31588	2.15	-16.33	-25.10
	16	6.95	0.26		3824	1.92	-14.58	-23.35

*The negative sign denotes an anodic mobility

10.2.1.1.3 Sequence dependence

The sequence dependence and ODN-ODN interactions were investigated using short-end hydrodynamic injection of mixtures containing a 16 bp strand consisting of a sequence non-complementary to the other double strands in the dsODN mixtures (16-CAT). The 16-CAT bp dsODN and a 16-COMP bp dsODN were analysed individually by normal injection (negative polarity) on a 30 cm (L_d) CFR PEPyM-*co*-PMMA random copolymer coated capillary in order to compare the mobilities.

Figure 10.7 shows the CE electropherograms and Table 10.8 contains the mobility data. Figure 10.7 shows that the 16-CAT bp dsODN had a longer t_m than the 16-COMP bp dsODN and hence a slower mobility (Table 10.8).

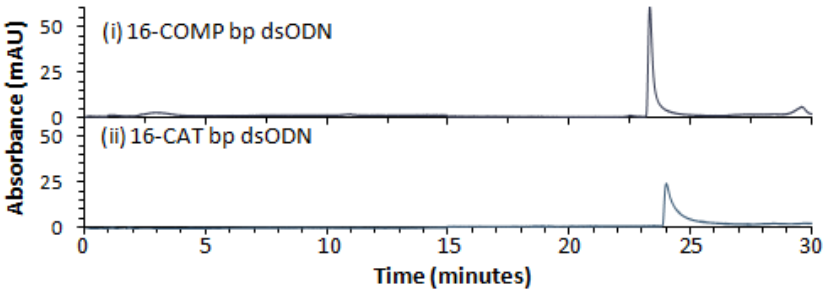

Figure 10.7. CE electropherograms of individual solutions of 16-COMP bp (i), and 16-CAT bp (ii), dsODNs (18 µM). Separation was performed on a CFR PEPyM-*co*-PMMA random copolymer (21/79) coated fused-silica capillary (30 cm L_d, 38 cm L_t, 75 µm id, 363 µm od) at -131.6 V cm^{-1} and 30 °C with UV detection at 260 nm for 30 min run time. The BGE was Tris-borate (100 mM)/urea (7 M). Samples were introduced hydrodynamically at 5000 Pa for 6 s.

Table 10.8. Calculation of t_m, μ_{app}, and μ_{obs} analysis of individual solutions of 16-COMP bp and 16-CAT bp dsODNs (18.6 µM) on a CFR PEPyM-*co*-PMMA random copolymer (21/79) coated fused-silica capillary.

Sample	t_m (min)	W_h (min)	N	v (m s^{-1})	μ_{app} x 10^{-9} (m^2 V^{-1} s^{-1})*	μ_{obs} x 10^{-9} (m^2 V^{-1} s^{-1})*
16-COMP bp	23.03	0.18	79826	2.17	-16.50	-25.27
16-CAT bp	24.02	0.27	42435	2.08	-15.82	-24.59

*The negative sign denotes an anodic mobility

Separation was compared to mixtures containing 16 bp strands with a complementary sequence (16-COMP). The migration and mobility data can be found in Table 10.9.

Table 10.9. Calculation of R_s and efficiency of separation of dsODN mixtures, comparing mixtures containing sequences that are complementary (16-COMP mixtures), and mixtures containing sequences that are non-complementary (16-CAT mixtures).

dsODN sample	Peak (bp)	t_m (min)	W_h	R_s	N	v x 10^{-4} (m s^{-1})	μ_{app} x 10^{-9} (m^2 V^{-1} s^{-1})*	μ_{obs} x 10^{-9} (m^2 V^{-1} s^{-1})*
16 bp and 16-CAT bp	16-COMP	6.64	0.18	0.56	7761	2.01	-15.26	-24.03
	16-CAT	6.89	0.35		2157	1.94	-14.71	-23.48
17 bp and 16-COMP bp	17	6.46	0.22	0.51	4848	2.06	-15.68	-24.46
	16-COMP	6.71	0.35		1990	1.99	-15.11	-23.88
17 bp and 16-CAT bp	17	6.37	0.28	1.01	2873	2.09	-15.92	-24.69
	16-CAT	6.91	0.35		2159	1.93	-14.68	-23.45
20 bp and 16-COMP bp	20	6.20	0.25	1.11	3296	2.15	-16.35	-25.12
	16-COMP	6.74	0.32		2525	1.98	-15.05	-23.82
20 bp and 16-CAT bp	20	6.11	0.29	1.20	2429	2.18	-16.58	-25.36
	16-CAT	6.82	0.41		1568	1.95	-14.85	-23.62

*The negative sign denotes an anodic mobility

10.2.1.2 Electrokinetic injection

10.2.1.2.1 Injection conditions

The effect of V_{inj} and t_{int} on the v_{int} of ODNs was investigated using short-end EKI. The mobility and R_s calculations can be found in Table 10.10.

Table 10.10. Calculation of R_s and efficiency of the separation of 16 bp and 20 bp dsODNs (18.6 µM) using different EKI methods on a CFR PEPyM-*co*-PMMA random copolymer (21/79) coated fused-silica capillary (8 cm L_d) at 35 °C.

EKI method	Peak (bp)	t_m (min)	W_h (min)	R_s	N	v x 10^{-4} (m s^{-1})	μ_{app} x 10^{-9} (m^2 V^{-1} s^{-1})*	μ_{obs} x 10^{-9} (m^2 V^{-1} s^{-1})*
5kV, 5 s	20	6.25	0.14	1.35	10565	2.13	-16.22	-25.00
	16	6.69	0.24		4205	1.99	-15.14	-23.93
5kV, 8 s	20	6.18	0.15	1.10	9913	2.16	-16.40	-25.18
	16	6.51	0.21		5508	2.05	-15.57	-24.36
5kV, 10 s	20	6.14	0.11	1.05	18706	2.17	-16.50	-25.28
	16	6.39	0.18		7316	2.09	-15.85	-24.64
5kV, 15 s	20	6.14	0.13	0.75	12435	2.17	-16.50	-25.29
	16	6.33	0.17		7552	2.11	-16.00	-24.79
7.5kV, 5 s	20	6.12	0.11	0.98	16258	2.18	-16.57	-25.35
	16	6.36	0.17		7365	2.10	-15.95	-24.73
7.5kV, 8 s	20	6.10	0.12	0.76	13773	2.18	-16.60	-25.39
	16	6.29	0.16		8427	2.12	-16.12	-24.90
7.5kV, 10 s	20	6.10	0.12	0.70	13652	2.19	-16.62	-25.41
	16	6.27	0.17		7963	2.13	-16.17	-24.96

*The negative sign denotes an anodic mobility

10.2.1.2.2 Voltage study

The effect of voltage on ODN migration using short-end EKI was investigated using a 16 bp and 20 bp dsODN mixture at 35 °C and 40 °C. Tables 10.11 and 10.12 contain the migration data and the associated mobility and R_s calculations for 35 °C and 40 °C, respectively.

Table 10.11. Calculation of R_s and efficiency of the separation of 16 bp and 20 bp dsODNs (18.6 μM) at 35 ^{o}C and varying voltages using a CFR PEPyM-*co*-PMMA random copolymer (21/79) coated fused-silica capillary (8 cm L_d).

Voltage (V cm^{-1})	Peak (bp)	t_m (min)	W_h (min)	R_s	N	v x 10^{-4} (m s^{-1})	μ_{app} x 10^{-9} (m^2 V^{-1} s^{-1})*	μ_{obs} x 10^{-9} (m^2 V^{-1} s^{-1})*
26.3	20	35.87	0.67	1.06	15905	0.37	-14.12	-22.90
	16	37.07	0.65		17808	0.36	-13.67	-22.44
39.5	20	23.02	0.45	1.08	14823	0.58	-14.67	-23.45
	16	23.80	0.41		18939	0.56	-14.19	-22.97
52.6	20	16.93	0.31	1.05	16951	0.79	-14.96	-23.73
	16	17.49	0.32		16816	0.76	-14.49	-23.26
65.8	20	13.17	0.23	1.03	17950	1.01	-15.39	-24.17
	16	13.60	0.27		14154	0.98	-14.90	-23.67
78.9	20	10.90	0.20	0.98	16615	1.22	-15.50	-24.27
	16	11.26	0.23		13336	1.18	-15.01	-23.78
92.1	20	9.24	0.17	0.95	16940	1.44	-15.67	-24.44
	16	9.55	0.21		11010	1.40	-15.16	-23.93
105.3	20	8.02	0.15	0.89	15143	1.66	-15.79	-24.57
	16	8.29	0.20		9155	1.61	-15.28	-24.05
118.4	20	7.09	0.14	0.91	13917	1.88	-15.88	-24.65
	16	7.34	0.18		9652	1.82	-15.34	-24.12
131.6	20	6.36	0.14	0.80	11272	2.10	-15.93	-24.71
	16	6.59	0.20		6285	2.02	-15.38	-24.15
144.7	20	5.75	0.13	0.87	11609	2.32	-16.01	-24.78
	16	5.96	0.15		8255	2.24	-15.46	-24.23
157.9	20	5.25	0.13	0.79	8760	2.54	-16.09	-24.86
	16	5.45	0.17		6003	2.45	-15.50	-24.27
171.1	20	4.82	0.11	0.90	10985	2.77	-16.18	-24.95
	16	5.00	0.13		8028	2.67	-15.58	-24.36
184.2	20	4.45	0.11	0.83	9038	3.00	-16.26	-25.03
	16	4.62	0.13		6883	2.89	-15.66	-24.44
197.4	20	4.13	0.10	0.85	9277	3.23	-16.35	-25.12
	16	4.30	0.13		5972	3.10	-15.71	-24.48
210.5	20	3.87	0.10	0.85	8280	3.45	-16.38	-25.15
	16	4.03	0.12		5762	3.31	-15.72	-24.50
223.7	20	3.63	0.09	0.96	8486	3.68	-16.43	-25.20
	16	3.79	0.11		6575	3.52	-15.72	-24.49
236.8	20	3.41	0.09	0.91	7264	3.91	-16.50	-25.28
	16	3.58	0.12		4688	3.73	-15.73	-24.51

Voltage ($V\ cm^{-1}$)	Peak (bp)	t_m (min)	W_h (min)	R_s	N	v x 10^{-4} ($m\ s^{-1}$)	μ_{app} x 10^{-9} ($m^2\ V^{-1}\ s^{-1}$)*	μ_{obs} x 10^{-9} ($m^2\ V^{-1}\ s^{-1}$)*
250.0	20	3.22	0.09	0.91	6960	4.14	-16.55	-25.33
	16	3.39	0.13		3910	3.93	-15.73	-24.51
263.2	20	3.05	0.09	1.11	6232	4.37	-16.60	-25.37
	16	3.23	0.09		6553	4.13	-15.71	-24.48
328.9	20	2.43	0.09	1.44	3899	5.49	-16.68	-25.45
	16	2.67	0.10		3883	5.00	-15.20	-23.98
394.7	20	2.09	0.10	1.29	2399	6.39	-16.18	-24.96
	16	2.29	0.09		3736	5.81	-14.73	-23.50

*The negative sign denotes an anodic mobility

Table 10.12. Calculation of R_s and efficiency of the separation of 16 bp and 20 bp dsODNs (18.6 μM) at 40 ^{o}C and varying voltages using a CFR PEPyM-*co*-PMMA random copolymer (21/79) coated fused-silica capillary (8 cm L_d).

Voltage (V cm^{-1})	Peak (bp)	t_m (min)	W_h (min)	R_s	N	v x 10^{-4} (m s^{-1})	μ_{app} x 10^{-9} (m^2 V^{-1} s^{-1})*	μ_{obs} x 10^{-9} (m^2 V^{-1} s^{-1})*
26.3	20	33.47	0.61	1.18	16823	0.40	-15.14	-23.91
	16	34.63	0.55		21936	0.39	-14.63	-23.40
39.5	20	20.90	0.36	1.17	18827	0.64	-16.16	-24.93
	16	21.61	0.35		20651	0.62	-15.63	-24.41
52.6	20	15.40	0.28	1.08	17054	0.87	-16.45	-25.22
	16	15.94	0.30		15363	0.84	-15.90	-24.67
65.8	20	12.18	0.27	0.86	11341	1.09	-16.64	-25.41
	16	12.58	0.29		10643	1.06	-16.11	-24.88
78.9	20	10.08	0.17	1.08	18535	1.32	-16.76	-25.53
	16	10.42	0.20		15098	1.28	-16.21	-24.98
92.1	20	8.59	0.16	0.99	16227	1.55	-16.85	-25.63
	16	8.89	0.19		11656	1.50	-16.29	-25.07
105.3	20	7.53	0.16	0.94	12254	1.77	-16.83	-25.61
	16	7.79	0.17		11008	1.71	-16.26	-25.03
118.4	20	6.70	0.13	0.98	14295	1.99	-16.80	-25.58
	16	6.95	0.17		9189	1.92	-16.20	-24.97
131.6	20	6.07	0.13	0.91	11402	2.20	-16.69	-25.47
	16	6.30	0.16		8089	2.12	-16.08	-24.85
144.7	20	5.57	0.13	0.95	10788	2.39	-16.54	-25.31
	16	5.80	0.16		6897	2.30	-15.87	-24.64
157.9	20	5.03	0.12	0.96	10607	2.65	-16.78	-25.55
	16	5.25	0.15		6402	2.54	-16.08	-24.85
171.1	20	4.64	0.11	0.91	9366	2.87	-16.81	-25.58
	16	4.85	0.16		5007	2.75	-16.08	-24.85
184.2	20	4.27	0.11	0.95	8981	3.12	-16.96	-25.73
	16	4.47	0.15		5238	2.98	-16.19	-24.96
197.4	20	3.96	0.11	0.88	6620	3.37	-17.07	-25.84
	16	4.15	0.15		4442	3.21	-16.26	-25.04
210.5	20	3.72	0.10	1.01	7293	3.59	-17.03	-25.80
	16	3.92	0.14		4669	3.40	-16.15	-24.92
223.7	20	3.45	0.12	0.89	4527	3.86	-17.26	-26.04
	16	3.66	0.15		3293	3.65	-16.30	-25.07
236.8	20	3.24	0.09	1.14	7162	4.12	-17.40	-26.17
	16	3.45	0.13		4135	3.87	-16.34	-25.11

Voltage ($V\ cm^{-1}$)	Peak (bp)	t_m (min)	W_h (min)	R_s	N	v x 10^{-4} ($m\ s^{-1}$)	μ_{app} x 10^{-9} ($m^2\ V^{-1}\ s^{-1}$)*	μ_{obs} x 10^{-9} ($m^2\ V^{-1}\ s^{-1}$)*
250.0	20	3.03	0.09	1.05	6014	4.40	-17.61	-26.39
	16	3.23	0.13		3441	4.13	-16.54	-25.31
263.2	20	2.89	0.10	1.16	4831	4.62	-17.54	-26.32
	16	3.11	0.12		3533	4.29	-16.31	-25.08
328.9	20	2.27	0.09	1.41	3202	5.88	-17.88	-26.65
	16	2.50	0.10		3600	5.34	-16.23	-25.00
394.7	20	1.95	0.06	0.86	5208	6.84	-17.32	-26.09
	16	2.05	0.08		3842	6.49	-16.44	-25.22

*The negative sign denotes an anodic mobility

10.2.1.2.3 Temperature study

The effect of temperature on ODN migration using short-end EKI was investigated using mixtures of 16 bp and 18 bp, and 16 bp and 20 bp dsODNs. Tables 10.13 and 10.14 contains the migration data and the associated mobility and R_s calculations for the 16 bp and 18 bp mixture, and the 16 bp and 20 bp mixture, respectively.

Table 10.13. Calculation of R_s and efficiency of the separation of 16 bp and 18 bp dsODNs (18.6 µM) at varying temperatures using a CFR PEPyM-*co*-PMMA random copolymer (21/79) coated fused-silica capillary.

Temp. (^oC)	Peak (bp)	t_m (min)	W_h (min)	R_s	N	v x 10^{-4} (m s^{-1})	μ_{app} x 10^{-9} (m^2 V^{-1} s^{-1})*	s_d x 10^{-9} (n = 2)	RSD (%)	μ_{obs} x 10^{-9} (m^2 V^{-1} s^{-1})*
15	18	7.82	0.08	0.26	47806	1.70	-12.95	0.008	0.06	-21.73
	16	7.88	0.19		9959	1.69	-12.86	0.014	0.11	-21.63
20	18	7.20	0.09	0.27	36691	1.85	-14.07	0.023	0.16	-22.84
	16	7.26	0.16		12049	1.84	-13.96	0.025	0.18	-22.74
25	18	6.80	0.09	0.27	29607	1.96	-14.90	0.000	0.00	-23.68
	16	6.85	0.14		12390	1.95	-14.78	0.005	0.03	-23.56
30	18	6.41	0.10	0.42	24354	2.08	-15.80	0.022	0.14	-24.57
	16	6.51	0.16		8966	2.05	-15.57	0.010	0.06	-24.34
35	18	6.10	0.12	0.70	15064	2.19	-16.61	0.017	0.11	-25.38
	16	6.25	0.14		11660	2.13	-16.21	0.021	0.13	-24.98
40	18	5.66	0.13	0.79	11039	2.36	-17.91	0.014	0.08	-26.68
	16	5.82	0.12		12645	2.29	-17.40	0.005	0.03	-26.17
45	18	5.48	0.13	0.96	9472	2.43	-18.50	0.366	1.98	-27.27
	16	5.71	0.16		7226	2.33	-17.73	0.354	2.00	-26.51
50	18	5.47	0.14	1.16	9080	2.44	-18.52	0.504	2.72	-27.29
	16	5.77	0.17		6292	2.31	-17.55	0.704	4.01	-26.32

*The negative sign denotes an anodic mobility

Table 10.14. Calculation of R_s and efficiency of the separation of 16 bp and 20 bp dsODNs (18.6 µM) at varying temperatures using a CFR PEPyM-*co*-PMMA random copolymer (21/79) coated fused-silica capillary.

Temp. (^oC)	Peak (bp)	t_m (min)	W_h (min)	R_s	N	v x 10^{-4} (m s^{-1})	μ_{app} x 10^{-9} (m^2 V^{-1} s^{-1})*	s_d x 10^{-9} (n = 2)	RSD (%)	μ_{obs} x 10^{-9} (m^2 V^{-1} s^{-1})*
15	20	7.65	0.13	0.49	19700	1.74	-13.24	0.09	0.71	-22.02
	16	7.78	0.18		10729	1.71	-13.03	0.07	0.50	-21.80
20	20	7.08	0.11	0.66	24455	1.88	-14.32	0.09	0.65	-23.09
	16	7.22	0.15		13326	1.85	-14.04	0.09	0.62	-22.81
25	20	6.63	0.10	0.68	23003	2.01	-15.28	0.05	0.33	-24.05
	16	6.77	0.13		15161	1.97	-14.97	0.05	0.31	-23.75
30	20	6.29	0.12	0.72	16365	2.12	-16.11	0.02	0.13	-24.88
	16	6.45	0.14		11391	2.07	-15.71	0.02	0.12	-24.49
35	20	5.89	0.13	0.80	10839	2.26	-17.20	0.04	0.21	-25.97
	16	6.08	0.14		10267	2.19	-16.67	0.04	0.24	-25.44
40	20	5.53	0.14	1.18	8846	2.41	-18.33	0.23	1.25	-27.10
	16	5.80	0.14		9971	2.30	-17.46	0.24	1.40	-26.23
45	20	5.59	0.14	1.25	8254	2.39	-18.14	0.16	0.88	-26.91
	16	5.92	0.17		7101	2.25	-17.13	0.19	1.13	-25.90
50	20	5.21	0.16	1.27	6063	2.56	-19.44	0.34	1.74	-28.21
	16	5.57	0.17		5821	2.39	-18.20	0.46	2.52	-26.97

*The negative sign denotes an anodic mobility

10.2.1.2.4 Sequence dependence

The sequence dependence and ODN-ODN interactions were investigated using short-end EKI of mixtures containing a 16 bp strand consisting of a sequence non-complementary to the other double strands in the dsODN mixtures (16-CAT). Separation was compared to mixtures containing 16 bp strands with a complementary sequence (16-COMP). The migration and mobility data can be found in Table 10.15.

Table 10.15. Calculation of R_s and efficiency of separation of dsODN mixtures, comparing mixtures containing sequences that are complementary (16-COMP mixtures), and mixtures containing sequences that are non-complementary (16-CAT mixtures).

dsODN sample	Peak (bp)	t_m (min)	W_h	R_s	N	v x 10^{-4} (m s^{-1})	μ_{app} x 10^{-9} (m^2 V^{-1} s^{-1})*	s_d x 10^{-9} (n = 2)	RSD (%)	μ_{obs} x 10^{-9} (m^2 V^{-1} s^{-1})*
16 bp and 16-CAT bp	16-COMP	3.10	0.07	0.52	9874	4.30	-16.35	0.08	0.48	-25.12
	16-CAT	3.19	0.14		2975	4.18	-15.87	0.08	0.50	-24.65
17 bp and 16-COMP bp	17	2.98	0.06	0.56	14806	4.48	-17.02	0.01	0.08	-25.80
	16-COMP	3.06	0.12		3542	4.35	-16.55	0.05	0.29	-25.32
17 bp and 16-CAT bp	17	2.97	0.09	0.89	5529	4.49	-17.08	0.003	0.02	-25.85
	16-CAT	3.16	0.17		2021	4.22	-16.02	0.06	0.38	-24.79
18 bp and 16-COMP bp	18	2.91	0.09	1.03	5377	4.57	-17.38	0.04	0.21	-26.16
	16-COMP	3.11	0.13		3067	4.28	-16.28	0.09	0.52	-25.05
18 bp and 16-CAT bp	20	2.90	0.09	1.24	6340	4.59	-17.45	0.04	0.24	-26.23
	16-CAT	3.14	0.14		2918	4.25	-16.15	0.14	0.88	-24.93
19 bp and 16-COMP bp	19	2.90	0.09	1.08	5639	4.60	-17.47	0.03	0.18	-26.24
	16-COMP	3.10	0.13		3225	4.30	-16.33	0.04	0.27	-25.10
19 bp and 16-CAT bp	20	2.86	0.10	1.23	4313	4.66	-17.69	0.05	0.29	-26.46
	16-CAT	3.10	0.12		3631	4.31	-16.36	0.08	0.52	-25.13
20 bp and 16-COMP bp	20	2.86	0.09	1.29	5193	4.66	-17.72	0.06	0.32	-26.49
	16-COMP	3.09	0.12		3573	4.31	-16.37	0.00	0.02	-25.14
20 bp and 16-CAT bp	20	2.85	0.11	1.35	3682	4.69	-17.81	0.08	0.47	-26.58
	16-CAT	3.11	0.12		3903	4.29	-16.31	0.03	0.18	-25.08

*The negative sign denotes an anodic mobility

10.2.1.2.5 Effect of ionic strength

The effect of ionic strength on the mobility of a mixture of 16 bp and 20 bp dsODNs was investigated by adding Tris-borate (200 mM), and NaCl (in varying amounts) to the BGE. The mobility and R_s calculations for the NaCl study can be found in Table 10.16.

Table 10.16. Calculation of R_s and efficiency of the separation of 16 bp and 20 bp dsODN mixture (18.6 µM) at varying BGE ionic strengths using a CFR PEPyM-*co*-PMMA random copolymer (21/79) coated fused-silica capillary.

[NaOH] added to BGE (mM)	Peak (bp)	t_m (min)	W_h (min)	R_s	N	v x 10^{-4} (m s^{-1})	μ_{app} x 10^{-9} (m^2 V^{-1} s^{-1})*	s_d x 10^{-9} (n = 3)	RSD (%)
0	20	6.30	0.14	0.94	10929	2.12	-16.09	-	-
	16	6.59	0.22		4902	2.02	-15.38	-	-
10	20	5.39	0.12	0.83	10376	2.47	-18.78	0.60	3.21
	16	5.59	0.15		8057	2.39	-18.14	0.46	2.55
30	20	5.61	0.13	0.79	10047	2.38	-18.06	0.02	0.13
	16	5.79	0.14		9463	2.30	-17.49	0.02	0.12
50	20	5.89	0.15	0.57	8176	2.26	-17.20	0.22	1.26
	16	6.05	0.18		6438	2.20	-16.76	0.15	0.88

*The negative sign denotes an anodic mobility

10.2.2 PS-ODNs

10.2.2.1 Effect of temperature on PS-ODN separation

The effect of temperature on PS-ODN migration was investigated on a CFR PEPyM-*co*-PMMA random copolymer coated capillary using short-end EKI in an attempt to improve the R_s of a mixture of 16* bp and 18* bp dsPS-ODNs. Table 10.17 contains the migration data and the associated mobility and R_s calculations for the 16* bp and 18* bp dsPS-ODN mixture.

Table 10.17. Calculation of R_s and efficiency of the separation of 16* bp and 18* bp dsPS-ODNs (8.5 µM) at varying temperatures using a CFR PEPyM-*co*-PMMA random copolymer coated fused-silica capillary.

Temp. (^oC)	Peak (bp)	t_m (min)	W_h (min)	R_s	N	v x 10^{-4} (m s^{-1})	μ_{app} x 10^{-9} (m^2 V^{-1} s^{-1})$^{\#}$	μ_{obs} x 10^{-9} (m^2 V^{-1} s^{-1})$^{\#}$
35	18*	3.49	0.05	0.28	29246	3.82	-14.52	-23.30
	16*	3.53	0.14		3333	3.77	-14.34	-23.11
40	18*	3.36	0.04	0.29	38013	0.00	-15.08	-23.85
	16*	3.41	0.14		3272	0.00	-14.88	-23.65
45	18*	3.29	0.04	0.32	46402	0.00	-15.41	-24.18
	16*	3.34	0.15		2732	0.00	-15.18	-23.95
50	18*	3.26	0.04	0.35	31012	0.00	-15.56	-24.33
	16*	3.32	0.17		2055	0.00	-15.26	-24.04
55	18*	3.27	0.04	0.34	37706	0.00	-15.50	-24.27
	16*	3.33	0.17		2146	0.00	-15.22	-23.99
60	18*	3.38	0.06	0.37	20457	0.00	-14.98	-23.75
	16*	3.46	0.20		1599	0.00	-14.62	-23.40

$^{\#}$The negative sign denotes an anodic mobility *Represents phosphorothioate backbone

10.2.2.2 Effect of ionic strength on PS-ODN separation

The effect of ionic strength on the mobility of a mixture of 16* bp and 18* bp dsPS-ODNs was investigated by adding Tris-borate (200 mM), and NaCl (in varying amounts) to the BGE. The mobility and R_s calculations for the NaCl study can be found in Table 10.18.

Table 10.18. Calculation of R_s and efficiency of the separation of 16* bp and 18* bp dsPS-ODNs (8.5 µM) at varying BGE ionic strengths using a CFR PEPyM-*co*-PMMA random copolymer (21/79) coated fused-silica capillary.

[NaOH] added to BGE (mM)	Peak (bp)	t_m (min)	W_h (min)	R_s	N	v x 10^{-4} (m s^{-1})	μ_{app} x 10^{-9} (m^2 V^{-1} s^{-1})[#]	s_d x 10^{-9} (n = 3)	RSD (%)	μ_{obs} x 10^{-9} (m^2 V^{-1} s^{-1})[#]
0	18*	7.41	0.11	0.41	23567	1.80	-13.67	-	-	-22.44
	16*	7.55	0.29		3828	1.77	-13.42	-	-	-22.19
10	18*	6.38	0.18	0.52	7117	2.09	-15.88	0.06	0.39	-24.66
	16*	6.56	0.22		5330	2.03	-15.46	0.09	0.57	-24.23
30	18*	6.65	0.14	0.42	12947	2.00	-15.23	0.10	0.67	-24.01
	16*	6.80	0.29		3140	1.96	-14.89	0.08	0.54	-23.67
50	18*	6.81	0.20	0.84	6621	1.96	-14.88	0.28	1.87	-23.66
	16*	7.15	0.29		3771	1.86	-14.17	0.04	0.29	-22.95

[#]The negative sign denotes an anodic mobility
*Represents phosphorothioate backbone